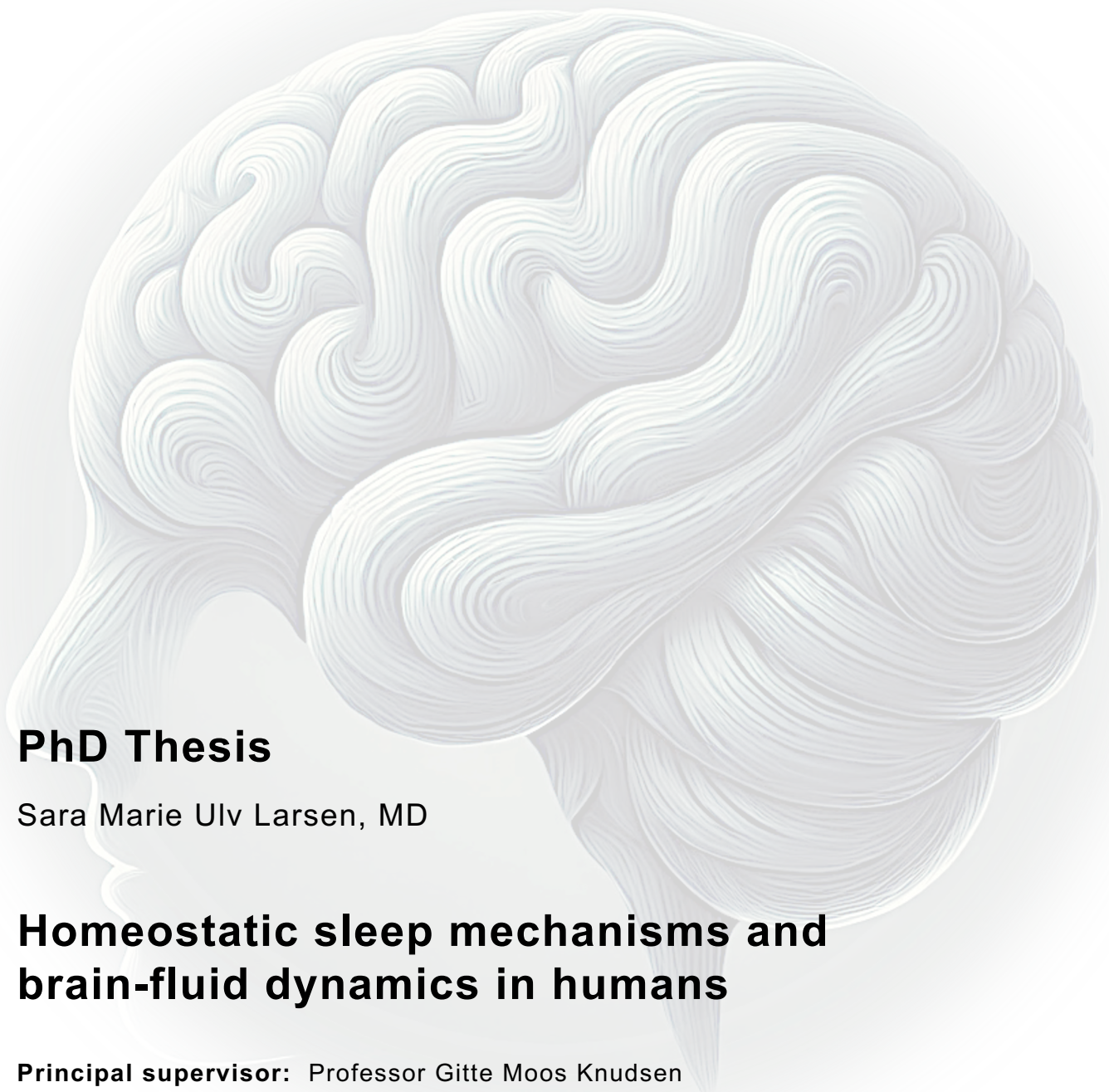


UNIVERSITY OF COPENHAGEN  
FACULTY OR DEPARTMENT



## PhD Thesis

Sara Marie Ulv Larsen, MD

# Homeostatic sleep mechanisms and brain-fluid dynamics in humans

**Principal supervisor:** Professor Gitte Moos Knudsen

This thesis has been submitted to the Graduate School of Health and Medical Sciences,  
University of Copenhagen on January 9<sup>th</sup>, 2025.

Name of department: Neurobiology Research Unit, Department of Neurology,  
Copenhagen University Hospital, Rigshospitalet, Copenhagen,  
Denmark

Author: Sara Marie Ulv Larsen, MD

Title: Homeostatic sleep mechanisms and brain-fluid dynamics in  
humans

Institutions: Neurobiology Research Unit, Copenhagen University Hospital  
Rigshospitalet & Faculty of Health and Medical Sciences,  
University of Copenhagen, Copenhagen, Denmark

Principal Supervisor: Professor Gitte Moos Knudsen,  
Neurobiology Research Unit,  
Copenhagen University Hospital Rigshospitalet

Co-supervisors: Dr. Sebastian Camillo Holst,  
Neurobiology Research Unit,  
Copenhagen University Hospital Rigshospitalet &

Submitted on: January 9, 2025

Date of defense: April 4, 2025

Assessment committee: Professor Adam Espe Hansen,  
Department of Diagnostic Radiology,  
Copenhagen University Hospital, Rigshospitalet  
Copenhagen, Denmark

Professor Rune Enger  
GliaLab and Letten Centre, Division of Anatomy  
Department of Molecular Medicine, Institute of Basic Medical  
Sciences, University of Oslo, Norway

Dr. Swati Rane Levendovszky  
Brain imaging Core, University of Washington,  
Seattle, Washington D.C., USA

Front page illustration created using DALL-E with ChatGPT..

# Contents

---

List of manuscripts .....	v
Acknowledgements .....	vi
Summary .....	vi
Dansk resumé .....	xi
Abbreviations .....	xiii
<b>BACKGROUND .....</b>	<b>1</b>
1. SLEEP ... ..	1
1.1 A night of sleep .....	1
1.2 Homeostatic sleep mechanisms .....	3
2. BRAIN FLUID DYNAMICS .....	4
2.1 The three fluid compartments.....	4
2.2 The glymphatic system.....	5
2.3 Physiological drivers of brain fluid flow in rodents.....	6
2.4 Sleep-dependent brain fluid flow and clearance in humans .....	7
3. AQP4 .....	8
3.1 AQP4 water channel.....	8
3.2 Genetic variants of the AQP4 gene .....	8
3.3 AQP4 SNPs in humans .....	8
4. IMAGING PHYSIOLOGICAL BRAIN OSCILLATION .....	9
4.1 MREG and MB .....	9
4.2 Physiological brain oscillations and sleep-wake regulation .....	10
4.3 From whole-brain images to MREG- and MB spectra.....	10
4.4 Use of data in previously submitted Master's thesis.....	11
<b>AIMS &amp; HYPOTHESES.....</b>	<b>12</b>
5. AIM OF PHD .....	12
5.1 Study I .....	12
5.2 Study II .....	12

5.3	Study III .....	12
5.4	Study IV .....	13
<b>METHODS .....</b>		<b>14</b>
6.	ETHICS, APPROVALS, AND REGISTRATIONS.....	14
7.	STUDY I .....	14
7.1	dbSNP .....	14
7.2	Genotyping.....	15
7.3	Population.....	15
7.4	Study design across Zürich sleep studies .....	16
7.5	Polysomnography .....	16
7.6	EEG analysis .....	17
7.7	Psychomotor performance .....	17
7.8	Subjective sleepiness.....	17
8.	STUDY II.....	18
8.1	Population .....	18
8.2	Scan sessions.....	18
8.3	Processing and evaluation of MREG data .....	18
9.	STUDY III & IV .....	19
9.1	Population .....	19
9.2	Study design .....	20
9.3	Pharmacological intervention with carvedilol .....	21
9.4	MRI sessions .....	21
9.5	MR acquisition .....	21
9.6	MR preprocessing .....	22
9.7	Spectral analysis.....	22
9.8	EEG and physiological data collected during MR.....	23
9.9	MR-EEG processing and scoring .....	24
9.10	Quantification of EEG delta power ratio.....	24
9.11	EEG outside of scanner environment .....	25
9.12	Nocturnal PSG recording.....	25
9.13	Minimal EEG setup during prolonged wakefulness.....	25
9.14	Psychomotor vigilance .....	26

9.15 Plasma norepinephrine .....	26
10. STATISTICS .....	27
10.1 Study I .....	27
10.2 Study II .....	28
10.3 Study III + IV .....	28
<b>RESULTS .....</b>	<b>31</b>
11. STUDY I .....	31
11.1 8-SNP AQP4-haplotype .....	31
11.2 AQP4-haplotype and NREM slow waves .....	32
11.3 AQP4-haplotype: Response to sleep deprivations.....	32
12. STUDY II.....	33
13. STUDY III.....	36
13.1 Sleep study cohort and vigilance state descriptives .....	36
13.2 Physiological brain oscillations across tissue types .....	37
13.3 LFOs, sleep deprivation and sleep pressure .....	37
13.4 NREM sleep and respiration- and cardiac-driven brain pulsations .....	37
13.5 Sleep depth, EEG delta power and the strength of respiration- and cardiac-driven brain pulsations.....	38
13.6 Systemic adrenergic antagonism and physiological brain oscillations	38
14. STUDY IV.....	41
14.1 MB-detected LFOs across brain tissue types .....	41
14.2 MB-detected LFOs and sleep deprivation .....	41
14.3 LFOs and plasma norepinephrine .....	41
14.4 NREM sleep and MB-detected respiration- and cardiac-driven brain pulsations.....	43
14.5 MB versus MREG.....	43
<b>DISCUSSION .....</b>	<b>45</b>
15. DISCUSSION.....	45
15.1 AQP4 haplotype modulates deep NREM sleep intensity and slow waves	45
15.2 MR-detected physiological brain oscillation and brain-fluid dynamics	46

15.3 Respiration- and cardiac driven brain pulsations correlate with sleep slow waves .....	47
15.4 LFOs and cerebrovascular oscillations .....	47
15.5 Cerebrovascular oscillations and heightened sleep pressure.....	48
15.6 Cerebrovascular oscillations and plasma norepinephrine.....	49
15.7 Adrenergic antagonism decreases LFOs and cardiac-driven brain pulsations.....	50
16. LIMITATIONS .....	51
<b>CONCLUSION.....</b>	<b>52</b>
<b>REFERENCES.....</b>	<b>53</b>
<b>APPENDIX .....</b>	<b>61</b>

## List of manuscripts

---

The thesis is based on the following manuscripts.

- 1) **Ulv Larsen SM**, Landolt HP, Berger W, Nedergaard M, Knudsen GM, Holst SC. Haplotype of the astrocytic water channel AQP4 is associated with slow wave energy regulation in human NREM sleep. *PLoS Biol.* May 2020.
- 2) **Ulv Larsen SM**<sup>1</sup>, Holst SC<sup>\*</sup>, Olsen AS, Ozenne B, Zilstorff DB, Brendstrup-Brix K, Weikop P, Pleinert S, Kiviniemi V, Jennum PJ, Nedergaard M, Knudsen GM. Sleep pressure promotes cerebrovascular oscillations while respiration- and cardiac-driven brain pulsations escalate with sleep intensity. *In revision at PLoS Biology, submitted Jan 2025. Previous version incl. study II published on medRxiv Oct 2024*<sup>1</sup>.
- 3) **Ulv Larsen SM**, Olsen AS, Zilstorff DB, Ozenne B, Pleinert S, Norberg CL, Brendstrup-Brix K, Weikop P, Jennum PJ, Nedergaard M, Holst SC, Knudsen GM. The role of norepinephrine and sleep deprivation on cerebrovascular oscillations in humans. *Manuscript in prep.*

Selected related articles not included in this thesis:

- i. Emily Eufaula Beaman, Anders Nissen Bonde, **Sara Marie Ulv Larsen**, Brice Ozenne, Terhi Johanna Lohela, Maiken Nedergaard, Gunnar Hilmar Gíslason, Gitte Moos Knudsen, Sebastian Camillo Holst. Blood–brain barrier permeable  $\beta$ -blockers linked to lower risk of Alzheimer’s disease in hypertension *Brain. Volume 146, Issue 3, March 2023, Pages 1141–1151*
- ii. Brendstrup-Brix K, **Ulv Larsen SM**, Lee HH, Knudsen GM. J Perivascular space diffusivity and brain microstructural measures are associated with circadian time and sleep quality. *Sleep Res.* 2024;33(6):e14226.

---

\* These authors contributed equally to the work

## Acknowledgements

---

Science thrives on collaboration, and over the past eight years—from my time as a research year student, through part-time research, and into my PhD—I’ve had the privilege of meeting some of the most remarkable, clever and interesting people imaginable. Not only at the Neurobiology Research Unit (NRU), but also in the labs and clinics I’ve collaborated with. While I cannot mention and thank everyone without writing a 10-page essay, please know that I’ve appreciated every discussion, piece of advice, coffee-maker meet-up, MR-scanner moment, conference, lunch, and laugh we’ve shared.

First and foremost, my deepest thanks to my supervisor, Professor Gitte Moos Knudsen. Thank you for masterfully guiding me and helping me find my own path in the world of sleep, brain-fluid dynamics, and neuroimaging. I’ve enjoyed our many hours spent discussing and interpreting data, and I’m in awe of your inexhaustible knowledge of neuroscience and your sharp eye for both the big picture and the smallest details. I hope some of that has rubbed off on me along the way. Thank you also to my co-supervisor, Sebastian Camillo Holst, for sparking my excitement about sleep and glymphatics and for trusting me with the sleep project—both when you first hired me on the project and later when you handed me the reins. I’m grateful to have had a supervisor who involved me in all phases of research from early on, and I appreciate that our meetings can still stretch on for hours – because the science discussions are simply too interesting to stop. To Professor Maiken Nedergaard: Thank you for taking on a mentorship role for me. I deeply appreciate your advice and perspective, and I greatly admire your approach to science and how you are always open and encouraging about new findings that may challenge our current understanding of the glymphatic system.

Thank you, Peter Jensen, Dorte Givard, and Birgit Tang, for being the backbone of NRU and for always staying ahead of potential issues on my behalf. Knowing there’s always a helping hand and a smile behind your doors has been a constant over the years. And thanks to Emilie Henriksen, Lone Freyr, and Gerda Thomsen for great help with MR-scans and project practicalities. How anyone does science without the likes of you is a riddle to me.

Thank you to the awesome group of people who have been part of the ‘glymphatics family’ at NRU. I’ve thoroughly enjoyed working with you all. Thank you Anders Stevnhoved Olsen, for being my partner-in-crime in MREG-analysis— and for always being up for a good biological-versus- methodological discussion. Everyone should have a research ‘sidekick’ like you. Thank you, Dorte Zielstorff and Simone Pleinert, for your delightful selves and for all the hours spent testing, scanning, and sleep-depriving study participants together. To Emily Beaman and Miriam Navarro, thanks for enthusiastic discussions and theories, and for letting me take part in your respective research projects.

To Kristoffer Brendstrup-Brix, for your sharp mind, thoroughness, and the calm atmosphere you bring. Thank you for taking such good care of my projects during my maternity leave – I don't think I could have left it with anyone more competent than you. Also a big thanks to the students who joined our group through the years: Oliver Iversen, Cecilie Nordberg, Nina Fultz, Ajla Sabitovic, Astrid Nielsen, Silja Vange, and Cathrine Lind. You've been a joy to work with, supervise, and learn from.

My deepest gratitude also goes to collaborators on the sleep projects from outside of NRU. Professors Poul Jørgen Jennum, Vesa Kiviniemi, and Hans-Peter Landolt; thank you for your invaluable advice and guidance. And to the wonderful people at the Center for Translational Neuromedicine at the University of Copenhagen, thank you for welcoming me into your lab, journal clubs, and data discussions. I'm so impressed and intrigued by the very cool research you do.

Thank you Brice Ozeanne, for teaching me about linear mixed models, and for your admirable patience and good humor about statistics (and for the galette recipe!). Thank you Claus Svarer, for your help with the ever-growing need for MREG data space, and for giving me the opportunity to supervise DTU students together with you. It taught me a lot.

Thank you to colleagues from the Danish Headache Center, the Memory Clinic and the Radiology Department at Rigshospitalet. While our clinical projects on brain-fluid dynamics in IHH and NPH patients didn't make it into the thesis, these projects were central to my PhD-time. I've enjoyed the positivity and ease of collaborations – and admire your deep knowledge and care about your patients. Thank you Professor Rigmor Højland, Nadja Skadkjær Hansen, and Johanne Severinsen for your tireless support and for finding IHH patients for me before other doctors 'got their hands on them'. I'll (almost) miss the calls and patient talks at odd hours, on Sundays, and during holidays. Thank you Professor Steen Hasselbalch, Hanne Naomi Wakabayashi, Sara Taudorf, Jonathan Carlsen and Professor Adam Espe Hansen for your help with coordinating (and performing) tap tests and MR scans of NPH patients – and for sharing in my excitement about intracranial pressure and brain pulsations. I look forward to our next steps.

Thank you to the two reasons I know that three *is* a party: To Vibeke Dam, for your open arms from my very first day at NRU– and for being the occasionally much-needed experienced voice in my head. Let's keep doing puzzles, pottery, vacations and garden-sharing for a long time. You can also keep borrowing Marc for the rock stuff. To Annette Johansen, for being an amazing wing-woman, brainstormer, fellow neuro-nerd and like-minded thinker. Here's to many more coffee-walks. If nothing else came out of this PhD, I'd still be grateful it brought you both into my life.

A huge thanks to all members of the Pink Ladies and Seven Dwarfs offices: Søren Vinther Larsen, Camilla Borgsted Larsen, Gjertrud Laurell, Drummond McCullough, Clara Madsen, Ruben Dörfel, Nakul Raval, Charlotte Nykjær and honorary member Kristian Jensen. Thank you for the good times, the great work vibes, and all your help and

input—you are a lovely bunch of admirable researchers. And to Lene Donovan, Melanie Ganz, and Hanne Demant, thank you for showing me that women can be badass neuroscientists and mothers of young ones at the same time.

Thank you, MK Olsen, for being my best colleague and discussion partner, my sharpest critic, my greatest supporter, and the best editor a girl could ask for. Large language models have nothing on your read-throughs and suggestions in my work.

And lastly, thanks to the many inspiring people up and down the halls of NRU who've filled the place with engaging conversations and a strong sense of community and 'home'; These include – but are not limited to – Patrick, Lars, Vibe, Kristian, Maja, Arafat, Pontus, Anjali, Sophia, Martin, Kristin, Giske, Cheng, Svitlana, and Oluf.

To Mom and Dad, thank you for your support in all the forms it takes. I'm grateful for the curiosity and sheer bloody-minded determination you've instilled in me. Thank you, also, for indoctrinating me throughout childhood to want to become both like my doctor mom and engineer dad, so that I ended up as a neuroscientist-doctor working with MR. It's a good place to be in life. To Jacob and Emil: I'll always be both older and taller than both of you, but I do still look up to you. I appreciate your continued interest in my ramblings and your ever-sobering requests that I publish something in 'Fyns Stifttidende' rather than in science journals. Thank you also to Marianne. I won the lottery when I gained you as a mother-in-law. I am very grateful for the way you stepped in during the final stage of my PhD—helping to provide both the mental and physical space I needed to finish.

Thank you, Julie, for being a sister-like anchor in life and for always offering fresh perspectives and alternative solutions to every conundrum I find myself in. And to Alex and Alicia, thank you for your friendship, wine-and-cake deliveries – and for lending me your vacation home to write. And thanks Alex, for gifting me the name *Aquaporina* and for forever embedding a melodic lyric in my brain whenever I hear the word *aquaporin*.. Thanks to the 'bubble' of friends from medical school through doctorhood, who've shared countless laughs, dances and career talks over the years.

To Bedstemor and Bedstefar; thank you for introducing me to the wonders of mathematics and chemistry, a love of books, nature, and lengthy philosophical discussions. To Farmor and Farfar; thank you for always taking an interest in my life, and for giving me some *synnejysk muld* under my feet. And to every other person in my extended family—both the one I grew up with and the one I gained in adult life; It's not lost on me how lucky I am to be surrounded by all of you.

And most importantly, thank you to my two boys. Nothing would be worth it without you, and science would certainly be a lot less exciting if I couldn't come home and rant far too much about it over a puzzle on the floor.

To Arthur, for making me laugh every day and giving it all some healthy perspective.  
To Marc, for everything.

## Summary

---

Sleep promotes cerebrospinal fluid (CSF) flow into and through the brain, which is essential for clearing metabolic waste. Preclinical studies describe how this sleep-dependent influx of CSF, also known as ‘the glymphatic system’, is facilitated by the water channel aquaporin-4 (AQP4) and driven by cerebrovascular oscillations and pressure waves generated by respiratory and cardiac cycles. While growing human evidence supports sleep's role in brain-fluid flow and waste removal, the mechanisms by which sleep regulates this flow remain largely unknown.

The aim of this thesis was to improve our understanding of the interplay between homeostatic sleep mechanisms and brain-fluid dynamics in humans. In study I, we first evaluated whether AQP4 water channel function modulates sleep-wake regulation by examining nocturnal sleep recordings and responses to sleep loss in individuals genotyped for a common AQP4 haplotype. In the subsequent two studies, we used the ultrafast brain imaging techniques Magnetic Resonance Encephalography (MREG) to measure physiological brain oscillations, thought to reflect brain fluid motion. Study II is a descriptive study, validating the physiological origin of MREG-detected brain oscillations through breath-holding and the Valsalva maneuver (known to influence cerebral vasomotion and cardiac activity). Study III examined how sleep deprivation, slow-wave-rich sleep, and pharmacological modulation of cerebrovascular pulsatility impact the strength of physiological brain oscillations in a circadian-controlled study, including a randomized, double-blind, placebo-controlled crossover administration of the  $\alpha 1$  and  $\beta$ -adrenergic antagonist carvedilol. Lastly, in study IV, we extended our investigations of cerebrovascular oscillation to examine their relationship with blood norepinephrine levels, using Multiband echo planar imaging (MB). This method offers higher spatial resolution, but slower imaging acquisition than MREG (4.6 images per second versus 10) and was collected alternately with MREG in study III.

**Study I** demonstrated that carriers of a low-AQP4-expressing variant of an AQP4 haplotype exhibit heightened slow-wave energy during nocturnal sleep and experience increased global alertness and less sleepiness during extended wakefulness.

**Study II** showed a causal link between both MREG-detected low-frequency oscillations (LFOs) and cerebral vasomotion and between MREG-detected brain pulsations in respiration- and cardiac frequency ranges and their corresponding physiological processes.

**Study III** found that sleep deprivation promotes LFOs, while slow-wave-rich sleep (stages N2 and N3) enhances respiration- and cardiac-driven brain pulsations in gray- and white matter, with their strength correlating with sleep depth and EEG delta power. Carvedilol also dampened LFOs, supporting that these reflect cerebrovascular oscillations.

**Study IV** showed that LFOs are modulated by norepinephrine in rested wakefulness and sleep, and further confirmed the observed effects of sleep deprivation on LFOs and slow-wave-rich sleep on respiration-driven brain pulsations.

**In conclusion**, this work presents the first human evidence linking brain fluid dynamics to sleep slow waves, heightened sleep pressure and norepinephrine. It also disentangles the effects of sleep deprivation and autonomic arousal from those of sleep itself and suggests that sleep may not be the sole driver of glymphatic flow, as cerebrovascular oscillations are regulated by heightened sleep need norepinephrine levels.

## Dansk resumé

---

Søvn fremmer cerebrospinalvæskens (CSF) strømning ind i og gennem hjernen, hvilket er afgørende for at fjerne metabolisk affald. Prækliniske studier beskriver, hvordan denne søvnafhængige tilstrømning af CSF, også kendt som det "glymfatiske system," faciliteres af vandkanalen aquaporin-4 (AQP4) og drives af cerebrovaskulære oscillationer samt trykbølger genereret af åndedræt og kardiovaskulære pulsationer. Selvom der er en stigende mængde evidens fra mennesker, der understøtter søvns rolle i hjernens væskestrøm og affaldsfjernelse, er mekanismerne, hvormed søvn regulerer denne strøm, stadig stort set ukendte.

Formålet med denne afhandling var at forbedre vores forståelse af samspillet mellem homeostatisk søvnmekanismer og hjernens væskedynamikker hos mennesker. I studie I undersøgte vi først, om funktionen af AQP4-vandkanalen modulerer søvn-vågenregulering ved at se på natlige søvnoptagelser og reaktioner på søvnmangel hos individer der var genotypet for en gængs AQP4-haplotype. I de efterfølgende to studier anvendte vi den ultrahurtige hjerneskaningsteknik, Magnetic Resonance Encephalografi (MREG), til at måle fysiologiske hjerneoscillationer, som menes at afspejle hjernens væskebevægelser. Studie II er et deskriptivt forsøg, der validerer den fysiologiske oprindelse af MREG-detekterede hjerneoscillationer gennem pausering af vejrtrækning og ved Valsalva-manøvren, hvoraf sidstnævnte påvirker cerebrovaskulære oscillationer og hjerteaktivitet). Studie III undersøgte, hvordan søvnmangel, dyb søvn med høj andel af slow waves og farmakologisk modulation af cerebrovaskulær pulsilitet påvirker styrken af fysiologiske hjerneoscillationer i et cirkadisk kontrolleret studie-setup, der inkluderer en randomiseret, dobbeltblind, placebo-kontrolleret crossover administration af den  $\alpha$ 1- og  $\beta$ -adrenerge antagonist carvedilol. Endelig udvidede vi i studie IV vores undersøgelser af cerebrovaskulære oscillationer ved at undersøge deres forhold til blodets noradrenalin niveau, ved hjælp af Multiband Echo Planar Imaging (MB). Denne metode har højere rumlig opløsning, men langsommere billedoptagelse end MREG (4,6 billeder per sekund mod 10) og blev indsamlet skiftevis med MREG som en del af studie III.

**Studie I** viste, at bærere af en lav-AQP4-udtrykkende variant af en AQP4-haplotype udviste øget slow-wave-aktivitet under natlig søvn og oplevede øget global årvågenhed og mindre søvnighed under søvndeprivation.

**Studie II** demonstrerede en kausal sammenhæng mellem både MREG-detekterede lav-frekvens oscillationer (LFO'e) og cerebral vasomotion samt mellem MREG-detekterede hjernepulsationer i åndedræts- og hjertefrekvensområder og deres tilsvarende underliggende fysiologiske processer.

**Studie III** viste, at øget søvnpres fremmer LFO'er, mens søvn med høj andel af slow waves (N2- og N3-stadier) forstærker åndedræts- og hjerteslags-drevne hjernepulsationer i grå og hvid substans i hjernen, hvor deres styrke korrelerer med søvnens

dybde og EEG-delta-kraft. Indgift af carvedilol dæmpede også LFO'er, hvilket understøtter, at disse afspejler cerebrovaskulære oscillationer.

**Studie IV** viste, at LFO'er moduleres af noradrenalin i både veludhvilet vågenhed og søvn og bekræftede yderligere de observerede effekter af øget søvnpres på LFO'er og slow-wave-rig søvn på åndedrætsdrevne hjernepulsationer.

**Overordnet** præsenterer dette arbejde den første menneskelige evidens, der forbinder hjernens væskedynamikker med søvnens slow waves, øget søvnpres og noradrenalin. Det adskiller også effekten af søvnmangel og autonom aktivering fra effekten af søvn og viser, at søvn muligvis ikke er den eneste drivkraft for glymfatiske CSF strømme, da cerebrovaskulære oscillationer reguleres af både øget søvnbehov og noradrenalin-niveauer.

## Abbreviations

---

APOE	Apolipoprotein E
AQP4	Aquaporin-4
BOLD	Blood-Oxygen-Level-Dependent
CEU	Utah Residents from North and West Europe (population in DbSNP database)
CSF	Cerebrospinal fluid
dB	Decibel
DNA	Deoxyribonucleic Acid
ECG	Electrocardiogram
EDTA	Ethylenediaminetetraacetic acid – used in blood collection tubes
EEG	Electroencephalography
EMG	Electromyogram
EOG	Electrooculogram
ESS	Epworth Sleepiness Scale
GM	Grey matter
H	Hours
Hom	Homozygote
HtMa	Haplotype Major: Homozygote for the major AQP4 haplotypes
HtMi	Haplotype Minor: Carrier of the minor AQP4 haplotype
Hz	Hertz
ICP	Intracranial pressure
IRR	Infinite Impulse Response - filter
ISF	Interstitial fluid
kHz	Kilo Hertz
k $\Omega$	Kilo Ohms
LD	Linkage disequilibrium
LFO	Low frequency brain oscillations
Log	Logarithm
MAF	Minor allele frequency
MB	Multiband echoplanar imaging
MEQ	Morningness-Eveningness Questionnaire
Mg	Milligram
Min	Minute
mm	Millimetre
mL	Millilitre
MR	Magnetic Resonance
MREG	Magnetic Resonance Encephalography
MRI	Magnetic Resonance Imaging
NE	Norepinephrine
NREM	Non rapid-eye-movement
p-NE	Plasma norepinephrine
PSG	Polysomnography

PSQI	Pittsburgh Sleep Quality Index
PVT	Psychomotor vigilance test
REM	Rapid-eye-movement
ROI	Region of interest
RS	Reaction speed
RT	Reaction time
Sec	Second
SEM	Standard error of the mean
SNP	Single nucleotide polymorphism
SSS	Stanford Sleepiness Scale
SWA	Slow wave activity
SWE	Slow wave energy
TIB	Time in bed
TSI	Toscany in Italy (population in DbSNP database)
WM	White matter

# Background

---

## 1. Sleep

Sleep is a naturally occurring state of altered consciousness, characterised by reduced responsiveness to sensory stimuli and diminished voluntary control over muscle activity. Unlike unconscious states such as coma, sleep is easily reversible and exhibits specific patterns of synchronized brain activity<sup>2</sup>. It is a near universal phenomenon in living organisms and likely evolved as early as 500 million years ago<sup>3</sup>. Sleep, or sleep-like behaviour, is present in most complex species alive today, in everything from jellyfish and bees to sharks and birds, indicating its importance for essential biological processes.

Sleep is important for maintaining physical health and cognitive performance, and is linked to memory consolidation, brain plasticity and synaptic downscaling<sup>4</sup>. Similarly, acute sleep deprivation impairs short term memory<sup>5</sup>, reduces vigilance and attention<sup>6</sup>, and, when prolonged, can lead to psychosis, anxiety, and disorientation.

However, despite the ubiquity and critical functions of sleep, the precise biological mechanisms behind sleep's restorative effects have long been a mystery to science.

The pioneering sleep researcher Dr. Allan Rechtschaffen eloquently described this paradox in 1971, saying

***“If sleep does not serve an absolutely vital function, then it is the biggest mistake the evolutionary process ever made”***

But now, in the last decade, a new theory has emerged that could possibly explain the purpose of sleep; namely, that sleep facilitates the clearance of waste products from the brain that accumulate during wakefulness.

### 1.1 A night of sleep

Every night, the human brain cycles through several stages of sleep, moving from lighter to deeper sleep and back again. This cycle occurs 4–6 times per night, with each cycle lasting about 90 minutes<sup>7</sup>.

Based on electroencephalography (EEG) recordings, which measure electrical activity in the brain via electrodes placed on the scalp, these sleep stages can be distinguished from one another<sup>8</sup>.

During non-rapid eye movement (NREM) sleep, the body is at rest, and brain activity is synchronized, displaying low-frequency, high-voltage EEG patterns. NREM stage 1 (N1) is a transitional stage between wakefulness and sleep, that represents the lightest form of sleep and is characterized by 4-7 Hz EEG activity. NREM stage 2 (N2) is an intermediate stage of sleep, marked by the appearance of K-complexes (<2 Hz) and sleep spindles (11–16 Hz) in the EEG. NREM stage 3 (N3) is referred to as deep sleep and is characterized by an abundance of slow, high-amplitude waves in the EEG frequency range ~1–4.5 Hz. These waves, also known as EEG slow waves or delta waves, are used as a measure of sleep depth<sup>9</sup>. Finally, rapid eye movement (REM) sleep is distinguished by EEG patterns resembling those of N1 sleep but is accompanied by muscle atonia and eye movements beneath closed eyelids.

About 80% of the night is spent in NREM sleep, while the remaining 20% is in REM sleep. Slow-wave sleep dominates the first third of the night, whereas the final third is characterized by lighter sleep and the longest REM episodes ( **Figure 1**).

Sleep architecture, as visualised by sleep-EEG, is partly genetically determined and highly consistent across nights within the same person. The heritability of NREM sleep EEG is as high as 90%, with the largest degree of variance in rhythms outside of the EEG delta power band<sup>10</sup>.

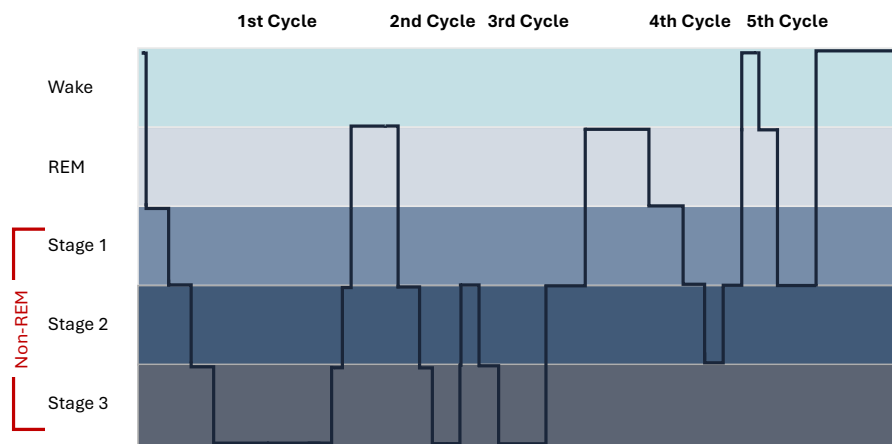


**Figure 1** - Example of sleep cycles in humans

*Illustration created by SM Ulv Larsen*

## 1.2 Homeostatic sleep mechanisms

Sleep is under homeostatic regulation. Simply put, the longer one stays awake, the greater the need for sleep and the deeper the subsequent sleep.

This concept of ‘sleep homeostasis’ was first described by Borbély in the 1980s. It details how sleep pressure steadily rises with time awake and dissipates during sleep, maintaining the balance between wakefulness and sleep<sup>11</sup>.

Slow-wave activity (SWA), as measured by EEG during NREM sleep, is a robust marker of homeostatic sleep regulation<sup>12</sup>. SWA accumulates in direct relation to the duration of prior wakefulness and decreases progressively during sleep, alongside the decline in sleep pressure<sup>13</sup>. Similarly, daytime naps reduce SWA during the following night<sup>14</sup>, while sleep deprivation leads to increased SWA at sleep onset<sup>15</sup>.

This compensatory response of the brain indicates an important and restorative function of slow waves. Supporting this, studies have shown that cortical areas more active during wakefulness – for example, while learning a new skill - generate higher SWA during the night than less active areas<sup>16,17</sup>.

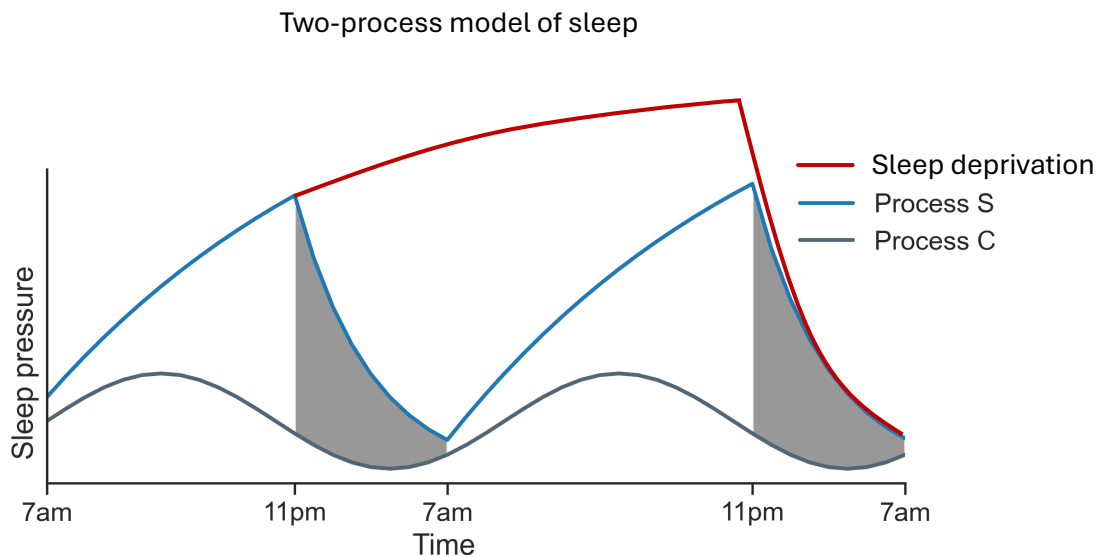


**Figure 2** - The two-process model of sleep

*Illustration created by SM Ulv Larsen*

Lastly, as outlined by the two-process model of sleep regulation, the circadian rhythm works alongside homeostatic sleep mechanisms in regulating sleep<sup>18</sup> (**Figure 2**). Governed by the brain's suprachiasmatic nucleus, the circadian rhythm aligns sleep and bodily functions with the 24-hour light-dark cycle, promoting wakefulness during daylight and sleep initiation during darkness. Therefore, any research investigating one of these processes must also consider the other\*.

Overall, homeostatic sleep mechanisms are essential for maintaining sleep quality and balance

## 2. Brain fluid dynamics

### 2.1 The three fluid compartments

The brain's fluid dynamics are critical for maintaining neural function and overall brain health<sup>19</sup>. Three primary fluid compartments—cerebrospinal fluid (CSF), interstitial fluid (ISF), and blood—exist within the skull and are balanced by complex regulatory mechanisms.

CSF, which is produced by the choroid plexus, circulates through the ventricles, subarachnoid space, and perivascular spaces, entering the brain parenchyma via passive diffusion and through the aquaporin-4 (AQP4) water channel<sup>20,21</sup>. This clear, colourless fluid performs several essential functions: it provides nutrients, removes metabolic waste, aids in immune defence, and cushions the brain and spinal cord. The average adult produces 500 mL of CSF daily, although only 150 mL is present at any given time, highlighting its constant turnover<sup>22</sup>.

Interstitial fluid occupies the extracellular space between neural cells and facilitates the exchange of nutrients, ions, and metabolic products at the cellular level. Its movement is driven by hydrostatic and osmotic pressure gradients, as well as mechanical forces like respiration, the heartbeat and blood vessel motion<sup>21,23</sup>.

---

\* We did so in the studies presented in this thesis. Therefore, I will leave it to another Ph.D. student, at another time, to elaborate further on this otherwise very interesting second regulator of sleep

The blood vessels supply oxygen and nutrients to the brain. Cerebral blood flow is tightly regulated to maintain consistent perfusion, even with changes in systemic blood pressure<sup>24</sup>. Additionally, neurovascular coupling dynamically directs blood flow to brain regions with heightened neuronal activity, ensuring their increased oxygen and metabolic demands are met<sup>25</sup>. The blood-brain barrier, formed by specialised endothelial cells, regulates substance exchange between blood and brain tissue<sup>26</sup>.

All these mechanisms rely on relatively constant intracranial pressure (ICP). To maintain this, and because the cranial vault cannot expand, any changes in the pressure or volume of one component, will affect the others directly in the opposite direction<sup>27</sup>.

## 2.2 The glymphatic system

Despite its high metabolic activity and a large daily turnover of proteins, the brain lacks a conventional lymphatic system to clear away waste products. In the body, blood and lymphatic vessels run together and blood capillaries provide a constant influx of a plasma ultrafiltrate to peripheral tissue, where permeable lymphatic capillaries then collect the metabolic waste and return it to the general circulation. Contrary to this, the blood-brain barrier in the brain restricts fluid and solute exchange across vessel walls and there are no lymphatic vessels in the brain tissue. Consequently, the brain depends on alternative routes for clearance<sup>28</sup>.

The recently discovered fluid network in the rodent brain, termed ‘the glymphatic system’ (so named for its dependence on glial cells), has been proposed as one such an alternative<sup>29</sup>.

The glymphatic model describes how, during sleep<sup>30</sup>, CSF flows from subarachnoid spaces into the perivascular spaces, which are low-resistant fluid pathways created by astrocytic endfeet ensheathing the brain vasculature<sup>31</sup>. From here, CSF enters the brain parenchyma through AQP4 water channels which permeate the astrocytic endfeet<sup>32</sup>, creating a net-inward flow of CSF through the brain, which causes both an exchange of CSF and ISF and a clearance of metabolic waste products<sup>29</sup>. This directional fluid flow is driven both by cerebrovascular oscillations and pressure waves generated by respiration and heartbeat<sup>21</sup>. Importantly, the magnitude of this flow is directly correlated with sleep slow waves and EEG delta power<sup>33,34</sup>. **Figure 3** illustrates the different components and routes described above.

Since glymphatic dysfunction is linked to tau and amyloid- $\beta$  accumulation<sup>35,36</sup>, which are implicated in the development of neurodegenerative diseases such as Alzheimer’s<sup>37</sup>,

advancing our understanding of this system holds potential not only for clarifying sleep's restorative role, but also for future treatment and prevention strategies of these conditions.

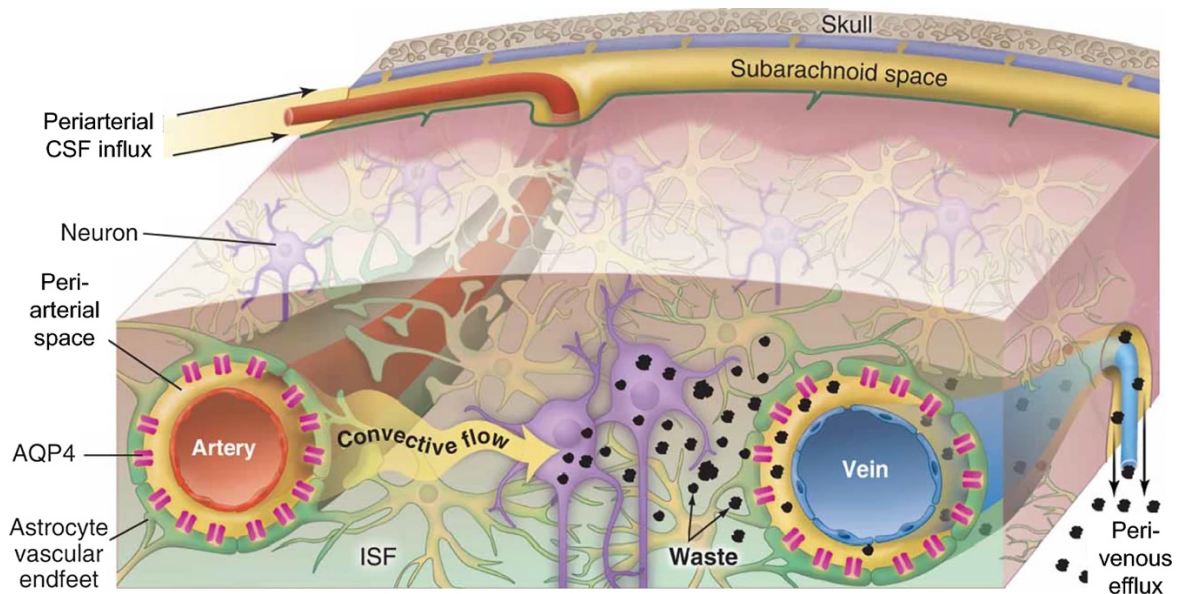


**Figure 3** - Model of glymphatic flow

Illustration from Ray et al. *Fluids and barriers of the CNS* vol 18,1 55. 2021. doi: <https://doi.org/10.1186/s12987-021-00290-z>. © CC-BY-4.0 licence (<https://creativecommons.org/licenses/by/4.0>)

### 2.3 Physiological drivers of brain fluid flow in rodents

The act of breathing and the beating of the heart both generate pressure waves that propagate through the brain and physically propel CSF along the perivascular spaces<sup>38,39</sup>.

The respiration is thought to drive brain fluid motion through its effect on intrathoracic pressure with each in- and expiration. This in turn causes cyclic changes in central venous pressure and, consequently – per the Monro-Kellie Doctrine – also in the ICP<sup>40,41</sup>.

The cardiac cycle induces pulsatile movements in the vasculature that ‘pump’ CSF through perivascular spaces<sup>39</sup>. Additionally, the dense network of arteries and arterioles in the brain suggests that cardiac-induced vascular pulsations also impact surrounding tissue<sup>21</sup>.

Cerebrovascular oscillations – also referred to as vasomotion – refer to the slow rhythmic constriction-dilation dynamics of the brain’s vasculature. These oscillations are integral to autoregulation, a physiological mechanism that ensures consistent cerebral blood flow

despite fluctuations in systemic blood pressure<sup>24</sup>. They stem from tonus changes of the vascular smooth muscle cells in the walls of vessels and have been shown to also drive CSF-flow along the periarterial spaces and into the brain parenchyma<sup>42,43</sup>.

Interestingly, recent evidence suggests that cerebrovascular oscillations in themselves take part in the sleep-wake regulation of fluid flow, as they show distinct constriction-dilation patterns across the sleep cycle<sup>44</sup>.

Studies with adrenergic agonists that increase heart rate and cardiac output have demonstrated enhanced CSF flow in perivascular spaces and improved CSF-ISF exchange, reinforcing the role of these physiological drivers in modulating CSF flow<sup>45,46</sup>.

## 2.4 Sleep-dependent brain fluid flow and clearance in humans

Although most extensively studied in rodents, emerging evidence support the existence of a sleep-dependent fluid flow and brain clearance mechanism in humans<sup>21</sup>.

Studies using intrathecal contrast agents and Magnetic Resonance Imaging (MRI) have recently shown a directional fluid flow in perivascular spaces of the human brain<sup>47</sup>, alike the one seen in rodents. Same method was used to demonstrate that acute and chronic sleep deprivation slow the clearance of these agents from the brain<sup>48,49</sup>, thus strongly indicating an important role of sleep in brain waste removal. Aligning with this, one night of sleep deprivation causes a significant increase in the amount of tau and amyloid- $\beta$  in CSF and brain parenchyma<sup>50-52</sup>, while Individuals suffering from Alzheimer's disease, known to have high amounts of CSF tau, have been shown to have disturbed sleep<sup>53</sup>.

Although these findings elegantly link sleep and sleep deprivation to the build-up and clearance of waste, they do not inform on what happens *during* sleep or how sleep pressure and slow-wave sleep might influence brain fluid dynamics.

To measure brain fluid flow during deep sleep – and preferentially during changing sleep stages or throughout the night –, requires non-invasive approaches that allow participants to sleep naturally while being continually measured.

Below, I outline two approaches – one indirect and one direct – that have gained increasing interest over the last decade.

## 3. AQP4

### 3.1 AQP4 water channel

As mentioned, the water channel AQP4 facilitates the flow of CSF from perivascular spaces into the brain parenchyma<sup>32</sup>. It is primarily located on the endfeet of the astrocytes that wrap around blood vessels, creating the perivascular spaces. AQP4 is selectively permeable to water and allows for a passive and bidirectional fluid flow. It is one of the most abundant molecules in the brain<sup>54</sup> and its inactivation in mice has been shown to reduce influx of CSF to the brain parenchyma<sup>32,55</sup> and increase amyloid- $\beta$  deposition<sup>56</sup>, underscoring its role in glymphatic flow and clearance.

### 3.2 Genetic variants of the AQP4 gene

The genetic variants within the AQP4 gene – the so-called single nucleotide polymorphisms (SNPs) – offer a possibility for investigating water channel function non-invasively in humans. An SNP is a variation in a single nucleotide in the DNA sequence at a specific position in the genome. If this variation exists in more than 5% of the population, it is classified as a common SNP. When two or more SNPs are frequently inherited together on the same chromosome, they can form a haplotype.

While most SNPs have no (known) impact, some can convey changes in the expression of their encoded proteins, e.g. water channel function, expression, localisation etc. Because of this rarity of known function, simply comparing ‘random’ SNPs between populations can at best establish associative links and, at worst, lead to false conclusions. Therefore, to ensure biologically meaningful comparison when assessing the effects of harbouring specific SNPs, it is preferable that these SNPs are pre-validated – either through *vitro* or *in vivo* studies, or large genetic association studies – as functional variants themselves or as part of a haplotype containing a functional SNP.

### 3.3 AQP4 SNPs in humans

Preclinical studies have identified some naturally occurring human AQP4 SNPs that impair water permeability and homeostasis of cells *in-vitro*<sup>57</sup>, as well as a single variant associated with a 15-20% change in AQP4 expression<sup>58</sup>, providing some potential targets for analysis. Moreover, a series of human studies have associated SNPs with speed of cognitive decline

in Alzheimer's disease<sup>59</sup>, leukoaraiosis<sup>60</sup> and oedema formation after traumatic brain injury and stroke<sup>61,62</sup>, suggesting a link between AQP4 water channel function and the development of neurological diseases associated with dysfunction of brain-fluid and clearance mechanisms.

Only recently however, has the link between AQP4 and sleep-wake mechanisms been explored by our group and others.

## 4. Imaging physiological brain oscillation

### 4.1 MREG and MB

Advances in accelerated imaging techniques have made it possible to study physiological brain oscillations in humans dynamically and non-invasively.

With high temporal resolutions, these novel MRI methods allow for detailed investigations of low frequency oscillations (LFOs) – believed to reflect cerebrovascular oscillations<sup>63</sup> - as well as brain pulsations driven by respiratory and cardiac cycles.

Currently, the two methods used for this are Magnetic Resonance Encephalography (MREG)<sup>64</sup> and Multiband echo planar imaging (MB)<sup>65</sup>. Both are functional T2\* weighted imaging methods that achieve high acquisition rates through different undersampling techniques\*. As such, in addition to detecting brain fluid dynamics originating from blood oxygenation (Blood-Oxygen-Level-Dependent, or BOLD signal), they can also measure dynamics arising from CSF spaces and interstitial fluid changes<sup>66</sup>.

MREG acquires 10 full three-dimensional images of the brain per second, making it well-suited for capturing all three types of physiological brain oscillations<sup>64</sup>. It has been proposed

---

\* A full dissertation could (also) be written comparing MREG and MB methods, including their undersampling techniques, signal-to-noise ratios, and sensitivities to neural activation and the default mode network. However, this is not the focus of this work. Instead, I build on the contributions of other brilliant researchers who established these methods as tools for assessing brain-fluid dynamics through their visualisation of cerebrovascular oscillations and respiration- and cardiac-driven pulsations.

Here, I focus on the biological interpretations and correlates between the signals, while I fully acknowledge that many other factors could influence the signals.

as a measure of glymphatic flow in the human brain<sup>67</sup>, with its signal reflecting either fluid motion propelled along by the physiological drivers and/or brain tissue distortions caused by pressure waves travel through the brain, which in turn are affected by factors such as brain elasticity and water content<sup>68,69</sup>.

The MB sequence offers superior spatial resolution and sampling rates between 0.33 – 4.6 Hz, possibly making it ideal for detecting LFOs, though less effective for capturing cardiac-driven brain pulsations. To date, MB has primarily been used to detect LFOs across the cortex and the coupled influx of CSF in the fourth ventricle<sup>70–73</sup>.

## 4.2 Physiological brain oscillations and sleep-wake regulation

Previous accelerated imaging studies have shown that LFOs increase in power during lighter sleep stages (N1 and N2)<sup>66,71</sup>, with some evidence suggesting this increase appears even earlier, during drowsiness in wakefulness<sup>72</sup>. Moreover, it has been shown that LFOs are strongest in lighter relative to deeper sleep, and that autonomic arousal may also play a role in their regulation<sup>70</sup>. This raises the question whether cerebrovascular oscillations are, in fact, coupled to sleep slow waves as previously suggested<sup>71</sup> - or if these oscillations regulate brain fluid independently of sleep?

Conversely, studies of respiration- and cardiac-driven brain pulsations have shown that their strength increase during lighter NREM sleep stages, with N2 sleep having more widespread effects on the brain than N1<sup>66,74</sup>. This aligns with the hypothesis that sleep enhances CSF influx and expands the extracellular space<sup>30</sup>. Notably, only MREG has been used to measure this.

Altogether, these findings suggest that brain-fluid dynamics in humans are regulated by sleep-wake mechanisms. However, no one has yet disentangled the effects of sleep pressure from those of sleep itself or controlled for circadian rhythm. Furthermore, the relationship between EEG slow waves and brain pulsations strength, as well as the effect of slow-wave-rich N3 sleep on cardiorespiratory brain pulsation, remains unexplored.

## 4.3 From whole-brain images to MREG- and MB spectra

**Figure 4** illustrates how the MREG (and, in our case, also MB) signal is converted from three-dimensional full-brain images into power spectra. Various approaches can be used to analyse both the images and the resulting spectra. However, consistent with prior research<sup>66,74</sup>, we evaluate the sum of spectral power within physiological frequency bands as measures of LFO, respiration- and cardiac-driven brain pulsation. A detailed description of the analysis pipeline can be found in Study III & IVs.

In the studies presented here, we focused on the 0.012-0.034 Hz frequency band when investigating LFOs. While previous studies have used the 0.01-0.1 Hz band<sup>70,71,74</sup>, we chose the narrower band as it has a physical correlate in clinical settings; namely the invasively measured ICP B-waves<sup>75</sup>. B-waves are known to increase with elevated ICP and have been shown to reflect cerebrovascular oscillations<sup>76</sup>, which aligns directly with our investigative goals. Interestingly, ICP B-waves are also influenced by sleep<sup>77,78</sup>, hinting at their relevance for our study.

For respiration- and cardiac-driven brain pulsations, we restricted our analyses to frequencies in the MREG/MB spectra centred around the concurrently measures respiration and heart rates. This was done to ensure that we were specifically measuring brain oscillations induced by respiratory and cardiac cycles.

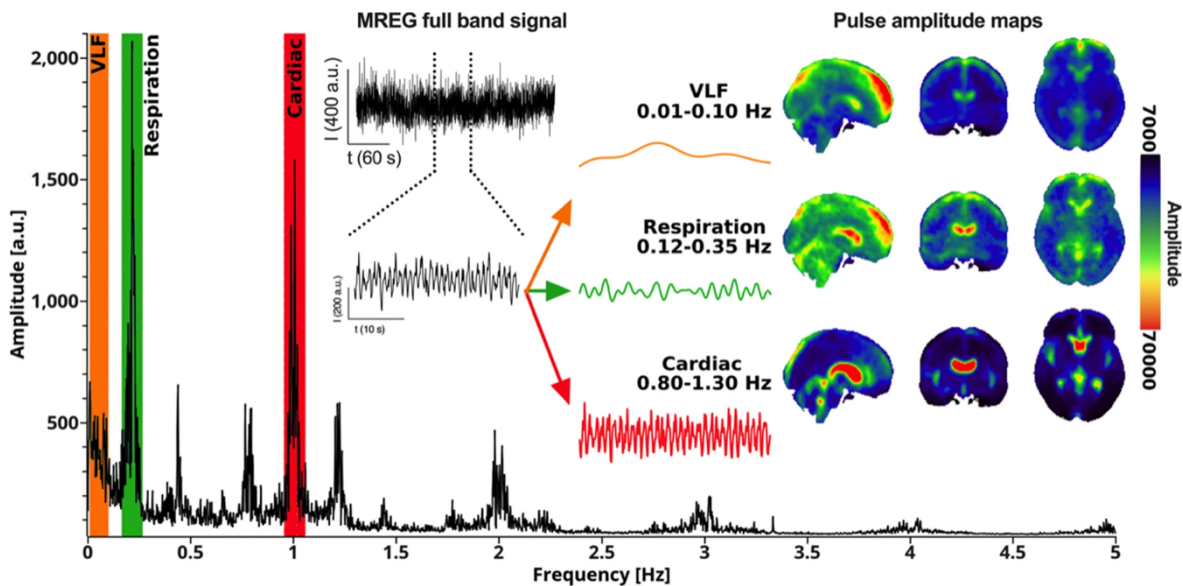


**Figure 4** - Illustration of MREG timeseries with its distinct pulsations in low frequency, respiratory and cardiac frequency ranges – as well as its related power spectrum.

Image from Hennig J et al. *MAGMA* vol 34,1: 85-108. 2021. doi: <https://doi.org/10.1007/s10334-020-00891-z>.  
 © CC-BY-4.0 licence (<https://creativecommons.org/licenses/by/4.0>)

#### 4.4 Use of data in previously submitted Master's thesis

Results from study I presented in sections 11.1 and 11.2. were included in preliminary forms in the author's Master's thesis, submitted in August of 2018. Analyses were subsequently expanded and the initial findings elaborated upon, prior publication PLoS Biology in 2020. The resulting paper is included as Study I in this thesis.

# Aims & Hypotheses

---

## 5. Aim of PhD

The overall aim of this thesis was to improve our understanding of the interplay between homeostatic sleep mechanisms and brain-fluid dynamics in humans.

### 5.1 Study I

In this genotyping study, we aimed to investigate the role of AQP4 in sleep-wake regulation. We did this through investigation of a common 8-SNP AQP4 haplotype. We hypothesized that if NREM slow waves regulate CSF fluid flow, then a reduced AQP4 expression might lead to a compensatory increase in slow-wave-rich NREM sleep.

### 5.2 Study II

In this descriptive study, we aimed to validate the physiological origin of MREG-detected physiological brain oscillations.

We hypothesized that:

- ♦ LFOs, if reflecting cerebrovascular oscillations, increase with the dynamic rise in ICP by the Valsalva Manoeuvre
- ♦ Respiration-related brain pulsations disappear during breath-holding
- ♦ Cardiac-related brain pulsations decrease in strength with the Valsalva Manoeuvre due to reduced cardiac output and blood pressure

### 5.3 Study III

In this study, we aimed to examine the distinct effects of sleep pressure, slow-wave-rich NREM sleep, sleep depth and EEG delta power on the strength of physiological brain oscillations, as detected with MREG. We hypothesized that

- ♦ Sleep deprivation is associated with a homeostatic drive towards enhanced physiological brain oscillations in wakefulness,

- ♦ NREM sleep further enhances these oscillations
- ♦ Physiological brain oscillation strength is proportional to sleep depth and EEG delta power

We further aimed to assess if systemic treatment with the  $\alpha$ 1- and  $\beta$ -adrenergic antagonist carvedilol would modulate these brain oscillations.

#### 5.4 Study IV

In this study, we aimed to investigate cerebrovascular oscillations across vigilance states at higher spatial resolution using the MB sequence, examining the effects of sleep deprivation and plasma norepinephrine levels.

Additionally, we aimed to investigate respiration- and cardiac-driven brain pulsations with MB to validate our findings in study III and compare the outcomes between MB and MREG.

## Methods

---

### 6. Ethics, approvals, and registrations

Study I consisted of data from prior studies conducted at the Institute of Pharmacology and Toxicology in Zurich, Switzerland. Study protocols were approved by the health ethics committee of the Canton of Zurich for research on human participants (Cantonal Ethics Committee reference numbers: E-39/2006, 2012–0398, E-24/2007, EK-Nr. 786, 2015–0424). As was previously required in Zürich, the oldest study<sup>79</sup> was approved by a local ethics committee for research on human participants.

Studies II and III/IV were conducted at Rigshospitalet, Copenhagen, Denmark. Approvals were granted by the Danish Ethics Committee of the Capital Region of Denmark (Study II ID: H-18048865, Study III/IV ID: H-16045933).

All studies were conducted in accordance with the Declaration of Helsinki and written and informed consent was obtained from all participants before the experiments.

### 7. Study I

This study investigates the association between common variants in the AQP4 gene and sleep-wake regulation in humans, using retrospectively genotyped blood samples from healthy participants from six previous sleep and sleep deprivation studies<sup>79–84</sup>.

#### 7.1 dbSNP

To determine common variants in the AQP4 gene, the dbSNP database (build 152) of the 1000 genome project was accessed<sup>85</sup>. Specifically, the European population data (TSI and CEU) was chosen to best represent the Swiss cohort. An initial search found 16 SNPs with a minor allele frequency above 20% in the chosen population. Subsequent linkage disequilibrium (LD) analysis found that eight of these (specifically rs162007, rs162008, rs63514, rs455671, rs335931, rs335930, rs335929, and rs16942851) constitute a distinct eight-SNP haplotype block ( $r^2 > 0,8$ ) consisting of a major haplotype (HtMA, incidence 76,7%) and a minor haplotype (HtMi, incidence 19,7%) – as illustrated in **Figure 5B**.

## 7.2 Genotyping

Genotyping was performed using genomic DNA extracted from 3mL fresh EDTA blood (wizard<sup>R</sup> Genomic DNA purification Kit, Promega, Madison, WI). Haplotyping was determined using the rs335931, rs335929, and rs16942851 (highlighted in **Figure 5A**) polymorphisms as representative tag SNPs and were analysed using Taqman1SNP Genotyping Assay (Life Technologies Europe B.V). All genotypes were replicated at least once for confirmation and allelic discrimination analysis was performed using statistical software SDS version 2.2.2 (applied Biosystems, Foster City, CA). As previous studies have shown a consistent association between specific apolipoprotein (APOE) genotypes and the risk of Alzheimer’s disease<sup>86</sup>, we performed additional analysis of the rs429358 and rs7412 APOE genotypes in our study population, using the same SNP genotyping procedure.

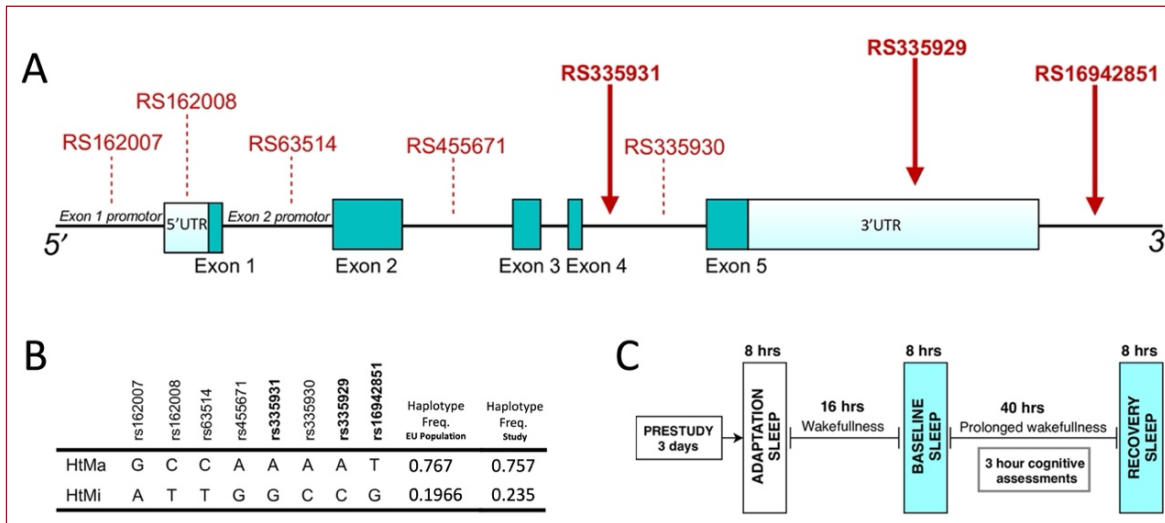


**Figure 5** – AQP4 gene, structure (A), haplotype (B) and study design across Zürich sleep studies (C)

Figure adapted from Ulv Ulv Larsen, et al., PLoS Biol. Vol 18,5 e3000623. 2020. doi: <https://doi.org/10.1371/journal.pbio.3000623>. © CC-BY-4.0 licence (<https://creativecommons.org/licenses/by/4.0>)

## 7.3 Population

The study cohort consisted of 134 healthy male participants from one of six previously conducted sleep deprivation studies. Participants were right-handed with no history of neurological or psychiatric disorders, no alcohol, substance or excessive caffeine use, and had not crossed any time zones for two months prior to participation. All reported being good sleepers with regular sleep schedules and no night- or shiftwork. Before inclusion in any of the studies, all participants were screened for undiagnosed sleep disorders and/or low

sleep efficiency in a laboratory setting. Nine of these participants were excluded for being over 60 years old.

71 participants were homozygous for the major allele (HtMa/HtMa), 7 were homozygous for the minor allele (HtMi/HtMi) and 45 were heterozygous (HtMa/HtMi). Two participants were carriers of a rare haplotypes and were excluded. This left a total of 123 participants for analysis. For the studies that included an intervention with one or more treatments, only the placebo arm was included for analysis.

#### 7.4 Study design across Zürich sleep studies

All six sleep studies had similar methodologies and lab setups, illustrated in **Figure 5C**. Participants were required to adhere to a strict 8/16-hour sleep schedule throughout the studies and refrained from any intake of caffeine or alcohol. Actigraphy, sleep-wake diaries, and saliva-caffeine and alcohol breath analysis were used to ensure compliance. After a three-day pre-study period, participants spent four consecutive days and nights in the sleep lab setting: An adaptation and a baseline night, followed by a 40-hour sleep deprivation period leading up to bedtime on the fourth day, after which a 10-hour recovery window was scheduled. Wakefulness during the sleep deprivation period was ensured by constant supervision and engagement by the research team.

#### 7.5 Polysomnography

Polysomnographic (PSG) recordings consisting of EEG, electrooculogram (EOG), submental myogram (EMG) and electrocardiogram (ECG) were recorded during both baseline nights and the recovery night using either PSA24 amplifiers (Braintronics Inc., Almere, the Netherlands;  $n = 16^{79}$ ) or Artisan systems (Micromed, Mogliano Veneto, Italy;  $n = 107^{80-84}$ ).

For PSA24 recordings, the analogue EEG signals were first high-pass (3 dB, 0.16 Hz) and low-pass (3 dB, 102 Hz) filtered, then sampled at 512 Hz and digitally low-pass filtered (3 dB, 49Hz). Finally, they were stored with a resolution of 128 Hz. The recordings from the Artisan's analogue EEG data were conditioned with a high-pass filter (3 dB, 0.15) a low-pass filter (3 dB, 67.2 Hz), and sampled with a frequency of 256 Hz.

Sleep stages were visually scored in 20-second epochs according to established standard criteria<sup>8</sup> by a single sleep expert, and arousal- and movement-related artefacts were visually identified and removed. Analysis was restricted to the first eight hours (480 minutes, 1440 epochs) after lights-off for both the baseline nights and the recovery period.

## 7.6 EEG analysis

For all six studies, four-second EEG spectra were derived using a fast Fourier transformation in Hanning Window, with a resolution of 0,25Hz in MATLAB (MathWorks Inc., Natick, MA). Averages of five consecutive four-second epochs were then matched to the scored sleep stages. The average of all artefact-free 20-second epochs with scored NREM sleep (stages 1-4, 0-20Hz) were then collated into an all-night spectrum.

Energy spectra were computed by multiplying all power values in the spectrum by amount of time in minutes spent in NREM sleep per night (or in the respective NREM sleep cycles, for separate analysis of those)<sup>87</sup>.

## 7.7 Psychomotor performance

All six studies included a Psychomotor Vigilance Test (PVT, Psychology SoftwareTools Inc., Pittsburgh, PA)<sup>88</sup>. While seated in front of a computer, participants were instructed to press the spacebar as quickly as possible after they saw a digital millisecond counter on the screen. Of the 123 included participants, 104 completed a digital PVT, while 19 were tested using a different analogue version and were excluded from analysis. All participants were given verbal instructions and allowed a practice sessions prior to testing. For each PVT trial, 100 stimuli were presented. The PVT was administered every three hours during the 40-hour sleep deprivation period. Variables recorded were median reaction time and lapses of attention (percentage of trials with reaction times >500ms)<sup>89</sup>. Prior to analysis, reaction times were converted to response speed = 1/reaction time.

## 7.8 Subjective sleepiness

Subjective feelings of sleepiness were assessed using the Stanford Sleepiness Scale (SSS)<sup>90</sup>. A validated German language version was administered every three hours, immediately prior to PVT sessions<sup>91</sup>. All 123 participants completed the SSS.

## 8. Study II

This study was a descriptive study, designed to assess the effects of breath-holding and the Valsalva manoeuvre on physiological brain oscillations detected with MREG

### 8.1 Population

Four healthy participants, two males and two females, aged between 31-40 were included. None had a history of major medical, neurological, or psychiatric conditions and none were on psychoactive medications.

### 8.2 Scan sessions

A single MRI-scan session was conducted between 4 and 6 pm local time. Participants repeated the following three manoeuvres (1 minute break in between each) while the MREG sequence ran continuously: 30 sec rest, 30 sec breath-hold and 30 sec Valsalva manoeuvre. This sequence of events was repeated for a total of three rounds. Participants had been instructed in and practiced the manoeuvres before entering the scanner with specific attention given to ensuring the participants not inhale before the breath-hold, to avoid performing a de facto low-pressure Valsalva manoeuvre.

Timings and instructions were displayed on screen in the scanner. Wakefulness was ensured by having the lights on and encouraging the participant to keep their eyes open. A running video feed of the participants eyes was provided to the MR-technician to monitor wakefulness.

Scanner model, setup, parameters, and data reconstruction methods were identical to those described in detail below for Studies III and IV.

### 8.3 Processing and evaluation of MREG data

MREG scans were divided into 25-30 second epochs equivalent to the three parts of the cycle, i.e. rest, breath-hold, and Valsalva. Data was high-pass filtered with a 10-order infinite impulse response (IIR) filter with a passband of 0.02 Hz. Frames with significant distortion from motion artefacts due to initiating or sustaining breath-hold or Valsalva were discarded. Subsequent analyses steps for the 30-second MREG epochs were performed as described in detail in Study III and IV.

Power peaks in the MREG spectra were visually assessed within physiological frequency ranges for respiration (0.14 – 0.5 Hz = 8.4 – 30 breaths per minute), heart rate (0.68 – 2 Hz = 41 – 120 beats per minute), and LFOs (< 0.1 Hz). However, interpretation of spectral power in LFO frequencies below 0.034 Hz had to be made with caution, due to the spectral resolution limit imposed by the 30-seconds window. Using the frequency wave equation  $\Delta f=1/T$  to determine the measurable frequency delta for our 30-second epochs gave a lower range of  $\Delta f=1/30=0.033\text{Hz}^{92}$ , whereas studies III and IV investigated LFO frequencies down to 0.012 Hz.

## 9. Study III & IV

Studies III and IV are based on data from a human sleep and sleep deprivation study. In this study, we applied accelerated neuroimaging techniques to examine cerebrovascular oscillations and respiration- and cardiac-driven brain pulsations across changing vigilance states and during pharmacological intervention with an adrenergic antagonist.

### 9.1 Population

Twenty healthy male participants aged between 18 and 29 years were included in and completed the study. Recruitment was done via local databases of individuals who had previously expressed an interest in participating in brain imaging studies, as well as the publicly available national test participant database ‘forsoegsperson.dk’. All were right-handed, spoke and read Danish, and had no history of high blood pressure, sleep disorder, neurological or psychiatric conditions, learning disabilities, or significant somatic illness. All were non-smokers with no concurrent use of relevant prescription drugs, or excessive alcohol or illicit substance use. None had performed shiftwork for three months prior to the study commencing. In the event that they had crossed two or more time-zones, a two-week recovery period per time-zone crossed was observed before enrolment. Before inclusion, participants underwent a polysomnographic screening in a controlled setting to ensure that no undiagnosed sleep disorders or low sleep efficiency was present. Additionally, the Morningness-eveningness (MEQ)<sup>93</sup>, Pittsburgh Sleep Quality Index (PSQI)<sup>94</sup>, and Epworth Sleepiness Scale (ESS)<sup>95</sup> questionnaires were administered as part of the screening to rule out anamnestic sleep disorders.

## 9.2 Study design

The full study design for this circadian-controlled sleep and sleep-deprivation study can be seen in **Figure 6**. The study was preregistered at ClinicalTrials.gov with identifier NCT03576664.

For 1 week prior to and throughout the entirety of the study period, participants were instructed to adhere to a strict 8/16-hour sleep/wake schedule (in-between sleep deprivation sessions). As in study I, compliance was monitored with actigraphy (Actiwatch spectrum, Philips Respironics) and a sleep diary. This was done to ensure that all measurements were performed at the same point of their circadian cycle and therefore at comparable sleep pressures. Caffeine intake was limited to  $\lesssim 200$  mg caffeine per day, ingested before 2 pm.

A total of three scan sessions of combined EEG/MRI were performed on separate days during the study period, between the hours of 6:30 pm and 8:30 pm. First, a well-rested scan after 11 hours of wakefulness, followed by two separate sleep deprivation scans following 35 hours of prolonged wakefulness, spaced 1 week apart. One hour before each of the sleep deprivation scans, participants were given either a carvedilol or placebo pill (see below).

For the three nights leading up to each of the sessions, as well as the two nights following sleep deprivation, participants slept in a controlled environment in a private room with window blinds, while fitted with a full PSG setup. For the periods of sleep-deprivation, participants were monitored with a minimal EEG setup at the lab's facilities and kept awake by research assistants (see below).

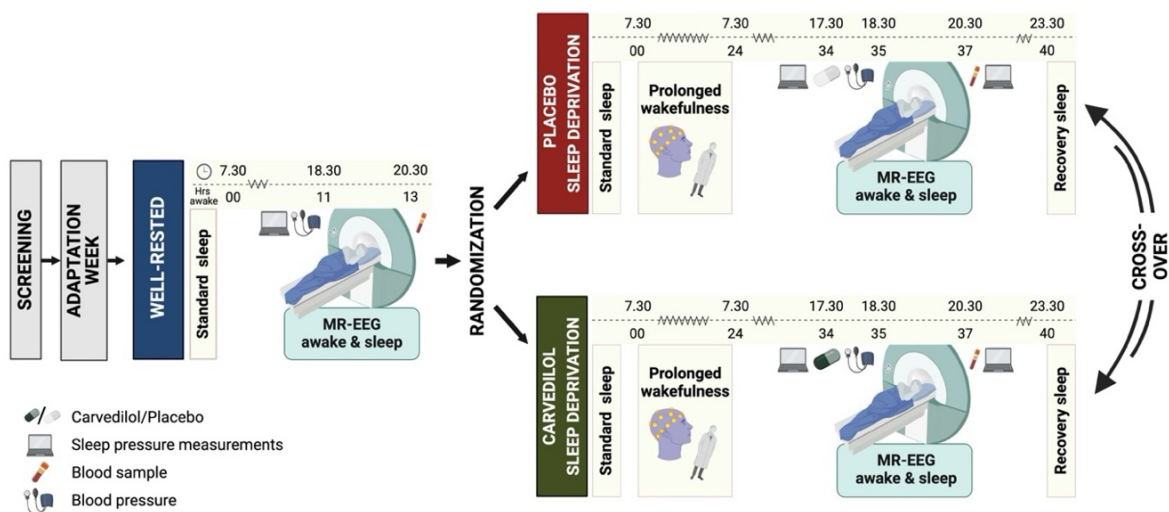


**Figure 6** - Study design for III+IV. Created with BioRender.com.

Figure reprinted from Ulv Larsen & Holst et al. (Appendix B). Published in preprint of paper on medRxiv in October 2024. doi: <https://doi.org/10.1101/2024.10.16.24315580>. The authors hold copyright.

### 9.3 Pharmacological intervention with carvedilol

Before sleep deprivation scans, participants were given either 25mg of carvedilol or a placebo, taken orally.

Blinding was ensured by using specially prepared and visually identical capsules, provided by the Capital Region Pharmacy. Participants were randomised at time of enrolment to a crossover of either placebo-carvedilol, or carvedilol-placebo by a third-party research administrator not otherwise involved in the study.

Capsules were administered one hour prior to the start of the scanning, to ensure a peak plasma concentration of carvedilol. To ensure participant safety, an unblinded assistant monitored and recorded blood-pressure and general wellbeing every 15 minutes for the hour prior the scanning sessions commencing. Results were not passed on to the investigators, but clear instructions and cut-off values for alerting investigators were predefined.

Participants were asked to guess their treatment allocation at the end of the study.

### 9.4 MRI sessions

MR scans were conducted on a Siemens (Erlangen, DE) MAGNETOM 3T Prisma scanner. We used a 64-channel head coil. Before scans, participants were fitted with an MR-compatible EEG-cap (see below), ECG, respiratory belt and a pulse oximeter. Moreover, they wore earplugs and memory foam cushions were used to both restrict head movement and alleviate pressure from the head-coil on the EEG electrodes.

During wakefulness opportunities, we monitored participants to ensure they kept their eyes open, and we talked to them in-between scans. During sleep opportunities, lights were turned off and participants were told they could relax and sleep. To aid sleep during sleep opportunities, we kept the scan sounds as constant as possible, with no or little pause between scans

### 9.5 MR acquisition

All scan sessions started with high-resolution, whole-brain structural T1 weighted image (MPRAGE) to provide an anatomical reference: Inversion time = 900 ms, TR = 1900 ms, TE = 2.52 ms, flip angle = 9°, slice thickness = 1 mm, slices = 208, in-plane resolution = 0.9x0.9, in-plane matrix = 256 x256.

Next, we alternated between the two functional sequences MREG and MB in a 2:1 ratio (MREG-MREG-MB). MREG1 is a single-shot sequence that undersamples k-space with a stack-of-spiral trajectory in three dimensions. The following parameters were used: TR =

100 ms, TE = 33, flip angle = 25°, field of view = 150 mm and voxel: 3x3x3 mm. After scan session, MREG was reconstructed with a MATLAB reconstruction tool 2, using L2-Tikhonov regularization with lambda 0.1 and a regularization parameter determined by the L-curve method.

The MB EPI sequence obtains its high temporal resolution by exciting and acquiring several slices at once, in our case with an acceleration factor of 8. Other parameters were TR = 215 ms, TE = 35 ms, flip angle = 24°, field of view = 229 mm, slices: 24, slice thickness = 4 mm and voxel: 3.6x3.6x4 mm.

## 9.6 MR preprocessing

All processing steps were done similarly for MREG and MB, unless otherwise specified. The first 10 seconds (MREG= 100 images, MB = 47 images) were excluded from the beginning of each scan to ensure steady-state signal saturation. The statistical Parametric Mapping software (SPM12, Wellcome Trust Center for Neuroimaging, UCL) in MATLAB (R2017b, The Mathworks, Inc.) was used for preprocessing and analysis. Motion correction was performed by first realigning all functional images to each other and then co-registering the first volume to the structural T1 image. This was done with the FSL Brain extraction tool and a fractional intensity threshold of 0.3. Next, the co-registered T1 image was segmented into grey matter (GM), white matter (WM) and CSF maps, in which voxels were only included if they had a probability of  $\geq 0.1$  for the relevant tissue type. A whole-brain mask was then defined as the combined GM, WM and CSF masks.

Next, we created a CSF region of interest (ROI) in the left ventricle in order to be able to evaluate CSF oscillations with as little inference from surrounding brain tissue as possible. This was done by manually selecting a midpoint in the left ventricle (MNI coordinates: 8,-10,24) and then drawing a sphere with a radius of 2 cm around it. Only voxels with segmentation-based CSF probabilities larger than 0.5 were included in this ventricle CSF ROI. Lastly, the CSF ROI was normalized to each scan session and used as ‘CSF’ in all analyses.

## 9.7 Spectral analysis

Spectral analysis was performed as outlined below and described in full detail in Appendix B (*preprint*<sup>1</sup>) and C.

For investigation of LFOs, we used the full 5-min MB/MREG sequences and assessed sum of spectral power within both a B-waves frequency band (0.5 – 2 waves per min = 0.008 – 0.033 Hz) and in a broader LFO band (0.01 – 0.1 Hz). Data from 5-min scans were high-pass filtered using a 10-order IIR filter (highpass 0.008 Hz) and spectral analysis was performed with a Hanning window and bin width of 0.00244 Hz. Scans were excluded if it had one or more epoch with framewise displacement >3 mm.

For investigation of brain pulsations related to respiratory and cardiac rhythms, we assessed 30-sec MREG/MB-spectra and assessed the sum of spectral power within individually tailored respiration and cardiac frequency bands.

First, data from all 5-min MB/MREG scans were high-pass filtered with a 10-order IIR filter (passband 0.1 Hz), and segmented into 30-sec epochs, temporally aligning with corresponding sleep-scored EEG epochs. For each 30-sec MREG/MB epoch, spectral analysis was performed with a Hanning window and a bin width of 0.02 Hz. The TAPAS PhysIO toolbox [65] was used to import data from the respiratory belt and pulse oximeter collected simultaneously with scans. MREG/MB and physio data were temporally aligned. Respiration- and heartrates for each 30 sec time series were defined as the frequency of the dominant peak within respiration (0.13 – 0.5 Hz; 7.8 – 30 min<sup>-1</sup>) and cardiac frequency ranges (0.67 – 2 Hz; 40.2 – 120 min<sup>-1</sup>) of 30-sec physio power spectra calculated with the MATLAB periodogram function.

These respiration and heart rates were then used to define the individually tailored 30-sec epoch-specific respiration and cardiac frequency bands in the MREG/MB spectra. Frequency ranges for respiration and cardiac bands in the MREG/MB spectra were defined as the epoch-wise respiration rate  $\pm 0.06$  Hz ( $= \pm 3$  bins) and the epoch-wise heart rate  $\pm 0.1$  Hz ( $= \pm 5$  bins), respectively. Epochs with framewise displacement  $> 3$  mm or with heart rates  $< 40$  or  $> 90$  heart beats per min and/or respiration rates  $< 8$  or  $> 25$  breaths per min were excluded.

5-min scans were included in LFO analysis if EEG experts had classified at least 80% (8/10 epochs) of the simultaneously recorded EEG epochs as either wakefulness or NREM sleep and only if they occurred in lights-on or lights-off conditions, respectively.

30-sec epochs were included in analyses if experts had classified the corresponding EEG as wakefulness, NREM sleep, N2 sleep or N3 sleep. For EEG delta power analysis, MREG/MB epochs were only included if neither of the experts had scored the corresponding EEG as ‘artefact’.

## 9.8 EEG and physiological data collected during MR

During scans, participants were fitted with an MRI-compatible EEG cap (Electrical Geodesics, Inc., Eugene, OR) with 256 EEG channels and a single reference electrode (Cz). The cap was sized according to the participants’ head circumference and prepared with an electrolyte shampoo solution. Cap placement was guided by positioning the reference electrode at the vertex and visual inspection of predetermined reference points according to

the 10-20 system. The cap was secured with a hair net and kept moist by a shower cap. Initial impedances were kept below 50 k $\Omega$ .

Two ECG electrodes were placed over the left 4<sup>th</sup> and 5<sup>th</sup> intercostal spaces. Both EEG and ECG data were acquired with a 1 kHz sampling rate and all cables were connected to a synchronization box to match acquisition to the MR scanner's clock frequency. Participants were additionally fitted with an MR-compatible respiration belt and pulse oximeter, wired directly to the scanner. *For further details, see Appendix B (preprint<sup>1</sup>) and C.*

### 9.9 MR-EEG processing and scoring

Removal of artefacts from the EEG was performed using MATLAB (R2014a, The MathWorks, Inc.). MR-induced gradient artefacts were removed with the average artefact subtraction method<sup>96</sup> and Ballistocardiographic artefacts were removed with the optimal basis sets approach<sup>97</sup>.

EEG recordings were visually scored in 30 second epochs by two independent experts, in accordance with standard American Academy of Sleep Medicine criteria<sup>98</sup> and using DOMINO software (Somnomedics, Germany). The experts were both blinded to participant, treatment allocation and scan condition (lights on or off) and were instructed to mark epochs with significant MR artefacts and aberrant non-physiological data as artefacts.

Final sleep staging of MR-EEG epochs was then done as follows; An epoch was classified as 'wakefulness' if it occurred before the first onset of NREM sleep stages N2 or N3 (scored by at least one expert) and if both experts agreed on 'wakefulness' or if one scored it as 'wakefulness' and the other scored it as 'artefact.' Epochs were designated as 'NREM sleep' if both experts independently classified them as either NREM sleep stage N2 or N3. Similarly, epochs were specifically categorized as 'N2 sleep' or 'N3 sleep' only if both experts consistently assigned the same respective classification. *A detailed description can be found in Appendix B (preprint<sup>1</sup>) and C.*

### 9.10 Quantification of EEG delta power ratio

Delta power ratio for each 30-second EEG epochs was calculated as the ratio of EEG band power (mV<sup>2</sup>) in the delta range (1–4 Hz) to the full power spectrum range (0.5–30 Hz).

EEG band power in each of these frequency ranges was computed as described in Appendix B (*preprint<sup>1</sup>*) as follows: EEG-data were first cleaned participant- and condition-wise by rejecting channels exceeding a kurtosis threshold of 5 using EEGlab's `pop_rejchan` function<sup>99</sup>. The leads C3-M2 and C4-M1 were then constructed either from their

corresponding channels ( $\text{Chan}_{\{C3\}} = 59$ ,  $\text{Chan}_{\{C4\}} = 183$ ,  $\text{Chan}_{\{M1\}} = 94$ ,  $\text{Chan}_{\{M2\}} = 190$ ) or, if rejected, an average of the neighbouring channels.

If EEG power in a 0.5-second window (with 0.25-second overlap) for the two leads exceeded 15 dB in the 35–120 Hz range, it was rejected as an artefact segment

In all epochs without artefact segments, we computed the bandpower ( $\text{mV}^2$ ) in the 1–4 Hz range and in the 0.5 – 30 Hz range for the two leads (and calculated the ratio).

The reported delta power ratio is a mean of the two leads. Epochs were only included in the final analyses if neither expert had classified the epochs as ‘artefact’ during sleep scoring.

### 9.11 EEG outside of scanner environment

The Somnoscreen Plus system (Somnomedics, Germany), a mobile battery-powered EEG device, was used for all recordings outside the scan sessions. A single expert, blinded to treatment and condition, visually scored 30-second epochs according to standard criteria<sup>98</sup>, accounting for artefact rejection and filter settings. Scoring was conducted using DOMINO software (Somnomedics, Germany)

### 9.12 Nocturnal PSG recording

18-electrode EEG-recordings according to the 10-20 system<sup>100</sup> were conducted simultaneously with EOG and ECG. Initial impedance values were kept below 6k $\Omega$ . Participants were asked to blink ten times in a row to announce that they were turning off the lights and going to bed, and again when they woke up and turned on the lights. A mandatory lights-off period of eight hours for the standard nights prior to study sessions and ten hours for recovery nights was set. EEG-analyses were redistricted to eight hours to ensure comparability between nights.

### 9.13 Minimal EEG setup during prolonged wakefulness

To ensure and monitor wakefulness during the 35-hour sleep deprivation, participants were fitted with a lightweight EEG setup with six electrodes and an EOG, which recorded continuously for the entire period. The EEG recorder was placed in a shoulder bag, allowing full freedom of movement for the participant.

### 9.14 Psychomotor vigilance

As in study I, a PVT (Psychology Software Tools Inc., Pittsburgh) was used to assess cognitive effects of prolonged wakefulness. To familiarize participants with the test, they completed a training session during the adaptation week. The test was administered in the well-rested condition after seven hours of wakefulness, in the sleep-deprived conditions after 31 hours of wakefulness, and immediately following the one-hour sleep opportunity at the end of every scan session. As in study I, the two validated PVT variables “median reaction time” and “lapses of attention” were recorded.

In study III/IV (and described in full in Appendix B (*preprint*<sup>1</sup>)), impaired psychomotor vigilance in sleep deprived conditions was evaluated by 1) quantifying the increase in median reaction time from rested wakefulness (value before sleep-deprived scan minus value before well-rested scan) and 2) the absolute number of lapses of attention before the sleep-deprived scan (Freeman-Tukey transformed  $\sqrt{x} + \sqrt{(x + 1)}$ ). Improvements in psychomotor vigilance due to sleep in the scanner were computed as the difference between values taken before and immediately after scans.

### 9.15 Plasma norepinephrine

Following each scan session, 6 mL of venous blood was collected in EDTA tubes. Samples were taken approximately 15 minutes after exiting the scanner. Plasma was then extracted via centrifugation at 2860 rpm for seven minutes at four degrees Celsius and then stored at -80 degrees until analysis. Levels of plasma norepinephrine (p-NE) were measured by batch microdialysis as specified by Weikop and colleagues<sup>101</sup>. Analysis was performed by a researcher blinded to the treatment and condition and the samples were analysed in random order. For further details on the method of analysis, please see the supplementary section in Appendix C.

## 10. Statistics

The following sections outline the statistical methods for each study. For further details, please see the included papers (Appendix A,B,C). P-values were considered significant only if they equal to or below 0.05.

### 10.1 Study I

All statistical analyses were conducted using SAS 9.4 (SAS Institute, Cary, NC). EEG energy was considered the primary outcome variable and was log-transformed before testing to mitigate skewness in the distribution.

For all significant EEG energy findings, the same analyses were conducted for EEG power.

Assessments of haplotype effects were conducted across nocturnal EEG data, subjective sleepiness measures and PVT performance as outlined below and described in full detail in Appendix A<sup>102</sup>.

Two- and three-way mixed-model ANOVAs with “genotype” (HtMa homozygotes vs. HtMi carriers) as a between-participant factor and, where relevant, “condition” (baseline vs. recovery), “NREM sleep episode” (1–4), “frequency bin” (1–81), clocktime, and prolonged wakefulness duration (day 1 vs. day 2) as within-participant factors.

Specifically for assessment of EEG spectra, we first performed two overall four-way mixed-model ANOVAs (for EEG power and EEG energy), that included all frequency bins, genotype, condition, and study to establish an overall effect of genotype on EEG.

In further assessment of single bins in the EEG spectra, we controlled for type I errors by only considering an effect significant if the following two criteria were met:

- 1) > 2 bins in the bin-by-bin (mixed model) showed a haplotype effect
- 2) The corresponding frequency band to the found significant bin (slow wave/delta, theta, alpha, spindle, beta) also showed a haplotype effect.

The final step implemented to control for type I errors was to investigate the sleep EEG bands using a hypothesis driven, fixed sequence procedure, in which EEG bands were listed based on their relevance for sleep-wake regulation as follows: (1) Delta/slow wave activity (0.75–4.5 Hz), (2) Spindles (12–15 Hz), (3) Theta (5–8 Hz), (4) Alpha (8–12 Hz), and (5) Beta (15–20 Hz) and tested for significance in that order.

Significant effects of interactions were localized using paired or unpaired two-tailed t-tests. Effect sizes (partial eta squared:  $\eta^2$ ) were calculated from corresponding mixed-model F-values and degrees of freedom.

## 10.2 Study II

As this study was a descriptive study with a low number of participants, no statistical calculations were performed.

## 10.3 Study III + IV

Statistical analyses and graphs were performed in R version (<http://www.R-project.org/>). The R package lme4 (version: 1.1.29) was used for mixed models, while lmerTest (version: 3.1.3) and LMM star (version: 0.8.9) were used for fitting linear mixed models, performing Wald's tests and estimating expected means and correlation parameters. Estimates are reported in means  $\pm$  standard error of the mean (SEM) unless explicitly stated otherwise.

Below is presented an overview of the statistical models used in study III and IV. A comprehensive description of all models used, and data included can be found in supplementary material for Appendix B.

### Primary outcomes

Sum of MB and MREG spectral power within the LFO, respiration, and cardiac frequency bands were considered the primary outcome variables. Band-wise spectral power was log transformed before analysis to mitigate skewness in the distribution.

### Linear mixed effects models

Linear mixed-effects models were used to estimate differences between conditions. Fixed effects were (where appropriate): Sleep deprivation (well-rested vs sleep deprived), vigilance state (awake vs NREM sleep), sleep depth (sleep deprived wakefulness vs N2 sleep vs N3 sleep), tissue type (GM vs WM vs CSF), treatment (placebo vs carvedilol), PVT measurement ('median reaction time' and 'lapses of attention') and EEG delta power ratio. Interactions between fixed effects were estimated for 'tissue type x vigilance' and 'treatment x vigilance'.

The following random effects were included: participant ID, scan session (well-rested, sleep-deprived 1 and sleep-deprived 2) and sleep opportunity (lights on scan, lights off scan), with sleep opportunity being nested into scan session itself nested into participant ID.

For all models used to analyse spectral power in respiration- and cardiac frequency ranges, the simultaneously recorded respiration and heart rates, respectively, were included in the model as fixed effects to account for the declining spectral power with higher frequencies.

Wald's tests were used to obtain p-values for the fixed effects. Estimated means were computed under specific conditions (e.g. sleep under sleep deprivation) from the linear mixed effects.

Estimated means (based on log transformed data) were used to calculate the percental changes presented throughout the result section by following equation:

$$\frac{EstimatedMean2 - EstimatedMean1}{EstimatedMean1} = xx\%$$

e.g. for effect of sleep deprivation on LFO spectral power in study III

$$\frac{10^{7.091} - 10^{6.748}}{10^{6.748}} = 120\%$$

### Correlations

Correlation coefficients for associations between log spectral power in Resp/Card/LFO frequency bands and delta power ratio as well as PVT measurements were deduced from mixed model estimates (denoted  $r_{adj}$ ) with approach described in Appendix B.

Pearson's correlation coefficients (denoted  $r$ ) were used to evaluate associations between NE levels and log LFO spectral power and to present reference values for  $r_{adj}$ .

### Pairwise testing

Where pairwise testing was appropriate, we conducted Student's two-tailed t-tests for data with a normal distribution and Wilcoxon signed-rank tests for data not normally distributed

### Data included in analysis

The amounts of participants per conditions and average amount of either 30-sec epochs or 5-min scans per participant per condition included in MREG and MB analysis is shown in Table 1 and Table 2 below.

Of note, in all analyses of LFO spectral power in the MB dataset, a mean per condition was calculated rather than including all 5 min scans. This was due to uneven distribution of scan per condition between participants.

**Table 1** - Distribution of analysed MREG data in sleep study

	Rested Awake	Sleep deprived placebo				Sleep deprived Carvedilol			
		Awake	Sleep	N2	N3	Awake	Sleep	N2	N3
<b>30-sec dataset</b>									
Participants (N)	<b>20</b>	<b>17</b>	<b>17</b>	<b>16</b>	<b>14</b>	<b>15</b>	<b>19</b>	<b>17</b>	<b>12</b>
Included epochs (N)	35.6 [28.1, 43.0]	10.8 [5.2, 16.3]	28.7 [20.2, 37.2]	14.5 [9.1, 19.9]	8.1 [4.5, 11.7]	9.5 [4.7, 14.4]	14.3 [13.2, 15.5]	14.6 [8.9, 20.3]	17.8 [7.1, 28.6]
<b>5-min dataset</b>									
Participants (N)	<b>19</b>	<b>12</b>	<b>14</b>	-	-	<b>12</b>	<b>17</b>	-	-
Included scans (N)	1.6 [1.3, 1.8]	1.1 [0.9, 1.3]	3.1 [2.1, 4.1]	-	-	1.3 [0.7, 1.8z]	3.3 [2.5, 4.1]	-	-

**Table 2** - Distribution of analysed MB data in sleep study

	Rested Awake	Sleep deprived placebo	
		Awake	Sleep
<b>30-sec dataset</b>			
Participants (N)	<b>18</b>	<b>8</b>	<b>15</b>
Included epochs (n)	16.7 [12.1, 21.2]	11.0 [7.2, 14.8]	12.5 [8.3, 16.8]
<b>5-min dataset</b>			
Participants (N)	<b>17</b>	<b>8</b>	<b>13</b>
Included scans (n)	1 [1, 1]	1 [1,1]	1.5 [1.1, 1.9]

Tables 1 & 2 adapted from Appendix B & C. Tables in appendix B have been published in preprint of paper on medRxiv in October 2024. doi: <https://doi.org/10.1101/2024.10.16.24315580>. The authors hold the copyright.

# Results

---

In the following sections, a summary of the main results from Study I, III and IV as well as results from study II are presented. Full details are provided in each of the manuscripts (Appendix A,B,C).

## 11. Study I

Analysis in this study are based on data from 123 healthy participants. We assessed the effect of being a carrier versus homozygous for a common AQP4 haplotype on sleep-wake regulation. Our primary outcome variable was NREM slow wave energy, a combined measure of slow wave activity and NREM sleep duration.

Results presented in sections 11.1 and 11.2. were included in preliminary forms in the author's Master's thesis, submitted in August of 2018. Analyses were subsequently expanded and the initial findings elaborated upon, prior publication PLoS Biology in 2020. The resulting paper is included as Study I in this thesis.

### 11.1 8-SNP AQP4-haplotype

The SNPs investigated here (rs335929, rs16942851 and rs335931) are all part of a common 8-SNP AQP4-haplotype (**Figure 5A**). The three genotyped SNPs were in Hardy-Weinberger equilibrium and had high pairwise linkage disequilibrium, thus justifying that all further analyses were done on the haplotype rather than on single SNPs.

Frequencies of the two haplotype variants HtMa and HtMi were 75.7% and 23.5%, respectively. This aligned with their expected incidences in a European population.

Throughout the study, 71 carriers of HtMi were compared to 52 individuals who were homozygous for HtMa. The distribution of HtMi-carriers versus HtMa homozygous was similar between the 6 studies ( $p > 0.21$ ). Demographics between the two groups can be seen in **Table 3**.

**Table 3** - Demographics for study I

	HtMa homozygotes	HtMi carriers	<i>p</i> -value
Sample size (N <sub>total</sub> = 123)	71	52	
Age (years)	24.1 ± 2.8	23.9 ± 3.0	0.69
BMI (kg/cm <sup>2</sup> )	22.4 ± 1.6	22.6 ± 2.1	0.40
Gender (% females)	12,7	3,8	0.12
Reported habitual sleep duration (h)	7.3 ± 0.7	7.4 ± 0.7	0.46
Trait anxiety (STAI)	33.25 ± 7.1	35.1 ± 8.5	0.19
Sleepiness (ESS)	6.6 ± 3.0	6.9 ± 2.9	0.61
Smoking (% yes)	2,8	1,9	1
Caffeine consumption (mg/day)	108.1 ± 100.3	129.9 ± 118.9	0.27
Alcohol consumption (drinks/week)	3.2 ± 2.7	2.8 ± 2.6	0.43
APOE genotype			
ε2 carrier	10	4	
ε3 carrier	42	36	
ε4 carrier	16	11	0.47

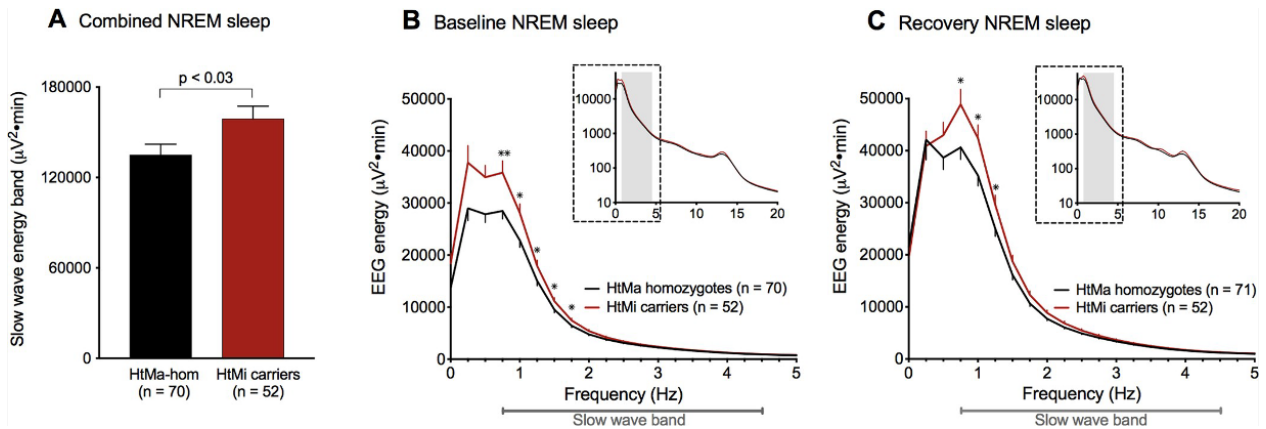
From Ulv Larsen. et al., *PLoS biology* vol. 18,5 e3000623. 2020. doi: <https://doi.org/10.1371/journal.pbio.3000623>. © CC-BY-4.0 licence (<https://creativecommons.org/licenses/by/4.0>).

## 11.2 AQP4-haplotype and NREM slow waves

HtMi carriers had higher NREM EEG slow wave energy than HtMa homozygotes ( $p < 0.03$ ). This was observed both in baseline sleep and during recovery sleep after 40 hours of prolonged wakefulness (“genotype x night”:  $p > 0.55$ ; Fig 7). Post hoc analyses of NREM slow wave activity confirmed the results, while no differences were seen in REM sleep. The AQP4-haplotype had a differential effect on NREM sleep across the first four sleep cycles of the night (haplotype x NREM episode”:  $p < 0.05$ ). Specifically, the haplotype primarily modulated NREM slow wave energy in the first two sleep cycles of both baseline and recovery sleep (Cycle 1+2 versus Cycle 3+4:  $p_{\text{both}} < 0.05$ )

## 11.3 AQP4-haplotype: Response to sleep deprivations

Reaction times and subjective sleepiness ratings throughout 40 hours of prolonged wakefulness showed that carriers of the HtMi haplotype coped slightly better with sleep deprivation than individuals homozygous for the HtMa haplotype, as they showed a smaller increase in sleepiness and delayed reaction times from day 1 to day 2 awake (“haplotype x day”:  $p_{\text{both}} < 0.04$ ). In the non-sleep deprived part of the wakefulness period (day 1), the measures were comparable.



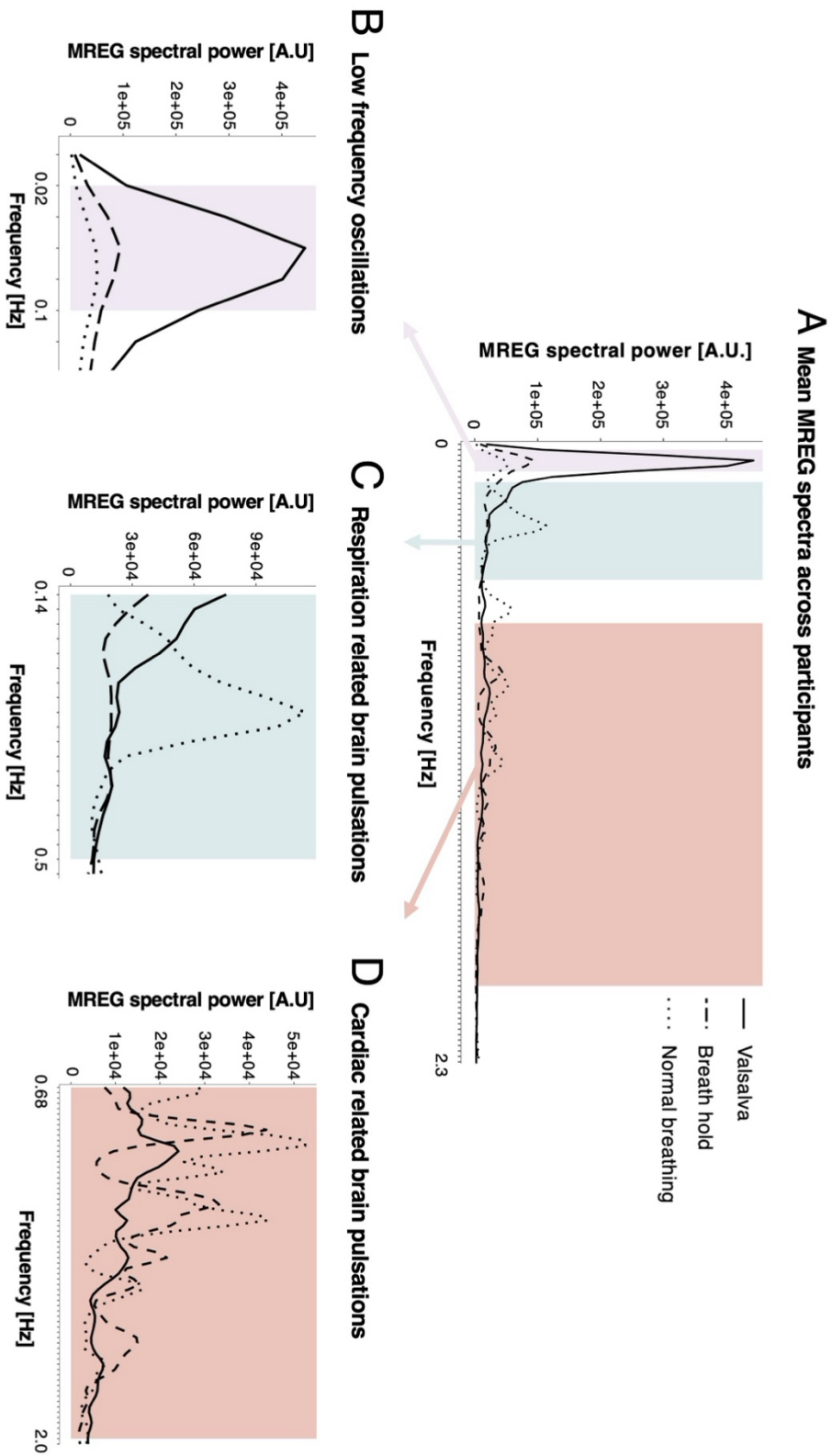
**Figure 7** – Combined NREM sleep for HtMA/HtMi (A), Baseline NREM sleep (B), Recovery NREM sleep (C)

Figure reprinted from Ulv Larsen et al. *PLoS Biol.* Vol 18,5 e3000623. 2020. doi: <https://doi.org/10.1371/journal.pbio.3000623>. © CC-BY-4.0 licence (<https://creativecommons.org/licenses/by/4.0>)

## 12. Study II

This descriptive study included 4 participant (2 males, 2 females). The effects of breath-holding and the Valsalva maneuver on power peaks within physiological frequency ranges of the MREG spectra were visually assessed.

We observed a large increase in MREG spectral power within LFO frequencies (< 0.1 Hz) during the Valsalva manoeuvre, compared to both normal breathing and breath-holding (**Figure 8A**). Breath-holding and the Valsalva manoeuvre were found to suppress spectral power peaks in respiratory frequencies (0.14 – 0.5 Hz; Fig 1A&C), while for cardiac-related peaks in the MREG spectra (0.68 – 2.0 Hz), we observed a reduction in spectral power during the Valsalva manoeuvre (**Figure 8B,C,D**). These patterns were consistently observed across all four participants (**Figure 9**). Due to the small sample size, no statistical tests were performed.



**Figure 8** – (A) MREG spectra across all participants, (B) LFOs, (C) Respiration-band, (D) Cardiac-band  
 Figure from Uiv Larsen & Holst et al, published as preprint on medRxiv in October 2024, doi: <https://doi.org/10.1101/2024.10.16.24315580>. The authors hold the copyright.  
 Preprint represents an earlier version of appendix B that included study II.

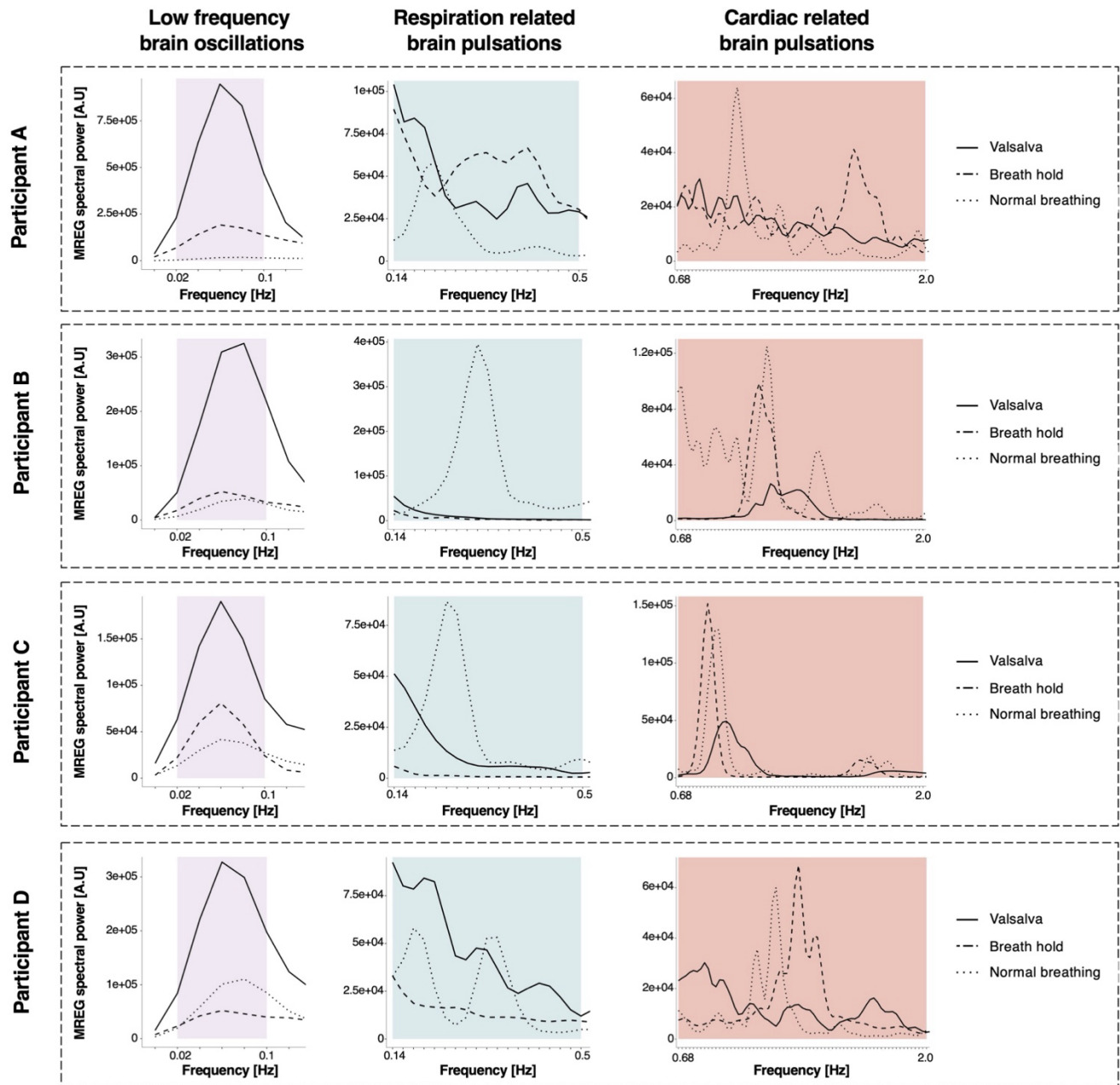


**Figure 9** - Separate MREG spectra for all four participants

Figure from Ulv Larsen & Holst et al., published as preprint on medRxiv in October 2024. doi: [http://doi.org/10.1101/2024.10.16.24315580](https://doi.org/10.1101/2024.10.16.24315580). The authors hold the copyright. Preprint represents an earlier version of appendix B that included study II.

## 13. Study III

This study included data from 20 male participants.

The primary outcome variables were the sum of power in LFO, respiratory and cardiac frequency bands of the MREG spectra (*see* Methods), which were considered measures of physiological brain oscillations at the respective frequencies. Distribution of participants and MREG-data included in analysis across conditions can be seen in Table 1. More details on results can be found in appendix B.

### 13.1 Sleep study cohort and vigilance state descriptives

All participants adhered to their prescribed 8-16-hour sleep schedules and had comparable sleep during standardized nights leading up to study days, confirming that all measures were performed at same circadian time-point. Wakefulness during sleep deprivation periods was confirmed with continuous EEG measurements, and increased sleep propensity before the sleep deprived scan sessions was confirmed by impaired psychomotor vigilance performance (reaction time:  $-0.035 \pm 0.005$  sec; lapses of attention  $+3.86 \pm 0.23$ ;  $p_{\text{both}} < 0.001$ ) and a borderline increase in awake EEG delta power ( $p = 0.05$ ). Neither respiration, heart rate, blood pressure or norepinephrine levels were significantly changed by sleep deprivation. NREM sleep during MREG-scans was associated with a strong increase in EEG delta power ( $p < 0.001$ ), which was greater in N3 than N2 sleep ( $p < 0.001$ ,  $N = 17$ ), and a  $\sim 10\%$  decrease in both respiration and heart rates ( $p < 0.001$ ).

In rested wakefulness, we observed a strong temporal relationship between measured respiration and heart rates and the frequency of their corresponding power peaks in the MREG spectra (Resp:  $r_{\text{adj}} = 0.97$ ; Card:  $r_{\text{adj}} = 1.00$ ;  $p_{\text{adj}} < 0.001$ )

**Table 4** - Demographics for study III/IV

	<b>Mean <math>\pm</math> SD</b>	<b>min – max</b>
<b>Age (years)</b>	24.1 $\pm$ 2.8	20 – 29
<b>Body mass index (kg/m<sup>2</sup>)</b>	22.7 $\pm$ 2.8	19.1 – 31.6
<b>Reported habitual sleep duration (h)</b>	7.6 $\pm$ 0.4	7.0 – 8.0
<b>Morningness-eveningness (MEQ)</b>	48.6 $\pm$ 6.4	38.9 – 61.0
<b>General daytime sleepiness (ESS)</b>	6.2 $\pm$ 3.0	2.0 – 13
<b>Sleep quality index (PSQI)</b>	3.0 $\pm$ 1.6	1.0 – 6.0

MEQ: Morningness-eveningness questionnaire, PSQI: Pittsburgh Sleep Quality Index, ESS: Epworth Sleepiness Scale.

Table adapted from Ulv Larsen & Holst et al. (Appendix B).

### 13.2 Physiological brain oscillations across tissue types

During rested wakefulness, MREG spectral power within the respiratory and cardiac frequency bands varied significantly across tissue types ('Tissue type main effect':  $p < 0.001$ ). Specifically, spectral power was markedly stronger in CSF compared to both grey and white matter ( $p_{all, adj} < 0.001$ ). Additionally, GM exhibited slightly higher spectral power than WM in both respiratory ( $p_{adj} = 0.052$ ) and cardiac frequency bands ( $p_{adj} = 0.014$ ).

For the LFO band, we observed no differences in MREG spectral power between tissue types.

### 13.3 LFOs, sleep deprivation and sleep pressure

Sleep deprivation (35 hours of wakefulness) caused MREG spectral power in the LFO frequency band (0.012 - 0.034 Hz) to increase by 120% ( $p = 0.030$ ) compared to rested wakefulness. This effect was consistent across tissue types.

When participants fell asleep in the scanner and entered NREM sleep stages N2 and N3, LFO spectral power was in-between that of rested wakefulness and sleep deprived wakefulness, but not significantly different from any of them (NREMsleep effect:  $p = 0.19$ ) (**Figure 10A-C**)

When we evaluated psychomotor vigilance (reaction time and attention lapses) as an indicator of sleep pressure, we discovered that LFO spectral power during sleep was correlated with both pre-scan psychomotor vigilance performance and the improvement in performance - reflected by faster reaction times and fewer lapses—after the nap in the scanner compared to before ( $p_{adj, all} < 0.05$ ) (**Figure 12**)

### 13.4 NREM sleep and respiration- and cardiac-driven brain pulsations

NREM sleep (combined stages N2 and N3) had a strong effect ( $p < 0.001$ ) on whole-brain MREG spectral power within the respiratory frequency band, causing an increase of 73% and 150% compared to sleep deprived and rested wakefulness, respectively.

A similar effect of sleep was observed in the cardiac frequency band ( $p = 0.003$ ), where the increased amounted to 35% and 42% (**Figure 10D-H**)

This enhancing effect of NREM sleep on spectral power was significantly greater in gray and white matter than in CSF, with increases of 70 and 75% in the respiratory frequency band and 92 and 110% in the cardiac frequency band ( $p_{adj, all} < 0.001$ ).

Sleep deprivation increased spectral power in the respiratory frequency range by +45% ( $p = 0.038$ ), an effect observed only in grey and white matter.

### 13.5 Sleep depth, EEG delta power and the strength of respiration- and cardiac-driven brain pulsations

In the respiration band, MREG spectral power increased in a dose-response-like manner from sleep deprived wakefulness to N2 sleep (+35%,  $p_{adj} = 0.047$ ) to N3 sleep (+ 57%,  $p < 0.001$ ). For cardiac spectral power, spectral power was higher in N3 sleep than in both N2 sleep (+39%,  $p_{adj} < 0.001$ ) and wakefulness (+58%,  $p_{adj} < 0.001$ ), while no difference was observed between N2 sleep and sleep deprived wakefulness. (Figure 11)

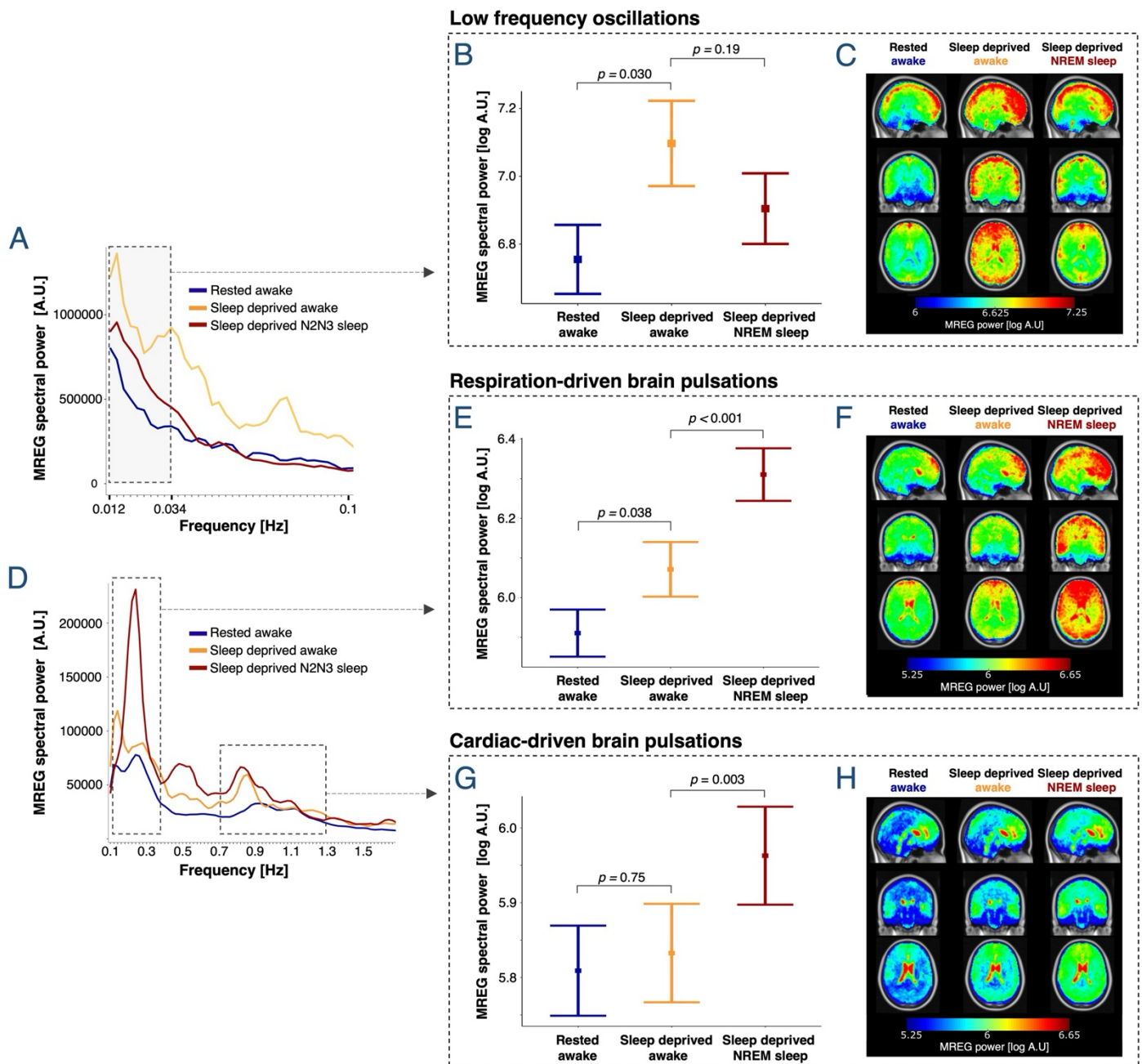
EEG delta power ratio correlated positively with MREG spectral power in both frequency ranges ( $p < 0.001$ ) (Figure 11)

### 13.6 Systemic adrenergic antagonism and physiological brain oscillations

Participants were not able to guess whether they had received carvedilol or placebo (Treatment guess accuracy: 54%), confirming successful blinding.

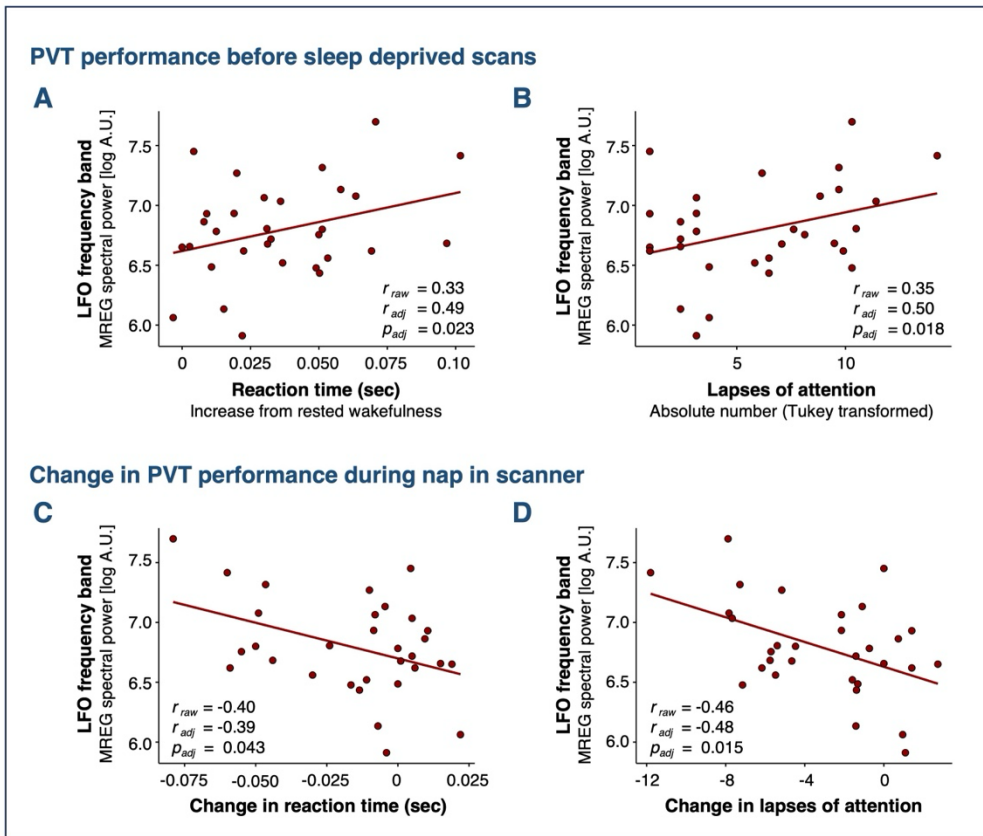
Treatment with the adrenergic antagonist carvedilol reduced p-NE levels ( $-479 \pm 113$  pg/mL,  $p_{adj} < 0.001$ ) and lowered mean arterial blood pressure by  $\sim 5$  %. During NREM sleep, carvedilol caused a reduction in MREG spectral power in both the LFO (-51%,  $p = 0.05$ ) and cardiac (-30%,  $p = 0.032$ ) frequency ranges.

This effect was not seen in sleep deprived wakefulness and carvedilol did not change relative or absolute time spent in sleep during scans. Respiratory spectral power was comparable in both sleep and wakefulness between the two conditions.



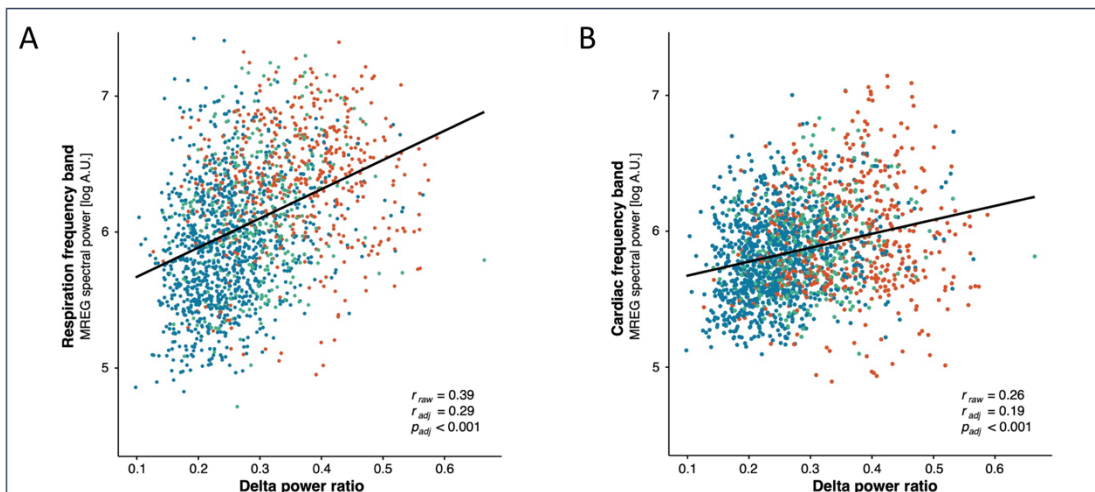
**Figure 10** - (A, D) Mean whole-brain MREG spectra across participants. (B, E, G) Estimated means  $\pm$  SEM and  $p$ -values are from linear mixed models evaluating effects of sleep deprivation and sleep on spectral power in LFO (B), respiration (E), and cardiac (G) frequency bands. (C, F, H) Whole-brain maps illustrate the regional spectral power [log A.U.] in the LFO, respiration and cardiac frequency bands across all 5-min scans (LFO) or 30-sec epochs (respiration and cardiac), averaged across first epochs/scans, then participants (warped into MNI space).

Figure reprinted from Ulv Larsen & Holst et al. (Appendix B). Published in preprint of paper on medRxiv in October 2024. doi: <https://doi.org/10.1101/2024.10.16.24315580>. The authors hold the copyright.



**Figure 12 - PVT performance**

Figure reprinted from Ulv Larsen & Holst et al. (Appendix B). Published in preprint of paper on medRxiv in October 2024. 1101/2024.10.16.24315580. The authors hold the copyright.



**Figure 11 – Delta power in respiration- and cardiac frequency bands**

Figure reprinted from Ulv Larsen & Holst et al. (Appendix B). Published in preprint of paper on medRxiv in October 2024. doi: <https://doi.org/10.1101/2024.10.16.24315580>. The authors hold the copyright.

## 14. Study IV

This study included data from 20 male participants and was based on MB data collected alternately with MREG data analysed in study III. The primary outcome variables were sum of MB spectral power in LFO, respiratory and cardiac frequency bands. MB-data included in analyses can be found in **Table 2**.

### 14.1 MB-detected LFOs across brain tissue types

In rested wakefulness, LFO spectral power was higher in GM than in both WM and CSF. CSF also showed significantly higher spectral power than WM (tissue type main effect:  $p < 0.001$ ) (**Figure 13**). This pattern was observed both within the B-wave band (0.011-0.034) and in the broader frequency band (0.011 – 0.1 Hz). However, visual inspection of the average MB spectrum across participant indicated that tissue differences were strongest below 0.05 Hz (**Figure 13**).

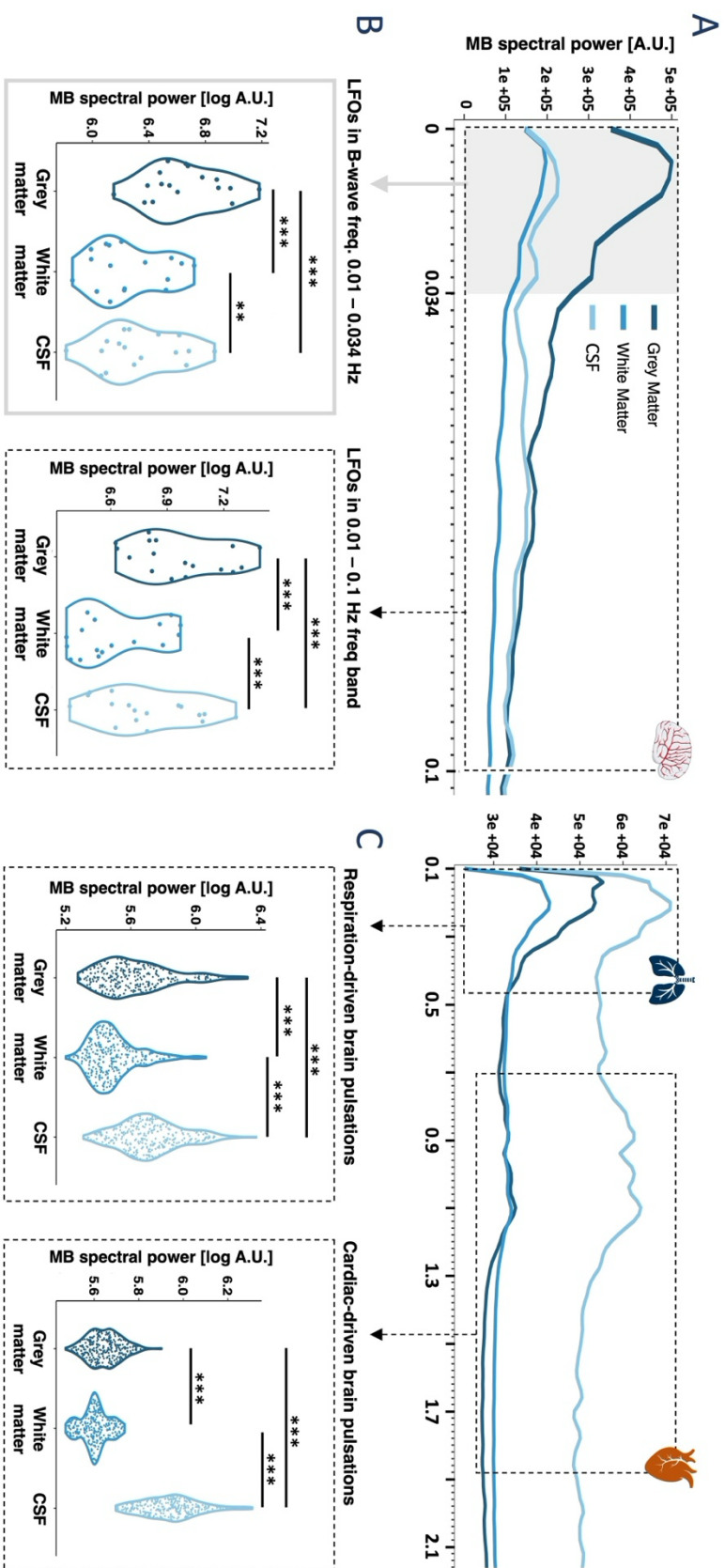
In the following, LFO results are reported for the 0.011–0.034 Hz band, with similar findings observed in the broader frequency band. Additional details can be found in Appendix C.

### 14.2 MB-detected LFOs and sleep deprivation

Participants had 91% higher MB spectral power in the LFO frequency band during sleep deprived wakefulness than in rested wakefulness ( $p < 0.001$ ). After falling asleep and entering NREM sleep stages N2 and N3, LFO spectral power dropped by 79 % ( $p = 0.011$ ). These effects were similar across tissue types. Sleep deprivation did not significantly increase respiration ( $p = 0.076$ ) or heart rates ( $p = 0.096$ ) collected concurrently with MB.

### 14.3 LFOs and plasma norepinephrine

Norepinephrine levels in plasma showed a positive correlation with LFO spectral power in rested wakefulness ( $r = 0.59$ ,  $p = 0.022$ ,  $N = 17$ ). This association persisted during sleep, where the change in LFO spectral power from rested wakefulness to sleep deprived NREM sleep (N2 & N3) correlated with the change in p-NE from rested to sleep deprived conditions ( $r = 0.24$ ,  $p = 0.57$ ,  $N = 8$ ). However, we did not find evidence that the increase in LFO spectral power with sleep deprivation was due to changes in p-NE ( $r = 0.68$ ,  $p = 0.044$ ,  $N = 9$ ) (**Figure 15**).



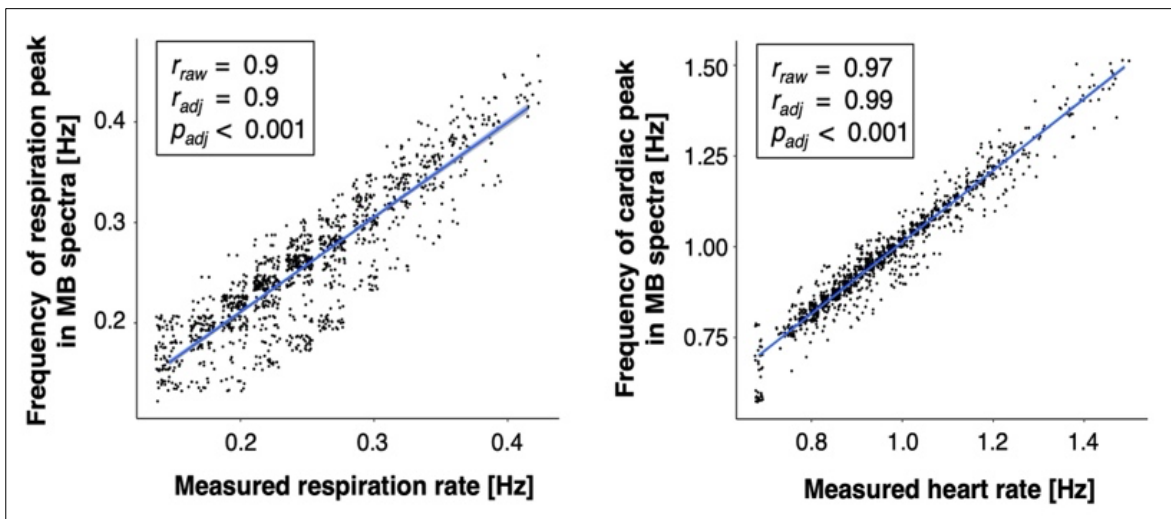
**Figure 13** – MB spectrum during rested wakefulness. (A) Mean MB spectra across participants. (B,C) Comparison of MB spectral power density across GM, WM and CSF.

Figure reprinted from Ulv-Larsen et al. (Appendix C).

## 14.4 NREM sleep and MB-detected respiration- and cardiac-driven brain pulsations

We found a strong correlation between measured respiration- and heart rates and the frequency of their corresponding power peaks in the MB spectra (Resp:  $r_{adj} = 0.9$ ,  $p_{adj} < 0.001$ ; Card:  $r_{adj} = 0.99$ ,  $p_{adj} < 0.001$ ) (**Figure 14**). In rested wakefulness, MB spectral power in both frequency bands was strongest in CSF, followed by GM and then WM (Tissue main effect:  $p < 0.001$ )

In the respiration frequency band, MB spectral power increased during NREM sleep (+77%,  $p = 0.006$ ) and correlated with EEG delta power ratio ( $r_{adj} = 0.15$ ,  $p_{adj} < 0.001$ ). In the cardiac frequency band, MB spectral power also correlated with EEG delta power ( $r_{adj} = 0.11$ ,  $p_{adj} < 0.001$ ) but did not differ significantly between wakefulness and sleep. Sleep deprivation had no effect in either frequency band.



**Figure 14** - Respiration- and cardiac MB frequency vs respiration- and heart rate

Figure reprinted from Ulv Larsen et al. (Appendix C).

## 14.5 MB versus MREG

Due to the 2:1 data acquisition ratio between MREG and MB, less data was available for MB analysis. To compare the two methods, we conducted a sensitivity analysis using a restricted MREG dataset directly matched to the MB data

Sleep deprivation increased LFO spectral power in the restricted MREG dataset, showing a similar effect size, but with lower significance than in the MB dataset (MREG<sub>Restrict</sub>: +98%,  $p = 0.04$ ). NREM sleep similarly increased respiratory frequency spectral power in MB and

the restricted MREG dataset (MREG<sub>Restrict</sub>: +74%,  $p < 0.001$ ), while sleep deprivation affected only MREG data. Unlike MB, the restricted MREG dataset showed a significant sleep-induced increase in cardiac spectral power (MREG<sub>Restrict</sub>: +28%,  $p = 0.05$ ; MB: +1.6%,  $p = 0.69$ ).

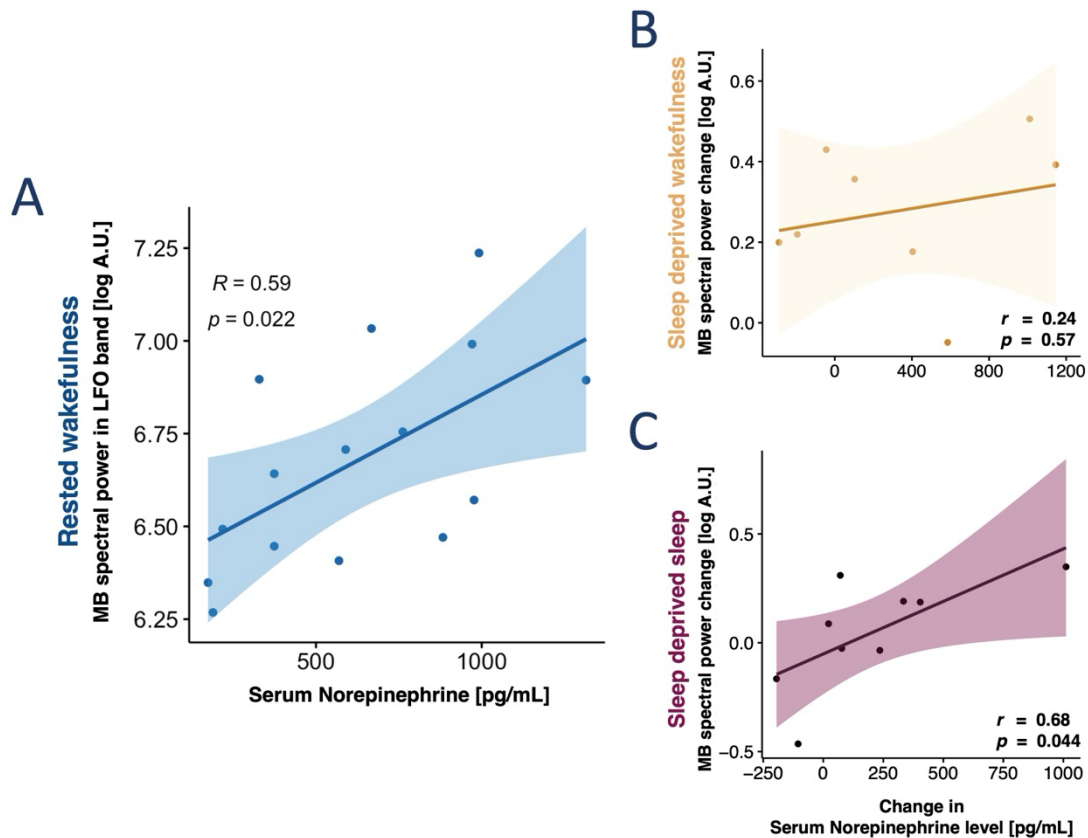


**Figure 15** – LFO spectral power vs p-NE levels (A) Correlation between p-NE and MB spectral power in LFO band (0.011-0.034 Hz) during rested wakefulness (B) Absolute change in p-NE level from rested to sleep deprived scans and absolute change in LFO MB spectral power from rested wakefulness to sleep deprived wakefulness (C) NREM sleep.

Figure reprinted from Ulv Larsen et al. (Appendix C).

## Discussion

---

### 15. Discussion

The discussion below spans studies I, II, III & IV. Detailed discussion of the individual studies are provided in [Appendix A, B](#) (with study II included in the preprint<sup>1</sup>) and C.

#### 15.1 AQP4 haplotype modulates deep NREM sleep intensity and slow waves

The AQP4 gene contains an 8-SNP haplotype linked to AQP4 expression. This haplotype, spanning the entire gene, includes two common variants: rs335929, associated with cognitive decline in Alzheimer's disease<sup>59</sup>, and rs162008, which reduces AQP4 expression by 15-20% in vitro<sup>58</sup>. Power analysis, based on EEG slow wave energy (0.75–4.5 Hz) variance and a targeted 5% effect size, determined that a sample size of 78 (39 per group) is sufficient. In a dominant analysis, 45 heterozygous and 7 homozygous carriers of the minor allele (HtMi) were compared to 71 individuals homozygous for the major allele (HtMa). The groups showed no differences in demographics, sleep architecture, or responses to sleep deprivation.

To assess whether the AQP4 haplotype affects homeostatic sleep-wake regulation, EEG energy in NREM sleep across predefined frequency bands, subjective sleepiness, and cognitive performance were analyzed using a fixed sequence procedure. EEG slow wave energy, a marker of sleep intensity and duration, was the primary outcome. Results revealed that HtMi carriers exhibited significantly higher slow wave energy (SWE) than HtMa homozygotes, supported by post hoc slow wave power analysis. No significant differences were found in spindle activity, other frequency bands, or REM sleep.

The findings suggest that the AQP4 haplotype modulates deep NREM sleep intensity, linking AQP4 expression to CSF-driven brain pulsations. Preclinical evidence supports this, showing that slow wave intensity is directly associated with glymphatic influx<sup>33</sup>, and the absence of AQP4 in mice leads to brain impairments after sleep deprivation<sup>51</sup>. These results imply that HtMi carriers compensate for reduced AQP4 expression by increasing SWE, possibly enhancing parenchymal CSF flow. This modulation was consistent across both baseline and recovery nights indicating its presence under normal and sleep-deprived conditions.

To examine whether the AQP4 haplotype influences the homeostatic decline of slow waves, EEG SWE was analyzed across the first four NREM episodes in baseline and recovery nights. HtMi carriers exhibited higher SWE, primarily during the early night when sleep

pressure is highest. This effect, masked by delayed REM onset in HtMa homozygotes, became clearer when the first two NREM episodes were combined. The results suggest AQP4-dependent modulation of NREM sleep intensity and its possible link to fluid exchange across the blood-brain barrier or CSF clearance.

To assess the cognitive effects of AQP4 haplotype modulation of SWE, psychomotor vigilance (PVT) and subjective sleepiness (SSS) were analyzed during prolonged wakefulness. HtMi carriers showed a smaller increase in sleepiness ratings and a less pronounced decline in PVT response speed from day 1 to day 2 compared to HtMa homozygotes. While lapses of attention were similar, the findings suggest cognitive consequences of altered AQP4 expression, particularly under sleep deprivation. These results link the AQP4 haplotype to NREM SWE modulation and its role in the restorative effects of sleep on cognition, warranting further investigation.

## 15.2 MR-detected physiological brain oscillation and brain-fluid dynamics

Here we establish for the first time that MR-detected brain pulsations in cardiac and respiratory frequency ranges are causally linked to their corresponding physiological processes. This is evidenced by the elimination of respiration-related peaks in the MREG-spectra during breath-holding and the suppression of cardiac-related peaks during the Valsalva manoeuvre. In further support of this causal relationship, we show that measured respiration- and heart rates are closely correlated with the frequencies of peaks in both the MREG- and MB-spectra in their respective frequency ranges.

The physiological interpretation of MREG-detected brain oscillations has previously been suggested to reflect either the direct imaging of brain fluid motion, signifying CSF exchanges in humans<sup>64,67</sup>, or imaged tissue oscillations induced by travelling pressure waves – and thus reflective of the underlying compliance of brain tissue, encompassing factors such as water content or tissue viscosity<sup>103,104</sup>. Our data supports this interpretation by demonstrating that both MREG- and MB-detected respiration- and cardiac-driven brain pulsations are significantly stronger in CSF than in grey and white matter. We also show that these pulsations are more pronounced in grey matter than in white matter. Considering that water content and viscosity vary across these three brain tissue types<sup>68,69</sup>, this suggests that the strength of the signal is directly related to water content in the parenchyma. As fluid flow in the parenchyma is conceivably intimately associated to the amount of water in the parenchyma, our data cannot distinguish whether we are measuring one or the other. However, it strongly implies that increase in CSF influx to the brain parenchyma will lead to increases in MREG detected brain pulsation.

Descriptions of the effects of breath-holding and the Valsalva Maneuver on physiological brain oscillations, along with the discussion thereof, were included in an earlier version of *Appendix B* and can be read in full detail in [this preprint](#)<sup>1</sup>

### 15.3 Respiration- and cardiac driven brain pulsations correlate with sleep slow waves

Indeed, when examining respiration- and cardiac-driven brain pulsations across vigilance states while controlling for circadian rhythms and sleep pressure, we found a significant increase during slow-wave-rich NREM sleep. Interestingly, this effect was more pronounced in gray and white matter than in CSF spaces, supporting a sleep-dependent increase in CSF influx into the brain parenchyma and an expansion of extracellular space, consistent with observations in mouse models<sup>105</sup>.

As initially intended, we also investigated the relationship between sleep slow waves and brain pulsations. We found that pulsation strength increased with sleep depth, being greater in N3 than N2 sleep, and correlated with EEG delta power, a measure of slow-wave activity. This association supports the hypothesis that synchronized neuronal activity during slow-wave sleep drives fluid and solute movement through the brain, as observed in rodent studies<sup>106</sup>.

Since EEG delta power is a marker of homeostatic sleep propensity<sup>12</sup>, its correlation with brain pulsation strength—and thereby brain fluid flow—suggests that these processes are homeostatically regulated and fundamental to sleep function. Our findings align with preclinical evidence linking EEG slow waves to CSF influx and perfusion in the brain parenchyma<sup>33</sup>.

Together with our findings in the AQ4-genotyping study, we thus here provide support for the hypothesis that, as in mice, human sleep and slow-wave activity facilitate CSF-interstitial fluid exchange, aiding in the clearance of waste products from the brain.

### 15.4 LFOs and cerebrovascular oscillations

For LFOs we observe that the dynamic increase in ICP while performing the Valsalva manoeuvre leads to a prominent increase in MREG spectral power in frequencies below 0.1 Hz<sup>1</sup>. As this effect mirrors the behaviour of ICP monitored B-waves (0.01 – 0.33 Hz), which are known to increase with rising ICP and are thought to reflect cerebrovascular oscillations, we here provide a (admittedly small) piece of causal evidence that MR-detected LFOs reflect cerebral vasomotion. Although the effect was quite pronounced across the examined individuals, we should of course keep in mind that this was a descriptive study of only four

4 participants – without statistical tests – which does limit the generalisability of our findings. Moreover, due to the timespans of the Valsalva manoeuvre (and breath-holding) of 30 seconds, all power estimates in frequencies below 0.033 Hz should, according to the Shannon-Nyquist theorem, be interpreted with caution.

However, the finding in MB data that LFOs are stronger in grey matter than in both white matter and CSF support the notion that they reflect a signal from the vasculature – which would be expected to be strongest where vascular density is highest. Although the tissue type effect was apparent in both the B-wave frequency band of 0.012-0.034 Hz and in the broader frequency band of 0.012-0.1Hz, the visual observation that the effects were largest in frequencies below 0.05 Hz lend further support to the hypothesis that MR-detected LFOs are, in fact, a non-invasive measure of B-waves – and therefore cerebrovascular oscillations.

Last, but not least, the acute intervention arm of our sleep and sleep deprivation study with carvedilol showed a significant dampening of LFOs during sleep. As carvedilol is a nonselective  $\beta$ 1-,  $\beta$ 2- and  $\alpha$ 1-adrenergic antagonist, which is known to inhibit smooth muscle contraction and thereby potentially decreases cerebral vasomotor activity, this creates a direct link between modulations of vasomotion and modulation of MR-detected LFOs. This finding mirrors preclinical work showing that systemic adrenergic agonism increases pulsatility of pial arteries and arterioles<sup>45,46</sup> thus adding a translational link to the hypothesis that LFOs originate from cerebrovascular oscillations.

## 15.5 Cerebrovascular oscillations and heightened sleep pressure

Having established that the measurements obtained using accelerated imaging at frequencies below 0.05 Hz likely reflect cerebrovascular oscillations, I will now explore the intriguing findings associated with these oscillations.

Contrary to what has previously been suggested, our study demonstrates that sleep deprivation, rather than sleep itself, enhances brain LFOs. This finding is important because LFOs – or cerebrovascular oscillations – are thought to drive cerebrospinal fluid flow in the perivascular spaces, facilitating brain clearance. Our results thus provide a new perspective on previous interpretations of the relationship between sleep and cerebrovascular oscillations in humans by Fultz et al.<sup>108</sup> and the Kiviniemi group, who did not account for the impact of sleep pressure and circadian rhythm on their measures.

This finding challenges the concept of sleep as a sole driver of glymphatic flow and indicates that as waste and sleep pressure builds up during the day and during sleep deprivation<sup>48</sup>, the brain has compensatory restorative clearance mechanisms in place. If this

is the case, it seems that cerebrovascular oscillations may either be under homeostatic regulation or may themselves play a role in the potential sleep-wake regulation of fluid flow in the brain.

Interestingly, we also observed a correlation between LFOs during sleep and objective markers of sleep pressure before sleep. We also saw that their strength during sleep relates to the improvement in psychomotor vigilance (i.e., improvement of reaction times and lapses of attention) from the nap in the scanner. This indicates a direct restorative function of cerebrovascular oscillation during sleep – even though they decreased from sleep deprived wakefulness to sleep.

This finding may explain the differences in findings between our, and earlier studies where we do not find any difference between rested wakefulness and N2N3 sleep, whereas others has found an increase with N1N2 sleep compared to wakefulness. As sleep pressure dissipates over time spent asleep, this might indicate that cerebrovascular oscillations are most active in the early and lighter sleep stages, while they may lower in intensity with time spent asleep. However, to understand this correlation with sleep pressure during sleep better, a future study would need to include both sleep deprivation and all three sleep stages, whereas we did unfortunately not have enough data to compare N2 and N3 sleep for LFOs.

## 15.6 Cerebrovascular oscillations and plasma norepinephrine

Following the observation of a significant increase in LFOs during sleep deprivation using MREG imaging, we analysed the MB data collected concurrently in our study. Given MB's higher spatial resolution, we hypothesized that it would offer greater sensitivity to cerebrovascular oscillations. This analysis aimed both to validate our sleep deprivation findings using an independent method and to explore the hypothesis proposed by Picchioni and colleagues<sup>109</sup> that autonomic arousal may drive cerebrovascular oscillations. Their group demonstrated that autonomic arousals during K-complexes in sleep better explained LFOs in the cortex and fourth ventricle than neural slow waves. To investigate this, we examined the relationship between LFO strength across sleep stages and plasma norepinephrine levels, a marker of autonomic arousal and sympathetic activity.

Our data shows that in rested wakefulness, levels of p-NE strongly correlate with LFO strength, and that this relationship persists during sleep, where an increase in p-NE from rested to sleep-deprived status correlates with the increase in LFO spectral power from rested wakefulness to NREM sleep (stages N2 and N3). Therefore, we can proudly present the first human evidence that cerebrovascular oscillations are modulated by plasma norepinephrine levels – and therefore possibly sympathetic activity.

As circulating norepinephrine levels are known to decrease during sleep, this aligns with our observation that LFOs are strongest in N1 sleep, followed by N2, and weakest in N3. These findings, combined with the observed effect of sleep pressure on LFOs, suggest that cerebrovascular oscillations during sleep may be influenced by a combination of accumulated sleep pressure, bursts of autonomic activity in lighter sleep stages, and fluctuations in norepinephrine levels linked to vigilance and sleep stage transitions. This is further supported by preclinical evidence from naturally sleeping mice<sup>110</sup>, which demonstrates that transitions between sleep stages, microarousals, and wakefulness are associated with distinct constriction-dilation dynamics in cerebral arteries and arterioles.

Intriguingly, however, the increase found in LFOs during sleep deprived wakefulness in MREG – and confirmed in MB data - was not explained by increases in sympathetic activity, as changes in norepinephrine levels from rested to sleep-deprived conditions did not correlate with changes in LFO strength. As such, our data indicates that sleep deprivation promotes cerebrovascular activity independently of sympathetic activity.

In summary, we propose the existence of two distinct modulators of cerebrovascular oscillations: sleep pressure and sympathetic activity.

### 15.7 Adrenergic antagonism decreases LFOs and cardiac-driven brain pulsations

Following administration of carvedilol, most of the vigilance-state related increases in LFO- and cardiac induced brain pulsations diminished, or even disappeared. Carvedilol is a nonselective  $\beta$ 1-,  $\beta$ 2- and  $\alpha$ 1-adrenergic antagonist, which decreases heart contractility, lowers blood pressure, causes vasodilation<sup>111,112</sup> and, presumably, decreases cerebrovascular oscillations. The dampening effect of carvedilol on the MREG-detected LFO brain pulsations thus provides evidence for these pulsations as a measure of cerebrovascular oscillation (or: vasomotion; b-waves), while for MREG-detected cardiac brain pulsation, it reiterates the causality between cardiac action and brain pulsations in the cardiac frequency band. Our findings mirror preclinical work showing that systemic adrenergic agonism increases pulsatility of pial arteries and arterioles<sup>45,46</sup>.

Initially, we implemented carvedilol to assess its impact on brain pulsations through central adrenoreceptor inhibition. Preclinical evidence suggest that NE-levels shape sleep microarchitecture<sup>113</sup> and that central inhibition of NE receptors increases CSF-ISF exchange in the brain parenchyma<sup>105,114</sup> and promotes clearance of metabolite<sup>115</sup>. This central effect of NE was supported by our own group in an epidemiological study<sup>116</sup>, showing that chronic treatment with blood-brain barrier permeable (but not impermeable)  $\beta$ -blockers including

carvedilol, is associated with lower risk of Alzheimer's disease. But given that we observed a systemic response to carvedilol yet found no difference between the placebo and carvedilol sessions in sleep patterns during MR scans and recovery sleep, we conclude that carvedilol did not reach the central nervous system (CNS). Although carvedilol is predicted to be highly brain penetrant, we suspect that a single acute dose has low CN penetration, possibly due to active ATP-dependent efflux that may reduce CNS exposure to the drug<sup>111,117</sup>.

## 16. Limitations

This thesis includes studies on human participants, where the vast majority were males. For the Zürich sleep studies it was out of our hands as the data was collected by a separate group, however, we made the conscious decision to only include young males in our sleep study, to eliminate the effects of menstrual cycle and age. This naturally limits the generalisability of our findings.

None of our studies investigated N1 sleep specifically, which is potentially an area of interest.

Our findings relating to p-NE levels are limited by their relatively low numbers of participants.

It should be noted that spectral power calculations, including those used for quantifying MREG dependent brain pulsations, decline as a function of increased frequency (often referred to as the 1/f-effect). To account for 1/f-effects, we included epoch-wise base-10 logarithm of respiration- and heart rates in our statistical models when we evaluated respiration- and cardiac induced brain pulsations, respectively. While this procedure slightly reduced the difference in MREG spectral power between sleep and wakefulness in respiration- and cardiac frequency bands, it reduces the potential confounding of the 1/f effect.

## Conclusion

---

The purpose of this thesis was to explore the relationship between homeostatic sleep mechanisms and brain fluid dynamics. We first found evidence linking aquaporin-4 channel function to sleep slow wave production in humans. While not causal, these findings support the hypothesis that homeostatic sleep slow waves contribute to regulating parenchymal CSF flow.

Next, we investigated brain fluid dynamics in real-time during changes in vigilance and sleep stages while controlling for circadian mechanisms. We observed that brain pulsations induced by respiratory and cardiac rhythms – likely reflecting fluid motion or parenchymal water content – increased with slow-wave-rich sleep. Their strength correlated with deeper sleep and higher EEG delta power, markers of increased slow wave production. Notably, this effect was stronger in gray and white matter than in CSF, suggesting a specific increase in parenchymal fluid flow with sleep and aligning with rodent evidence of a sleep-dependent waste-clearing flow of CSF through the brain.

We also examined low-frequency oscillations (LFOs), believed to reflect cerebrovascular oscillations involved in propelling CSF through perivascular spaces. Contrary to current beliefs, we found that LFOs were strongly enhanced by sleep deprivation rather than sleep and correlated with plasma norepinephrine during both rested wakefulness and sleep. This suggests that LFOs may be regulated by both sleep pressure and sympathetic activity.

Collectively, our studies advance understanding of the interplay between homeostatic sleep mechanisms, vasomotor activity, brain fluid dynamics, and potentially, the clearance of waste products from the brain.

## References

---

1. Larsen SMU, Holst SC, Olsen AS, et al. Sleep pressure propels cerebrovascular oscillations while sleep intensity correlates with respiration- and cardiac-driven brain pulsations. Published online October 17, 2024:2024.10.16.24315580. doi:10.1101/2024.10.16.24315580
2. Cirelli C, Tononi G. Is Sleep Essential? *PLOS Biology*. 2008;6(8):e216. doi:10.1371/journal.pbio.0060216
3. Keene AC, Duboue ER. The origins and evolution of sleep. *J Exp Biol*. 2018;221(Pt 11):jeb159533. doi:10.1242/jeb.159533
4. Tononi G, Cirelli C. Sleep and the price of plasticity: from synaptic and cellular homeostasis to memory consolidation and integration. *Neuron*. 2014;81(1):12-34. doi:10.1016/j.neuron.2013.12.025
5. Belenky G, Wesensten NJ, Thorne DR, et al. Patterns of performance degradation and restoration during sleep restriction and subsequent recovery: a sleep dose-response study. *J Sleep Res*. 2003;12(1):1-12. doi:10.1046/j.1365-2869.2003.00337.x
6. Van Dongen HPA, Maislin G, Mullington JM, Dinges DF. The cumulative cost of additional wakefulness: dose-response effects on neurobehavioral functions and sleep physiology from chronic sleep restriction and total sleep deprivation. *Sleep*. 2003;26(2):117-126. doi:10.1093/sleep/26.2.117
7. Cajochen C, Reichert CF, Münch M, et al. Ultradian sleep cycles: Frequency, duration, and associations with individual and environmental factors—A retrospective study. *Sleep Health: Journal of the National Sleep Foundation*. 2024;10(1):S52-S62. doi:10.1016/j.sleh.2023.09.002
8. Kales A, Rechtschaffen A, University of California LA, Brain Information Service, National Institute of Neurological Diseases and Blindness (U.S.). *A Manual of Standardized Terminology, Techniques and Scoring System for Sleep Stages of Human Subjects*. United States Government Printing Office; 1968.
9. Dijk DJ. Regulation and Functional Correlates of Slow Wave Sleep. *Journal of Clinical Sleep Medicine*. 2009;5(2 suppl):S6-S15. doi:10.5664/jcsm.5.2S.S6
10. Buckelmüller J, Landolt HP, Stassen HH, Achermann P. Trait-like individual differences in the human sleep electroencephalogram. *Neuroscience*. 2006;138(1):351-356. doi:10.1016/j.neuroscience.2005.11.005
11. Borbély AA, Daan S, Wirz-Justice A, Deboer T. The two-process model of sleep regulation: a reappraisal. *J Sleep Res*. 2016;25(2):131-143. doi:10.1111/jsr.12371
12. Borbély AA. A two process model of sleep regulation. *Hum Neurobiol*. 1982;1(3):195-204.
13. Achermann P, Borbély AA. Mathematical models of sleep regulation. *Front Biosci*. 2003;8:s683-693. doi:10.2741/1064
14. Vyazovskiy VV, Kopp C, Wigger E, Jones MEE, Simpson ER, Tobler I. Sleep and rest regulation in young and old oestrogen-deficient female mice. *J Neuroendocrinol*. 2006;18(8):567-576. doi:10.1111/j.1365-2826.2006.01452.x

15. Borbély AA, Baumann F, Brandeis D, Strauch I, Lehmann D. Sleep deprivation: effect on sleep stages and EEG power density in man. *Electroencephalogr Clin Neurophysiol*. 1981;51(5):483-495. doi:10.1016/0013-4694(81)90225-x
16. Huber R, Ghilardi MF, Massimini M, Tononi G. Local sleep and learning. *Nature*. 2004;430(6995):78-81. doi:10.1038/nature02663
17. Kattler H, Dijk DJ, Borbély AA. Effect of unilateral somatosensory stimulation prior to sleep on the sleep EEG in humans. *J Sleep Res*. 1994;3(3):159-164. doi:10.1111/j.1365-2869.1994.tb00123.x
18. Borbély AA, Achermann P. Sleep homeostasis and models of sleep regulation. *J Biol Rhythms*. 1999;14(6):557-568. doi:10.1177/074873099129000894
19. Abbott NJ, Pizzo ME, Preston JE, Janigro D, Thorne RG. The role of brain barriers in fluid movement in the CNS: is there a “glymphatic” system? *Acta Neuropathol*. 2018;135(3):387-407. doi:10.1007/s00401-018-1812-4
20. Damkier HH, Brown PD, Praetorius J. Cerebrospinal fluid secretion by the choroid plexus. *Physiol Rev*. 2013;93(4):1847-1892. doi:10.1152/physrev.00004.2013
21. Rasmussen MK, Mestre H, Nedergaard M. Fluid transport in the brain. *Physiol Rev*. 2022;102(2):1025-1151. doi:10.1152/physrev.00031.2020
22. Spector R, Robert Snodgrass S, Johanson CE. A balanced view of the cerebrospinal fluid composition and functions: Focus on adult humans. *Exp Neurol*. 2015;273:57-68. doi:10.1016/j.expneurol.2015.07.027
23. Lei Y, Han H, Yuan F, Javed A, Zhao Y. The brain interstitial system: Anatomy, modeling, in vivo measurement, and applications. *Prog Neurobiol*. 2017;157:230-246. doi:10.1016/j.pneurobio.2015.12.007
24. Cipolla MJ. *The Cerebral Circulation*. Morgan & Claypool Life Sciences; 2009. Accessed January 8, 2025. <http://www.ncbi.nlm.nih.gov/books/NBK53081/>
25. Zhu WM, Neuhaus A, Beard DJ, Sutherland BA, DeLuca GC. Neurovascular coupling mechanisms in health and neurovascular uncoupling in Alzheimer’s disease. *Brain*. 2022;145(7):2276-2292. doi:10.1093/brain/awac174
26. Wu D, Chen Q, Chen X, Han F, Chen Z, Wang Y. The blood–brain barrier: Structure, regulation and drug delivery. *Sig Transduct Target Ther*. 2023;8(1):1-27. doi:10.1038/s41392-023-01481-w
27. Mokri B. The Monro-Kellie hypothesis: applications in CSF volume depletion. *Neurology*. 2001;56(12):1746-1748. doi:10.1212/wnl.56.12.1746
28. Hablitz LM, Nedergaard M. The Glymphatic System: A Novel Component of Fundamental Neurobiology. *J Neurosci*. 2021;41(37):7698-7711. doi:10.1523/JNEUROSCI.0619-21.2021
29. Bohr T, Hjorth PG, Holst SC, et al. The glymphatic system: Current understanding and modeling. *iScience*. 2022;25(9):104987. doi:10.1016/j.isci.2022.104987
30. Xie L, Kang H, Xu Q, et al. Sleep drives metabolite clearance from the adult brain. *Science*. 2013;342(6156):373-377. doi:10.1126/science.1241224
31. Iliff JJ, Wang M, Liao Y, et al. A paravascular pathway facilitates CSF flow through the brain parenchyma and the clearance of interstitial solutes, including amyloid  $\beta$ . *Sci Transl Med*. 2012;4(147):147ra111. doi:10.1126/scitranslmed.3003748

32. Mestre H, Hablitz LM, Xavier AL, et al. Aquaporin-4-dependent glymphatic solute transport in the rodent brain. *eLife*. 7. doi:10.7554/eLife.40070
33. Hablitz LM, Vinitsky HS, Sun Q, et al. Increased glymphatic influx is correlated with high EEG delta power and low heart rate in mice under anesthesia. *Sci Adv*. 2019;5(2):eaav5447. doi:10.1126/sciadv.aav5447
34. Jiang-Xie LF, Drieu A, Bhasiin K, Quintero D, Smirnov I, Kipnis J. Neuronal dynamics direct cerebrospinal fluid perfusion and brain clearance. *Nature*. 2024;627(8002):157-164. doi:10.1038/s41586-024-07108-6
35. Lopes DM, Wells JA, Ma D, et al. Glymphatic inhibition exacerbates tau propagation in an Alzheimer's disease model. *Alzheimer's Research & Therapy*. 2024;16(1):71. doi:10.1186/s13195-024-01439-2
36. Harrison IF, Ismail O, Machhada A, et al. Impaired glymphatic function and clearance of tau in an Alzheimer's disease model. *Brain*. 2020;143(8):2576-2593. doi:10.1093/brain/awaa179
37. Villemagne VL, Burnham S, Bourgeat P, et al. Amyloid  $\beta$  deposition, neurodegeneration, and cognitive decline in sporadic Alzheimer's disease: a prospective cohort study. *The Lancet Neurology*. 2013;12(4):357-367. doi:10.1016/S1474-4422(13)70044-9
38. Changes in intrathoracic pressure, not arterial pulsations, exert the greatest effect on tracer influx in the spinal cord - PubMed. Accessed January 7, 2025. <https://pubmed.ncbi.nlm.nih.gov/35135574/>
39. Mestre H, Tithof J, Du T, et al. Flow of cerebrospinal fluid is driven by arterial pulsations and is reduced in hypertension. *Nat Commun*. 2018;9(1):4878. doi:10.1038/s41467-018-07318-3
40. Hall A, O'Kane R. The best marker for guiding the clinical management of patients with raised intracranial pressure-the RAP index or the mean pulse amplitude? *Acta Neurochir (Wien)*. 2016;158(10):1997-2009. doi:10.1007/s00701-016-2932-z
41. Wilson MH. Monroe-Kellie 2.0: The dynamic vascular and venous pathophysiological components of intracranial pressure. *J Cereb Blood Flow Metab*. 2016;36(8):1338-1350. doi:10.1177/0271678X16648711
42. van Veluw SJ, Hou SS, Calvo-Rodriguez M, et al. Vasomotion as a Driving Force for Paravascular Clearance in the Awake Mouse Brain. *Neuron*. 2020;105(3):549-561.e5. doi:10.1016/j.neuron.2019.10.033
43. Holstein-Rønsbo S, Gan Y, Giannetto MJ, et al. Glymphatic influx and clearance are accelerated by neurovascular coupling. *Nat Neurosci*. 2023;26(6):1042-1053. doi:10.1038/s41593-023-01327-2
44. Bojarskaite L, Vallet A, Bjørnstad DM, et al. Sleep cycle-dependent vascular dynamics in male mice and the predicted effects on perivascular cerebrospinal fluid flow and solute transport. *Nat Commun*. 2023;14(1):953. doi:10.1038/s41467-023-36643-5
45. Harrison IF, Siow B, Akilo AB, et al. Non-invasive imaging of CSF-mediated brain clearance pathways via assessment of perivascular fluid movement with diffusion tensor MRI. Behrens TE, Okell TW, eds. *eLife*. 2018;7:e34028. doi:10.7554/eLife.34028

46. Iliff JJ, Wang M, Zeppenfeld DM, et al. Cerebral arterial pulsation drives paravascular CSF-interstitial fluid exchange in the murine brain. *J Neurosci.* 2013;33(46):18190-18199. doi:10.1523/JNEUROSCI.1592-13.2013
47. Yamamoto EA, Bagley JH, Geltzeiler M, et al. The perivascular space is a conduit for cerebrospinal fluid flow in humans: A proof-of-principle report. *Proceedings of the National Academy of Sciences.* 2024;121(42):e2407246121. doi:10.1073/pnas.2407246121
48. Eide PK, Vinje V, Pripp AH, Mardal KA, Ringstad G. Sleep deprivation impairs molecular clearance from the human brain. *Brain.* 2021;144(3):863-874. doi:10.1093/brain/awaa443
49. Chen L, Qi X, Zheng J. Altered Regional Cortical Brain Activity in Healthy Subjects After Sleep Deprivation: A Functional Magnetic Resonance Imaging Study. *Front Neurol.* 2018;9. doi:10.3389/fneur.2018.00588
50. Shokri-Kojori E, Wang GJ, Wiers CE, et al.  $\beta$ -Amyloid accumulation in the human brain after one night of sleep deprivation. *Proc Natl Acad Sci U S A.* 2018;115(17):4483-4488. doi:10.1073/pnas.1721694115
51. Holth JK, Fritschi SK, Wang C, et al. The sleep-wake cycle regulates brain interstitial fluid tau in mice and CSF tau in humans. *Science.* 2019;363(6429):880-884. doi:10.1126/science.aav2546
52. Lucey BP, Hicks TJ, McLeland JS, et al. Effect of sleep on overnight cerebrospinal fluid amyloid  $\beta$  kinetics. *Ann Neurol.* 2018;83(1):197-204. doi:10.1002/ana.25117
53. Brzecka A, Leszek J, Ashraf GM, et al. Sleep Disorders Associated With Alzheimer's Disease: A Perspective. *Front Neurosci.* 2018;12:330. doi:10.3389/fnins.2018.00330
54. Nagelhus EA, Ottersen OP. Physiological roles of aquaporin-4 in brain. *Physiol Rev.* 2013;93(4):1543-1562. doi:10.1152/physrev.00011.2013
55. Haj-Yasein NN, Vindedal GF, Eilert-Olsen M, et al. Glial-conditional deletion of aquaporin-4 (Aqp4) reduces blood-brain water uptake and confers barrier function on perivascular astrocyte endfeet. *Proc Natl Acad Sci USA.* 2011;108(43):17815-17820. doi:10.1073/pnas.1110655108
56. Harrison IF, Ismail O, Machhada A, et al. Impaired glymphatic function and clearance of tau in an Alzheimer's disease model. *Brain.* 2020;143(8):2576-2593. doi:10.1093/brain/awaa179
57. Sorani MD, Zador Z, Hurowitz E, Yan D, Giacomini KM, Manley GT. Novel variants in human Aquaporin-4 reduce cellular water permeability. *Hum Mol Genet.* 2008;17(15):2379-2389. doi:10.1093/hmg/ddn138
58. Woo J, Kim JE, Im JJ, et al. Astrocytic water channel aquaporin-4 modulates brain plasticity in both mice and humans: a potential gliogenetic mechanism underlying language-associated learning. *Mol Psychiatry.* 2018;23(4):1021-1030. doi:10.1038/mp.2017.113
59. Burfeind KG, Murchison CF, Westaway SK, et al. The effects of noncoding aquaporin-4 single-nucleotide polymorphisms on cognition and functional progression of Alzheimer's disease. *Alzheimers Dement (N Y).* 2017;3(3):348-359. doi:10.1016/j.trci.2017.05.001

60. Yadav BK, Oh SY, Kim NK, Shin BS. Association of rs2075575 and rs9951307 polymorphisms of AQP-4 gene with leukoaraiosis. *J Stroke Cerebrovasc Dis.* 2014;23(5):1199-1206. doi:10.1016/j.jstrokecerebrovasdis.2013.10.017
61. Kleffner I, Bungeroth M, Schiffbauer H, Schäbitz WR, Ringelstein EB, Kuhlenbäumer G. The role of aquaporin-4 polymorphisms in the development of brain edema after middle cerebral artery occlusion. *Stroke.* 2008;39(4):1333-1335. doi:10.1161/STROKEAHA.107.500785
62. Dardiotis E, Paterakis K, Tsivgoulis G, et al. AQP4 tag single nucleotide polymorphisms in patients with traumatic brain injury. *J Neurotrauma.* 2014;31(23):1920-1926. doi:10.1089/neu.2014.3347
63. Wang Y, van Gelderen P, de Zwart JA, et al. Cerebrovascular activity is a major factor in the cerebrospinal fluid flow dynamics. *Neuroimage.* 2022;258:119362. doi:10.1016/j.neuroimage.2022.119362
64. Hennig J, Kiviniemi V, Riemenschneider B, et al. 15 Years MR-encephalography. *MAGMA.* 2021;34(1):85-108. doi:10.1007/s10334-020-00891-z
65. Barth M, Breuer F, Koopmans PJ, Norris DG, Poser BA. Simultaneous multislice (SMS) imaging techniques. *Magn Reson Med.* 2016;75(1):63-81. doi:10.1002/mrm.25897
66. Helakari H, Korhonen V, Holst SC, et al. Human NREM Sleep Promotes Brain-Wide Vasomotor and Respiratory Pulsations. *J Neurosci.* 2022;42(12):2503-2515. doi:10.1523/JNEUROSCI.0934-21.2022
67. Kiviniemi V, Wang X, Korhonen V, et al. Ultra-fast magnetic resonance encephalography of physiological brain activity - Glymphatic pulsation mechanisms? *J Cereb Blood Flow Metab.* 2016;36(6):1033-1045. doi:10.1177/0271678X15622047
68. Budday S, Nay R, de Rooij R, et al. Mechanical properties of gray and white matter brain tissue by indentation. *J Mech Behav Biomed Mater.* 2015;46:318-330. doi:10.1016/j.jmbbm.2015.02.024
69. Whittall KP, MacKay AL, Graeb DA, Nugent RA, Li DK, Paty DW. In vivo measurement of T2 distributions and water contents in normal human brain. *Magn Reson Med.* 1997;37(1):34-43. doi:10.1002/mrm.1910370107
70. Picchioni D, Özbay PS, Mandelkow H, et al. Autonomic arousals contribute to brain fluid pulsations during sleep. *NeuroImage.* 2022;249:118888. doi:10.1016/j.neuroimage.2022.118888
71. Fultz NE, Bonmassar G, Setsompop K, et al. Coupled electrophysiological, hemodynamic, and cerebrospinal fluid oscillations in human sleep. *Science.* 2019;366(6465):628-631. doi:10.1126/science.aax5440
72. Gonzalez-Castillo J, Fernandez IS, Handwerker DA, Bandettini PA. Ultra-slow fMRI fluctuations in the fourth ventricle as a marker of drowsiness. *Neuroimage.* 2022;259:119424. doi:10.1016/j.neuroimage.2022.119424
73. Williams SD, Setzer B, Fultz NE, et al. Neural activity induced by sensory stimulation can drive large-scale cerebrospinal fluid flow during wakefulness in humans. *PLOS Biology.* 2023;21(3):e3002035. doi:10.1371/journal.pbio.3002035
74. Helakari H, Järvelä M, Väyrynen T, et al. Effect of sleep deprivation and NREM sleep stage on physiological brain pulsations. *Front Neurosci.* 2023;17:1275184. doi:10.3389/fnins.2023.1275184

75. Spiegelberg A, Preuß M, Kurtcuoglu V. B-waves revisited. *Interdisciplinary Neurosurgery*. 2016;6:13-17. doi:10.1016/j.inat.2016.03.004
76. Auer LM, Sayama I. Intracranial pressure oscillations (B-waves) caused by oscillations in cerebrovascular volume. *Acta Neurochir (Wien)*. 1983;68(1-2):93-100. doi:10.1007/BF01406205
77. Droste DW, Krauss JK, Berger W, Schuler E, Brown MM. Rhythmic oscillations with a wavelength of 0.5–2 min in transcranial Doppler recordings. *Acta Neurologica Scandinavica*. 1994;90(2):99-104. doi:10.1111/j.1600-0404.1994.tb02687.x
78. Krauss JK, Droste DW, Bohus M, et al. The relation of intracranial pressure B-waves to different sleep stages in patients with suspected normal pressure hydrocephalus. *Acta neurochir*. 1995;136(3):195-203. doi:10.1007/BF01410626
79. Rétey JV, Adam M, Gottselig JM, et al. Adenosinergic mechanisms contribute to individual differences in sleep deprivation-induced changes in neurobehavioral function and brain rhythmic activity. *J Neurosci*. 2006;26(41):10472-10479. doi:10.1523/JNEUROSCI.1538-06.2006
80. Bodenmann S, Xu S, Luhmann UFO, et al. Pharmacogenetics of modafinil after sleep loss: catechol-O-methyltransferase genotype modulates waking functions but not recovery sleep. *Clin Pharmacol Ther*. 2009;85(3):296-304. doi:10.1038/clpt.2008.222
81. Valomon A, Holst SC, Borrello A, et al. Effects of COMT genotype and tolcapone on lapses of sustained attention after sleep deprivation in healthy young men. *Neuropsychopharmacology*. 2018;43(7):1599-1607. doi:10.1038/s41386-018-0018-8
82. Bachmann V, Klaus F, Bodenmann S, et al. Functional ADA polymorphism increases sleep depth and reduces vigilant attention in humans. *Cereb Cortex*. 2012;22(4):962-970. doi:10.1093/cercor/bhr173
83. Hefti K, Holst SC, Sovago J, et al. Increased metabotropic glutamate receptor subtype 5 availability in human brain after one night without sleep. *Biol Psychiatry*. 2013;73(2):161-168. doi:10.1016/j.biopsych.2012.07.030
84. Weigend S, Holst SC, Meier J, Brock M, Kohler M, Landolt HP. Prolonged Waking and Recovery Sleep Affect the Serum MicroRNA Expression Profile in Humans. *Clocks & Sleep*. 2019;1(1):75-86. doi:10.3390/clockssleep1010008
85. Home - SNP - NCBI. Accessed January 7, 2025. <https://www.ncbi.nlm.nih.gov/snp/>
86. Yu JT, Tan L, Hardy J. Apolipoprotein E in Alzheimer's disease: an update. *Annu Rev Neurosci*. 2014;37:79-100. doi:10.1146/annurev-neuro-071013-014300
87. Dmitrienko A, D'Agostino R. Traditional multiplicity adjustment methods in clinical trials. *Stat Med*. 2013;32(29):5172-5218. doi:10.1002/sim.5990
88. Dinges DF, Powell JW. Microcomputer analyses of performance on a portable, simple visual RT task during sustained operations. *Behavior Research Methods, Instruments, & Computers*. 1985;17(6):652-655. doi:10.3758/BF03200977
89. Lim J, Dinges DF. Sleep deprivation and vigilant attention. *Ann N Y Acad Sci*. 2008;1129:305-322. doi:10.1196/annals.1417.002
90. Hoddes E, Dement W, Zarcone V. The development and use of the Stanford Sleepiness Scale (SSS). *Psychophysiology*. 1971;9:150.
91. Sturm A., Clarenbach P., Largiadèr F. & Wicki O. Checkliste Schlafstörungen. Checklisten der aktuellen Medizin. *Thieme*. Published online 1997.

92. Jerri AJ. The Shannon sampling theorem—Its various extensions and applications: A tutorial review. *Proceedings of the IEEE*. 1977;65(11):1565-1596. doi:10.1109/PROC.1977.10771
93. Horne JA, Ostberg O. A self-assessment questionnaire to determine morningness-eveningness in human circadian rhythms. *Int J Chronobiol*. 1976;4(2):97-110.
94. Buysse DJ, Reynolds CF, Monk TH, Berman SR, Kupfer DJ. The Pittsburgh Sleep Quality Index: a new instrument for psychiatric practice and research. *Psychiatry Res*. 1989;28(2):193-213. doi:10.1016/0165-1781(89)90047-4
95. Johns MW. A New Method for Measuring Daytime Sleepiness: The Epworth Sleepiness Scale. *Sleep*. 1991;14(6):540-545. doi:10.1093/sleep/14.6.540
96. Allen PJ, Josephs O, Turner R. A method for removing imaging artifact from continuous EEG recorded during functional MRI. *Neuroimage*. 2000;12(2):230-239. doi:10.1006/nimg.2000.0599
97. Niazy RK, Beckmann CF, Iannetti GD, Brady JM, Smith SM. Removal of FMRI environment artifacts from EEG data using optimal basis sets. *Neuroimage*. 2005;28(3):720-737. doi:10.1016/j.neuroimage.2005.06.067
98. Berry RB, Budhiraja R, Gottlieb DJ, et al. Rules for scoring respiratory events in sleep: update of the 2007 AASM Manual for the Scoring of Sleep and Associated Events. Deliberations of the Sleep Apnea Definitions Task Force of the American Academy of Sleep Medicine. *J Clin Sleep Med*. 2012;8(5):597-619. doi:10.5664/jcsm.2172
99. Delorme A, Makeig S. EEGLAB: an open source toolbox for analysis of single-trial EEG dynamics including independent component analysis. *J Neurosci Methods*. 2004;134(1):9-21. doi:10.1016/j.jneumeth.2003.10.009
100. Klem GH, Lüders HO, Jasper HH, Elger C. The ten-twenty electrode system of the International Federation. The International Federation of Clinical Neurophysiology. *Electroencephalogr Clin Neurophysiol Suppl*. 1999;52:3-6.
101. Weikop P, Kehr J, Scheel-Krüger J. Reciprocal effects of combined administration of serotonin, noradrenaline and dopamine reuptake inhibitors on serotonin and dopamine levels in the rat prefrontal cortex: the role of 5-HT1A receptors. *J Psychopharmacol*. 2007;21(8):795-804. doi:10.1177/0269881107077347
102. Ulv Larsen SM, Landolt HP, Berger W, Nedergaard M, Knudsen GM, Holst SC. Haplotype of the astrocytic water channel AQP4 is associated with slow wave energy regulation in human NREM sleep. *PLoS Biol*. 2020;18(5):e3000623. doi:10.1371/journal.pbio.3000623
103. Sloots JJ, Biessels GJ, Zwanenburg JJM. Cardiac and respiration-induced brain deformations in humans quantified with high-field MRI. *Neuroimage*. 2020;210:116581. doi:10.1016/j.neuroimage.2020.116581
104. Dreha-Kulaczewski S, Joseph AA, Merboldt KD, Ludwig HC, Gärtner J, Frahm J. Inspiration is the major regulator of human CSF flow. *J Neurosci*. 2015;35(6):2485-2491. doi:10.1523/JNEUROSCI.3246-14.2015
105. Xie L, Kang H, Xu Q, et al. Sleep drives metabolite clearance from the adult brain. *Science*. 2013;342(6156):373-377. doi:10.1126/science.1241224

106. Jiang-Xie LF, Drieu A, Bhasiin K, Quintero D, Smirnov I, Kipnis J. Neuronal dynamics direct cerebrospinal fluid perfusion and brain clearance. *Nature*. 2024;627(8002):157-164. doi:10.1038/s41586-024-07108-6
107. Kubíková T, Kochová P, Tomášek P, Witter K, Tonar Z. Numerical and length densities of microvessels in the human brain: Correlation with preferential orientation of microvessels in the cerebral cortex, subcortical grey matter and white matter, pons and cerebellum. *J Chem Neuroanat*. 2018;88:22-32. doi:10.1016/j.jchemneu.2017.11.005
108. Fultz NE, Bonmassar G, Setsompop K, et al. Coupled electrophysiological, hemodynamic, and cerebrospinal fluid oscillations in human sleep. *Science*. 2019;366(6465):628-631. doi:10.1126/science.aax5440
109. Picchioni D, Özbay PS, Mandelkow H, et al. Autonomic arousals contribute to brain fluid pulsations during sleep. *Neuroimage*. 2022;249:118888. doi:10.1016/j.neuroimage.2022.118888
110. Bojarskaite L, Vallet A, Bjørnstad DM, et al. Sleep cycle-dependent vascular dynamics in male mice and the predicted effects on perivascular cerebrospinal fluid flow and solute transport. *Nat Commun*. 2023;14(1):953. doi:10.1038/s41467-023-36643-5
111. Bart J, Dijkers ECF, Wegman TD, et al. New positron emission tomography tracer [(11)C]carvedilol reveals P-glycoprotein modulation kinetics. *Br J Pharmacol*. 2005;145(8):1045-1051. doi:10.1038/sj.bjp.0706283
112. Dulin B, Abraham WT. Pharmacology of carvedilol. *Am J Cardiol*. 2004;93(9A):3B-6B. doi:10.1016/j.amjcard.2004.01.003
113. Kjaerby C, Andersen M, Hauglund N, et al. Memory-enhancing properties of sleep depend on the oscillatory amplitude of norepinephrine. *Nat Neurosci*. 2022;25(8):1059-1070. doi:10.1038/s41593-022-01102-9
114. Lilius TO, Blomqvist K, Hauglund NL, et al. Dexmedetomidine enhances glymphatic brain delivery of intrathecally administered drugs. *J Control Release*. 2019;304:29-38. doi:10.1016/j.jconrel.2019.05.005
115. Benveniste H, Lee H, Ding F, et al. Anesthesia with Dexmedetomidine and Low-dose Isoflurane Increases Solute Transport via the Glymphatic Pathway in Rat Brain When Compared with High-dose Isoflurane. *Anesthesiology*. 2017;127(6):976-988. doi:10.1097/ALN.0000000000001888
116. Beaman EE, Bonde AN, Larsen SMU, et al. Blood-brain barrier permeable  $\beta$ -blockers linked to lower risk of Alzheimer's disease in hypertension. *Brain*. 2023;146(3):1141-1151. doi:10.1093/brain/awac076
117. Elsinga PH, Hendrikse NH, Bart J, Vaalburg W, van Waarde A. PET Studies on P-glycoprotein function in the blood-brain barrier: how it affects uptake and binding of drugs within the CNS. *Curr Pharm Des*. 2004;10(13):1493-1503. doi:10.2174/1381612043384736

## Appendix

---

- A. **Ulv Larsen SM**, Landolt HP, Berger W, Nedergaard M, Knudsen GM, Holst SC. Haplotype of the astrocytic water channel AQP4 is associated with slow wave energy regulation in human NREM sleep. *PLoS Biol.* May 2020.
- B. **Ulv Larsen SM\***, Holst SC\*, Olsen AS, Ozenne B, Zilstorff DB, Brendstrup-Brix K, Weikop P, Pleinert S, Kiviniemi V, Jennum PJ, Nedergaard M, Knudsen GM. Sleep pressure promotes cerebrovascular oscillations while respiration- and cardiac-driven brain pulsations escalate with sleep intensity. *Submitted to PLoS Biology January 2025. Previous version incl. study II published on medRxiv Oct 2024<sup>1</sup>.*
- C. **Ulv Larsen SM**, Olsen AS, Zilstorff DB, Ozenne B, Pleinert S, Norberg CL, Brendstrup-Brix K, Weikop P, Jennum PJ, Nedergaard M, Holst SC, Knudsen GM. The role of norepinephrine and sleep deprivation on cerebrovascular oscillations in humans. *Manuscript in prep.*

---

\* These authors contributed equally to the work

# Appendix A

---

## SHORT REPORTS

# Haplotype of the astrocytic water channel AQP4 is associated with slow wave energy regulation in human NREM sleep

Sara Marie Ulv Larsen<sup>1</sup>, Hans-Peter Landolt<sup>2,3,4,5</sup>, Wolfgang Berger<sup>3,4,6</sup>, Maiken Nedergaard<sup>7</sup>, Gitte Moos Knudsen<sup>1,8</sup>, Sebastian Camillo Holst<sup>1,5\*</sup>

**1** Neurobiology Research Unit, Copenhagen University Hospital, Rigshospitalet, Copenhagen, Denmark, **2** Institute of Pharmacology & Toxicology, University of Zurich, Zurich, Switzerland, **3** Zurich Center for Integrative Human Physiology, University of Zurich, Zurich, Switzerland, **4** Neuroscience Center Zurich, University and ETH Zurich, Zurich, Switzerland, **5** Sleep & Health Zurich, University Center of Competence, Zurich, Switzerland, **6** Institute of Medical Molecular Genetics, University of Zurich, Schlieren, Switzerland, **7** Center for Translational Neuromedicine, University of Copenhagen, Copenhagen, Denmark, **8** Faculty of Health and Medical Sciences, University of Copenhagen, Copenhagen, Denmark

\* [holst@nru.dk](mailto:holst@nru.dk)



## OPEN ACCESS

**Citation:** Ulv Larsen SM, Landolt H-P, Berger W, Nedergaard M, Knudsen GM, Holst SC (2020) Haplotype of the astrocytic water channel AQP4 is associated with slow wave energy regulation in human NREM sleep. *PLoS Biol* 18(5): e3000623. <https://doi.org/10.1371/journal.pbio.3000623>

**Academic Editor:** Paul Shaw, Washington University, St. Louis, UNITED STATES

**Received:** December 9, 2019

**Accepted:** April 2, 2020

**Published:** May 5, 2020

**Peer Review History:** PLOS recognizes the benefits of transparency in the peer review process; therefore, we enable the publication of all of the content of peer review and author responses alongside final, published articles. The editorial history of this article is available here: <https://doi.org/10.1371/journal.pbio.3000623>

**Copyright:** © 2020 Ulv Larsen et al. This is an open access article distributed under the terms of the [Creative Commons Attribution License](https://creativecommons.org/licenses/by/4.0/), which permits unrestricted use, distribution, and reproduction in any medium, provided the original author and source are credited.

**Data Availability Statement:** Individual anonymized observations that underlie the data summarized in the figures are included in [S1–S5](#) Data files. For further information or details please

## Abstract

Cerebrospinal fluid (CSF) flow through the brain parenchyma is facilitated by the astrocytic water channel aquaporin 4 (AQP4). Homeostatically regulated electroencephalographic (EEG) slow waves are a hallmark of deep non-rapid eye movement (NREM) sleep and have been implicated in the regulation of parenchymal CSF flow and brain clearance. The human *AQP4* gene harbors several single nucleotide polymorphisms (SNPs) associated with AQP4 expression, brain-water homeostasis, and neurodegenerative diseases. To date, their role in sleep-wake regulation is unknown. To investigate whether functional variants in *AQP4* modulate human sleep, nocturnal EEG recordings and cognitive performance were investigated in 123 healthy participants genotyped for a common eight-SNP *AQP4*-haplotype. We show that this *AQP4*-haplotype is associated with distinct modulations of NREM slow wave energy, strongest in early sleep and mirrored by changes in sleepiness and reaction times during extended wakefulness. The study provides the first human evidence for a link between AQP4, deep NREM sleep, and cognitive consequences of prolonged wakefulness.

## Introduction

Glial-dependent cerebrospinal fluid (CSF) flow through the brain parenchyma, by some termed the glymphatic system, facilitates the removal of waste by generating a convective flow of CSF and interstitial fluid [1,2]. Evidence suggests that the pathway relies on 3 main processes: Firstly, bulk flow of CSF through perivascular spaces is generated by arterial pulsations from the heartbeat and potentially to a lesser extent by pulsations from the respiration [3]. Secondly, movements of CSF from the perivascular space into the brain parenchyma relies on the water channel aquaporin 4 (AQP4), which is highly expressed on astrocytic vascular endfeet

contact the Neurobiology Research Unit in Copenhagen (Dr. Holst: [holst@nru.dk](mailto:holst@nru.dk), or MD Ulv Larsen: [sara.larsen@nru.dk](mailto:sara.larsen@nru.dk)) or the Psychopharmacology Laboratory at the University of Zurich (Prof. Landolt: [landolt@pharma.uzh.ch](mailto:landolt@pharma.uzh.ch)).

**Funding:** This project has received funding from the European Union's Horizon 2020 research and innovation programme under the Marie Skłodowska-Curie grant agreement No 798131 (to SCH), by a fellowship from the Copenhagen University hospital, Rigshospitalet R151-A6534 (to SMUL) and by grants from the Swiss National Science Foundation 31-67060.01; 310000-120377; 3100A0-107874; 320030\_135414; 320030\_163439 (to HPL). The funders had no role in study design, data collection and analysis, decision to publish, or preparation of the manuscript.

**Competing interests:** The authors have declared that no competing interests exist.

**Abbreviations:** APOE, Apolipoprotein E; AQP4, aquaporin 4; CSF, cerebrospinal fluid; ECG, electrocardiogram; EEG, electroencephalographic; EMG, electromyogram; EOG, electrooculogram; HtMa, HtMi; LD, linkage disequilibrium; MAF, minor allele frequency; NREM, non-rapid eye movement; PVT, psychomotor vigilance test; SNP, single nucleotide polymorphism; SSS, Stanford sleepiness scale; SWE, slow wave energy.

[1,4]. Mice lacking AQP4 show a strong reduction in parenchymal CSF influx [4,5] and increased interstitial beta-amyloid depositions [6], which is ameliorated by sleep deprivation [7]. Thirdly, the inward flow of CSF through AQP4 channels mainly occurs during non-rapid eye movement (NREM) sleep [8], and in preclinical studies, glymphatic flow is positively correlated with slow wave intensity during different types of anesthesia [9].

Emerging data support the existence of sleep driven CSF movements and clearance in the human brain. Increased levels of intracerebral tau and  $\beta$ -amyloid have been observed in healthy adults after sleep loss [10,11], and recently sleep dependent pulsations in the fourth ventricle were demonstrated in the human brain [12]. To date, however, no studies have described the link between AQP4 and human sleep-wake regulation or investigated whether genetic modulation of AQP4 may have restorative effects on cognitive functions after sleep loss.

The gene encoding AQP4 is located on chromosome 18 (18q11.2–q12.1) [13] (Fig 1). Several thousand single nucleotide polymorphisms (SNPs) in the noncoding regions of AQP4 have so far been identified, and their function(s) in the normal and diseased human brain is an active area of research. Human AQP4 SNPs have been shown to impair cellular water permeability and water homeostasis in vitro [14]. Moreover, an array of studies have associated human AQP4 SNPs with neurological disorders including Alzheimer's disease progression [15], vascular depression phenotype [16], leukariosis [17], outcome after traumatic head injury [18], edema formation [19,20], and the risk of stroke [21]. These findings suggest a link between AQP4 and the development of brain diseases associated with waste deposition and fluid movements. Recently, a single variant within AQP4 was associated with a 15% to 20% change in AQP4 expression [22].

Here, we aimed to investigate the role of AQP4 in human sleep-wake regulation. We hypothesized that if NREM slow waves are the endogenous regulator of CSF brain pulsations, then a reduced expression of AQP4 should be associated with a compensatory increase in deep NREM sleep (Fig 1A). To investigate this association, a haplotype spanning AQP4 was genotyped a priori in a previously collected sample of 123 healthy participants from controlled sleep deprivation studies. Data from all-night electroencephalographic (EEG) recordings in baseline and recovery sleep as well as measurements of subjective sleepiness and global alertness throughout 40 hours of prolonged wakefulness were analyzed (Fig 1E).

## Results and discussion

### The AQP4-gene harbors an 8-SNP haplotype associated with AQP4 expression

Initial examination of SNPs in the AQP4-gene revealed a conserved haplotype spanning the entire gene with 2 common variants (Fig 1B). This haplotype consists of 8 SNPs, including rs335929 implicated in cognitive decline in Alzheimer's patients [15] and rs162008 demonstrated to reduce AQP4 expression [22]. Based on overall variance in EEG slow wave energy (SWE; 0.75–4.5 Hz) and the a priori aim to detect an effect size of at least 5%, power analysis suggests a required sample size of 78 (39 per group) as sufficient (see Methods). The AQP4-haplotypes were compared by means of dominant analysis, whereby 45 heterozygous subjects and 7 homozygotes were denoted as carriers of the minor allele (HtMi) and compared to 71 individuals homozygous for the major allele (HtMa) variant (S1 Data). The 2 groups did not differ in demographic characteristics (S1 and S2 Tables), presented with similar sleep architecture, and had a normal response to sleep deprivation (S3 Table).

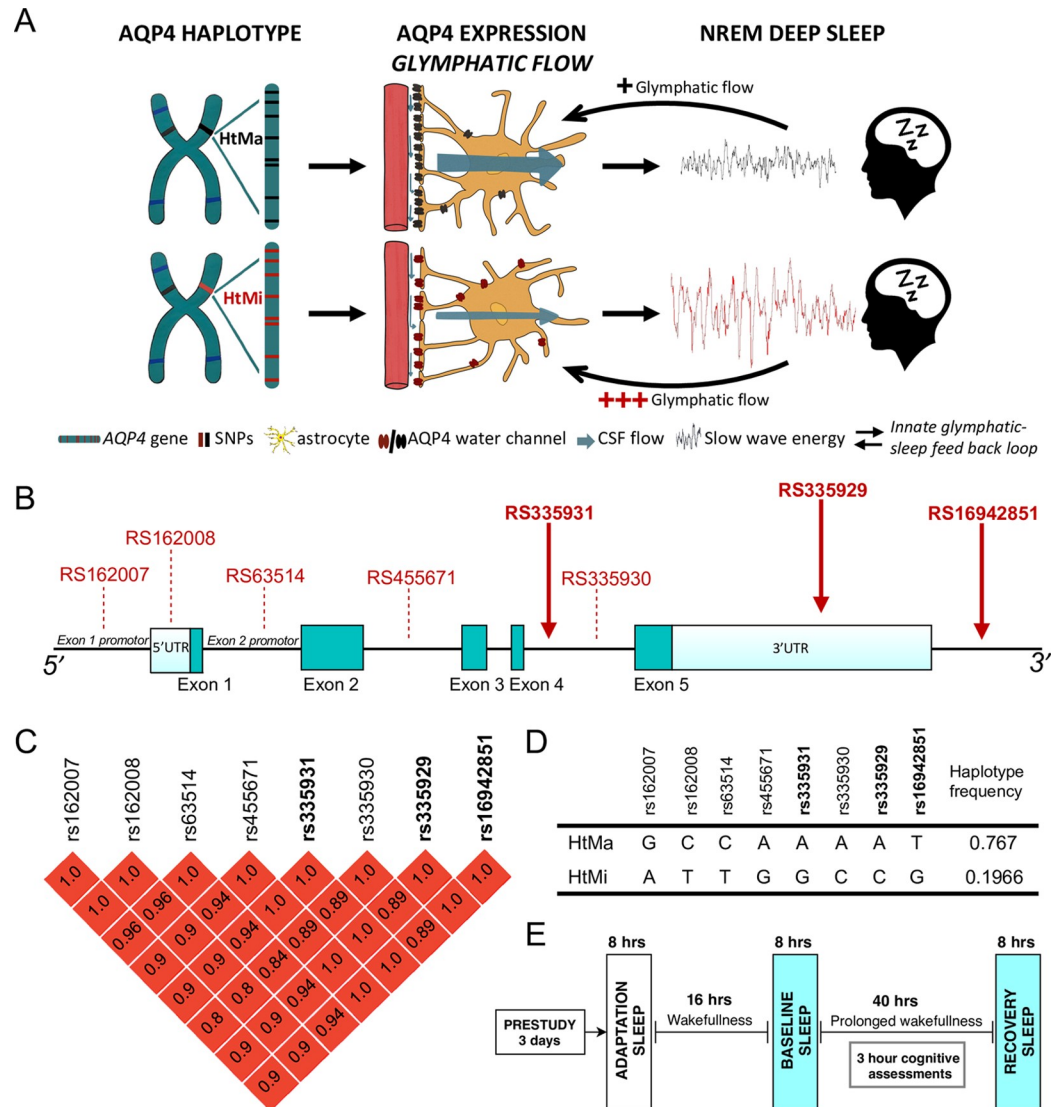


**Fig 1. Hypothesized role of the human AQP4-haplotype investigated in a controlled sleep deprivation study.** (A) Based on the genetic modulation of AQP4 protein expression [22], we hypothesized that the high AQP4 expressing variant of the AQP4-haplotype (HtMa; black) presents with improved glymphatic flow compared to the low AQP4 expressing HtMi variant (red). Assuming that NREM slow waves are the endogenous regulator of glymphatic flow, the HtMa variant require less SWE to initiate glymphatic flow than the HtMi variant, establishing an innate glymphatic-sleep feedback loop. (B) Physical map of the AQP4 gene and the location of the 8 haplotype SNPs. The 3 SNPs genotyped in this sample are marked with full red arrows. Dark green blocks: coding exons; light blue blocks: 5'- and 3'-untranslated regions. (C) LD block among the AQP4 SNPs in the investigated haplotype. The pairwise LD coefficients ( $r^2$ ) of SNPs in the LD block are color-scaled in red tones with dark red indicating perfect LD ( $r^2 = 1$ ). (D) Table shows bases at the 8 different SNP locations in the AQP4 gene for the 2 haplotypes HtMa (76.7%) and HtMi (19.7%) and their respective frequencies in the CEU and TSI populations, representative of the investigated Swiss cohort. A total of 3.7% of CEU and TSI are predicted to be carriers of rare haplotype variants [23]. Frequencies in investigated study population were close to the prediction (HtMa: 75.7%; HtMi: 23.5; others: 0.7%; S1 Data). (E) Visualization of study design common for all subjects included from 6 separate studies. After a minimum 3-day inclusion period with monitored bedtimes and no caffeine intake, all study participants underwent an adaptation night in the laboratory before baseline sleep, 40 hours prolonged wakefulness and a recovery night, adding up to more than 1,950 hours ( $123 \times 2 \times 8$  hours) of included sleep EEG recordings. Subjective sleepiness ratings and the approximately 10 min PVT were performed at 3-hour intervals. AQP4, aquaporin 4; CEU, Utah Residents from North and West Europe; EEG, electroencephalographic; HtMa, Major allele of haplotype; HtMi, Minor allele of haplotype; LD, linkage disequilibrium; NREM, non-rapid eye movement; PVT, psychomotor vigilance test; SNP, single nucleotide polymorphism; SWE, slow wave energy; TSI, Toscani in Italy;

<https://doi.org/10.1371/journal.pbio.3000623.g001>

## AQP4-haplotype is associated with a distinct modulation of slow waves in NREM sleep

The sleep EEG is genetically determined, with NREM sleep exhibiting up to 90% heritability [24], making it one of the most hereditary human traits described. To investigate whether the AQP4-haplotype modulates homeostatic sleep-wake regulation, EEG energy in predefined frequency bands in NREM sleep in baseline and recovery nights and the evolution of subjective sleepiness as well as cognitive performance measures were compared between the AQP4-haplotypes by a fixed sequence procedure [25] (see [Methods](#)). EEG SWE, which is a combined measure of sleep intensity and duration and is one of the best validated markers of sleep propensity in humans [26], was defined as the primary outcome variable. EEG quantification revealed that the HtMi carriers produced more SWE than the HtMa homozygotes (“genotype”:  $P < 0.03$ ; [Fig 2A](#)), an effect paralleled by post hoc slow wave power analysis ([S2 Fig](#)). These effects were not observed in the spindle range ( $P > 0.77$ ) or any other frequency band ( $P > 0.33$ ), nor in REM sleep ([S1 Fig](#)). The demonstrated AQP4-haplotype modulation of SWE documents an association between the intensity of deep NREM sleep and the expression of the AQP4-water channel, a relationship that may be central for CSF-driven brain pulsations. Given how recent preclinical evidence show that the intensity of slow waves is directly linked to glymphatic influx [9] and that the complete removal of AQP4 in mice results in brain impairments after sleep deprivation [7], this suggests an important role of AQP4-mediated clearance during sleep. The results appear in line with our initial hypothesis, suggesting that to compensate for a genetic reduction in AQP4 expression [22], AQP4 HtMi carriers increase SWE during NREM sleep, perhaps by an up-regulation of parenchymal CSF flow ([Fig 1A](#)). Interestingly, the AQP4-haplotype modulation was similar in baseline—and recovery nights (“genotype x night”:  $F_{1,120} = 0.37$ ;  $P > 0.55$ ;  $\eta_p^2 = 0.31\%$ ), proposing that the AQP4 modulation is present both under normal sleep conditions and following the sleep homeostatic challenge.

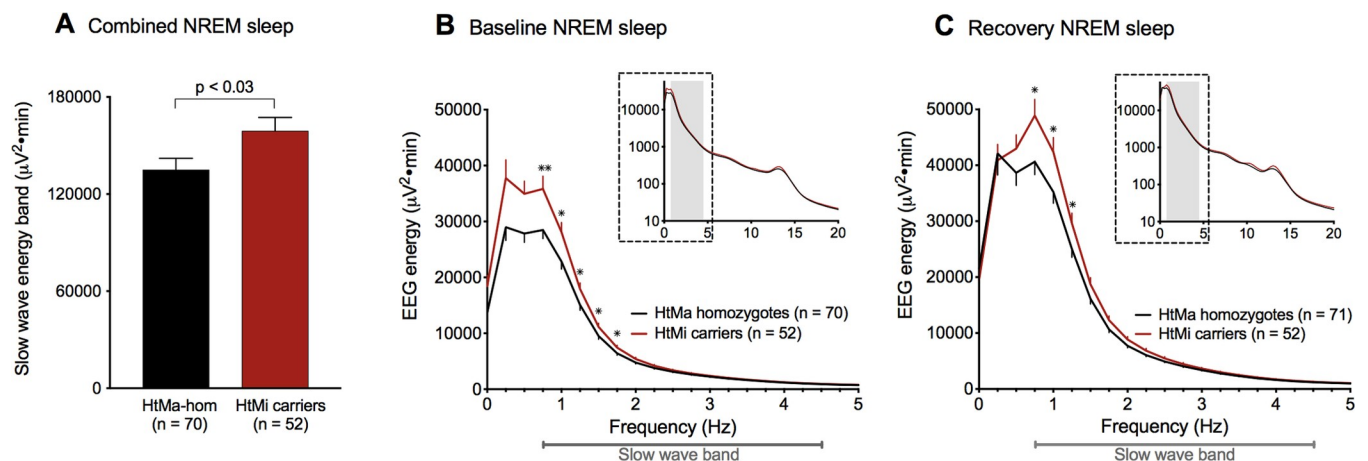


**Fig 2. AQP4-haplotype is associated with EEG energy regulation in the slow wave range.** Comparison of EEG energy (EEG power  $\times$  time) across baseline and recovery nights in the slow wave range (0.75–4.5 Hz) within the AQP4 haplotype variants HtMa homozygotes (black) and HtMi carriers (red). To minimize false positive results, EEG data was analyzed by a hypothesis-driven fixed sequence procedure that only revealed significant effects of AQP4 in the whole-night slow wave band, which was significantly increased in the AQP4 HtMi-carrier group when compared to HtMa homozygotes (A; “genotype”:  $F_{1,121} = 5.0$ ;  $P < 0.03$ ;  $\eta_p^2 = 3.95\%$ ). The effect was similar in baseline (B) and recovery (C) conditions and confined to the 0.75–2 Hz band. Inserts (B and C) represent full NREM sleep spectra for 0–20 Hz on log10 scale with gray shading indicating the slow wave band ([S2 Data](#)). Data represent mean  $\pm$  SEM. By-bin unpaired two-tailed  $t$  tests: \* $P < 0.05$ , \*\* $P < 0.01$ . AQP4, aquaporin 4; EEG, electroencephalographic; HtMa, Major allele of haplotype; HtMi, Minor allele of haplotype; NREM, non-rapid eye movement.

<https://doi.org/10.1371/journal.pbio.3000623.g002>

To localize the AQP4-dependent effect in the slow wave range, bin-wise frequency analysis was performed and revealed significantly higher energy in the 0.75 to 2 Hz range for the HtMi carriers than the HtMa homozygotes (Fig 2B and 2C and S2 and S5 Datas).

### EEG markers of sleep homeostasis in NREM sleep are associated with the AQP4-haplotype

To investigate whether the AQP4 haplotype modulates the well-known homeostatic decline of slow waves across sleep, EEG SWE was quantified across the first 4 NREM sleep episodes in baseline and recovery nights. Consistent with the all-night sleep EEG analysis, a main effect of the AQP4 haplotype was observed (“haplotype”:  $P < 0.03$ ; Fig 3A–3B), confirming the overall increased SWE levels in the HtMi-carrier group. Importantly, however, the haplotype effect was not constant across the night. Rather, AQP4 HtMi carriers showed increased EEG energy mainly in the early part of the night (“haplotype x NREM episode”:  $P < 0.05$ ; Fig 3A–3B) when sleep pressure is highest (S3 Data). This finding may suggest an AQP4-dependent homeostatic modulation of NREM sleep. The effect in the first NREM episode was masked by a small delay in REM onset ( $8.9 \pm 4.3$  min) in the HtMa homozygotes compared to the HtMi-carrier group (“haplotype”:  $F_{1,121} = 4.3$ ;  $P < 0.05$ ;  $\eta_p^2 = 3.41\%$ ; S3 Table), making the AQP4-haplotype modulation clearer when the first 2 NREM episodes were combined (Fig 3 inserts). The increased SWE in the low AQP4 protein expressing HtMi carriers indicates regulatory feedback between sleep intensity and AQP4 dependent water exchange (Fig 1A). Future studies are warranted to better understand whether the increase in SWE is also associated with increased CSF clearance or perhaps indicates that sleep intensity is related to an exchange of fluids across the blood brain barrier.

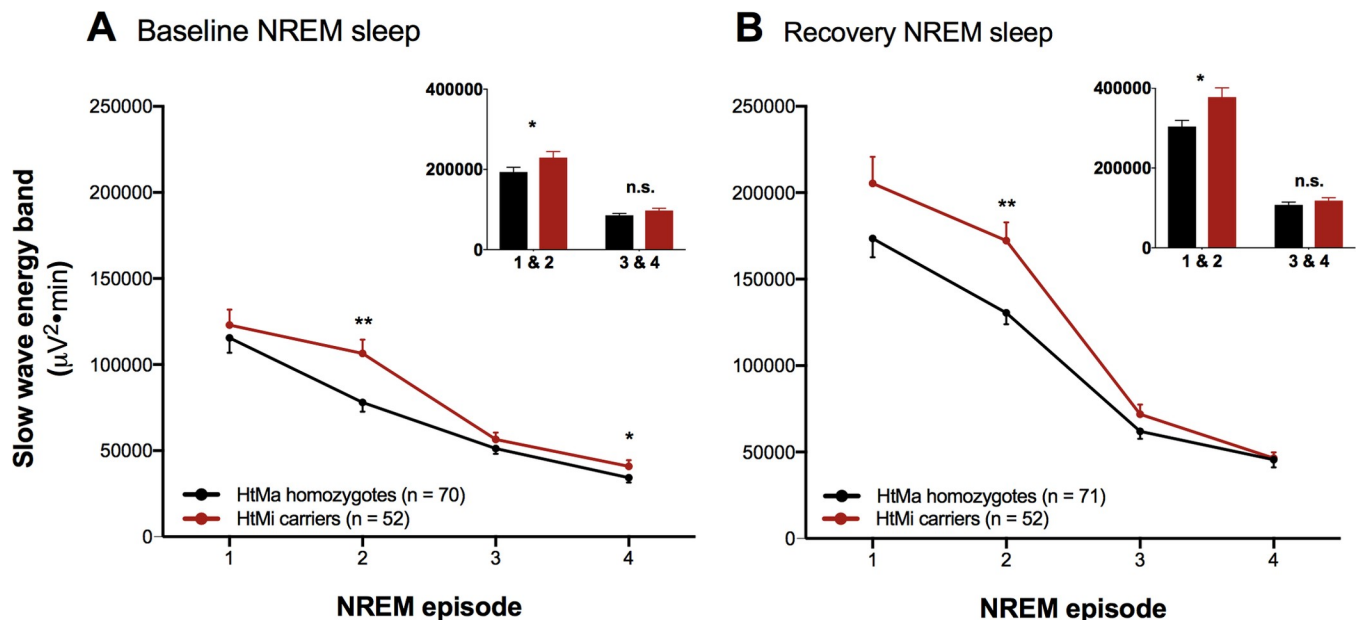


**Fig 3. Time course of EEG slow wave production is associated with the AQP4 haplotype.** To probe the role of AQP4 on sleep-wake regulation, SWE across the first 4 NREM episodes (A and B) was investigated. The data confirmed the previously detected overall increase in SWE in the AQP4 HtMi carriers (red) compared to the HtMa homozygote (black) group (“haplotype”:  $F_{1,121} = 5.39$ ;  $P < 0.03$ ,  $\eta_p^2 = 4.26\%$ ). Moreover, a significant AQP4-haplotype modulation across the first 4 NREM episodes was observed (“haplotype x NREM episode”:  $F_{3,843} = 2.65$ ;  $P < 0.05$ ;  $\eta_p^2 = 0.93\%$ ), an effect that was strongest in the second NREM episode. AQP4 HtMi carriers were found to have increased SWE mainly in the early part of the night (figure inserts). Spectral energy values of the slow wave band (0.75–4.5 Hz) in NREM sleep episodes 1 through 4 and the second part of the night (early: 1 and 2, late: 3 and 4) are plotted for the 2 haplotype groups for both baseline and recovery sleep (S3 Data). Data represent mean  $\pm$  SEM. Unpaired two-tailed  $t$  tests: \* $P < 0.05$ , \*\* $P < 0.01$ . AQP4, aquaporin 4; EEG, electroencephalographic; HtMa, Major allele of haplotype; HtMi, Minor allele of haplotype; NREM, non-rapid eye movement; SWE, slow wave energy.

<https://doi.org/10.1371/journal.pbio.3000623.g003>

## The AQP4-haplotype is associated with a modulation of subjective and objective responses to prolonged wakefulness

To probe whether the AQP4-haplotype modulation of SWE has cognitive consequences, we investigated psychomotor vigilance performance (psychomotor vigilance test, PVT) and subjective sleepiness (Stanford sleepiness scale, SSS) across prolonged wakefulness in the 2 genetic groups (see Fig 1E). Subjective sleepiness ratings revealed that HtMi carriers coped slightly better with sleep deprivation than HtMa homozygotes and showed a smaller increase in sleepiness ratings from day 1 to day 2 (“haplotype x day”:  $P < 0.04$ ; Fig 4A). Importantly, median response speed on the PVT mirrored the effects on subjective sleepiness with the HtMi carriers reducing their speed slightly less than HtMa homozygotes (“haplotype x day”:  $P < 0.04$ ; Fig 4B), despite comparable speeds on day 1. Effects for lapses of attention were visually similar yet did not reach significance (Fig 4C and S4 Data). These data suggest that alterations in AQP4-expression have cognitive consequences, unveiled during sleep deprivation. Our data extend the recently described connection between slow waves, neuronal activation, and CSF flow in the fourth ventricle [12], by showing that the AQP4 haplotype is associated with a modulation of NREM SWE and the restorative effect of sleep on cognitive functions. The low number of included HtMi homozygotes did not allow us to test whether the observed effects on sleep follow a dose response relationship, a question that should be addressed in future studies. Although we cannot rule out possible confounding associations between the AQP4 haplotype and other sleep regulating genes, our observations may indirectly suggest that AQP4-dependent fluid flow within the neuropil is regulated by EEG slow waves during NREM sleep.

## Conclusion

Our data highlights that subjects carrying the low AQP4-expressing HtMi variant of the AQP4-haplotype have enhanced SWE mainly in early NREM episodes and cope slightly better with prolonged wakefulness. Given that SNPs associated with the HtMi variant affect the cognitive decline in Alzheimer’s patients [15], the here described modulation of sleep intensity by the

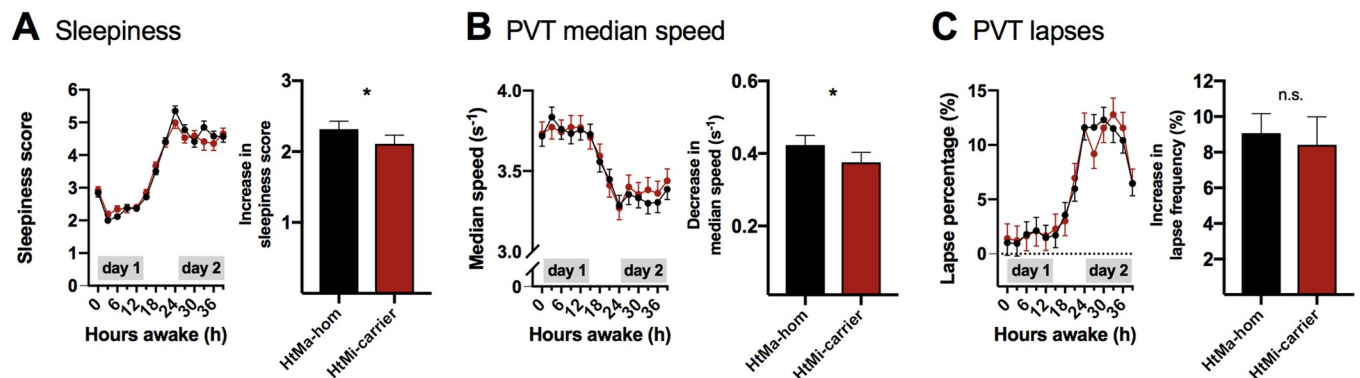


**Fig 4. Objective and subjective measures of sleep deprivation is affected by the AQP4 haplotype.** Subjective sleepiness ratings on the SSS and objective alertness measures by the PVT. SSS scores (A), median speed (B), and attention lapses (C) on the PVT were quantified at 3-hour intervals across the 40 hours of prolonged wakefulness. Three-way linear mixed-model analysis revealed strong differences between day 1 and day 2 (“day”:  $F_{all} > 442$ ,  $p < 0.0001$ ) and moderate modulations of clock time ( $F_{all} > 4.6$ ,  $p < 0.0005$ ) and by the “day x clock time” interaction ( $F_{all} > 3.5$ ,  $p < 0.004$ ) in all 3 measures. Comparison of subjective sleepiness between the 71 HtMa homozygotes (black) and the 52 HtMi carriers (red) of the AQP4 haplotype revealed that the HtMi group coped slightly better with prolonged wakefulness than the HtMa homozygotes (“haplotype x day”:  $F_{1,364} = 4.5$ ;  $P < 0.04$ ;  $\eta_p^2 = 1.22\%$ ; Panel A right). Intriguingly, the AQP4-haplotype dependent modulation of sleepiness was mirrored by a similar effect on PVT median speed performance among the 60 HtMa homozygotes and 44 HtMi carriers that were tested (“haplotype x day”:  $F_{1,1041} = 4.7$ ;  $P < 0.04$ ;  $\eta_p^2 = 0.45\%$ ; Panel B right), an effect similar yet not significant for lapses of attention (“haplotype x day”:  $F_{1,1041} = 0.1$ ,  $p > 0.78$ , Panel C right; S4 Data). Data represent estimated mean  $\pm$  SEM. \*  $p < 0.05$  from the corresponding “haplotype x day” interaction. AQP4, aquaporin 4; hom: Homozygote; HtMa, Major allele of haplotype; HtMi, Minor allele of haplotype; PVT, psychomotor vigilance test; SSS, Stanford sleepiness scale.

<https://doi.org/10.1371/journal.pbio.3000623.g004>

*AQP4* haplotype provides a tantalizing link between Alzheimer's disease, sleep intensity, and *AQP4* in humans. Although future studies are warranted to better understand the underlying molecular mechanisms governing this effect, the data are consistent with the hypothesized impact from the glymphatic pathway. It also supports the hypothesis that sleep slow waves are part of the regulatory machinery of parenchymal CSF flow. Further studies investigating the *AQP4* haplotype and its association to sleep-associated brain functions are warranted.

## Methods

### Ethics statement

The study protocols were approved by the ethics committee of the Canton of Zurich for research on human subjects (Cantonal Ethics Committee reference numbers: E-39/2006 [29]; 2012-0398 [30]; E-24/2007 [31]; EK-Nr. 786 [32]; 2015-0424 [33]). As previously required, the oldest data set [28] was approved by local institutional review board. Subjects were recruited by public advertisements seeking participants for scientific studies or via billboard advertisements at the university buildings in Zurich. All subjects received a monetary compensation for their participation. Written and informed consent was obtained from all participants before the experiments as required according to the principles in the Declaration of Helsinki.

### SNPs of the *AQP4* gene and haplotype analysis

To investigate genetic modulations of *AQP4*, common variants in the *AQP4* gene were explored using the dbSNP database build 152 (<https://www.ncbi.nlm.nih.gov/snp/>). The initial search in the 1000 genome project database within dbSNP revealed 32 SNPs with a global minor allele frequency (MAF) above 5%. Only 16 of these were common (MAF above 20%) in the European population data representative of the investigated Swiss cohort (CEU and TSI populations). Linkage disequilibrium (LD) analysis showed that 8 of the 16 SNPs (rs162007, rs162008, rs63514, rs455671, rs335931, rs335930, rs335929, and rs16942851) form a distinct haplotype with SNPs in high LD ( $r^2 > 0.8$ ; Fig 1C). Further LD analysis of the haploblock revealed that these 8 SNPs form 2 common variants of the haplotype: a major haplotype (HtMa) with a 76.7% incidence and a minor haplotype (HtMi) with a 19.7% incidence (for further details, see Fig 1). Based on the 1000 genome database, this haplotype is widely detected across the European, American, and east Asian and south Asian populations.

### Genotyping of *AQP4* SNPs

Genomic DNA extracted from 3 mL fresh EDTA-blood (wizard<sup>R</sup> Genomic DNA purification Kit, Promega, Madison, WI) was used for genotyping. The rs335931, rs335929, and rs16942851 polymorphisms of *AQP4* were chosen as tag SNPs to represent the haplotype and were determined using Taqman<sup>®</sup> SNP genotyping Assay (Life Technologies Europe B.V.; see also S2 Table). Allelic discrimination analysis was performed with SDS version 2.2.2 software (applied Biosystems, Foster City, CA). All genotypes were replicated at least once for independent confirmation.

The MAFs of the genotyped variants were in accordance with MAFs predicted by the dbSNP database (S2 Table). All 3 SNPs were in Hardy-Weinberger equilibrium. Pairwise LD coefficients ( $r^2$ ) were calculated between rs335929, rs16942851, and rs335931 confirming high LD ( $r^2 > 0.95$ ). The 2 haplotypes and allele frequencies are shown in Fig 1.

Because of the well-established association between Alzheimer disease risk and Apolipoprotein E (APOE) genotype [27], we checked the distribution of APOE genotypes (rs429358 and rs7412) among the *AQP4*-haplotype groups using the same Taqman<sup>®</sup> SNP genotyping

approach. The analysis revealed that the distribution was similar in HtMa homozygotes and HtMi carriers ( $p > 0.47$ ; [S1 Table](#)).

## Study population

To examine the impact of the genetic haplotype of *AQP4* on the sleep EEG, we investigated data from 134 healthy participants of 6 previously published sleep deprivation studies [28–33]. All studies were conducted under strictly controlled conditions in the sleep lab of the Institute of Pharmacology and Toxicology at the University of Zürich, Switzerland, using similar protocols and methodology ([Fig 1E](#)). Two carriers of rare haplotypes as well as 9 older participants with an age above 60 years were excluded from the analysis. The total sample thereby included 71 individuals homozygous for the major allele (HtMa/HtMa), 45 heterozygous (HtMa/HtMi), and 7 homozygous for the minor allele (HtMi/HtMi). Given the low number of minor allele homozygotes, a HtMi-carrier group (HtMi/HtMi and HtMa/HtMi alleles) was created ( $n = 52$ ). Dominant analysis was performed with the aim of investigating the consequence of harboring the minor *AQP4* haplotype. No difference in the distribution of the *AQP4* haplotype between the 6 studies was observed ( $p > 0.21$ ). In studies that included the administration of one or more treatments [28–30], only data from the placebo arm were analyzed.

Study participants were right-handed healthy volunteers with a medical history free of neurological and psychiatric disorders. They were drug and medication abstinent and reported being good sleepers with regular bedtimes and no shift or night work. No participants passed through time zones or consumed excessive amounts of alcohol or caffeine in the 2 months prior to study enrollment. Before inclusion, participants underwent a screening night in the sleep laboratory to check for undiagnosed sleep disorders or low sleep efficiency ( $<85\%$ ; see [S1](#) and [S3](#) Tables).

## Sleep study protocol

The 6 study protocols were very similar and were performed as follows: In the final 3 days leading up to the sleep studies, participants were required to keep a strict 8-hour/16-hour sleep schedule and to refrain from caffeine (coffee, tea, cola drinks, chocolate, and energy drinks) and alcohol intake. Compliance with these requirements was verified by actigraphy from a wrist activity monitor, sleep-wake diaries, and determination of saliva caffeine as well as breath alcohol levels upon arrival in the sleep lab.

The sleep studies consisted of a block of 4 consecutive nights (see [Fig 1E](#)): First and second nights served as adaptation and baseline nights, respectively. The subjects were then kept awake for 40 hours (i.e., for 2 days, skipping one night of sleep) until bedtime on the fourth night, when they were given a 10-hour sleep opportunity for recovery. During the period of prolonged wakefulness, the participants were constantly supervised by members of the research team and engaged in studying, playing games, watching films, and occasionally taking a walk outside the laboratory.

## Polysomnographic recordings

Continuous all-night polysomnographic recordings were performed on all baseline and recovery nights. The EEG, electrooculogram (EOG), submental electromyogram, (EMG) and electrocardiogram (ECG) were recorded using the polysomnographic amplifiers PSA24 (Braintronics Inc., Almere, the Netherlands;  $n = 16$ ) [28] and Artisan<sup>®</sup> from Micromed (Mogliano Veneto, Italy;  $n = 107$ ) [29–33]. In the recordings obtained with the PSA24 recording system, the analogue EEG signals were conditioned by a high-pass filter (3 dB at 0.16 Hz) and a low-pass filter (3 dB at 102 Hz), sampled at 512 Hz, digitally low-pass filtered (3 dB at 49 Hz), and stored with a resolution of 128 Hz. In the recordings obtained with the Artisan<sup>®</sup> recording system, analogue EEG data were conditioned with a high-pass filter (3 dB at 0.15

Hz), a low-pass filter (3 dB at 67.2 Hz), and sampled with a frequency 256 Hz. Sleep stages were visually scored in 20-second epochs according to standard criteria [34], and arousal- and movement-related artifacts were visually identified and removed. The data from the C3M2 derivation are reported. In both conditions, the analyses were restricted to the first 8 hours (480 min) after lights-off.

### EEG analyses

Four second EEG spectra (fast Fourier transform routine, Hanning Window, frequency resolution 0.25 Hz) were calculated with MATLAB (MathWorks Inc., Natick, MA), and EEG power spectra of 5 consecutive 4-second epochs were averaged and matched with the scored sleep stages.

The first 4 NREM episodes were defined according to current standards [35]. The all-night power spectra represent the average of all artifact-free 20-second values in NREM sleep (stages 1–4) between 0 and 20 Hz. The energy spectra contain all values of spectral power multiplied by time (minutes) spent in NREM sleep per night (480 minutes) or in the respective NREM sleep episodes. The energy calculations factors in a more relevant quantitative interpretation of the spectra [25].

### Cognitive testing and sleepiness ratings

The PVT is a simple reaction time task implemented in e-Prime software (Psychology Software Tools Inc., Pittsburgh, PA), in which subjects are instructed to press a button as quickly as possible with their right index finger when they see a digital millisecond counter that starts to scroll in the center of the computer screen [36]. Nineteen individuals were excluded from analysis because they performed a different, noncomputerized version of the task, resulting in a sample size of 104 subjects for the PVT task analyses. Moreover, because a subset of participants underwent neuroimaging on the second day of sleep deprivation, some performance measures are missing on day 2. Subjects received oral instructions and performed a training session prior to study start. For each PVT trial; 100 stimuli were presented (random interstimulus intervals: 2–10 s). Two extensively validated PVT variables were quantified [37,38]: “lapses of attention” (defined as the percentage of trials with reaction times longer than 500 ms) and median response speed (based on inverse reaction times). Immediately prior to all PVT assessments, a validated German version of the SSS was administered [39]. The sleepiness ratings of all 123 subjects were included in the analyses.

### Statistical analyses

All statistical analyses were performed with SAS 9.4 x64 software (SAS institute, Cary, North Carolina) and performed across nocturnal EEG data, subjective sleepiness and PVT performance measures. To approximate a normal distribution, EEG energy was log-transformed prior to statistical tests. Two- and three-way mixed-model analysis of variance were performed with the between-subjects factor “genotype” (HtMa homozygotes versus HtMi carriers) and the relevant within-subject factors: “condition” (baseline versus recovery), “NREM sleep episode” (1–4), “frequency bin” (bin 1–81), clock time (8, 11, 14, 17, 20, 23 o'clock), and the duration of prolonged wakefulness (day 1 versus day 2). For the nocturnal EEG data, 2 overall four-way mixed-model analysis were performed (for EEG power and EEG energy), which included all frequency bins, genotype, condition, and study (“bin x genotype x night”:  $P < 0.0001$ ). Further analysis was only performed because a significant effect of genotypes was established. Moreover, to control for type I error caused by multiple comparison, the significance levels for these primary 2 overall mixed models were set to  $\alpha < 0.025$  (Bonferroni correction  $\alpha = 0.05/2$ ). Type I errors were further controlled by only considering significant effects relevant when

the following 2 criteria were met: (A) more than 2 bins in the by-bin (mixed model) analysis of variance were below  $\alpha = 0.05$  and (B) the corresponding frequency band (slow wave/delta, theta, alpha, spindle, beta) was also significant at  $\alpha$  level = 0.05. The final step implemented to control for type I errors was to investigate the sleep EEG bands using a hypothesis driven, fixed sequence procedure [25], in which EEG bands were listed based on their relevance for sleep-wake regulation as follows: (1) Delta/slow wave activity (0.75–4.5 Hz), (2) Spindles (12–15 Hz), (3) Theta (5–8 Hz), (4) Alpha (8–12 Hz), and (5) Beta (15–20 Hz) and tested in that order. Only if the previously tested band revealed a significant genotype modulation, statistical testing of the subsequent band was performed.

Based on the log-transformed EEG SWE data, a priori power analysis revealed that to determine a 5% difference between haplotypes with a simple two-tailed  $t$  test ( $\alpha = 0.05$ ), a total sample size of 78 subjects (Cohen's  $d$ : 0.833; SWE mean:  $5 \log[\mu V^2 \text{min}] \pm 2.5\%$ ; standard deviation:  $0.3 \log[\mu V^2 \text{min}]$ ) are required (G\*Power 3.1.9.2; Die Heinrich-Heine-Universität Düsseldorf).

When a significant main effect or interaction was discovered, appropriate paired or unpaired two-tailed  $t$  tests were used to localize differences within and between groups. If not stated otherwise, only significant effects or results are reported. Effect sizes (partial eta squared:  $\eta_p^2$ ) were calculated from corresponding mixed-model F-values and degrees of freedom. Effect sizes of 0.0099, 0.0588, and 0.1379 are considered small, moderate, and large, respectively [40,41].

## Supporting information

**S1 Fig. REM energy analysis.** REM energy analysis for AQP4 HtMa homozygous (black lines) and HtMi carriers (red lines) across baseline (A) nor recovery (B) nights. No significant modulation by the AQP4 haplotype was observed (“haplotype”:  $F_{1,21} = 0.07$ ;  $P > 0.79$ ), confirming that the sleep EEG modulations are selective to the NREM slow wave range (S5 Data). Plots represent means; error bars represent SEM. (Insert) Full NREM sleep spectra for 0 to 20 Hz on log10 scale. AQP4, aquaporin 4; EEG, electroencephalographic; HtMa, Major allele of haplotype; HtMi, Minor allele of haplotype; NREM, non-rapid eye movement; REM, rapid eye movement.

(TIF)

**S2 Fig. AQP4-haplotype is associated with a modulation of EEG power in the slow wave range.** Comparison of EEG spectral power across baseline and recovery nights in the slow wave band (0.75–4.5 Hz) within the AQP4-haplotype variants HtMa homozygotes (black) and HtMi carriers (red). The AQP4 HtMi carriers had higher spectral power than the HtMa homozygotes (A; “genotype”:  $F_{1,121} = 4.2$ ;  $P < 0.05$ ). The effect was similar in baseline (B) and recovery sleep (C) conditions and confined to the 0.75 to 1.25 Hz band. Inserts in panels B and C represent full NREM sleep spectra for 0 to 20 Hz on log10 scale. Gray shading indicating the slow wave band (S2 Data). Data represents means  $\pm$  SEM. By-bin unpaired two-tailed  $t$  tests; \* $P < 0.05$  (only performed in the slow wave range). AQP4, aquaporin 4; EEG, electroencephalographic; HtMa, Major allele of haplotype; HtMi, Minor allele of haplotype; NREM, non-rapid eye movement.

(TIF)

**S1 Table. Demographics.** Demographic characteristics of the 123 healthy adult volunteers, who participated in one of six 40-hour sleep deprivation studies from the Zürich sleep lab where AQP4 HtMa homozygotes and HtMi allele carriers were genotyped. No demographic differences between the 2 AQP4-haplotype groups was observed, nor was there a difference in haplotype distribution among the 6 studies (Fishers exact  $t$  test,  $p > 0.21$ ). Given the low number of females in the 6 included studies, a potential interaction between AQP4 haplotype and

gender could not be addressed in the current paper. German versions and validated German translations of questionnaires were used to assess lifestyle and personality traits. Questionnaires included ESS [42] and STAI [43]. Caffeine consumption was estimated based on average caffeine contents per serving (coffee: 100 mg, tea: 30 mg, cola drink: 40 mg [2 dL], energy drink: 80 mg [2 dL], chocolate: 50 mg [100 g]). The APOE genotype, known to modulate Alzheimer disease progression, was evenly distributed among the *AQP4* haplotype groups. *P* values are calculated from students two-tailed *t* tests or Fisher's exact test where appropriate. APOE, Apolipoprotein E; AQP4, aquaporin 4; ESS, Epworth Sleepiness Scale; HtMa, Major allele of haplotype; HtMi, Minor allele of haplotype; STAI, State-Trait Anxiety Inventory. (DOCX)

**S2 Table. Investigated SNPs.** Alleles: presented as [major allele/minor allele]. Position: Position of SNP in gene. Location: Location of single nucleotide polymorphism on chromosome 18 in the genome. Assay ID: ThermoFisher Taqman® SNP genotype assay ID nr.  $MAF_{\text{predicted}}$ : MAF predicted by dbSNP analysis tool in a CEU and TSI population (to approximate the Swiss population).  $MAF_{\text{study}}$ : MAF in the entire genotyped study population ( $n = 134$ ), including 2 rare genotypes and 9 elderly subjects excluded from analysis. dbSNP, The Single Nucleotide Polymorphism Database; CEU, Utah Residents from North and West Europe; MAF, minor allele frequency; SNP, single nucleotide polymorphism; TSI, Toscani in Italy; (DOCX)

**S3 Table. Visually scored sleep variables.** Data on the visually scored sleep variables and their modulation by sleep deprivation and the *AQP4* haplotype. Values represent mean  $\pm$  SEM in baseline and recovery nights for the 2 haplotype groups. Analysis of the recovery nights were restricted to 480 minutes. Sleep efficiency: percentage of total sleep time per 480 min. Stages N1–N3: NREM sleep stages (N3 refers to slow wave sleep). Sleep latency: time from lights-out to the first occurrence of N2 sleep. REM sleep latency: time from sleep onset to the first occurrence of REM sleep. *F*- and *P* values: two-way mixed-model ANOVA with factors “genotype” (HtMa homozygotes, HtMi carriers), “condition” (baseline, recovery), and their interaction. AQP4, aquaporin 4; HtMa, Major allele of haplotype; HtMi, Minor allele of haplotype; MT, movement time; NREM, non-rapid eye movement; REM, rapid eye movement; TIB, time in bed; TST, total sleep time; WASO, wakefulness after sleep onset. (DOCX)

**S1 Data. Individual genotyping and haplotyping.**  
(XLSX)

**S2 Data. Individual whole-night NREM spectral power and spectral energy data.** NREM, non-rapid eye movement.  
(XLS)

**S3 Data. Individual NREM spectral power and spectral energy data for the first 4 NREM episodes.** NREM, non-rapid eye movement.  
(XLSX)

**S4 Data. Individual data for PVT median speed, PVT lapses, and SSS ratings.** PVT, psychomotor vigilance test; SSS, Stanford sleepiness scale.  
(XLSX)

**S5 Data. Individual whole-night REM spectral power and spectral energy data.** REM, rapid eye movement.  
(XLSX)

## Acknowledgments

We thank Dr. Marianna Di Chiara, Laura van Bommel, Silke Feil, and Dr. Samuel Koller for their assistance with *AQP4* genotyping, and Dr. Brice Ozenne for his assistance with statistical analysis.

## Author Contributions

**Conceptualization:** Sara Marie Ulv Larsen, Hans-Peter Landolt, Maiken Nedergaard, Sebastian Camillo Holst.

**Data curation:** Sara Marie Ulv Larsen, Hans-Peter Landolt, Wolfgang Berger, Sebastian Camillo Holst.

**Formal analysis:** Sara Marie Ulv Larsen, Hans-Peter Landolt, Sebastian Camillo Holst.

**Funding acquisition:** Sara Marie Ulv Larsen, Hans-Peter Landolt, Maiken Nedergaard, Gitte Moos Knudsen, Sebastian Camillo Holst.

**Investigation:** Sara Marie Ulv Larsen, Hans-Peter Landolt, Gitte Moos Knudsen, Sebastian Camillo Holst.

**Methodology:** Sara Marie Ulv Larsen, Hans-Peter Landolt, Wolfgang Berger, Sebastian Camillo Holst.

**Project administration:** Sara Marie Ulv Larsen, Hans-Peter Landolt, Sebastian Camillo Holst.

**Resources:** Sara Marie Ulv Larsen, Hans-Peter Landolt, Wolfgang Berger, Gitte Moos Knudsen, Sebastian Camillo Holst.

**Supervision:** Hans-Peter Landolt, Wolfgang Berger, Maiken Nedergaard, Gitte Moos Knudsen, Sebastian Camillo Holst.

**Validation:** Sara Marie Ulv Larsen, Hans-Peter Landolt, Sebastian Camillo Holst.

**Visualization:** Sara Marie Ulv Larsen, Maiken Nedergaard, Sebastian Camillo Holst.

**Writing – original draft:** Sara Marie Ulv Larsen, Sebastian Camillo Holst.

**Writing – review & editing:** Sara Marie Ulv Larsen, Hans-Peter Landolt, Wolfgang Berger, Maiken Nedergaard, Gitte Moos Knudsen, Sebastian Camillo Holst.

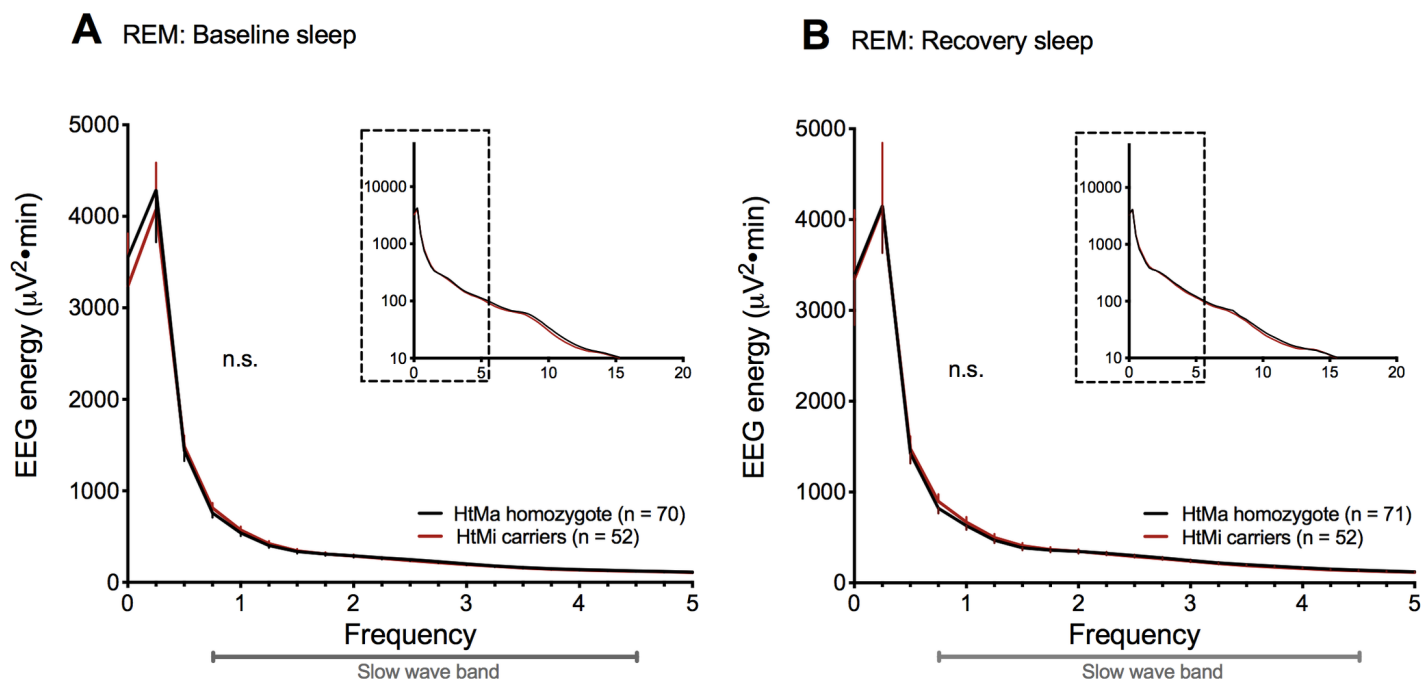
## References

1. Plog BA, Nedergaard M. The glymphatic system in CNS health and disease: past, present and future. *Annu Rev Pathol.* 2018 Jan 24; 13:379–94. <https://doi.org/10.1146/annurev-pathol-051217-111018> PMID: 29195051
2. Benveniste H, Lee H, Volkow ND. The Glymphatic Pathway. *Neuroscientist.* 2017 Jan 1; <https://doi.org/10.73858417691030>
3. Mestre H, Tithof J, Du T, Song W, Peng W, Sweeney AM, et al. Flow of cerebrospinal fluid is driven by arterial pulsations and is reduced in hypertension. *Nat Commun.* 2018 19; 9(1):4878. <https://doi.org/10.1038/s41467-018-07318-3> PMID: 30451853
4. Mestre H, Hablitz LM, Xavier AL, Feng W, Zou W, Pu T, et al. Aquaporin-4-dependent glymphatic solute transport in the rodent brain. *Elife.* 2018 18;7.
5. Haj-Yasein NN, Vindedal GF, Eilert-Olsen M, Gundersen GA, Skare Ø, Laake P, et al. Glial-conditional deletion of aquaporin-4 (*Aqp4*) reduces blood-brain water uptake and confers barrier function on perivascular astrocyte endfeet. *Proc Natl Acad Sci USA.* 2011 Oct 25; 108(43):17815–20. <https://doi.org/10.1073/pnas.1110655108> PMID: 21990350
6. Liff JJ, Wang M, Liao Y, Plogg BA, Peng W, Gundersen GA, et al. A paravascular pathway facilitates CSF flow through the brain parenchyma and the clearance of interstitial solutes, including amyloid  $\beta$ . *Sci Transl Med.* 2012 Aug 15; 4(147):147ra111.

7. Zhang R, Liu Y, Chen Y, Li Q, Marshall C, Wu T, et al. Aquaporin 4 deletion exacerbates brain impairments in a mouse model of chronic sleep disruption. *CNS Neurosci Ther*. 2019 Jul 31;
8. Xie L, Kang H, Xu Q, Chen MJ, Liao Y, Thiyagarajan M, et al. Sleep drives metabolite clearance from the adult brain. *Science*. 2013 Oct 18; 342(6156):373–7. <https://doi.org/10.1126/science.1241224> PMID: 24136970
9. Hablitz LM, Vinitzky HS, Sun Q, Stæger FF, Sigurdsson B, Mortensen KN, et al. Increased glymphatic influx is correlated with high EEG delta power and low heart rate in mice under anesthesia. *Sci Adv*. 2019 Feb; 5(2):eaav5447.
10. Holth JK, Fritschi SK, Wang C, Pedersen NP, Cirrito JR, Mahan TE, et al. The sleep-wake cycle regulates brain interstitial fluid tau in mice and CSF tau in humans. *Science*. 2019 22; 363(6429):880–4. <https://doi.org/10.1126/science.aav2546> PMID: 30679382
11. Shokri-Kojori E, Wang G-J, Wiers CE, Demiral SB, Guo M, Kim SW, et al.  $\beta$ -Amyloid accumulation in the human brain after one night of sleep deprivation. *Proc Natl Acad Sci USA*. 2018 24; 115(17):4483–8. <https://doi.org/10.1073/pnas.1721694115> PMID: 29632177
12. Fultz NE, Bonmassar G, Setsompop K, Stickgold RA, Rosen BR, Polimeni JR, et al. Coupled electrophysiological, hemodynamic, and cerebrospinal fluid oscillations in human sleep. *Science*. 2019 01; 366(6465):628–31. <https://doi.org/10.1126/science.aax5440> PMID: 31672896
13. Nagelhus EA, Ottersen OP. Physiological Roles of Aquaporin-4 in Brain. *Physiol Rev*. 2013 Oct; 93(4):1543–62. <https://doi.org/10.1152/physrev.00011.2013> PMID: 24137016
14. Sorani MD, Zador Z, Hurowitz E, Yan D, Giacomini KM, Manley GT. Novel variants in human Aquaporin-4 reduce cellular water permeability. *Hum Mol Genet*. 2008 Aug 1; 17(15):2379–89. <https://doi.org/10.1093/hmg/ddn138> PMID: 18511455
15. Burfeind KG, Murchison CF, Westaway SK, Simon MJ, Erten-Lyons D, Kaye JA, et al. The effects of noncoding aquaporin-4 single-nucleotide polymorphisms on cognition and functional progression of Alzheimer's disease. *Alzheimers Dement (N Y)*. 2017 Sep; 3(3):348–59.
16. Westermair AL, Munz M, Schaich A, Nitsche S, Willenborg B, Muñoz Venegas LM, et al. Association of Genetic Variation at AQP4 Locus with Vascular Depression. *Biomolecules*. 2018 Dec 5; 8(4).
17. Yadav BK, Oh S-Y, Kim N-K, Shin B-S. Association of rs2075575 and rs9951307 polymorphisms of AQP-4 gene with leukoaraiosis. *J Stroke Cerebrovasc Dis*. 2014 Jun; 23(5):199–206. <https://doi.org/10.1016/j.jstrokecerebrovasdis.2013.10.017> PMID: 24582793
18. Dardiotis E, Paterakis K, Tsivgoulis G, Tsintou M, Hadjigeorgiou GF, Dardiotis M, et al. AQP4 tag single nucleotide polymorphisms in patients with traumatic brain injury. *J Neurotrauma*. 2014 Dec 1; 31(23):1920–6. <https://doi.org/10.1089/neu.2014.3347> PMID: 24999750
19. Henker C, Kriesen T, Fürst K, Goody D, Glass Å, Pützer BM, et al. Effect of 10 different polymorphisms on preoperative volumetric characteristics of glioblastoma multiforme. *J Neurooncol*. 2016 Feb; 126(3):585–92. <https://doi.org/10.1007/s11060-015-2005-9> PMID: 26603163
20. Kieffner I, Bungeoth M, Schiffbauer H, Schäbitz W-R, Ringelstein EB, Kuhlenbäumer G. The role of aquaporin-4 polymorphisms in the development of brain edema after middle cerebral artery occlusion. *Stroke*. 2008 Apr; 39(4):1333–5. <https://doi.org/10.1161/STROKEAHA.107.500785> PMID: 18309154
21. Dardiotis E, Siokas V, Marogianni C, Aloizou A-M, Sokratous M, Paterakis K, et al. AQP4 tag SNPs in patients with intracerebral hemorrhage in Greek and Polish population. *Neuroscience Letters*. 2019 Mar 23; 696:156–61. <https://doi.org/10.1016/j.neulet.2018.12.025> PMID: 30578930
22. Woo J, Kim JE, Im JJ, Lee J, Jeong HS, Park S, et al. Astrocytic water channel aquaporin-4 modulates brain plasticity in both mice and humans: a potential gliogenetic mechanism underlying language-associated learning. *Mol Psychiatry*. 2018 Apr; 23(4):1021–30. <https://doi.org/10.1038/mp.2017.113> PMID: 29565042
23. National cancer institute [internet]. Tool for calculation of population specific haplotype frequencies [cited 2020 April 15]. Available from: <https://ldlink.nci.nih.gov/?tab=ldhap>
24. Buckelmüller J, Landolt H-P, Stassen HH, Achermann P. Trait-like individual differences in the human sleep electroencephalogram. *Neuroscience*. 2006; 138(1):351–6. <https://doi.org/10.1016/j.neuroscience.2005.11.005> PMID: 16388912
25. Dmitrienko A, D'Agostino R. Traditional multiplicity adjustment methods in clinical trials. *Stat Med*. 2013 Dec 20; 32(29):5172–218. <https://doi.org/10.1002/sim.5990> PMID: 24114861
26. Skorucak J, Arbon EL, Dijk D-J, Achermann P. Response to chronic sleep restriction, extension, and subsequent total sleep deprivation in humans: adaptation or preserved sleep homeostasis? *Sleep*. 2018 Jul 1; 41(7).
27. Yu J-T, Tan L, Hardy J. Apolipoprotein E in Alzheimer's disease: an update. *Annu Rev Neurosci*. 2014; 37:79–100. <https://doi.org/10.1146/annurev-neuro-071013-014300> PMID: 24821312

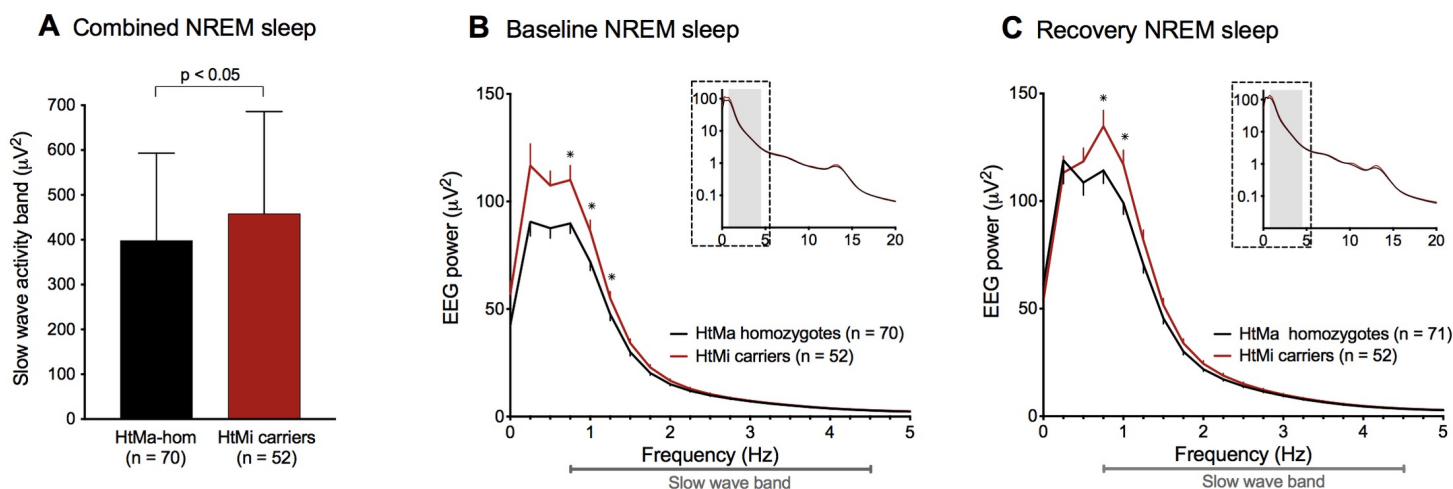
28. Rétey JV, Adam M, Gottselig JM, Khatami R, Dürr R, Achermann P, et al. Adenosinergic mechanisms contribute to individual differences in sleep deprivation-induced changes in neurobehavioral function and brain rhythmic activity. *J Neurosci*. 2006 Oct 11; 26(41):10472–9. <https://doi.org/10.1523/JNEUROSCI.1538-06.2006> PMID: 17035531
29. Bodenmann S, Xu S, Luhmann UFO, Arand M, Berger W, Jung HH, et al. Pharmacogenetics of modafinil after sleep loss: catechol-O-methyltransferase genotype modulates waking functions but not recovery sleep. *Clin Pharmacol Ther*. 2009 Mar; 85(3):296–304. <https://doi.org/10.1038/clpt.2008.222> PMID: 19037200
30. Valomon A, Holst SC, Borrello A, Weigend S, Müller T, Berger W, et al. Effects of COMT genotype and tolcapone on lapses of sustained attention after sleep deprivation in healthy young men. *Neuropsychopharmacology*. 2018 Jun; 43(7):1599–607. <https://doi.org/10.1038/s41386-018-0018-8> PMID: 29472644
31. Bachmann V, Klaus F, Bodenmann S, Schäfer N, Brugger P, Huber S, et al. Functional ADA polymorphism increases sleep depth and reduces vigilant attention in humans. *Cereb Cortex*. 2012 Apr; 22(4):962–70. <https://doi.org/10.1093/cercor/bhr173> PMID: 21734253
32. Hefti K, Holst SC, Sovago J, Bachmann V, Buck A, Ametamey SM, et al. Increased metabotropic glutamate receptor subtype 5 availability in human brain after one night without sleep. *Biol Psychiatry*. 2013 Jan 15; 73(2):161–8. <https://doi.org/10.1016/j.biopsych.2012.07.030> PMID: 22959709
33. Weigend S, Holst SC, Meier J, Brock M, Kohler M, Landolt H-P. Prolonged Waking and Recovery Sleep Affect the Serum MicroRNA Expression Profile in Humans. *Clocks & Sleep*. 2019 Mar; 1(1):75–86.
34. Kales A, Rechtschaffen A, University of California LA, Brain Information Service, National Institute of Neurological Diseases and Blindness (U.S.). A manual of standardized terminology, techniques and scoring system for sleep stages of human subjects. Washington, DC: United States Government Printing Office; 1968.
35. Feinberg I, Floyd TC. Systematic trends across the night in human sleep cycles. *Psychophysiology*. 1979 May; 16(3):283–91. <https://doi.org/10.1111/j.1469-8986.1979.tb02991.x> PMID: 220659
36. Durmer JS, Dinges DF. Neurocognitive consequences of sleep deprivation. *Semin Neurol*. 2005 Mar; 25(1):117–29. <https://doi.org/10.1055/s-2005-867080> PMID: 15798944
37. Doran SM, Van Dongen HP, Dinges DF. Sustained attention performance during sleep deprivation: evidence of state instability. *Arch Ital Biol*. 2001 Apr; 139(3):253–67. PMID: 11330205
38. Lim J, Dinges DF. Sleep deprivation and vigilant attention. *Ann N Y Acad Sci*. 2008; 1129:305–22. <https://doi.org/10.1196/annals.1417.002> PMID: 18591490
39. Sturm A., Clarenbach P., Largiadèr F. & Wicki O. Checkliste Schlafstörungen. Checklisten der aktuellen Medizin. Thieme; 1997.
40. Cohen Jacob. Statistical power analysis for the behavioral sciences. 2nd ed. New York: Academic Press; 2013. 567 p.
41. Richardson JTE. Eta squared and partial eta squared as measures of effect size in educational research. *Educational Research Review*. 2011; 6:135–47.
42. Bloch KE, Schoch OD, Zhang JNN, Russi EW. German version of the Epworth Sleepiness Scale. *Respiration*. 1999; 66:440–447. <https://doi.org/10.1159/000029408> PMID: 10516541
43. Spielberger CD, Gorsuch RL, Lushene RE. Manual for the State-Trait Anxiety Inventory. Consulting Psychologists Press. 1970;

Supplementary



S1 Fig REM energy analysis.

REM energy analysis for AQP4 HtMa homozygous (black lines) and HtMi carriers (red lines) across baseline (A) nor recovery (B) nights. No significant modulation by the AQP4 haplotype was observed (“haplotype”:  $F_{1,21} = 0.07$ ;  $P > 0.79$ ), confirming that the sleep EEG modulations are selective to the NREM slow wave range (S5 Data). Plots represent means; error bars represent SEM. (Insert) Full NREM sleep spectra for 0 to 20 Hz on log10 scale. AQP4, aquaporin 4; EEG, electroencephalographic; HtMa, Major allele of haplotype; HtMi, Minor allele of haplotype; NREM, non-rapid eye movement; REM, rapid eye movement.



S2 Fig AQP4-haplotype is associated with a modulation of EEG power in the slow wave range.

Comparison of EEG spectral power across baseline and recovery nights in the slow wave band (0.75–4.5 Hz) within the AQP4-haplotype variants HtMa homozygotes (black) and HtMi carriers (red). The AQP4 HtMi carriers had higher spectral power than the HtMa homozygotes (A; “genotype”:  $F_{1,121} = 4.2$ ;  $P < 0.05$ ). The effect was similar in baseline (B) and recovery sleep (C) conditions and confined to the 0.75 to 1.25 Hz band. Inserts in panels B and C represent full NREM sleep spectra for 0 to 20 Hz on log10 scale. Gray shading indicating the slow wave band (S2 Data). Data represents means  $\pm$  SEM. By-bin unpaired two-tailed t tests; \* $P < 0.05$  (only performed in the slow wave range). AQP4, aquaporin 4; EEG, electroencephalographic; HtMa, Major allele of haplotype; HtMi, Minor allele of haplotype; NREM, non-rapid eye movement.

**S1 Table**  
**Demographics**

	HtMa homozygotes	HtMi carriers	P-value
Sample size (n <sub>total</sub> = 123)	71	52	
Age (years)	24.1 ± 2.8	23.9 ± 3.0	0.69
BMI (kg/cm <sup>2</sup> )	22.4 ± 1.6	22.6 ± 2.1	0.40
Gender (% females)	12,7	3,8	0.12
Reported habitual sleep duration (h)	7.3 ± 0.7	7.4 ± 0.7	0.46
Trait anxiety (STAI)	33.25 ± 7.1	35.1 ± 8.5	0.19
Sleepiness (ESS)	6.6 ± 3.0	6.9 ± 2.9	0.61
Smoking (% yes)	2,8	1,9	1
Caffeine consumption (mg/day)	108.1 ± 100.3	129.9 ± 118.9	0.27
Alcohol consumption (drinks/week)	3.2 ± 2.7	2.8 ± 2.6	0.43
APOE genotype			
ε2 carrier	10	4	
ε3 carrier	42	36	
ε4 carrier	16	11	0.47

S1 Table. Demographics.

Demographic characteristics of the 123 healthy adult volunteers, who participated in one of six 40-hour sleep deprivation studies from the Zürich sleep lab where AQP4 HtMa homozygotes and HtMi allele carriers were genotyped. No demographic differences between the 2 AQP4-haplotype groups was observed, nor was there a difference in haplotype distribution among the 6 studies (Fishers exact t test,  $p > 0.21$ ). Given the low number of females in the 6 included studies, a potential interaction between AQP4 haplotype and gender could not be addressed in the current paper. German versions and validated German translations of questionnaires were used to assess lifestyle and personality traits. Questionnaires included ESS [42] and STAI [43]. Caffeine consumption was estimated based on average caffeine contents per serving (coffee: 100 mg, tea: 30 mg, cola drink: 40 mg [2 dL], energy drink: 80 mg [2 dL], chocolate: 50 mg [100 g]). The APOE genotype, known to modulate Alzheimer disease progression, was evenly distributed among the AQP4 haplotype groups. P values are calculated from students two-tailed t tests or Fisher's exact test where appropriate. APOE, Apolipoprotein E; AQP4, aquaporin 4; ESS, Epworth Sleepiness Scale; HtMa, Major allele of haplotype; HtMi, Minor allele of haplotype; STAI, State-Trait Anxiety Inventory.

**S2 Table. Investigated single nucleotide polymorphisms (SNPs)**

	Alleles	position	Location in genome	Assay ID	MAF <sub>predicted</sub>	MAF <sub>stu</sub>
rs335931	A / G	Intron 4-5	Chr.18: 26859108	C__11630001_10	0.202	0.243
rs335929	A / C	3UTR	Chr.18: 26855623	C__1303566_10	0.202	0.235
rs16942851	T / G	Downstream of 3UTR	Chr.18: 26851725	C__33451186_20	0.202	0.239

S2 Table. Investigated SNPs

Alleles: presented as [major allele/minor allele]. Position: Position of SNP in gene. Location: Location of single nucleotid polymorphism on chromosome 18 in the genome. Assay ID: Thermofisher Taqman® SNP genotype assay ID nr. MAF<sub>predicted</sub>: MAF predicted by dbSNP analysis tool in a CEU and TSI population (to approximate the Swiss population). MAF<sub>study</sub>: MAF in the entire genotyped study population (n = 134), including 2 rare genotypes and 9 elderly subjects excluded from analysis. dbSNP, The Single Nucleotide Polymorphism Database; CEU, Utah Residents from North and West Europe; MAF, minor allele frequency; SNP, single nucleotide polymorphism; TSI, Toscani in Italy;

**S3 Table. Visually scored sleep variables**

	HtMa-hom (n = 71)		HtMi carriers (n = 52)		'Genotype'		'Condition'		'Genotype' x 'Condition'	
	Baseline	Recovery	Baseline	Recovery	F <sub>1,121</sub>	P	F <sub>1,121</sub>	P	F <sub>1,121</sub>	P
<b>Sleep efficiency (%)</b>	94.0 ± 0.4	97.5 ± 0.2	94.1 ± 0.5	97.8 ± 0.2	0.3	0.59	131.0	<0.0001	0.1	0.75
<b>Sleep latency (min)</b>	14.7 ± 1.3	3.5 ± 0.3	14.8 ± 1.6	3.4 ± 0.6	0	0.97	119.4	<0.0001	0.01	0.92
<b>REM sleep latency (min)</b>	76.0 ± 3.5	81.3 ± 4.9	68.5 ± 2.9	71.0 ± 3.9	4.3	0.04	1.1	0.31	0.2	0.71
<b>Stage N1 (min)</b>	30.9 ± 2.0	14.8 ± 1.2	26.9 ± 1.9	12.1 ± 1.5	2.3	0.13	218.4	<0.0001	0.4	0.55
<b>Stage N2 (min)</b>	215.7 ± 4.1	201.6 ± 4.8	219.9 ± 5.2	207.3 ± 5.6	0.6	0.45	25.9	<0.0001	0.08	0.77
<b>Stage N3 (min)</b>	95.3 ± 4.1	149.2 ± 4.9	101.4 ± 5.5	151.2 ± 5.7	0.3	0.56	687.1	<0.0001	1.1	0.29
<b>NREM sleep (min)</b>	316.4 ± 3.5	352.8 ± 3.1	323.6 ± 3.2	359.2 ± 3.8	2.5	0.11	204.5	<0.0001	0.02	0.89
<b>REM sleep (min)</b>	109.0 ± 2.8	101.9 ± 3.1	103.0 ± 2.7	99.0 ± 3.6	1.4	0.25	6.27	0.014	0.5	0.49
<b>TST (min)</b>	450.9 ± 2.0	467.5 ± 1.0	451.3 ± 2.3	469.6 ± 0.8	0.5	0.50	126.5	<0.0001	0.3	0.59
<b>MT (min)</b>	6.7 ± 0.6	6.7 ± 0.6	6.5 ± 0.6	5.8 ± 0.6	0.5	0.49	1.7	0.20	1.4	0.25
<b>WASO (min)</b>	7.0 ± 1.2	1.1 ± 0.3	5.9 ± 1.5	1.2 ± 0.4	0.3	0.61	35.0	<0.0001	0.4	0.52
<b>TIB (min)</b>	479.7 ± 0	479.4 ± 0.6	479.6 ± 0.1	480 ± 0	0.5	0.47	0.01	0.92	1.0	0.32

S3 Table. Visually scored sleep variables.

Data on the visually scored sleep variables and their modulation by sleep deprivation and the AQP4 haplotype. Values represent mean ± SEM in baseline and recovery nights for the 2 haplotype groups. Analysis of the recovery nights were restricted to 480 minutes. Sleep efficiency: percentage of total sleep time per 480 min. Stages N1–N3: NREM sleep stages (N3 refers to slow wave sleep). Sleep latency: time from lights-out to the first occurrence of N2 sleep. REM sleep latency: time from sleep onset to the first occurrence of REM sleep. F- and P values: two-way mixed-model ANOVA with factors "genotype" (HtMa homozygotes, HtMi carriers), "condition" (baseline, recovery), and their interaction. AQP4, aquaporin 4; HtMa, Major allele of haplotype; HtMi, Minor allele of haplotype; MT, movement time; NREM, non-rapid eye movement; REM, rapid eye movement; TIB, time in bed; TST, total sleep time; WASO, wakefulness after sleep onset.

# Appendix B

---

# Sleep deprivation promotes cerebrovascular oscillations while respiration- and cardiac-driven brain pulsations escalate with sleep intensity

Sara Marie Ulv Larsen<sup>1,2,†</sup>, Sebastian Camillo Holst<sup>1,3,†</sup>, Anders Stevnhoved Olsen<sup>1,4</sup>, Brice Ozenne<sup>1,5</sup>, Dorte Bonde Zilstorff<sup>1</sup>, Kristoffer Brendstrup-Brix<sup>1</sup>, Pia Weikop<sup>6</sup>, Simone Pleinert<sup>1</sup>, Vesa Kiviniemi<sup>7,8</sup>, Poul Jørgen Jennum<sup>9,10</sup>, Maiken Nedergaard<sup>2,6,11</sup>, Gitte Moos Knudsen<sup>1,10\*</sup>

## Affiliations

<sup>1</sup>Neurobiology Research Unit, Copenhagen University Hospital, Rigshospitalet; DK-2100 Copenhagen, Denmark.

<sup>2</sup>Faculty of Health and Medical Sciences (SUND), University of Copenhagen; DK-2200 Copenhagen, Denmark.

<sup>3</sup>Roche Pharma Research and Early Development, Neuroscience and Rare Diseases, Roche Innovation Center Basel; CH-4070 Basel, Switzerland.

<sup>4</sup>Department of Applied Mathematics and Computer Science, Technical University of Denmark; DK-2800 Kgs. Lyngby, Denmark.

<sup>5</sup>Department of Public Health, Section of Biostatistics, University of Copenhagen; DK-1353 Copenhagen, Denmark.

<sup>6</sup>Center for Translational Neuromedicine, University of Copenhagen; DK-2200 Copenhagen, Denmark.

<sup>7</sup>Oulu Functional Neuroimaging (OFNI), Department of Diagnostic Radiology, Oulu University Hospital; FI-90014 Oulu, Finland.

<sup>8</sup>Biocenter Oulu, Oulu University; FI-90014 Oulu, Finland.

<sup>9</sup>Danish Center for Sleep Medicine, Department of Clinical Neurophysiology, Copenhagen University Hospital, Rigshospitalet; DK-2600 Glostrup, Denmark.

<sup>10</sup>Department of Clinical Medicine, University of Copenhagen; DK-2200 Copenhagen, Denmark.

<sup>11</sup>Center for Translational Neuromedicine, Department of Neurosurgery, University of Rochester Medical Center; Rochester, NY 14642, USA

† These authors contributed equally to this work

## \*Corresponding author:

Gitte Moos Knudsen, MD, DMsc

Neurobiology Research Unit, Rigshospitalet

8 Inge Lehmanns Vej, DK-2100 Copenhagen, Denmark

Email: [gmk@nru.dk](mailto:gmk@nru.dk)

**Short title:** Sleep deprivation, sleep intensity and brain oscillations in humans

**Keywords:** Magnetic Resonance Encephalography; Brain fluid dynamics; Glymphatic system; NREM sleep; sleep depth; sleep need; vasomotion

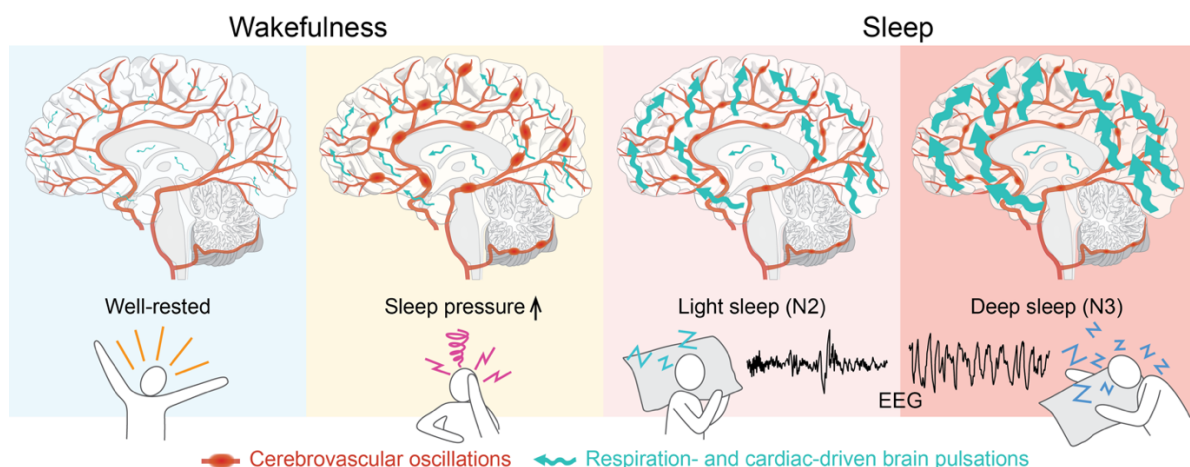
**Preprint:** An earlier version of this manuscript was deposited at medRxiv under a CC-BY-NC-ND licence. **Doi:** <https://doi.org/10.1101/2024.10.16.24315580>

## Abstract

The waste-clearing flow of cerebrospinal fluid through the brain is driven by cerebrovascular, respiratory, and cardiac forces. Growing evidence suggests that sleep facilitates this flow in humans, yet the role of homeostatic sleep mechanisms remains largely unknown.

In a circadian-controlled sleep and sleep deprivation study, we used accelerated neuroimaging to investigate how sleep pressure and slow-wave-rich sleep affect physiological brain oscillations, which are believed to reflect brain fluid dynamics in humans. We also examined the origin of low frequency brain oscillations (LFOs) by pharmacologically modulating vascular oscillations with the adrenergic antagonist carvedilol. We find that sleep deprivation increases LFOs (0.012 – 0.34 Hz) more than sleep does, with LFOs during sleep correlating with cognitive measures of sleep pressure. Conversely, slow-wave-rich sleep (stages N2 and N3) enhances physiological brain pulsations driven by the respiration and cardiac cycles, particularly within grey and white matter. The strength of these brain pulsations escalates with sleep depth (N3 > N2) and correlates with EEG delta power, a measure of slow wave activity. Moreover, carvedilol dampens LFOs, supporting that these reflect cerebrovascular oscillations. In summary, our findings indicate that sleep pressure promotes cerebrovascular oscillations, while sleep slow waves synchronise with respiration- and cardiac-driven pulsations in the brain parenchyma. Together, this suggests that homeostatic sleep mechanisms are integral to human brain fluid dynamics and potentially also waste clearance.

## Graphical abstract



Heightened sleep pressure (following 35 hours of wakefulness) promotes cerebrovascular oscillations (yellow box). Slow-wave-rich NREM sleep enhances physiological brain pulsations driven by the respiration and cardiac cycles – more so in grey and white matter than in CSF spaces (red boxes). The respiration- and cardiac-driven brain pulsations also intensify with deeper sleep (N3 > N2) and correlate with EEG delta power, which is a measure of slow-wave activity (light vs dark red boxes).

## Introduction

Deep sleep is essential for maintaining a healthy brain function. A prominent characteristic of deep non-rapid eye movement (NREM) sleep is the presence of slow, homeostatically regulated, high amplitude waves in the electroencephalogram (EEG) delta range (0.5 to 4.5 Hz) [1]. These EEG slow waves are increased by sleep deprivation [2,3] and have been implicated in multiple basic physiological processes, including brain plasticity [4], memory consolidation [5] and metabolic and immune system function [6]. Emerging preclinical evidence indicates that slow waves also play an important role in brain fluid dynamics [7]. During NREM sleep, cerebrospinal fluid (CSF) flows from perivascular spaces into and through the brain parenchyma, causing an increase in interstitial space volume and an exchange of CSF and interstitial fluid [8–10]. This influx of CSF strongly correlates with EEG slow waves [9,11] and facilitates the clearance of metabolic waste from the rodent brain [8,12,13] through a process known as ‘the glymphatic system’ [14].

While sleep promotes brain fluid flow, it is driven by an interplay of low frequency cerebrovascular oscillations, respiration and the cardiac cycle. Respiratory and cardiac rhythms generate pressure waves that physically propel CSF into and through the parenchyma [15,16], while cerebrovascular oscillations, or vasomotion, propel CSF-flow along periarterial spaces and into the brain [17,18]. Additionally, recent discoveries suggest that cerebrovascular vasomotor activity may also help regulate fluid flow, as the sleep-wake cycle and neural activity affect both the constriction-dilation dynamics of the brain vasculature and the size of and flow within perivascular spaces [18–20]. This critical role of physiological drivers for glymphatic flow is underscored by pharmacological studies, demonstrating that enhancing arterial pulsatility via systemically administered adrenergic agonist directly affects both CSF-flow within perivascular spaces and CSF-interstitial fluid exchange throughout the mouse brain [21,22].

Accumulating evidence supports the role of sleep in facilitating brain fluid flow and waste clearance in humans. A night of sleep is associated with increases in brain diffusivity, CSF production, and CSF volume [23–25], while light NREM sleep enhances CSF flow into the fourth ventricle [26]. Consistent with this, diffusivity in white matter regions of the brain decreases from morning to evening [27] and sleep deprivation results in reduced clearance of contrast agent from the brain [28] as well as increased accumulation of tau and  $\beta$ -amyloid in the CSF and brain parenchyma [29–31]. Further aligning with findings from rodent studies, intracranial pressure (ICP) measurements of B-waves (0.5 – 2 waves pr min), which are thought to reflect cerebrovascular oscillations [32], are also influenced by sleep stage [33,34].

Novel accelerated brain imaging techniques, such as Magnetic Resonance Encephalography (MREG) [35], have emerged as valuable tools for investigating brain-fluid dynamics in humans. MREG achieves temporal resolutions on the order of milliseconds, enabling non-invasive

assessments of low frequency brain oscillations (LFOs) as well as brain pulsations induced by the respiratory and cardiac cycles [36,37]. Previous studies have shown that NREM sleep (N1 and N2) enhances all three types of physiological brain oscillations [38], with sleep effects involving larger brain regions in N2 than in N1 sleep [39]. Additionally, drowsiness increases LFOs in the fourth ventricle during wakefulness [40], while sleep deprivation increases brain-wide LFOs in N1 sleep [39]. Although the influence of circadian factors and sleep propensity on these findings remains unclear, they do suggest that MREG-detected physiological brain oscillations can serve as a real-time measure of vigilance state-induced changes in brain fluid flow in humans.

Our study aimed to establish how the strength of these brain oscillations correlate with heightened sleep pressure, slow-wave-rich NREM sleep, sleep depth and EEG delta power, while controlling for circadian rhythm, time of day and caffeine intake. To do this, we assessed the association between simultaneously acquired MREG and EEG signals in healthy individuals during well-rested wakefulness, after 35 hours of prolonged wakefulness, and during NREM sleep stages N2 and N3. Moreover, we examined the effect of pharmacologically induced vasodilation using the  $\alpha$ 1- and  $\beta$ -adrenergic antagonist carvedilol (Fig 1).

We hypothesized that 1) sleep deprivation is associated with a homeostatic drive towards enhanced physiological brain oscillations in wakefulness, 2) NREM sleep further enhances these oscillations, 3) the strength of physiological brain oscillations is proportional to sleep depth and EEG delta power, and 4) adrenergic antagonism modulates physiological brain oscillations.

# Results

## Study cohort and descriptives

The study included 20 healthy males with anamnestic and polysomnographically verified normal sleep (Table 1; Fig. S1). Three MR/EEG scans sessions were conducted after an average of 11 and 35 hours of wakefulness (standardised time: ~18.30 – 20.30; Table S1). Participants adhered to their sleep-wake schedules, verified by actigraphy and sleep diary, ensuring that all scans were performed at same circadian timepoint. Wakefulness during sleep deprivation was confirmed with continuous EEG recordings (Table S1). Sleep patterns were comparable across the three standardised nights leading up to scan days (Table S2). During well-rested scans, participants were mostly awake, but once sleep-deprived, they quickly entered NREM sleep stages N2 and N3 (Fig. S2).

Increased sleep propensity due to sleep deprivation was confirmed by higher awake EEG delta power in sleep-deprived compared to well-rested scans (delta power ratio:  $+0.033 \pm 0.017$  AU,  $p = 0.051$ ,  $N = 20$ ) and impaired psychomotor vigilance performance before scan sessions (reaction time:  $-0.035 \pm 0.005$  sec; lapses of attention  $+3.86 \pm 0.23$ ;  $p_{\text{both}} < 0.001$ ,  $N = 20$ ). When sleep deprived, plasma norepinephrine levels (measured after scan sessions) increased numerically ( $+268.8 \pm 114.5$  pg/mL,  $p_{\text{adj}} = 0.074$ ,  $N = 20$ , Fig. S3).

As expected, NREM sleep was associated with a strong increase in EEG delta power ( $+0.081 \pm 0.014$  AU,  $p < 0.001$ ,  $N = 20$ ) compared to sleep-deprived wakefulness, with N3 exhibiting higher EEG delta power than N2 sleep ( $p < 0.001$ ,  $N = 17$ ). NREM sleep also showed a small drop in respiration ( $-9\%$ ,  $p = 0.01$ ) and heart rate ( $-11\%$ ,  $p < 0.001$ ) (Table S3). Treatment blinding was successful; participants guessed whether they received carvedilol or placebo before the two sleep-deprived scans only at chance level (guess accuracy: 54%).

**Table 1 Demographics**

	<b>Mean <math>\pm</math> SD</b>	<b>min – max</b>
<b>Age (years)</b>	24.1 $\pm$ 2.8	20 – 29
<b>Body mass index (kg/m<sup>2</sup>)</b>	22.7 $\pm$ 2.8	19.1 – 31.6
<b>Reported habitual sleep duration (h)</b>	7.6 $\pm$ 0.4	7.0 – 8.0
<b>Morningness-eveningness (MEQ)</b>	48.6 $\pm$ 6.4	38.9 – 61.0
<b>General daytime sleepiness (ESS)</b>	6.2 $\pm$ 3.0	2.0 – 13
<b>Sleep quality index (PSQI)</b>	3.0 $\pm$ 1.6	1.0 – 6.0

Demographic characteristics of the twenty healthy males included in the study. MEQ: Morningness-eveningness questionnaire, PSQI: Pittsburgh Sleep Quality Index, ESS: Epworth Sleepiness Scale.

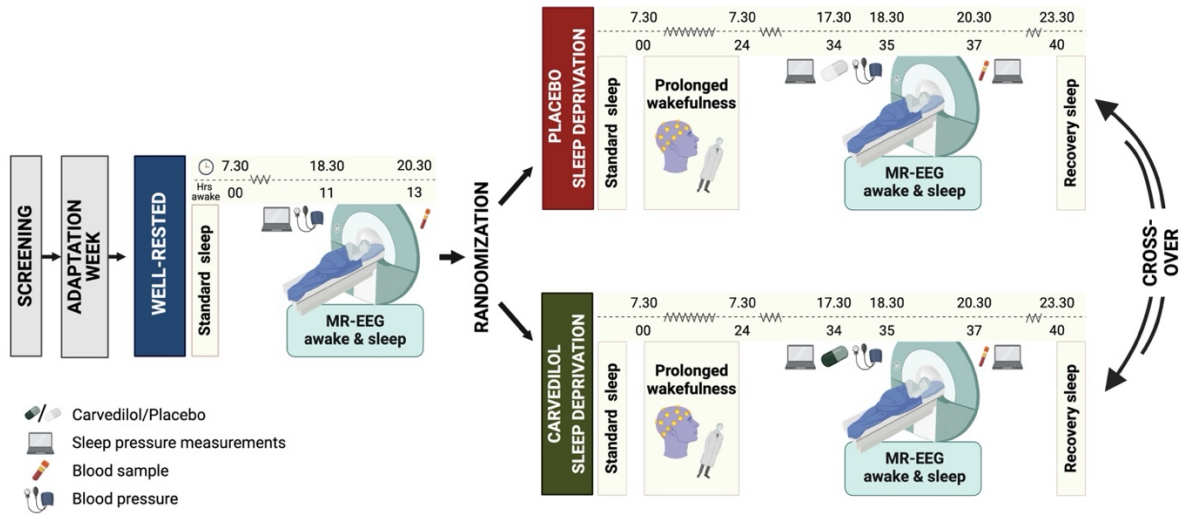


**Figure 1. Study design of the sleep study.** A well-rested and two sleep-deprived study sessions were conducted in the evenings at similar circadian time points. All three MR/EEG scans included a period of wakefulness followed by a sleep opportunity. Before the two sleep-deprived scans, participants received either a placebo or 25 mg of the adrenergic antagonist carvedilol in a double-blind, randomized, cross-over manner.  $N = 20$ . Figure created with BioRender.com.

## Sleep deprivation enhances spectral power in the LFO frequency band

Effects of sleep deprivation and NREM sleep on whole-brain LFOs (0.012 – 0.034 Hz) were evaluated in 5-min MREG-scans from well-rested and sleep-deprived placebo scan sessions (Table S4; see methods).

Sleep deprivation caused a 120% increase in awake spectral power within the LFO frequency band (estimated mean in well-rested ( $10^{6.748}$ ) versus sleep-deprived wakefulness ( $10^{7.091}$ ),  $120\% = (10^{7.091} - 10^{6.748}) / 10^{6.748}$ ,  $p = 0.030$ ; Fig. 2B). During sleep deprived NREM sleep (stages N2 and N3), LFO spectral power was in-between that of rested wakefulness and of sleep deprived wakefulness, with no significant effect of sleep observed ( $p = 0.19$ ; Fig 2A-C).

To investigate the relationship between sleep pressure and LFOs, we next examined the association between LFO spectral power and psychomotor vigilance, as quantified with the Psychomotor vigilance test (PVT). We observed a correlation between LFO spectral power during NREM sleep and pre-scan PVT performance (lapses of attention:  $r_{adj} = 0.50$ ,  $p = 0.018$ ; reaction time:  $r_{adj} = 0.49$ ,  $p = 0.023$ ; Fig. 3A-B). Improvement in PVT performance after a nap in the scanner (i.e. shorter reaction time and fewer lapses) also correlated positively with strength of LFO spectral power during NREM sleep (lapses:  $r_{adj} = -0.48$ ,  $p = 0.015$ ; reaction time:  $r_{adj} = -0.39$ ,  $p = 0.043$ ; Fig. 3C-D). We observed no such correlation during wakefulness ( $p_{all} > 0.5$ ).

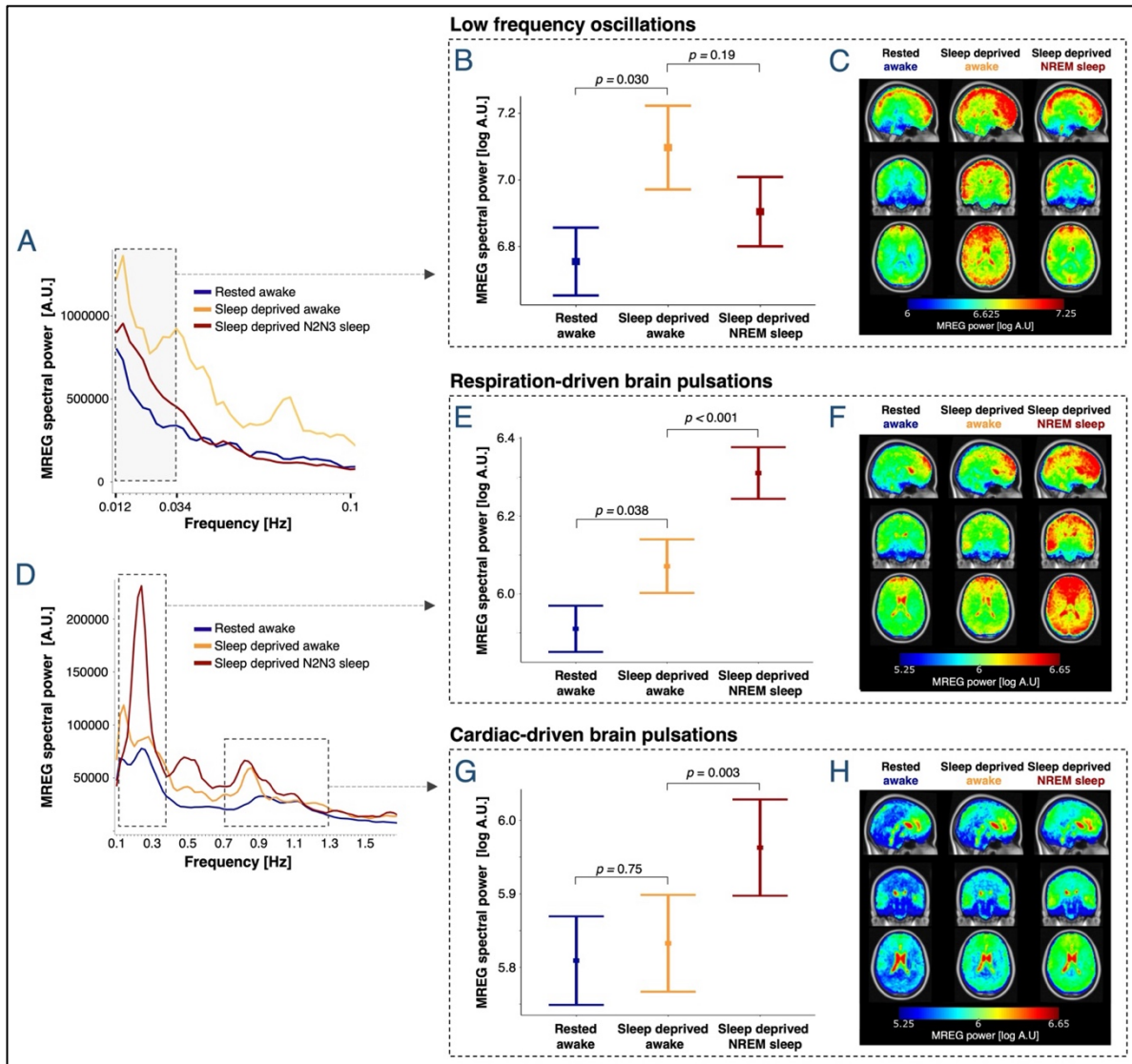


**Figure 2. Sleep deprivation increases LFOs, while NREM sleep is the primary enhancer of respiration- and cardiac-driven brain pulsations.** (A, D) Mean whole-brain MREG spectra across participants. Dashed boxes denote frequency ranges for LFOs (0.012–0.034 Hz) and for respiration- and cardiac-related. (B, E, G) Estimated means  $\pm$  SEM and  $p$ -values are from linear mixed models evaluating effects of sleep deprivation and NREM sleep on log spectral power. (C, F, H) Whole-brain maps illustrate the regional spectral power [log A.U.] in the LFO, respiration and cardiac frequency bands across all 5-min scans (LFO) or 30-sec epochs (respiration and cardiac), averaged across first epochs/scans, then participants (warped into MNI space).  $N$  included in analyses = 20 (see Tables S3 and S4 for number of participants in the three conditions).

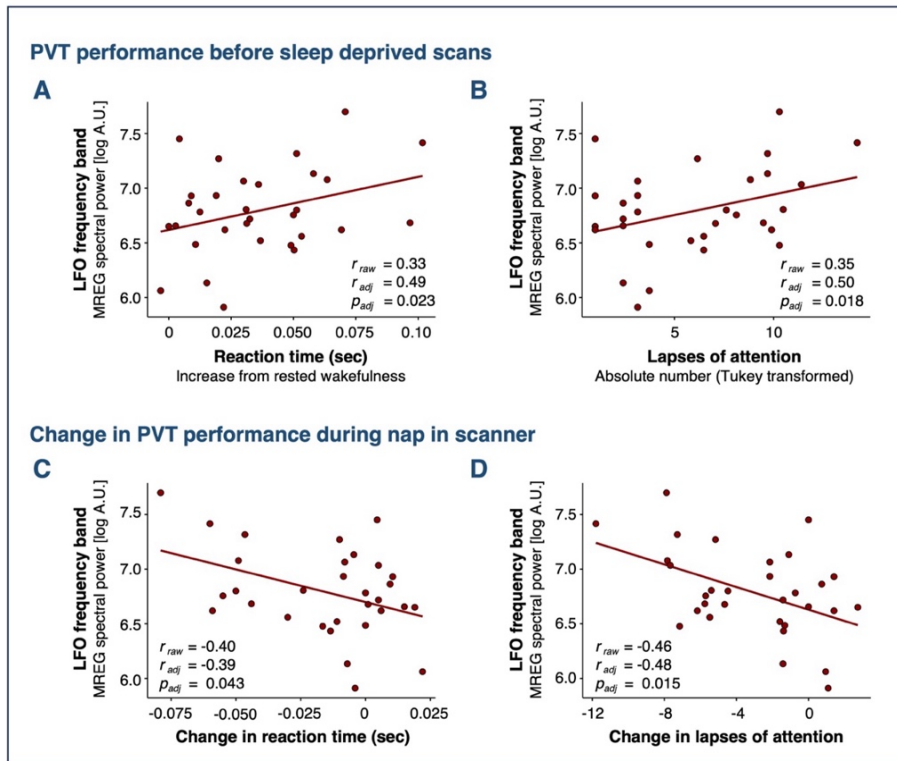


**Fig. 3. PVT performance is associated with LFOs during sleep.** (A, B) Correlations between pre-scan measures of impaired PVT performance (i.e. longer reaction times and more lapses of attention) and intensity of LFO spectral power during sleep. (C, D) Improvement in PVT performance (i.e. lower reaction time and less lapses) from before to after nap in scanner correlates with strength of LFO spectral power during sleep. Data from both sleep deprived scans are included. Dots represent mean LFO spectral power during NREM sleep (stages N2 or N3).  $r_{raw}$  denotes Pearson's correlation coefficient.  $r_{adj}$  and  $p_{adj}$  denote estimates from linear mixed models adjusted for treatment and repeated measures.  $N_{placebo} = 14$ ,  $N_{carvedilol} = 17$ .

### NREM sleep enhances spectral power in the respiration and cardiac frequency bands; N3 more so than N2 sleep

The effects of sleep deprivation, NREM sleep and sleep depth on brain pulsations driven by respiratory and cardiac forces were evaluated by assessing MREG spectral power within individually tailored respiration- and cardiac frequency bands (see methods) in 30-sec epochs from well-rested and sleep-deprived placebo scans (Tables S3 & S5).

Compared to rested wakefulness, awake sleep-deprived participants had increased whole-brain spectral power within the respiration (+45%,  $p = 0.038$ , Fig. 2D, E-F), but not in the cardiac frequency band (+6%,  $p = 0.75$ , Fig. 2D, G-H). When participants fell asleep and entered NREM sleep (pooled N2 and N3), we observed a strong increase in whole-brain spectral power in both the respiration (+73%,  $p < 0.001$ , Fig. 2D, E-F) and cardiac frequency bands (+35%,  $p = 0.003$ , Fig. 2D, G-H). Compared to rested wakefulness, sleep deprived NREM sleep increased spectral power by 150% and 42% in the respiration and cardiac frequency bands, respectively ( $p < 0.001$ ).

Sleep depth also influenced respiration- and cardiac-driven brain pulsations. In the respiration frequency band, N2 sleep was associated with a 35% increase in spectral power compared to sleep-deprived wakefulness ( $p_{adj} = 0.047$ ), while N3 sleep further increased spectral power by 57% ( $p_{adj} < 0.001$ ) (Fig. 4A-C). In the cardiac frequency band, spectral power was higher during N3 sleep than during both N2 sleep (+39%,  $p_{adj} < 0.001$ ) and sleep-deprived wakefulness (+58%,  $p_{adj} < 0.001$ ). No statistically significant change in cardiac spectral power was observed when comparing sleep-deprived wakefulness to N2 sleep ( $p_{adj} = 0.19$ ) (Fig. 4A & D-E). We did not observe any correlation between PVT performance and spectral power in the respiration and cardiac frequency bands.

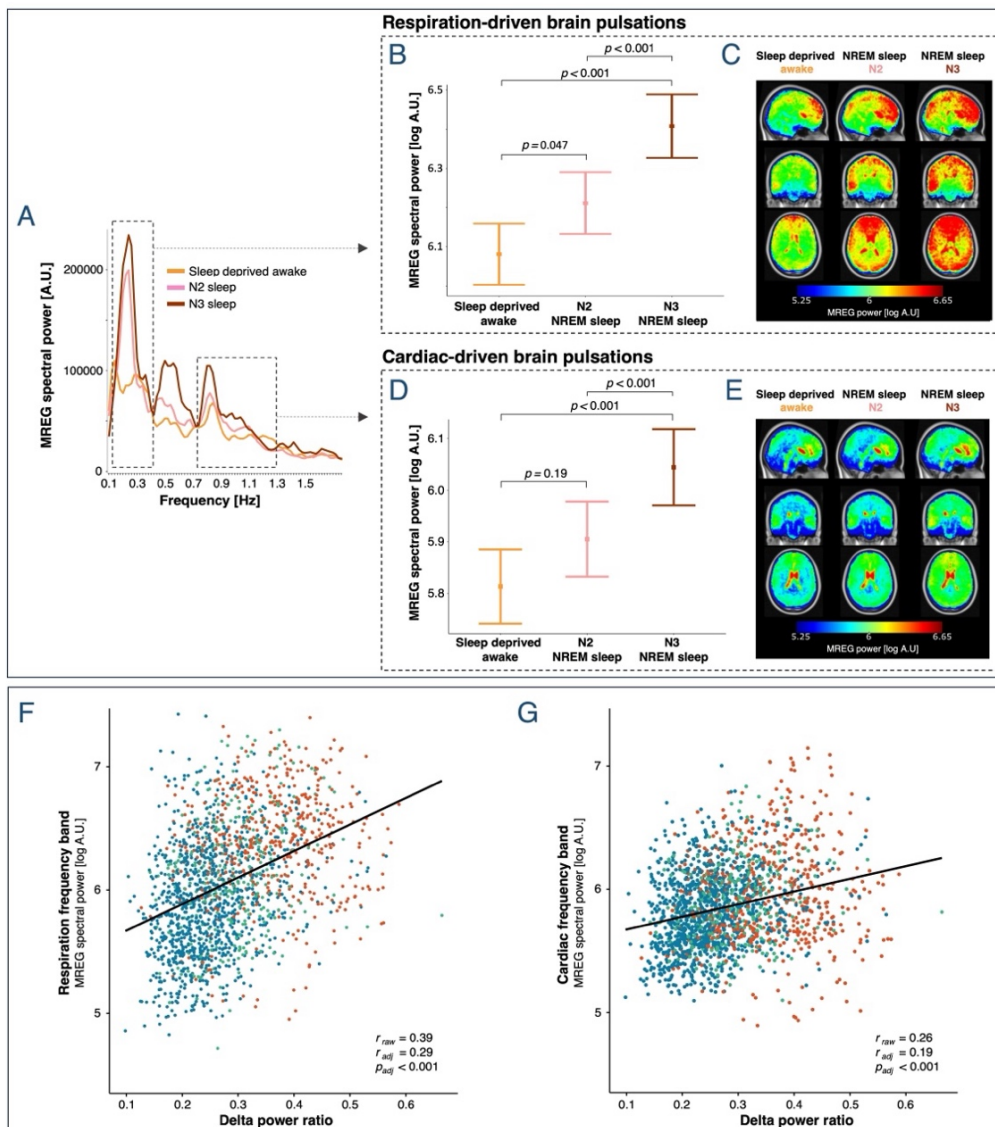


**Figure 4. Strength of respiration- and cardiac-driven brain pulsations correlates with sleep depth and EEG delta power.** (A) Mean whole-brain MREG spectra across participants for sleep-deprived wakefulness, N2 sleep and N3 sleep (placebo scans). Dashed boxes denote frequency ranges, in which respiration- and cardiac-related peaks are found (B, D) Estimated means  $\pm$  SEM and p-values from linear mixed models evaluating the effect of sleep depth on

log spectral power. All p-values have been adjusted for multiple comparison. **(C, E)** Whole-brain maps illustrate the regional spectral power [log A.U.] in the respiration and cardiac frequency bands across all 30-sec epochs, averaged across first epochs, then participants (warped into MNI space).  $N = 19$  (see Table S5 for number of participants in each of the conditions). **(F, G)** EEG delta power ratio versus simultaneously acquired spectral power in the respiration and cardiac frequency bands in all 30-sec epochs from both rested and sleep-deprived placebo scans. Colours represent the scored sleep stages (blue: rested wakefulness; red: NREM sleep stage 2 and 3; green: uncertain scorings) and are included for visualisation, but were not included in analysis.  $r_{raw}$  denotes Pearson's correlation coefficient.  $r_{adj}$  and  $p_{adj}$  denote adjusted estimates from linear mixed models.  $N_{resp} = 19$  and  $N_{card} = 20$ .

## **EEG delta-power during MR-imaging correlates with spectral power in respiration and cardiac frequency bands**

To validate the found effects of NREM sleep and sleep depth on respiration- and cardiac-driven brain pulsations in a quantitative and sleep-stage independent manner, we quantified EEG delta-power ratio across all 30-sec epochs from well-rested and sleep-deprived placebo scans, irrespective of their scored vigilance state (Fig. 4, lower panel). This showed a positive correlation between EEG delta power ratio and whole-brain spectral power in both the respiration ( $r_{raw} = 0.39$ ,  $r_{adj} = 0.27$ ,  $p_{adj} < 0.001$ ; Fig. 4F) and cardiac ( $r_{raw} = 0.26$ ,  $r_{adj} = 0.19$ ,  $p_{adj} < 0.001$ ; Fig. 4G) frequency bands. This positive association was identifiable in most participants (Fig. S4).

## **NREM sleep primarily enhances spectral power in respiration and cardiac frequency bands in grey and white matter**

To explore whether the strength of physiological brain oscillations differ between grey matter (GM), white matter (WM) and CSF, we analysed data from well-rested and sleep-deprived placebo scans. During rested wakefulness, LFO spectral power was consistent across tissue types (Fig. 5A). In sleep deprivation, LFO spectral power also increased to a similar extent in GM, WM and CSF ('tissue type'  $\times$  'sleep deprivation' interaction:  $p = 0.96$ ; Fig. S5A). Similarly, no interactions were observed between NREM sleep and tissue type for LFOs ( $p = 0.92$ ; Fig. 5B&C).

By contrast, in the respiration and cardiac frequency bands, spectral power varied significantly across CSF, GM and WM ('tissue type' main effect:  $p < 0.001$ ). During rested wakefulness, CSF showed notably higher spectral power than both GM (respiration band: +101%,  $p_{adj} < 0.001$ ; cardiac band: +1030%,  $p_{adj} < 0.001$ ) and WM (respiration band: +118%  $p_{adj} < 0.001$ ; cardiac band: +1153%,  $p_{adj} < 0.001$ ). Additionally, participants had higher spectral power in GM than in WM in the well-rested condition (respiration band: +9%,  $p = 0.017$ ,  $p_{adj} = 0.052$ ; cardiac band: +11%,  $p = 0.005$ ,  $p_{adj} = 0.014$ ; Fig. 5A).

The effect of NREM sleep on respiration- and cardiac-driven brain pulsations was more pronounced in GM and WM than in CSF, with a significant interaction effect between vigilance state and tissue type ( $p < 0.001$ ; Fig. 5B&C). Specifically, GM and WM exhibited 70% and 75%

stronger increases in spectral power during NREM sleep than CSF in the respiration band, and 92% and 110% stronger increases than CSF in the cardiac band ( $p_{adj, all} < 0.001$ ). When evaluated separately, all tissue types showed significant effects of NREM sleep on spectral power in both respiration- and cardiac frequency bands (respiration band<sub>(all)</sub>:  $p < 0.001$ ; cardiac band<sub>(all)</sub>:  $p < 0.01$ ). Additionally, sleep deprivation interacted with tissue type in the respiration band ( $p < 0.001$ ), with effects confined to GM ( $p = 0.045$ ) and WM ( $p = 0.054$ ) (Fig. S5B&C).

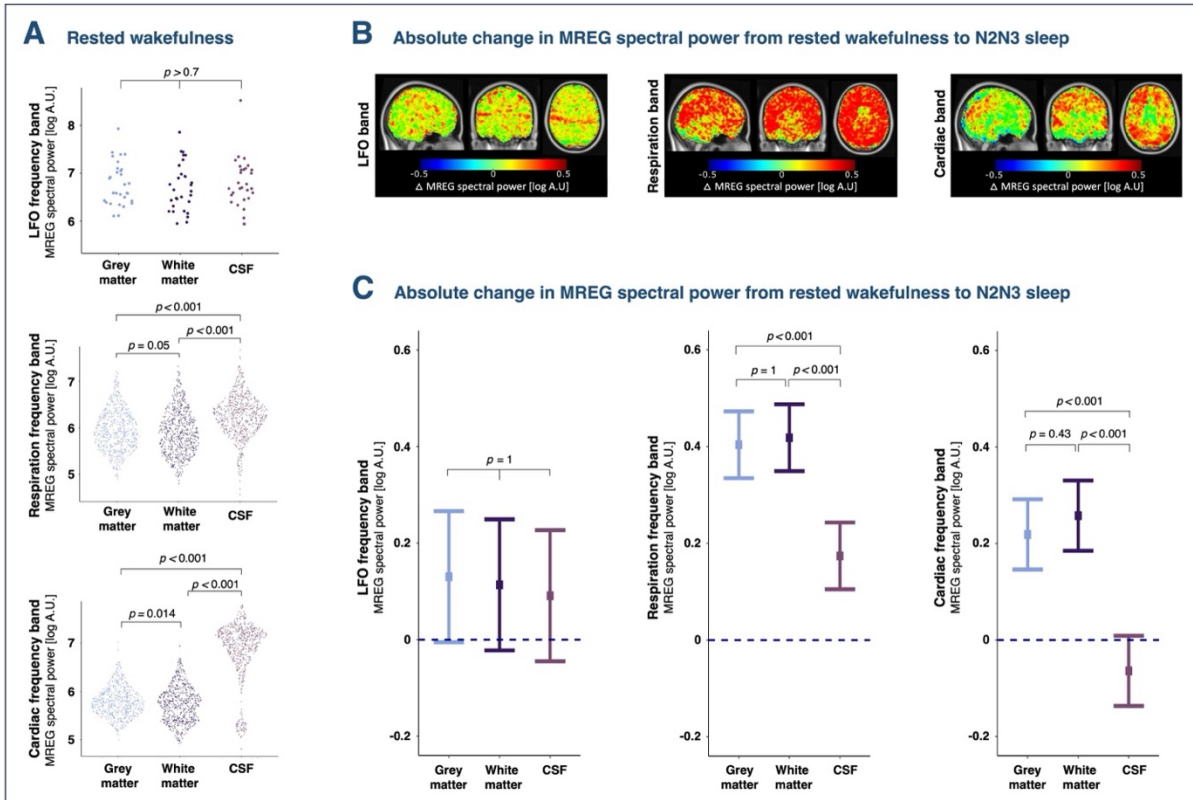


**Figure 5. Sleep has a greater effect on respiration- and cardiac-driven brain pulsations in grey and white matter than in CSF.** (A) Difference in brain oscillations strength between grey matter, white matter and CSF in ventricles in rested wakefulness. Each data point represents a 30-sec epoch from a single participant. (B) Brain maps illustrate the averages of participant-wise absolute differences in spectral power between rested wakefulness and NREM sleep (stages N2 and N3) in LFO, respiration on cardiac frequency bands. Whole-brain spectral power maps of individually calculated voxel-wise differences were warped into MNI space and averaged across participants. (C) Changes in estimated means of log spectral from rested wakefulness to N2-N3 NREM sleep.  $p$ -values represent interaction effects between tissue type and sleep from linear mixed models and are adjusted for multiple comparisons.  $N = 20$  (see Tables S3 and S4 for number of participants in each condition).

## Adrenergic antagonism decreases spectral power in LFO and cardiac frequency bands

Treatment with the adrenergic antagonist carvedilol demonstrated the anticipated systemic effects: It reduced plasma norepinephrine levels [41] ( $-479 \pm 113$  pg/mL,  $p_{adj} < 0.001$ ,  $N = 20$ ; Fig. S3), lowered mean arterial blood pressure by  $\sim 5\%$  ( $-4.4 \pm 0.9$  mmHg,  $p < 0.001$ ,  $N = 20$ ), and

did not alter respiration or heart rates (Table S3). Carvedilol also did not change absolute or relative time spent in wakefulness or sleep during scans (Fig. S2) and only had minor effects on recovery sleep (Table S6). During NREM sleep, carvedilol was associated with a decrease in LFO spectral power (-51%,  $p = 0.050$ ), while this was not the case during wakefulness (-35%,  $p = 0.32$ ) (Fig. 6A-C). Similarly, carvedilol significantly reduced spectral power in the cardiac frequency band during NREM sleep (-30%,  $p = 0.032$ ), but not during wakefulness (Fig. 6D, G-H). In the respiration frequency band, carvedilol intervention showed comparable spectral power outcome as placebo during both sleep-deprived wakefulness and NREM sleep ('treatment':  $p = 0.56$ , 'NREMsleep<sub>carvedilol</sub>':  $p < 0.001$ , Fig. 6D&E-F).

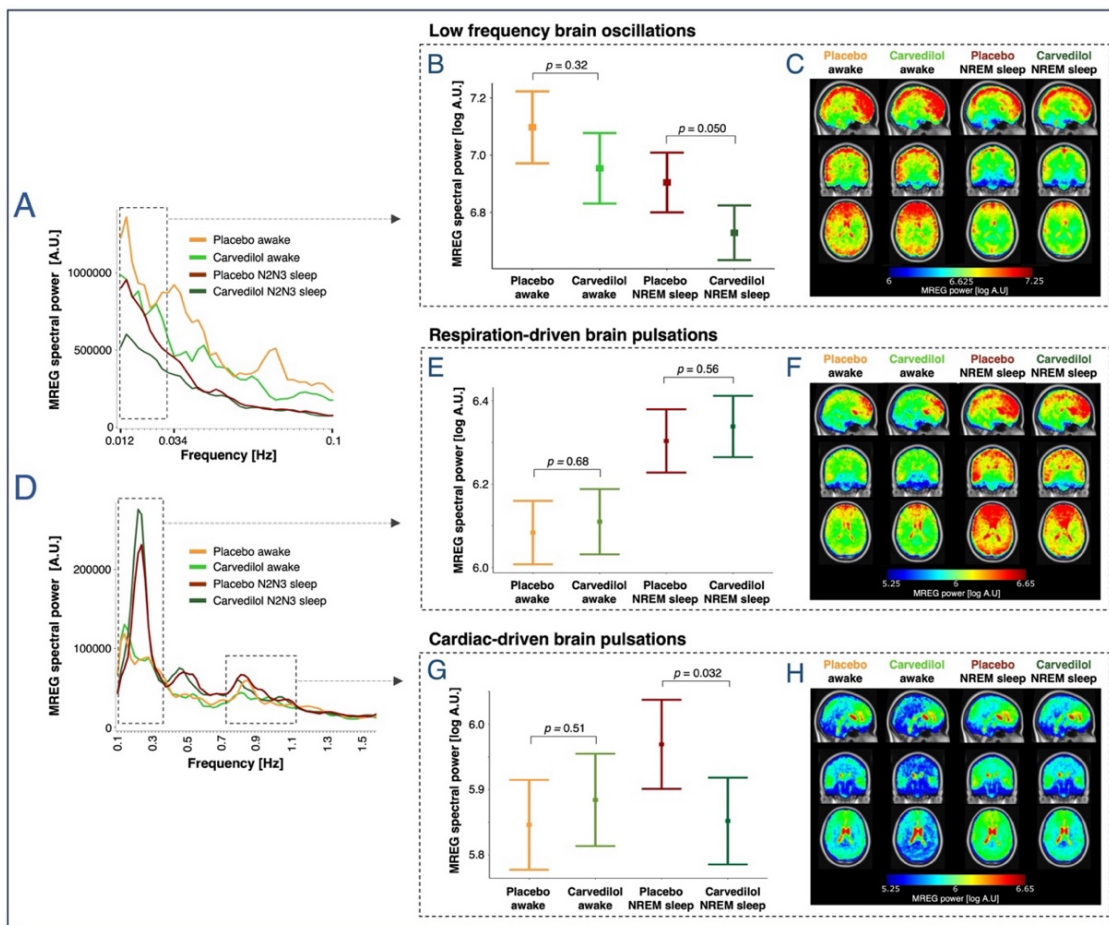


**Figure 6. The  $\alpha 1$  and  $\beta$ -adrenergic antagonist carvedilol attenuates LFOs and cardiac-driven brain pulsations during sleep.** (A, D) Mean whole-brain MREG spectra across participants in the sleep-deprived scans for placebo wakefulness, placebo NREM sleep, carvedilol wakefulness and carvedilol NREM sleep. Dashed boxes denote frequency ranges for LFOs (0.012–0.034 Hz) and for respiration- and cardiac-related peaks. (B, E, G) Estimated means  $\pm$  SEM and  $p$ -values are from linear mixed models evaluating the effect of treatment and NREM sleep. (C, F, H) Brain maps illustrate regional MREG spectral power [log A.U.] in the LFO, respiration and cardiac frequency bands across participants, averaged across first all 5-min scans (LFO) or 30-sec epochs (respiration and cardiac) per participant, then across participants (warped into MNI space).  $N = 20$  (see Tables S3 and S4 for number of participants in each of the three conditions).

## Discussion

In this circadian-controlled sleep and sleep deprivation study, we demonstrate that heightened sleep pressure promotes cerebrovascular oscillations, while sleep depth and EEG delta power correlate with the strength of brain pulsations driven by respiratory and cardiac forces (illustrated in Fig. 7).

Physiological brain oscillations, as visualised with MRI, have been suggested to reflect either the magnitude of brain fluid motion [36,37] or the underlying compliance of brain tissue, encompassing factors such as water content and tissue viscosity [42,43]. Our data support this interpretation for respiration- and cardiac-induced brain pulsations demonstrating that, irrespective of vigilance state, these pulsations are significantly stronger in CSF than in both grey and white matter. During rested wakefulness, they are also more pronounced in grey matter compared to white matter. Considering that water content and viscosity vary across these three brain tissue types [44,45], our results indicate that water content is directly associated with the strength of MREG-detected respiration- and cardiac-driven brain pulsations, and that increases in CSF influx to the brain parenchyma will amplify these pulsations. For LFOs, we observed no differences in oscillation strength across tissues types, supporting that MR-detected brain oscillations below 0.1 Hz reflect global cerebral vasomotion and its temporally associated effects on CSF inflow and oscillations [26,46]. Notably, we discovered that intervention with the adrenergic antagonist carvedilol – which is known to inhibit smooth muscle contraction and thereby potentially decreases cerebral vasomotor activity [47,48] – was associated with a reduction in both LFOs and cardiac-driven brain pulsations during sleep. This novel finding provides compelling evidence supporting the hypothesis that LFOs originate from cerebrovascular oscillations.

A novel finding of our study is that sleep deprivation has a greater effect on LFOs than sleep itself. Specifically, MREG-detected LFOs increase at a whole-brain level after 35 hours of wakefulness, compared to both rested wakefulness and subsequent periods of NREM sleep stages N2 and N3. Additionally, LFO strength during sleep correlates with pre-sleep measures of impaired psychomotor vigilance, which is a well-established marker of homeostatic sleep pressure, or the biological need to sleep [49,50]. In line with this, we also found a positive correlation between LFO strength during sleep and improvements in psychomotor vigilance from before to after the nap. Collectively, this suggests sleep pressure as a strong driver of cerebrovascular oscillations and that these oscillations play an important role in restoration of performance during sleep. Supporting this notion, a recent MREG study showed that healthy individuals exhibit stronger LFOs during sleep-deprived N1 sleep than during rested N1 sleep

[39]. While previous studies in humans have demonstrated that NREM sleep stages N1 and N2 increase LFO strength [26,39,51], they did not differentiate the effects of sleep deprivation from those of sleep itself, nor did they account for circadian influences or sleep pressure at scan onset. In the present study, we address these gaps, demonstrating that LFOs are already elevated during sleep-deprived wakefulness and therefore propose that earlier reports of LFOs in sleep have been confounded by sleep pressure effects. Sleep stage might also influence LFOs. ICP B-waves, which are believed to reflect cerebrovascular oscillations [32], have been reported to occur more frequently in N1 and N2 sleep [33,34] and less so during deeper sleep [52]. Similarly, both the slow oscillating CSF inflow through the fourth ventricle and its simultaneous global signal are strongest in N1 sleep, followed by N2 sleep, and weakest in N3 sleep [46]. Given that sleep pressure dissipates over time spent asleep [3], this indicates that cerebrovascular oscillations are strongest at the beginning of sleep, when sleep pressure is at its peak and individuals typically reside in lighter sleep stages. Since plasma norepinephrine was borderline increased during sleep deprivation, we also tested for an association between (change in) norepinephrine levels and LFOs measured in sleep deprived wakefulness or sleep, but found none. There were also no significant changes in blood pressure, heart and respiration rates in sleep-deprived wakefulness compared to rested wakefulness. That is, we do not find evidence that autonomic arousal alone explains the observed increases in LFOs, as proposed by Picchioni and colleagues [46]. Taken together, these findings indicate that cerebral vasomotion intensifies as the need for sleep increases, which is especially compelling as cerebrovascular oscillations are believed to be a key driver of CSF influx to the brain parenchyma [17], or glymphatic flow. This suggests that as sleep pressure builds up, the brain activates restorative brain clearance mechanisms.

Expanding on previous findings [39,51], we show that slow-wave-rich NREM sleep (pooled N2 and N3 sleep) enhances respiration- and cardiac-driven brain pulsations at a global brain level, and as a novel finding, we show that sleep-effect are more pronounced in grey and white matter than in CSF. As the strength of these physiological brain pulsations relates to tissue water content, we propose that this finding supports a sleep-dependent increase in CSF influx to the brain parenchyma and expansion of extracellular space volume in humans, similar to observations made in the mouse brain [8,10].

We further demonstrate that the strength of respiration- and cardiac-driven brain pulsations increases with the sleep depth, showing greater pulsatility in N3 than in N2 sleep, and correlates positively with EEG delta power, which is a measure of slow wave activity. A recent study on shallower NREM sleep[39] agrees with these results, reporting that respiration- and cardiac-driven brain pulsations encompass larger brain regions in N2 than in N1 sleep. Although our data cannot determine how brain fluid flow increases with sleep intensity, as we did not observe significant

increases in cerebrovascular oscillations by sleep, the association between sleep slow waves – i.e. deeper sleep and higher delta power – and brain pulsation strength strongly support the recent suggestion that the synchronous neuronal activity of slow-wave sleep drive fluid and solute movement physio-mechanically into and through the brain [11,53]. As EEG delta power is also an established marker of homeostatic sleep propensity [2,54], its close association with respiration- and cardiac-driven brain pulsation strength, and thus brain fluid flow, implies that this may be homeostatically regulated and an integral function of human sleep. Our results closely mirror preclinical work demonstrating that CSF influx and perfusion through the brain parenchyma is associated with EEG slow waves [9,11]. Consequently, we here provide support for the hypothesis that humans - alike mice – have a sleep- and slow-wave dependent exchange of CSF and interstitial fluid, clearing the brain of waste products.

Although smaller than during sleep, we also noted an increase in respiration-driven brain pulsations in grey and white matter during sleep-deprived wakefulness. We speculate this may indicate increased CSF influx to the brain parenchyma due to elevated LFOs during sleep deprivations, or alternatively, it may highlight the link between brain fluid dynamics and EEG slow waves, given the slight rise in EEG delta power after 35 hours of wakefulness.

Preclinical studies suggest that central inhibition of noradrenergic receptors increases CSF influx [8,55] and brain clearance [56]. However, as our participants received only a single peroral dose of carvedilol, which is known to enter the brain in minimal amounts [48,57], we believe that its main pharmacological effects were on the cardiovascular system. Consistent with this, we observed reductions blood pressure, plasma norepinephrine, cardiac-driven brain pulsations and LFOs, and found no discernible differences in sleep patterns between placebo and carvedilol sessions. Furthermore, the strength of respiration driven brain pulsations observed under the placebo condition was largely replicated with carvedilol. These findings mirror preclinical evidence that systemic administration of adrenergic agonists increases cortical artery pulsatility [21,22].

Our study is not without limitations. To eliminate the influence of age and menstrual cycle on sleep and circadian rhythm [58], we only included young males. While preclinical studies have not found any male/female differences in glymphatic flow,[59] this limits the generalizability of our findings. Also, there is no consensus in the literature on the appropriate frequency range for brain LFOs. We chose a range consistent with B-waves (0.01 – 0.034 Hz), whereas others have applied a broader band (~ 0.01 – 0.1 Hz) [26,38]. In a posthoc analysis, we assessed whether using a 0.01 – 0.1 Hz band would alter our results and found them consistent with the band used in our study. Nonetheless, this is the first study to carefully control for effects of sleep pressure, time of day, circadian rhythm, and alcohol and caffeine intake when evaluating how vigilance state influences physiological brain oscillations.

## **Conclusion**

Our investigation unveils that, following 35 hours of wakefulness, LFO intensify throughout the entire brain and that objective measures of sleep pressure exhibit a positive correlation with the magnitude of LFOs during sleep. Additionally, our study reveals that pharmacological modulation of vascular pulsatility dampens LFOs, providing compelling evidence supporting that LFOs represent cerebrovascular oscillations. These important findings offer crucial insights into how the vasomotor system in the brain responds to sleep deprivation, potentially serving as a means to mitigate the accumulation of brain waste products. Furthermore, we illustrate that as sleep depth increases, brain pulsations induced by respiration and cardiac activity intensify in both grey and white matter. As these brain pulsations likely reflect brain fluid flow, our observation aligns with preclinical evidence of a slow-wave-dependent influx of CSF into the brain parenchyma. These new findings collectively contribute to our understanding of the intricate dynamics of homeostatic sleep mechanisms, vasomotor activity, brain fluid flow and the clearance of waste products from the brain.

## Materials and methods

### Study design

We conducted a circadian-controlled sleep and sleep deprivation study that included a double-blind, placebo-controlled, cross-over administration of the non-selective  $\beta$ 1-,  $\beta$ 2- and  $\alpha$ 1-adrenergic antagonist carvedilol (Fig. 1). The study was preregistered at ClinicalTrials.gov (NCT03576664) and conducted at Rigshospitalet in Copenhagen (Denmark), between January 2018 and May 2019. Approval was granted by the Danish ethics committee of the Capital Region of Denmark (journal ID: H-16045933) and the study adhered to the principles of Declaration of Helsinki.

During an adaptation week and throughout the study period, participants followed a strict 8 h sleep, 16 h wake protocol. Sleep-wake rhythms were monitored continuously with actigraphy (Actiwatch spectrum, Philips Respironics) and a sleep diary to ensure that all measurements were performed during the same circadian phase and at comparable sleep propensities. Furthermore, participants were not allowed to drink alcohol and daily caffeine consumption was limited to two or less cups of coffee ( $\leq$  200 mg caffeine/day) taken no later than 2 pm. Three EEG/MRI scan sessions were conducted on separate days in the evening (standardised time:  $\sim$ 18.30-20.30): A well-rested scan scheduled after 11 hours of wakefulness followed by two sleep-deprived scans performed after 35 hours of wakefulness. Sleep-deprived scans were performed one week apart. Participants received either placebo or 25 mg of carvedilol one hour before scan start, as carvedilol reaches peak plasma concentration within 1-2 hours [47]. Placebo and carvedilol were administered in identical capsules (manufactured and distributed by Capital Region Pharmacy) and participants were randomised to either the placebo-carvedilol or carvedilol-placebo sequence analysis (10 in each) by a research administrator not otherwise involved in data collection or. All three EEG/MRI scans sessions included a period of wakefulness (well-rested scan:  $\sim$  45 min; sleep-deprived scans:  $\sim$ 30 min) followed by an one-hour sleep opportunity. During the awake period, lights were on, and participants were continuously monitored to ensure they remained awake with eyes open. During sleep opportunities, lights were turned off, the scanner environment was kept as quiet as possible, and participants were told to relax and that they were allowed to sleep. Participants' blood pressure was measured before and immediately after scan sessions and a blood sample to quantify plasma norepinephrine level was collected  $\sim$ 15 min after scans had ended. Sleep pressure was assessed with psychomotor vigilance test (PVT) performance before and after all scan sessions.

During the nights leading up to each of the three study periods and during the two nights following the sleep deprivation scans, participants slept in a controlled sleep environment

monitored with polysomnography (PSG). The prolonged wakefulness periods were monitored with a minimal EEG setup and participants were continuously supervised by members of the research team (see *supplementary methods*).

## **Study population**

Twenty healthy males, aged 18–29 years, were included in and completed the sleep study (see consort flow diagram in Fig. S1). Participants were recruited from a local database of individuals interested in participating in brain imaging studies and via a national test subject recruitment database ('www.forsøgsperson.dk'). All participants were right-handed, fluent in Danish, had normal blood pressure, reported no sleep issues when questioned systemically and had no prior or current neurological or psychiatric disorders, learning disabilities, severe somatic diseases, or any use of prescription drugs of relevance for the study. All were non-smokers and did not have excessive use of alcohol or illicit drugs and had not performed shiftwork three months prior to study participation. Participants who had crossed two or more time zones were required to have at least 14 days of recovery per time zone before enrolment. Before inclusion, participants underwent a PSG screening night to rule out undiagnosed sleep disorders or low sleep efficiency (defined as < 85%). Written informed consent was obtained from all participants before enrolment in the studies.

## **MRI acquisition**

Simultaneous EEG and MRI was performed on a Siemens (Erlangen, DE) MAGNETOM 3T Prisma scanner with a 64-channel head coil. Structural images were acquired using a high-resolution, whole-brain, T1-weighted MPRAGE scan with the following parameters: Inversion time = 900 ms, repetition time = 1900 ms, echo time = 2.52 ms, flip angle = 9°, in-plane matrix = 256 × 256, in-plane resolution = 0.9 × 0.9 mm, slices = 208, slice thickness = 1.0 mm. For accelerated functional MRI imaging, we used a MREG sequence obtained from the University of Freiburg.[60,61] MREG allows for 3D whole-brain imaging with a repetition time of 100 ms at a resolution of 3x3x3 mm using a stack-of-spirals k-space undersampling trajectory. Further scan parameters were: 3D matrix size = 64x64x50, echo time = 33 ms, flip angle = 25°, field of view = 150 mm and a gradient spoiling of 0.1 (for  $n = 3$ , gradient spoiling was 1.0) [35].

Participants were fitted with an MRI-compatible EEG-cap as well as a respiratory belt and a pulse oximeter wired directly to the scanner. They also wore earplugs to reduce scanner noise, and head cushions were used to restrict head movement. During sleep opportunities, scans alternated between 5-min MREG and 5-min multiband echo-planar sequences (the latter data not reported here) to maintain a steady noise level.

## **MREG and structural brain data preprocessing**

MREG data were reconstructed with a MATLAB reconstruction tool provided by the sequence developers [62], using L2-Tikhonov regularization with  $\lambda = 0.2$  and a regularization parameter determined by the L-curve method. To ensure steady-state signal saturation, the first 10 seconds of data (= 100 images) were excluded from all MREG scans. Next, MREG data were preprocessed and analysed using Statistical Parametric Mapping software (SPM12, Wellcome Trust Center for Neuroimaging, UCL) in MATLAB (R2017b, The Mathworks, Inc.), including motion correction, which was performed by realignment and co-registration of the high-resolution T1 structural image to the MREG data. Co-registration was enhanced with FSL's Brain Extraction Tool, employing a fractional intensity threshold of 0.3 on the first functional volume of each MREG scan, to which the structural image was co-registered. Subsequently, the co-registered structural images were segmented into grey matter, white matter, and CSF maps.

In order to evaluate CSF oscillations with as little interference of surrounding tissue and vascular pulsations as possibly, we created a CSF ROI in the left lateral ventricle: We marked a sphere with a radius of 2 cm around a manually selected midpoint of the left ventricle defined in MNI space (MNI coordinates: (8,-10,24)), keeping only the voxels with a segmentation-based CSF probability larger than 0.5. The ventricle ROI were then normalized to each scan session and used to assess CSF oscillations in tissue-type analyses.

## **EEG acquisitions during MRI**

To monitor sleep and wakefulness during scans, participants wore a MRI-compatible EEG cap (Electrical Geodesics, Inc., Eugene, OR) with 256 EEG channels and a single reference electrode (Cz). The cap was selected based on participants' head circumference and prepared with an electrolyte/shampoo solution. Cap placement was aided by positioning the reference electrode at the vertex and visual inspection of predetermined reference points. The cap was secured with a net and kept moist by a shower cap. Impedances were kept below 50 k $\Omega$ . Two electrocardiographic (ECG) electrodes were placed on the left side of the sternum, at the 4<sup>th</sup> and 5<sup>th</sup> intercostal spaces. Optical cables from the cap were routed along the side of the head inside the MRI head coil. EEG and ECG data were acquired with a 1 kHz sampling rate and all cables were connected to a synchronization box to match acquisition to the MR scanner clock frequency. Removal of gradient and ballistocardiographic artefacts from the EEG was performed with MATLAB (R2014a, The MathWorks, Inc.) using standard methods in a stepwise approach (see *supplementary methods*).

## **Sleep scoring and EEG delta power ratio**

EEG recordings were visually scored in 30 second (sec) epochs in accordance with standard AASM criteria (American Academy of Sleep Medicine, 2007) using DOMINO scoring software (Somnomedics, Germany). To accurately quantify sleep in the MR environment, EEG recordings were scored by two independent experts blinded to subject, treatment and scan type (lights on or lights off). In addition, scorers were also instructed to mark epochs with residual MR artefacts and aberrant non-physiological data as “artefacts”. The overall agreement between the two scorers was 73%, which is similar to what would be expected for standard sleep scorings in a non-MR environment [63].

Final sleep staging for EEG epochs was determined by consensus between experts as follows: 30-sec epochs were labelled as ‘wakefulness’ if they occurred before the first onset of NREM sleep stages N2 or N3 (scored by either expert) and if both experts agreed on ‘wakefulness’ or if one scored it as ‘wakefulness’ and the other scored it as ‘artifact.’ Epochs were classified as ‘NREM sleep’ if both experts scored them as either NREM sleep stage N2 or N3, while epochs were only classified as ‘N2 sleep’ or ‘N3 sleep’ if both experts scored them as such. Delta power ratio was quantified for all 30-sec epochs as the ratio between the computed EEG band power ( $\text{mV}^2$ ) in the 1 – 4 Hz range and in the 0.5 – 30 Hz range (*details in supplementary methods*).

## **MREG data analysis**

For analysis of LFOs, we used the full 5-min MREG sequences and assessed spectral power within a frequency range based on the clinically described B-waves (0.5–2 waves pr. min) [64]. For each 5-min MREG scan (corresponding to 10 scored EEG epochs), data were high-pass filtered with a 10-order IIR filter (highpass 0.008 Hz). Spectral analysis was then performed for individual voxels in a whole-brain mask consisting of all voxels with either a grey matter, white matter, or CSF probability larger than 0.1, using the MATLAB periodogram function with a Hanning window and bin width of 0.00244 Hz. Next, the voxel-wise MREG spectra were averaged to create respective whole-brain or tissue-type-specific MREG power spectra. 5-min scans with framewise displacement >3 mm in one or more 30-sec epoch were excluded from analysis. To avoid spill-over effects from the bandpass filtering, the exact frequency interval for LFO analysis was set to 0.01221 – 0.03418 Hz (~ 0.7–2.1 waves pr. min). 5-min MREG scans were selected for LFO-analysis if EEG experts had classified at least 80% (8/10 epochs) of the simultaneously recorded EEG epochs as either wakefulness or NREM sleep and only if they occurred in lights-on or lights-off conditions, respectively.

For analysis of respiration- and cardiac-driven brain pulsations, we used a 30-sec dataset and assessed spectral power in individually tailored respiration and cardiac frequency bands.

Data from all 5-min MREG scans were high-pass filtered with a 10-order IIR filter (passband 0.1 Hz), and segmented into 30-sec epochs, which were temporally aligned with corresponding sleep-scored EEG epochs. For each 30-sec epoch, spectral analysis was performed as described for the 5-min dataset, but with a bin width of 0.02 Hz. Epochs with a framewise displacement above 3 mm were excluded ( $n = 91$  epochs). We defined epoch-by-epoch heart rate and respiration frequencies using temporally aligned data from the respiratory belt and the pulse oximeter, imported using the TAPAS PhysIO toolbox.[65] The dominant peaks in respiration (0.13 – 0.5 Hz; 7.8 – 30  $\text{min}^{-1}$ ) and cardiac frequency ranges (0.67 – 2 Hz; 40.2 – 120  $\text{min}^{-1}$ ) were determined from the periodogram-determined power spectrum of each 30-sec epoch of physiological data. The epoch-by-epoch peak frequencies for respiration and heart rates were then used to define the individually tailored 30-sec epoch-specific respiration and cardiac frequency bands in the MREG spectra. Frequency ranges for the epoch-wise respiration and cardiac bands were defined as the epoch-wise respiration rate  $\pm 0.06$  Hz ( $= \pm 3$  bins), and the epoch-wise heart rate  $\pm 0.1$  Hz ( $= \pm 5$  bins), respectively. 30-sec epochs with non-physiological values ( $< 40$  or  $> 90$  heart beats per min. and/or  $< 8$  or  $> 25$  breaths per min.) were excluded. 30-sec MREG epochs were selected for sleep- and sleep deprivation analyses if experts had classified the corresponding EEG as wakefulness, NREM sleep, N2 sleep or N3 sleep. For EEG delta power analysis, MREG epochs were only included if neither of the experts had scored the corresponding EEG as ‘artifact’.

## **Psychomotor vigilance**

A psychomotor vigilance test (PVT; e-Prime software, Psychology Software Tools Inc., Pittsburgh) was used to assess cognitive effects of prolonged wakefulness [66]. PVT is a simple reaction time task in which participants press the space key as quickly as possible upon seeing a digital millisecond counter on the computer screen. A total of 100 stimuli are presented at random interstimulus intervals of 2–10 sec. Participants completed a training session during the adaptation week and performed the PVT before (rested: 7 hour awake; sleep-deprived: 31 hour awake) and immediately after scans (following an 1-hour sleep opportunity) (Fig. 1). Two validated PVT variables were quantified [49,50]: “median reaction time” and “lapses of attention (reaction time  $> 500$  ms). Impaired psychomotor vigilance due to sleep deprivation was evaluated by 1) quantifying the increase in median reaction time from rested wakefulness (measure before sleep-deprived scan – measure before well-rested scan) and 2) the absolute number of lapses of attention before the sleep-deprived scan (Freeman-Tukey transformed:  $\sqrt{x} + \sqrt{(x + 1)}$ ). Improvements in psychomotor vigilance due to sleep in the scanner were computed as the difference between measures taken before and immediately after scans.

## Statistical analyses

MREG spectral power within LFO, respiration and cardiac frequency bands (calculated as sum of spectral power within frequency range) from well-rested (awake scan), sleep deprived placebo (awake and sleep scan) and sleep deprived carvedilol scan sessions (awake and sleep scan) was log transformed to mitigate skewness in the distribution before being analysed using linear mixed models. Linear mixed models included sleep deprivation (well-rested vs sleep-deprived), vigilance state (awake vs NREM sleep), sleep depth (sleep-deprived awake vs N2 vs N3), tissue type (grey matter vs white matter vs CSF), treatment (placebo vs carvedilol; randomised to sleep deprived scan session 1 and 2), PVT measurements ('median reaction time' and 'lapses of attention') and delta power ratio as additive fixed effects, with interactions between vigilance state and tissue type as well as between vigilance state and treatment. Subject ID, scan session (well-rested, sleep-deprived session 1, sleep-deprived session 2) and sleep opportunity (lights on, lights off) were included as random intercepts with sleep opportunity being nested into scan session itself nested into subject ID. To account for the impact of declining spectral power as a function of higher frequencies[67], respiration or heart rates recorded simultaneously with MREG-scans were included as fixed effects in all models assessing spectral power within respiration or cardiac frequency bands. P-values for testing fixed effects were obtained using Wald tests. The expected log spectral power at various conditions (e.g. sleep-deprived under carvedilol) was computed from the mixed model estimates to illustrate the model fit.

Associations between (i) PVT measurements and mean log spectral power within LFO, respiration and cardiac frequency bands in 5-min scans/30-sec epochs and (ii) delta power ratio and log spectral power within respiration and cardiac frequency bands in 30sec epochs were assessed with Wald tests obtained from linear mixed models (denoted  $p_{adj}$ ). Corresponding correlations coefficients were deduced from mixed model estimates (denoted  $r_{adj}$ ). For reference, Pearson's correlation coefficients for associations between (i) and (ii) were also evaluated (regardless of subject ID, scan session, sleep opportunity, respiration- and heart rates and treatment) and denoted  $r_{raw}$ .

Where pairwise testing was appropriate, we conducted Student's two-tailed t-tests for data with a normal distribution and Wilcoxon signed-rank tests for data not normally distributed. P-values equal to or below 0.05 were considered significant except in analyses where three levels of a fixed effect were evaluated (and compared pairwise). Here, P-values were adjusted for multiple comparison using Bonferroni correction. If not otherwise specified, estimates are reported as mean SEM. All analyses were performed with the statistical software R (<http://www.R-project.org/>). The R packages lme4 (version: 1.1.29), lmerTest (version: 3.1.3), and LMMstar

(version: 0.8.9) were used for, respectively, fitting random intercept models, performing Wald tests, and estimating expected means and correlation parameters.

For detailed descriptions of all statistical models applied throughout the paper and power calculations, see *supplementary methods*.

## **Data availability**

All data and code that support the findings of this study are available from the corresponding author, upon reasonable request.

## **Acknowledgments**

We would like to thank Helle Leonthin for sleep staging and Emily Beaman, Cecilie Lerche Nordberg and members of the Center for Translational Neuromedicine lab for their assistance with data collection and supervision of proper sleep deprivation. We also thank Dan Xue from the Center for Translational Neuromedicine for assistance with illustrations.

## **Funding**

The research reported in this work was funded by the H2020 Marie Skłodowska-Curie Actions grant: H2020-MSCA-IF-2017-798131 (SCH); the Lundbeck Foundation grant: R264-2017-2778 (SCH); the Lundbeck Foundation grant: R279-2018-1145 (GMK); the Independent Research Fund Denmark grant: 0134-00454B & 7025-00090B (GMK); the Independent Research Fund; Rigshospitalet Forskningspuljer grant: R151-A6534 (GMK); the EU Joint Programme - Neurodegenerative Disease Research 2022-120 (VK, GMK, MN). The funders had no role in research conceptualization, study design, data collection and analyses, decision to publish or manuscript preparation.

## **Author contributions**

GMK, SCH, MN and PJJ conceptualised and designed the study. SCH and SMUL set up the sleep study protocol. SCH, SMUL, DBZ and SP were responsible for data collection. SMUL conducted analyses of sleep study data with the help of SCH, ASO, DBZ and KBB. DBZ scored EEG-data. ASO preprocessed EEG- and neuroimaging data from the sleep study and evaluated voxel-wise spectral power. PW measured norepinephrine levels in plasma from sleep study. BO set up statistical models and helped interpret model outcomes and visualise results. VK and PJJ gave technical support and conceptual advice on EEG and MREG-data collection and analysis. GMK, MN and PJJ supervised the project. SMUL, SCH and GMK wrote and prepared the manuscript.

All authors contributed to the interpretation of result and have all approved the final version of the manuscript.

## Competing interests

S.C.H. is currently an employee of Roche Pharma, which is unrelated to the contents of this manuscript. All other authors declare no competing interests.

## References

1. Borbély AA, Daan S, Wirz-Justice A, Deboer T. The two-process model of sleep regulation: a reappraisal. *J Sleep Res.* 2016;25: 131–143. doi:10.1111/jsr.12371
2. Borbély AA. A two process model of sleep regulation. *Hum Neurobiol.* 1982;1: 195–204.
3. Borbély AA, Achermann P. Sleep homeostasis and models of sleep regulation. *J Biol Rhythms.* 1999;14: 557–568.
4. Crunelli V, Lőrincz ML, Connelly WM, David F, Hughes SW, Lambert RC, et al. Dual function of thalamic low-vigilance state oscillations: rhythm-regulation and plasticity. *Nat Rev Neurosci.* 2018;19: 107–118. doi:10.1038/nrn.2017.151
5. Wunderlin M, Züst MA, Hertenstein E, Fehér KD, Schneider CL, Klöppel S, et al. Modulating overnight memory consolidation by acoustic stimulation during slow-wave sleep: a systematic review and meta-analysis. *Sleep.* 2021;44: zsaa296. doi:10.1093/sleep/zsaa296
6. Krueger JM, Frank MG, Wisor JP, Roy S. Sleep function: Toward elucidating an enigma. *Sleep Medicine Reviews.* 2016;28: 46–54. doi:10.1016/j.smrv.2015.08.005
7. Rasmussen MK, Mestre H, Nedergaard M. Fluid transport in the brain. *Physiol Rev.* 2022;102: 1025–1151. doi:10.1152/physrev.00031.2020
8. Xie L, Kang H, Xu Q, Chen MJ, Liao Y, Thiyagarajan M, et al. Sleep drives metabolite clearance from the adult brain. *Science.* 2013;342: 373–377. doi:10.1126/science.1241224
9. Hablitz LM, Vinitsky HS, Sun Q, Stæger FF, Sigurdsson B, Mortensen KN, et al. Increased glymphatic influx is correlated with high EEG delta power and low heart rate in mice under anesthesia. *Sci Adv.* 2019;5: eaav5447. doi:10.1126/sciadv.aav5447
10. Ding F, O'Donnell J, Xu Q, Kang N, Goldman N, Nedergaard M. Changes in the composition of brain interstitial ions control the sleep-wake cycle. *Science.* 2016;352: 550–555. doi:10.1126/science.aad4821
11. Jiang-Xie L-F, Drieu A, Bhasiin K, Quintero D, Smirnov I, Kipnis J. Neuronal dynamics direct cerebrospinal fluid perfusion and brain clearance. *Nature.* 2024;627: 157–164. doi:10.1038/s41586-024-07108-6

12. Iliff JJ, Wang M, Liao Y, Plogg BA, Peng W, Gundersen GA, et al. A paravascular pathway facilitates CSF flow through the brain parenchyma and the clearance of interstitial solutes, including amyloid  $\beta$ . *Sci Transl Med*. 2012;4: 147ra111. doi:10.1126/scitranslmed.3003748
13. Lundgaard I, Lu ML, Yang E, Peng W, Mestre H, Hitomi E, et al. Glymphatic clearance controls state-dependent changes in brain lactate concentration. *J Cereb Blood Flow Metab*. 2017;37: 2112–2124. doi:10.1177/0271678X16661202
14. Hablitz LM, Nedergaard M. The Glymphatic System: A Novel Component of Fundamental Neurobiology. *J Neurosci*. 2021;41: 7698–7711. doi:10.1523/JNEUROSCI.0619-21.2021
15. Mestre H, Tithof J, Du T, Song W, Peng W, Sweeney AM, et al. Flow of cerebrospinal fluid is driven by arterial pulsations and is reduced in hypertension. *Nat Commun*. 2018;9: 4878. doi:10.1038/s41467-018-07318-3
16. Liu S, Bilston LE, Flores Rodriguez N, Wright C, McMullan S, Lloyd R, et al. Changes in intrathoracic pressure, not arterial pulsations, exert the greatest effect on tracer influx in the spinal cord. *Fluids Barriers CNS*. 2022;19: 14. doi:10.1186/s12987-022-00310-6
17. van Veluw SJ, Hou SS, Calvo-Rodriguez M, Arbel-Ornath M, Snyder AC, Frosch MP, et al. Vasomotion as a Driving Force for Paravascular Clearance in the Awake Mouse Brain. *Neuron*. 2020;105: 549-561.e5. doi:10.1016/j.neuron.2019.10.033
18. Holstein-Rønsbo S, Gan Y, Giannetto MJ, Rasmussen MK, Sigurdsson B, Beinlich FRM, et al. Glymphatic influx and clearance are accelerated by neurovascular coupling. *Nat Neurosci*. 2023;26: 1042–1053. doi:10.1038/s41593-023-01327-2
19. Bojarskaite L, Vallet A, Bjørnstad DM, Gullestad Binder KM, Cunen C, Heuser K, et al. Sleep cycle-dependent vascular dynamics in male mice and the predicted effects on perivascular cerebrospinal fluid flow and solute transport. *Nat Commun*. 2023;14: 953. doi:10.1038/s41467-023-36643-5
20. Murdock MH, Yang C-Y, Sun N, Pao P-C, Blanco-Duque C, Kahn MC, et al. Multisensory gamma stimulation promotes glymphatic clearance of amyloid. *Nature*. 2024;627: 149–156. doi:10.1038/s41586-024-07132-6
21. Iliff JJ, Wang M, Zeppenfeld DM, Venkataraman A, Plog BA, Liao Y, et al. Cerebral arterial pulsation drives paravascular CSF-interstitial fluid exchange in the murine brain. *J Neurosci*. 2013;33: 18190–18199. doi:10.1523/JNEUROSCI.1592-13.2013
22. Harrison IF, Siow B, Akilo AB, Evans PG, Ismail O, Ohene Y, et al. Non-invasive imaging of CSF-mediated brain clearance pathways via assessment of perivascular fluid movement with diffusion tensor MRI. Behrens TE, Okell TW, editors. *eLife*. 2018;7: e34028. doi:10.7554/eLife.34028
23. Demiral ŞB, Tomasi D, Sarlls J, Lee H, Wiers CE, Zehra A, et al. Apparent diffusion coefficient changes in human brain during sleep - Does it inform on the existence of a glymphatic system? *Neuroimage*. 2019;185: 263–273. doi:10.1016/j.neuroimage.2018.10.043
24. Tuura RO, Volk C, Callaghan F, Jaramillo V, Huber R. Sleep-related and diurnal effects on brain diffusivity and cerebrospinal fluid flow. *Neuroimage*. 2021;241: 118420. doi:10.1016/j.neuroimage.2021.118420

25. Steffensen AB, Edelbo BL, Barbuskaite D, Andreassen SN, Olsen MH, Møller K, et al. Nocturnal increase in cerebrospinal fluid secretion as a circadian regulator of intracranial pressure. *Fluids and Barriers of the CNS*. 2023;20: 49. doi:10.1186/s12987-023-00451-2
26. Fultz NE, Bonmassar G, Setsompop K, Stickgold RA, Rosen BR, Polimeni JR, et al. Coupled electrophysiological, hemodynamic, and cerebrospinal fluid oscillations in human sleep. *Science*. 2019;366: 628–631. doi:10.1126/science.aax5440
27. Voldsbekk I, Maximov II, Zak N, Roelfs D, Geier O, Due-Tønnessen P, et al. Evidence for wakefulness-related changes to extracellular space in human brain white matter from diffusion-weighted MRI. *Neuroimage*. 2020;212: 116682. doi:10.1016/j.neuroimage.2020.116682
28. Eide PK, Vinje V, Pripp AH, Mardal K-A, Ringstad G. Sleep deprivation impairs molecular clearance from the human brain. *Brain*. 2021;144: 863–874. doi:10.1093/brain/awaa443
29. Shokri-Kojori E, Wang G-J, Wiers CE, Demiral SB, Guo M, Kim SW, et al.  $\beta$ -Amyloid accumulation in the human brain after one night of sleep deprivation. *Proc Natl Acad Sci USA*. 2018;115: 4483–4488. doi:10.1073/pnas.1721694115
30. Holth JK, Fritschi SK, Wang C, Pedersen NP, Cirrito JR, Mahan TE, et al. The sleep-wake cycle regulates brain interstitial fluid tau in mice and CSF tau in humans. *Science*. 2019;363: 880–884. doi:10.1126/science.aav2546
31. Lucey BP, Hicks TJ, McLeland JS, Toedebusch CD, Boyd J, Elbert DL, et al. Effect of sleep on overnight cerebrospinal fluid amyloid  $\beta$  kinetics. *Ann Neurol*. 2018;83: 197–204. doi:10.1002/ana.25117
32. Auer LM, Sayama I. Intracranial pressure oscillations (B-waves) caused by oscillations in cerebrovascular volume. *Acta Neurochir (Wien)*. 1983;68: 93–100. doi:10.1007/BF01406205
33. Droste DW, Krauss JK, Berger W, Schuler E, Brown MM. Rhythmic oscillations with a wavelength of 0.5–2 min in transcranial Doppler recordings. *Acta Neurologica Scandinavica*. 1994;90: 99–104. doi:10.1111/j.1600-0404.1994.tb02687.x
34. Krauss JK, Droste DW, Bohus M, Regel JP, Scheremet R, Riemann D, et al. The relation of intracranial pressure B-waves to different sleep stages in patients with suspected normal pressure hydrocephalus. *Acta neurochir*. 1995;136: 195–203. doi:10.1007/BF01410626
35. Assländer J, Zahneisen B, Hugger T, Reisert M, Lee H-L, LeVan P, et al. Single shot whole brain imaging using spherical stack of spirals trajectories. *NeuroImage*. 2013;73: 59–70. doi:10.1016/j.neuroimage.2013.01.065
36. Hennig J, Kiviniemi V, Riemenschneider B, Barghoorn A, Akin B, Wang F, et al. 15 Years MR-encephalography. *MAGMA*. 2021;34: 85–108. doi:10.1007/s10334-020-00891-z
37. Kiviniemi V, Wang X, Korhonen V, Keinänen T, Tuovinen T, Autio J, et al. Ultra-fast magnetic resonance encephalography of physiological brain activity - Glymphatic pulsation mechanisms? *J Cereb Blood Flow Metab*. 2016;36: 1033–1045. doi:10.1177/0271678X15622047

38. Helakari H, Korhonen V, Holst SC, Piispala J, Kallio M, Väyrynen T, et al. Human NREM Sleep Promotes Brain-Wide Vasomotor and Respiratory Pulsations. *J Neurosci*. 2022;42: 2503–2515. doi:10.1523/JNEUROSCI.0934-21.2022
39. Helakari H, Järvelä M, Väyrynen T, Tuunanen J, Piispala J, Kallio M, et al. Effect of sleep deprivation and NREM sleep stage on physiological brain pulsations. *Front Neurosci*. 2023;17: 1275184. doi:10.3389/fnins.2023.1275184
40. Gonzalez-Castillo J, Fernandez IS, Handwerker DA, Bandettini PA. Ultra-slow fMRI fluctuations in the fourth ventricle as a marker of drowsiness. *Neuroimage*. 2022;259: 119424. doi:10.1016/j.neuroimage.2022.119424
41. Azevedo ER, Kubo T, Mak S, Al-Hesayen A, Schofield A, Allan R, et al. Nonselective versus selective beta-adrenergic receptor blockade in congestive heart failure: differential effects on sympathetic activity. *Circulation*. 2001;104: 2194–2199. doi:10.1161/hc4301.098282
42. Dreha-Kulaczewski S, Joseph AA, Merboldt K-D, Ludwig H-C, Gärtner J, Frahm J. Inspiration is the major regulator of human CSF flow. *J Neurosci*. 2015;35: 2485–2491. doi:10.1523/JNEUROSCI.3246-14.2015
43. Sloots JJ, Biessels GJ, Zwanenburg JJM. Cardiac and respiration-induced brain deformations in humans quantified with high-field MRI. *NeuroImage*. 2020;210: 116581. doi:10.1016/j.neuroimage.2020.116581
44. Budday S, Nay R, de Rooij R, Steinmann P, Wyrobek T, Ovaert TC, et al. Mechanical properties of gray and white matter brain tissue by indentation. *J Mech Behav Biomed Mater*. 2015;46: 318–330. doi:10.1016/j.jmbbm.2015.02.024
45. Whittall KP, Mackay AL, Graeb DA, Nugent RA, Li DKB, Paty DW. In vivo measurement of T2 distributions and water contents in normal human brain. *Magnetic Resonance in Medicine*. 1997;37: 34–43. doi:10.1002/mrm.1910370107
46. Picchioni D, Özbay PS, Mandelkow H, de Zwart JA, Wang Y, van Gelderen P, et al. Autonomic arousals contribute to brain fluid pulsations during sleep. *NeuroImage*. 2022;249: 118888. doi:10.1016/j.neuroimage.2022.118888
47. McTavish D, Campoli-Richards D, Sorkin EM. Carvedilol. A review of its pharmacodynamic and pharmacokinetic properties, and therapeutic efficacy. *Drugs*. 1993;45: 232–258. doi:10.2165/00003495-199345020-00006
48. Bart J, Dijkers ECF, Wegman TD, de Vries EGE, van der Graaf WTA, Groen HJM, et al. New positron emission tomography tracer [11C]carvedilol reveals P-glycoprotein modulation kinetics. *British Journal of Pharmacology*. 2005;145: 1045–1051. doi:10.1038/sj.bjp.0706283
49. Doran SM, Van Dongen HP, Dinges DF. Sustained attention performance during sleep deprivation: evidence of state instability. *Arch Ital Biol*. 2001;139: 253–267.
50. Basner M, Dinges DF. Maximizing Sensitivity of the Psychomotor Vigilance Test (PVT) to Sleep Loss. *Sleep*. 2011;34: 581–591. doi:10.1093/sleep/34.5.581

51. Helakari H, Korhonen V, Holst SC, Piispala J, Kallio M, Väyrynen T, et al. Human NREM Sleep Promotes Brain-Wide Vasomotor and Respiratory Pulsations. *J Neurosci.* 2022;42: 2503–2515. doi:10.1523/JNEUROSCI.0934-21.2022
52. Virtanen J, Näsi T, Noponen T, Toppila J, Salmi T, Ilmoniemi RJ. Slow spontaneous hemodynamic oscillations during sleep measured with near-infrared spectroscopy. *Diffuse Optical Imaging III.* SPIE; 2011. pp. 23–31. doi:10.1117/12.889480
53. Bohr T, Hjorth PG, Holst SC, Hrabětová S, Kiviniemi V, Lilius T, et al. The glymphatic system: Current understanding and modeling. *iScience.* 2022;25: 104987. doi:10.1016/j.isci.2022.104987
54. Achermann P, Borbély AA. Low-frequency (<1 Hz) oscillations in the human sleep electroencephalogram. *Neuroscience.* 1997;81: 213–222. doi:10.1016/S0306-4522(97)00186-3
55. Lilius TO, Blomqvist K, Hauglund NL, Liu G, Stæger FF, Bærentzen S, et al. Dexmedetomidine enhances glymphatic brain delivery of intrathecally administered drugs. *Journal of Controlled Release.* 2019;304: 29–38. doi:10.1016/j.jconrel.2019.05.005
56. Beaman EE, Bonde AN, Ulv Larsen SM, Ozenne B, Lohela TJ, Nedergaard M, et al. Blood–brain barrier permeable  $\beta$ -blockers linked to lower risk of Alzheimer's disease in hypertension. *Brain.* 2022; awac076. doi:10.1093/brain/awac076
57. Elsinga PH, Hendrikse NH, Bart J, Vaalburg W, van Waarde A. PET Studies on P-glycoprotein function in the blood-brain barrier: how it affects uptake and binding of drugs within the CNS. *Curr Pharm Des.* 2004;10: 1493–1503. doi:10.2174/1381612043384736
58. Baker FC, Driver HS. Circadian rhythms, sleep, and the menstrual cycle. *Sleep Medicine.* 2007;8: 613–622. doi:10.1016/j.sleep.2006.09.011
59. Giannetto M, Xia M, Stæger FF, Metcalfe T, Vinitzky HS, Dang JAML, et al. Biological sex does not predict glymphatic influx in healthy young, middle aged or old mice. *Sci Rep.* 2020;10: 16073. doi:10.1038/s41598-020-72621-3
60. Hennig J, Kiviniemi V, Riemenschneider B, Barghoorn A, Akin B, Wang F, et al. 15 Years MR-encephalography. *Magn Reson Mater Phy.* 2021;34: 85–108. doi:10.1007/s10334-020-00891-z
61. Hennig J, Zhong K, Speck O. MR-Encephalography: Fast multi-channel monitoring of brain physiology with magnetic resonance. *NeuroImage.* 2007;34: 212–219. doi:10.1016/j.neuroimage.2006.08.036
62. Hugger T, Zahneisen B, LeVan P, Lee KJ, Lee H-L, Zaitsev M, et al. Fast Undersampled Functional Magnetic Resonance Imaging Using Nonlinear Regularized Parallel Image Reconstruction. *PLOS ONE.* 2011;6: e28822. doi:10.1371/journal.pone.0028822
63. Norman RG, Pal I, Stewart C, Walsleben JA, Rapoport DM. Interobserver agreement among sleep scorers from different centers in a large dataset. *Sleep.* 2000;23: 901–908.
64. Spiegelberg A, Preuß M, Kurtcuoglu V. B-waves revisited. *Interdisciplinary Neurosurgery.* 2016;6: 13–17. doi:10.1016/j.inat.2016.03.004

65. Frässle S, Aponte EA, Bollmann S, Brodersen KH, Do CT, Harrison OK, et al. TAPAS: An Open-Source Software Package for Translational Neuromodeling and Computational Psychiatry. *Frontiers in Psychiatry*. 2021;12. Available: <https://www.frontiersin.org/articles/10.3389/fpsy.2021.680811>
66. Lim J, Dinges DF. Sleep deprivation and vigilant attention. *Ann N Y Acad Sci*. 2008;1129: 305–322. doi:10.1196/annals.1417.002
67. Gerster M, Waterstraat G, Litvak V, Lehnertz K, Schnitzler A, Florin E, et al. Separating Neural Oscillations from Aperiodic 1/f Activity: Challenges and Recommendations. *Neuroinform*. 2022;20: 991–1012. doi:10.1007/s12021-022-09581-8

## Supplementary Material for

Sleep deprivation promotes cerebrovascular oscillations while respiration- and cardiac-driven brain pulsations escalate with sleep intensity

Sara Marie Ulv Larsen<sup>1,2,†</sup>, Sebastian Camillo Holst<sup>1,3,†</sup>, Anders Stevnhoved Olsen<sup>1,4</sup>, Brice Ozenne<sup>1,5</sup>, Dorte Bonde Zilstorff<sup>1</sup>, Kristoffer Brendstrup-Brix<sup>1</sup>, Pia Weikop<sup>6</sup>, Simone Pleinert<sup>1</sup>, Vesa Kiviniemi<sup>7,8</sup>, Poul Jørgen Jennum<sup>9,10</sup>, Maiken Nedergaard<sup>2,6,11</sup>, Gitte Moos Knudsen<sup>1,10\*</sup>

### Corresponding author:

Gitte Moos Knudsen

Email: [gmk@nru.dk](mailto:gmk@nru.dk)

s

### This PDF file includes:

- Supplementary methods
- Figures S1 to S5
- Tables S1 to S6
- Supplementary References

## Supplementary Figures

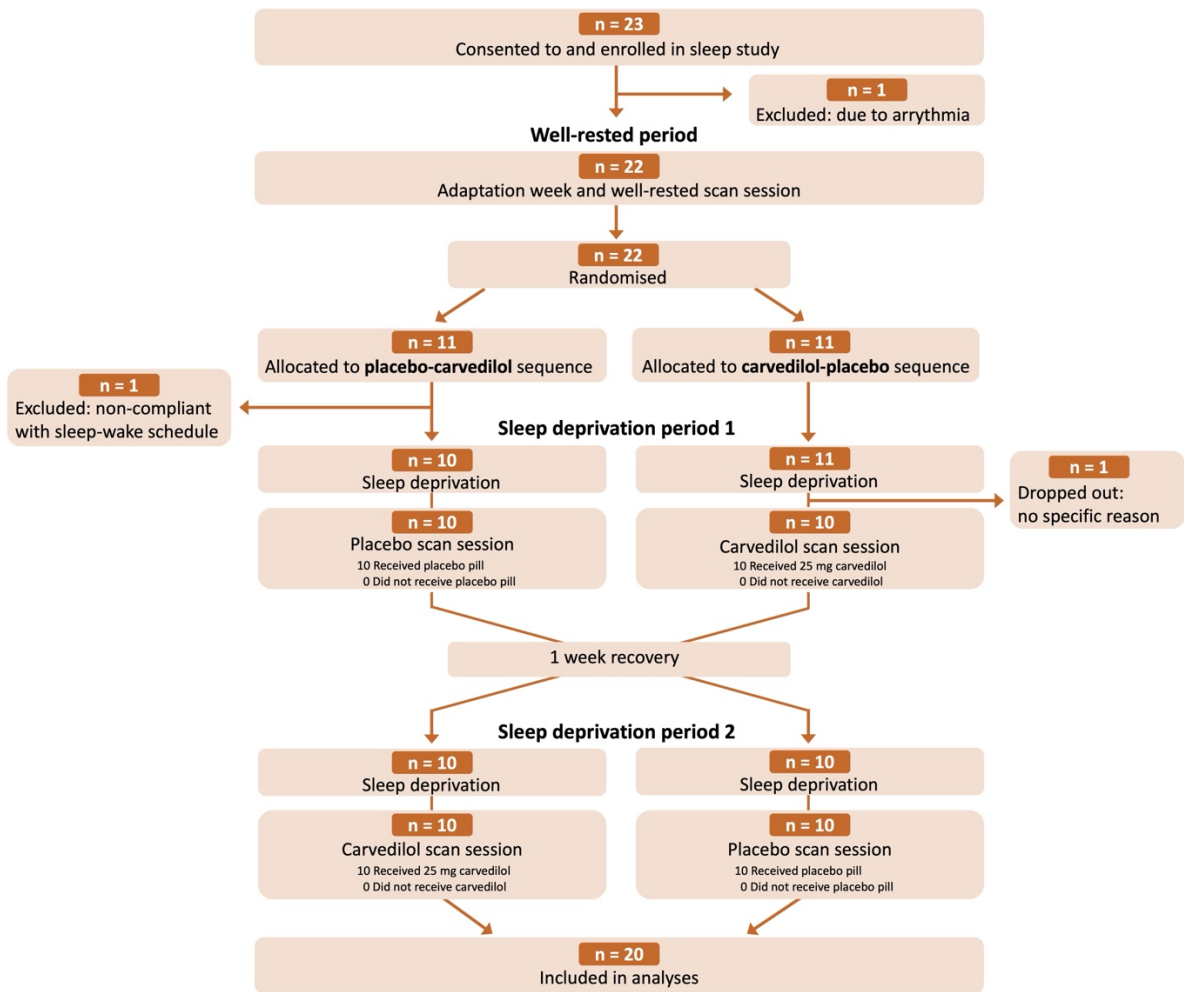


**Fig. S1.** Consort flow diagram presenting number of research volunteers enrolled, excluded, allocated to intervention sequence and who completed the study and were included in analyses.

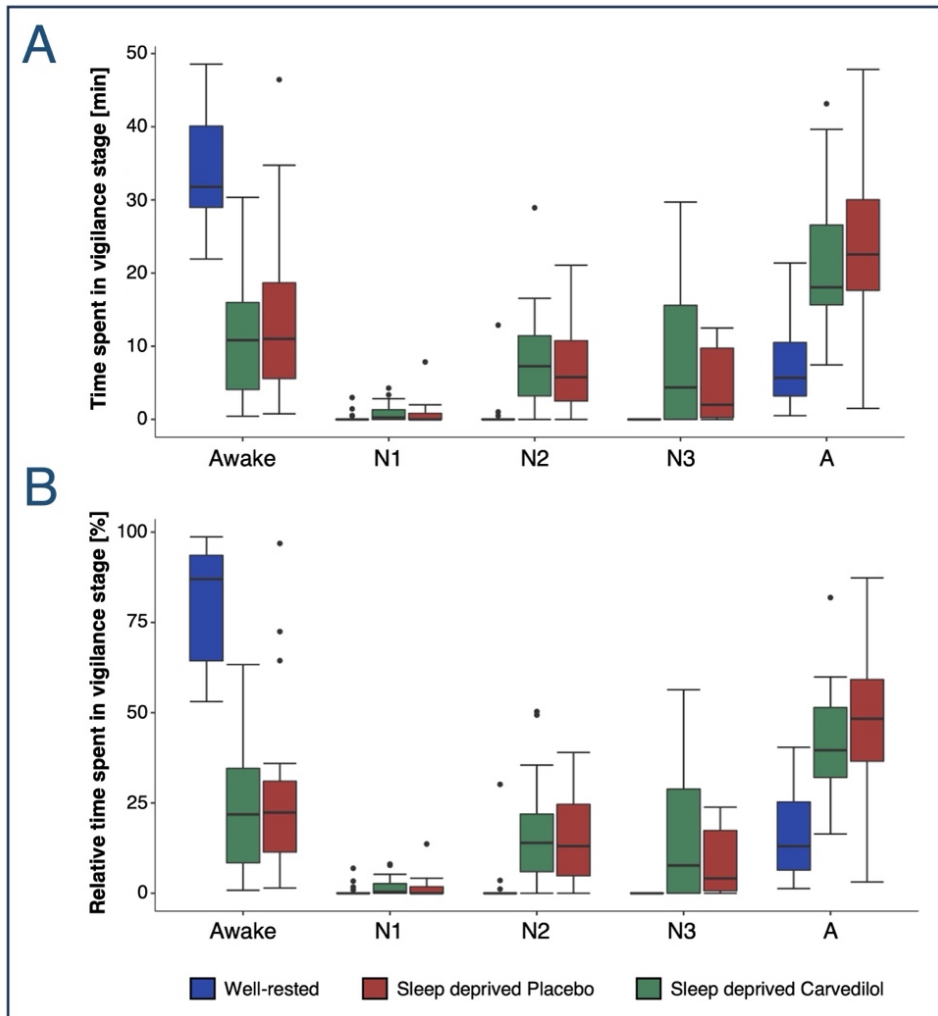


**Fig. S2. EEG-recorded vigilance states during MR-EEG sessions.** Boxplots illustrate absolute (**A**) and relative (**B**) time spent in wakefulness and NREM sleep stages N1, N2 and N3 during rested and sleep-deprived (placebo and carvedilol) scan sessions. All 30-sec EEG epochs recorded simultaneously with MR-scans were included in analyses. EEG-epochs were included in analyses when the two independent EEG scorers agreed on staging. Epochs with scorer disagreement and epochs scored as artifacts were categorized as 'A'. There is no difference between carvedilol and placebo conditions (Student's paired t-test,  $p_{all} > 0.05$ ). Box-plot elements include: median (center line), upper and lower quartiles (box limits), 1.5x interquartile range (whiskers) and outliers (points).  $N = 20$ .

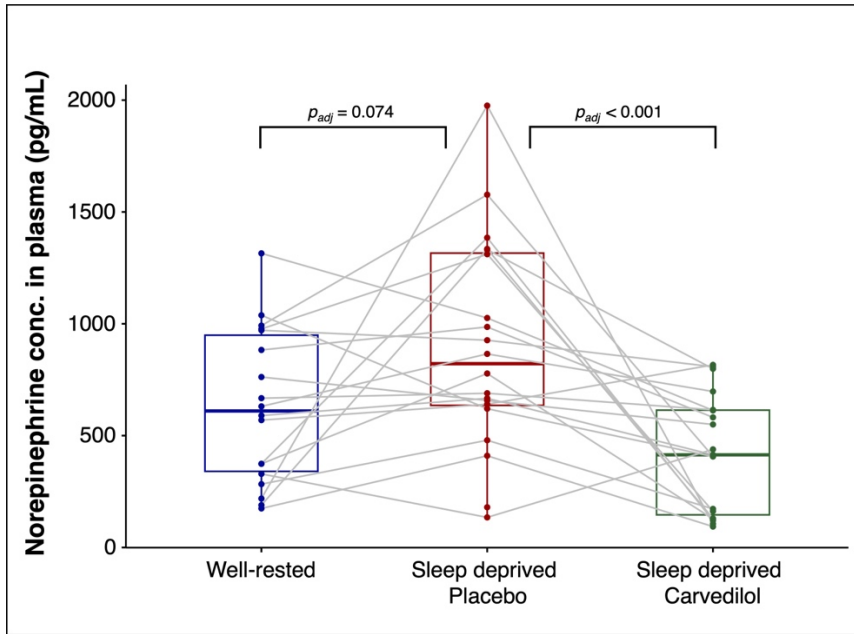


**Fig. S3. Plasma norepinephrine (pg/mL) immediately after all scans.** Normal range: 200-1700 pg/mL.  $p$ -values are from a linear mixed model have been adjusted for multiple comparisons with Bonferroni correction. Box-plot elements include: median (center line), upper and lower quartiles (box limits) and 1.5x interquartile range (whiskers).  $N = 20$ .

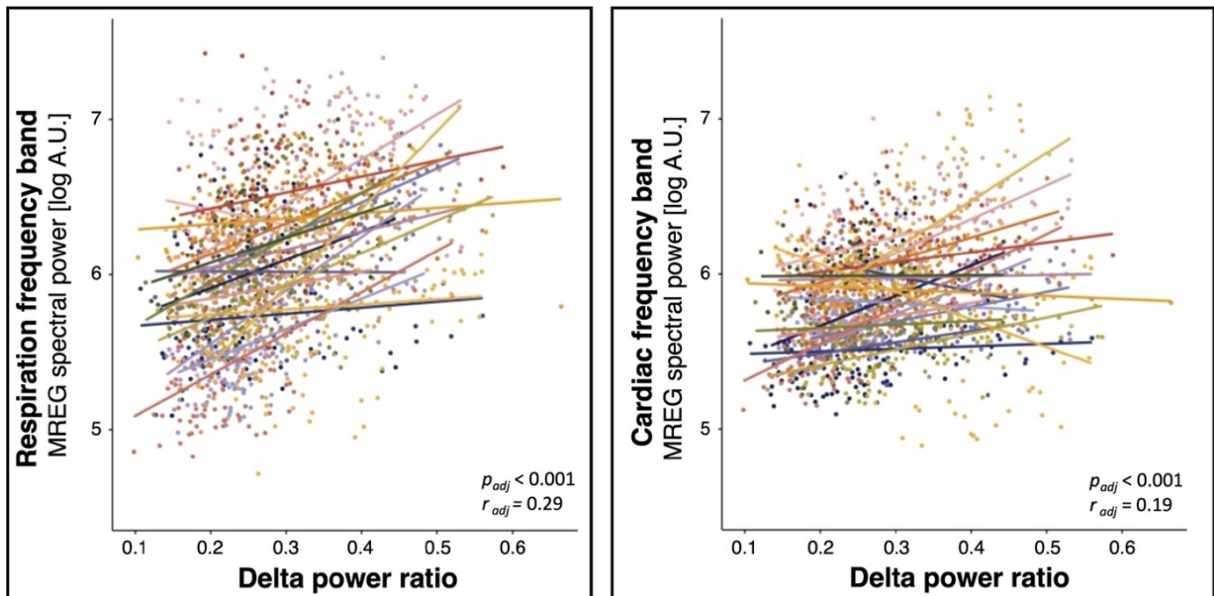


**Fig. S4. Participant-wise correlations between EEG delta power ratio as recorded simultaneously with MREG-imaging, and spectral power.** Each dot represents a 30 sec epoch and each participant's data is shown with a unique colour.  $r_{est}$  &  $p_{est}$  are estimated correlation coefficient and estimated  $p$ -value from linear mixed models, where repeated measurements are taken into account. **(A)** A positive slope was observed for 17 of 19 participants in the respiration frequency band, and of these 13 were statistically significantly positively correlated. **(B)** For the cardiac band, 16 of 20 participants were positive and 11/20 had a significant positive slope.

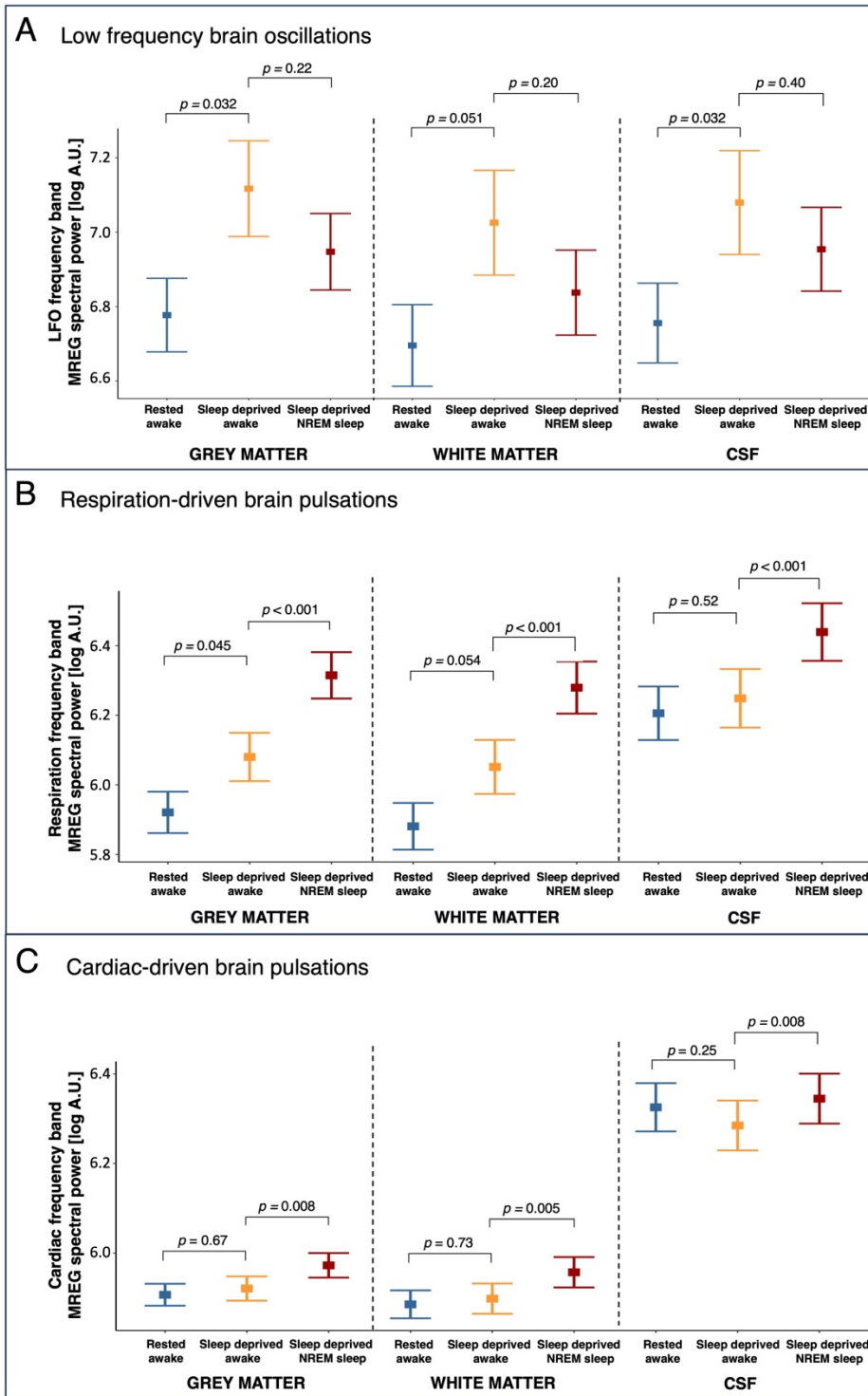


**Fig. S5. Effects of sleep deprivation and NREM sleep (combined N2 and N3) on brain oscillations across grey matter, white matter and CSF.** Results from sensitivity analyses of the effects of sleep deprivation and NREM sleep on MREG power in the (A) LFO, (B) respiration, and (C) cardiac frequency bands across three tissue types (grey matter, white matter and CSF). Error plots represent estimates (estimated means  $\pm$  SEM) from linear mixed models, run separately for each tissue type.

## Supplementary Tables

**Table S1 Wakefulness period leading up to MR/EEG scan sessions**

	Before well-rested	Sleep deprived scans		
		Before placebo	Before carvedilol	Diff. in wakefulness: placebo vs carvedilol
Hours from wake-up-time to scan start (h)	11.1 ± 0.4	34.9 ± 0.3	34.8 ± 0.3	$p = 0.21$
Prolonged wakefulness EEG-recording (h)	-	29.7 ± 3.2	28.5 ± 5.8	$p = 0.33$
NREM sleep (min)	-	1.4 ± 5.2	0.8 ± 1.7	$p = 0.56$
REM sleep (min)	-	0.0 ± 0.0	0.0 ± 0.0	NA

Time period participants spent awake between waking up from their 8-hours standardised sleep to the beginning of scan sessions.  $p$ -values represent results from students paired t-tests. All data are shown as mean ± SD.  $N = 20$ . NREM sleep: Non-rapid eye movement sleep stages N1-N3, REM sleep: Rapid eye movement sleep

**Table S2 Standardised sleep during nights before study days**

	Before well-rested	Before sleep deprived placebo	Before sleep deprived carvedilol	Diff. between nights
TIB (h)	7.9 ± 0.2	7.9 ± 0.3	7.9 ± 0.1	$p = 0.34$
TST (h)	7.4 ± 0.3	7.4 ± 0.3	7.4 ± 0.3	$p = 0.16$
Sleep efficiency (%)	93.6 ± 3.4	94.4 ± 2.7	93.8 ± 3.5	$p = 0.25$
NREM sleep (h)	5.5 ± 0.3	5.4 ± 0.4	5.4 ± 0.4	$p = 0.21$

Data across the three EEG-monitored nights of 8-hr standardised sleep leading up to study days. Estimates and  $p$ -values are from a linear mixed model (hours of NREM sleep) and Friedman tests (TIB, TST & Sleep efficiency). All data are shown as mean ± SD.  $N = 20$ . TIB: time in bed, TST: Total sleep time, Sleep efficiency: % time spent asleep of time spent in bed (after lights are off), NREM sleep: duration of NREM sleep stages N1, N2 and N3

**Table S3 30-sec dataset for evaluation of respiration- and cardiac-driven brain pulsations**

	Well-rested wakefulness	Placebo		Carvedilol	
		Sleep deprived wakefulness	Sleep deprived sleep (N2&N3)	Sleep deprived wakefulness	Sleep deprived sleep (N2&N3)
Participants in analysis (N)	20	17	17	15	19
Included 30-sec epochs (n)	35.6 [28.1, 43.0]	10.8 [5.2, 16.3]	28.7 [20.2, 37.2]	9.5 [4.7, 14.4]	33.8 [25.6, 42.1]
Respiration rate ( $\text{min}^{-1}$ )	15.2 [14.1, 16.4]	16.2 [14.9, 17.7]	14.9 [13.7, 16.2]	16.2 [14.8, 17.7]	14.3 [13.2, 15.5]
Heart rate ( $\text{min}^{-1}$ )	60.9 [57.5, 64.4]	59.5 [56.1, 63.1]	53.8 [50.8, 57.1]	59.6 [56.2, 63.2]	54.8 [51.7, 58.0]
MAP (mmHg)	91.3 [89.4, 93.3]	92.5 [90.1, 94.9]		88.2 [85.8, 90.5]	
Pulse pressure (mmHg)	45.7 [42.4, 48.9]	45.2 [42.1, 48.2]		44.3 [40.7, 47.9]	

Data included in 30-sec dataset for analyses of sleep deprivation- and NREM sleep effects on spectral power in respiration and cardiac frequency bands. Values are shown as mean and 95% confidence intervals and are determined from linear mixed models to account for interindividual variance. Participants in analysis: Number of participants included for analysis in each condition with at least one 30-sec MREG-epoch with EEG-confirmed vigilance state (see methods). Respiration and heart rates: Physiological measurements recorded simultaneously with MREG. Respiration and heart rates are estimated for all 30-sec MREG epochs and used to determine epoch-wise respiration and cardiac frequency bands. MAP (mean arterial blood pressure =  $1/3 \times$  diastolic blood pressure +  $2/3 \times$  systolic blood pressure) and pulse pressure (difference between systolic and diastolic blood pressure) are averages of blood pressure measurements performed immediately before and after scans.

**Table S4 5-min dataset for evaluation of LFOs**

	Well-rested wakefulness	Placebo		Carvedilol	
		Sleep deprived wakefulness	Sleep deprived sleep (N2&N3)	Sleep deprived wakefulness	Sleep deprived sleep (N2&N3)
Participants in analysis (N)	19	12	14	12	17
Included 5-min scans (n)	1.6 [1.3, 1.8]	1.1 [0.9, 1.3]	3.1 [2.1, 4.1]	1.3 [0.7, 1.8]	3.3 [2.5, 4.1]

Data included in 5-min dataset for analyses of sleep deprivation and NREM sleep effects on spectral power in the LFO frequency band (0.012 - 0.034 Hz). Values are shown as mean and 95% confidence intervals and are determined from linear mixed models to account for interindividual variance. Participants in analysis: Number of participants included in analysis in each condition, with at least one 5-min MREG scan with 80% (8/10 epochs) EEG-confirmed vigilance state (see methods).

**Table S5 30-sec dataset for evaluation of sleep depth effects**

	Placebo		Carvedilol	
	N2 sleep	N3 sleep	N2 sleep	N3 sleep
Participants in analysis (N)	16	14	17	12
Included 30-sec epochs (n)	14.5 [9.1, 19.9]	8.1 [4.5, 11.7]	14.6 [8.9, 20.3]	17.8 [7.1, 28.6]
Respiration rate (min <sup>-1</sup> )	14.5 [13.4, 15.6]	14.4 [13.3, 15.6]	14.2 [13.4, 15.3]	13.6 [12.6, 14.7]
Heart rate (min <sup>-1</sup> )	52.3 [49.5, 55.2]	53.9 [51.0, 56.9]	54.6 [51.8, 57.6]	54.5 [51.6, 57.5]

Data included in 30-sec data set for sleep depth analyses. Values are shown as mean and 95% confidence intervals and are determined from linear mixed models to account for interindividual variance. Participants included in analysis: Number of participants in each condition who had at least one 30-sec epoch, where EEG-scorers agreed on either N2 or N3 NREM sleep. Respiration and heart rates were recorded simultaneously with MREG and estimated for all 30-sec MREG-epochs and subsequently used to determine epoch-wise respiration and cardiac.

**Table S6 Recovery nights after sleep deprivation**

	Recovery sleep		Treatment effect
	Placebo	Carvedilol	
TIB: Time in bed (h)	8.0 ± 0.0	7.9 ± 0.3	$p = 0.37^{\perp}$
TST: total sleep time (h)	7.8 ± 0.1	7.7 ± 0.4	$p = 0.39^{\perp}$
Sleep efficiency (%)	97.3 ± 1.5	97.1 ± 1.6	$p = 0.60^{\perp}$
Sleep latency (h)	0.1 ± 0.1	0.1 ± 0.1	$p = 0.71^{\perp}$
REM latency (h)	1.4 ± 0.8	1.2 ± 0.7	$p = 0.27$
NREM total (%)	70.6 ± 3.8	70.9 ± 3.5	$p = 0.51$
REM total (%)	26.8 ± 3.9	26.3 ± 3.6	$p = 0.38$
Stage N1 (%)	3.5 ± 2.3	2.6 ± 1.2	$p = 0.03^{\perp}$
Stage N2 (%)	37.4 ± 5.9	39.4 ± 7.0	$p = 0.10$
Stage N3 (%)	29.7 ± 7.2	28.9 ± 8.4	$p = 0.76$
WASO (%)	1.4 ± 0.9	1.7 ± 1.2	$p = 0.31$

Characteristics of EEG-recorded recovery sleep after sleep deprivation in each treatment arm. Analyses were restricted to the first 8 hours (480 minutes). Sleep stages are presented as percentages of total time in bed. All data are shown as mean ± SD.  $p$ -values are from paired students  $t$ -tests or Wilcoxon signed rank tests (denoted  $\perp$ ).  $N = 20$ . TIB: time in bed, TST: total sleep time, Sleep latency and REM latency: time from lights-off to the first occurrence of stage N2 sleep, WASO: wakefulness after sleep onset

## Supplementary Methods

### Removal of MR-induced artifacts on EEG

First, the Average Artefact Subtraction method was used to eliminate gradient artefacts. This creates a template gradient artefact by using the MR-trigger signal as a time-locking event and then averaging across the nearest 30 artefacts, in a moving window on high-pass filtered data [1]. Second, the Optimal Basis Sets approach was used to adaptively remove ballisto-cardiographic artefacts over time. This approach uses the ECG R-peak as a time-locking event and combines the local moving average template construction with a combination of basis functions, derived from a principal component analysis of the gradient cleaned EEG-signal [2].

### Quantitative analysis of EEG during MRI

For quantitative analysis of EEG, data were cleaned subject- and condition-wise by rejecting channels exceeding a kurtosis threshold of 5 using EEGLab's `pop_rejchan` function [3]. The leads C3-M2 and C4-M1 were constructed either from preselected channels ( $\text{Chan}_{\{C3\}} = 59$ ,  $\text{Chan}_{\{C4\}} = 183$ ,  $\text{Chan}_{\{M1\}} = 94$ ,  $\text{Chan}_{\{M2\}} = 190$ ) or, if these were rejected, an average of the neighbouring channels. Artefact segments were rejected from the two leads in 0.5s windows with 0.25s overlap if the power in the 35-120Hz range exceeded 15dB. Delta power ratio was quantified epoch-wise in the two leads using MATLAB's `bandpower` function on epoch data, where artefact segments had been rejected. Bandpower ( $\text{mV}^2$ ) was computed in the 1– 4 Hz range and in the 0.5 – 30 Hz range, where relative delta-power was defined as the ratio of the two. The reported delta power ratio is a mean of the two leads. 30-sec epochs classified as “artefact” by either of the two EEG-scorers were excluded from analysis of EEG delta power ratio.

### Polysomnography and prolonged wakefulness EEG recordings

All sleep and wakefulness EEGs recorded outside the MR environment were recorded using the battery powered and transportable SomnoScreen Plus system (Somnomedics, Germany). Impedance values were kept below 6k $\Omega$  at the beginning of all recordings. Overnight PSG recordings were performed in private rooms with blinded windows. Data across 18 EEG electrodes, placed according to the internationally standardized 10–20 system [4], were recorded simultaneously with submental electromyogram, electrooculogram (EOG) and ECG. In order to define the overnight sleep periods, participants were asked to blink ten times when they went to bed and turned off the light and again when they woke up and turned on the light. Participants were prescribed a fixed ‘lights on’ and ‘lights off’ time of an 8-hour (standard night) or 10-hour (recovery night) sleep opportunity and data analysis was restricted to a maximum of eight hours

(480 minutes) to enable comparisons between nights.

To monitor vigilance during the two periods of sleep deprivation, participants were fitted with a minimal EEG setup with 6 EEG electrodes and EOG. These EEG data were recorded continuously throughout the wakefulness periods. When the EEG equipment was fitted, the recorder was placed in a bag, which allowed participants to move around freely.

A single expert, blinded to treatment condition, visually scored the EEG recordings in 30-sec epochs according to standard AASM criteria (American Academy of Sleep Medicine, 2007), taking artefact rejection and filter settings into consideration. Scoring was performed using DOMINO software (Somnomedics, Germany).

## **Statistical models for all reported results**

### ***(i) Sleep study cohort and descriptives:***

Paired two-tailed Student's t-tests were used to compare the mean time intervals from wake-up time to scan start and the mean time spent in NREM/REM sleep during the periods of prolonged wakefulness prior to scans (Table S1), as well as the relative time spent in wakefulness/sleep during MR-scans carvedilol and placebo conditions (Fig. S2) between. Paired t-tests were also used to evaluate the difference in reaction time and lapses of attention between rested wakefulness and sleep deprived wakefulness.  $N = 20$ .

Sleep during the standardised nights leading up to the three study sessions was compared by evaluating PSG-recorded sleep patterns across the nights (Table S2). A linear mixed model including night type (before-well-rested vs before-placebo vs before-carvedilol) as a fixed effect and subject ID and study week (week 1-3) as random intercepts (study week being nested into subject ID), was used to evaluate mean differences in 'Hours of NREM sleep (h)'. P-value for testing the fixed effect was obtained using a Wald test. Friedman tests were used to evaluate differences in 'Time in bed (h)', 'Total sleep time (h)' and 'sleep efficiency (%)' between the three nights, as these measures were not normally distributed.  $N = 20$ .

Effect of sleep deprivation and NREM sleep on EEG delta power ratio as well as on respiration- and heart rates (recorded simultaneously with MREG) were assessed in 30sec epochs from well-rested (awake scans) and sleep deprived placebo (awake and sleep scans) conditions (Table S3) using linear mixed models. Sleep deprivation (well-rested vs. sleep-deprived) and vigilance state (awake vs NREM sleep) were included as additive fixed effects and Subject ID, scan session (well-rested, sleep-deprived scan 1, sleep-deprived scan 2) and sleep opportunity (lights on, lights off) were included as random intercepts with sleep opportunity being nested into scan session itself nested into subject ID. This linear mixed model will be referred to as LMM-ii. P-values for testing fixed effects were obtained using Wald tests.  $N = 20$ .

**(ii) Sleep deprivation enhances spectral power in the LFO frequency band:**

Effects of sleep deprivation and NREM sleep on whole-brain LFOs were evaluated in 5 min MREG scans from well-rested (awake scans) and sleep deprived placebo (awake and NREM sleep scans) conditions. Whole-brain spectral power within the LFO band was calculated by summing the spectral power of all bins included in the 0.01221 – 0.03418 Hz frequency range, after which it was log transformed to mitigate skewness in the distribution before being analysed. A linear mixed model with same fixed and random effect structure as LMM-*i* was used for analysis and P-values for testing fixed effects were obtained using Wald tests. The expected log spectral power at various conditions (e.g. sleep-deprived wakefulness) was computed from the mixed model estimates to illustrate the model fit (Fig. 2B and Fig. S5A).  $N = 20$  (number of participants with data in each of the three conditions can be seen in Table S4).

The correlation between mean log spectral power in the LFO band (in either sleep deprived awake or NREM sleep scans) and PVT measurements (either pre-scan measurements or difference between pre- and post-scan measurements) was assessed considering two measurements per individual: one from placebo- and one from carvedilol conditions. A Wald test for the association between spectral power and PVT measures was obtained from a linear mixed model based on subject ID and adjusted for treatment and scan session nr (denoted  $\rho_{adj}$ ). The corresponding correlation coefficient ( $r_{adj}$ ) was evaluated (without proximation) as follows:

We introduce the following notations:

- $Y_{1,j}$  and  $Y_{2,j}$  denote the spectral power at, respectively, placebo and carvedilol for individual  $j$ .
- $Z_{1,j}$  and  $Z_{2,j}$  denote the PVT measurement at, respectively, placebo and carvedilol for individual  $j$ .
- $X_j$  denotes the covariates relative to individual  $j$ , here scan week.

We are interested the following correlation coefficient between spectral power and PVT measures:

$$r_{adj} = cor(Y_{1,j}, Z_{1,j}|X) = cor(Y_{2,j}, Z_{2,j}|X)$$

assumed to be independent of the treatment and scan week. We estimate this correlation under the following linear mixed model:

$$Y_{t,j} = \alpha_t + \beta X_{t,j} + u_j + \varepsilon_{t,j}$$

$$Z_{t,j} = \mu_t + \gamma X_{t,j} + v_j + \xi_{t,j}$$

Where  $\begin{bmatrix} u_j \\ v_j \end{bmatrix} \sim N\left(\begin{bmatrix} 0 \\ 0 \end{bmatrix}, \begin{bmatrix} \tau_1 & \tau_{12} \\ \tau_{12} & \tau_2 \end{bmatrix}\right)$  and  $\begin{bmatrix} \varepsilon_{t,j} \\ \xi_{t,j} \end{bmatrix} \sim N\left(\begin{bmatrix} 0 \\ 0 \end{bmatrix}, \begin{bmatrix} \sigma_1^2 & r_{adj}\sigma_1\sigma_2 \\ r_{adj}\sigma_1\sigma_2 & \sigma_2^2 \end{bmatrix}\right)$

using restricted maximum likelihood (REML).

For reference, Pearson correlation coefficients between mean log LFO spectral power and PVT measures were evaluated (regardless of subject ID, treatment and scan session nr) and denoted  $r_{raw}$  (Fig. 4F-G).  $N_{awake} = 16$  and  $N_{sleep} = 17$ .

***(iii) NREM sleep enhances MREG spectral power in the respiration and cardiac frequency bands; N3 more so than N2 sleep:***

Effects of sleep deprivation and NREM sleep on whole-brain respiration- and cardiac-driven brain pulsations were evaluated in 30sec epochs from well-rested (awake scans) and sleep deprived placebo (awake and NREM sleep scans) conditions. Whole-brain spectral power within individually tailored respiratory- and cardiac frequency bands were log transformed to mitigate skewness in the distribution before being analysed using a linear mixed model with the same random effect structure as LMM-*i* and the same fixed effects with the addition of the base-10 logarithm of simultaneously recorded respiration or heart rates.  $N = 20$  (number of participants with data in each of the three conditions can be seen in Table S3).

Effects of sleep depth on spectral power within respiratory and cardiac frequency bands were evaluated in all 30sec epochs from the sleep deprived placebo condition classified as either wakefulness, N2 sleep or N3 sleep (see 'MREG data analysis'). Analyses were performed as described above, but with sleep depth (sleep-deprived awake vs N2 vs N3) included as an additive fixed effect together with respiration or heart rates (log transformed).  $N = 19$  (number of participants with data in each of the three conditions can be seen in Table S5).

P-values for testing fixed effects in both of the above linear mixed models were obtained using Wald tests. The expected log spectral power at the various conditions (e.g. sleep-deprived wakefulness) was computed from the mixed model estimates under mean respiration or heart rates of all 30-sec epochs included in the respective analyses – and used to illustrate the model fit (Fig. 2E&G, Fig. S5B-C and Fig. 4B&D).

***(iv) EEG delta-power during MREG-imaging correlates with the MREG spectral power in respiration and cardiac frequency bands:***

The association between log spectral power in individually tailored respiration- and cardiac frequency bands and simultaneously recorded delta power ratios was evaluated in all 30-sec epochs from well-rested and sleep deprived placebo scans, regardless of their visually scored vigilance and/or sleep states (see 'Quantitative analyses of EEG during MRI').

We performed a linear mixed model with the same random effect structure as LMM-*i*, but with EEG delta power ratio and respiration or heart rates (log transformed) included as fixed effects. The reported p-value (denoted  $p_{adj}$ ) is the one of the delta power ratio in the mixed model.

The corresponding correlation coefficient ( $r_{\text{adj}}$ ) was deduced from the mixed model estimates using an approximation suggested by Lipsitz et al. [5]:  $r = \beta / \sqrt{\beta^2 + df \sigma_{\hat{\beta}}^2}$ , where  $\beta$  denotes the delta power ratio parameter in the mixed model,  $\sigma_{\hat{\beta}}$  its standard error, and  $df$  its degree of freedoms. For reference, Pearson correlation coefficients were evaluated (regardless of subject ID) and denoted  $r_{\text{raw}}$ . For reference, Pearson correlation coefficients between delta power ratio and log spectral power in all included 30-sec epochs were evaluated (regardless of subject ID, respiration and heart rates, scan week and sleep opportunity) and denoted  $r_{\text{raw}}$  (Fig. 4F-G & Fig. S4).  $N = 20$ .

***(v) NREM sleep primarily enhances spectral power in the respiration and cardiac frequency bands in grey and white matter:***

To explore whether the strength of brain oscillations differed between tissue types, we assessed spectral power within LFO, cardiac and respiratory frequency bands in grey matter, white matter and CSF. Data from well-rested (awake) and sleep deprived placebo (awake and NREM sleep) conditions were included in analysis and a linear mixed model with the same random effect structure as LMM-ii and the same fixed effects with the addition of tissue type (GM vs WM vs CSF) and respiration or heart rates (log transformed; only for resp./card. frequency bands) and the interaction between vigilance state and tissue type. P-values and estimates to illustrate the model fits (Fig. 5C) were calculated as described in (ii) and (iii).  $N = 20$  (number of participants with data in each of the three conditions can be seen in Tables S3 and S4).

***(vi) Adrenergic antagonism decreases spectral power in LFO and cardiac frequency bands:***

Effects of carvedilol (randomised to sleep-deprived session 1 or sleep-deprived session 2) were assessed as follows: Paired two-tailed Student's t-tests were used to compare blood pressure (Table S3) and sleep characteristics during recovery sleep (REM latency, NREM total, REM total, Stage N2, stage N3; Table S4) between placebo and carvedilol conditions. For recovery sleep characteristics not normally distributed (TIB, TST, Sleep efficiency, Sleep latency, Stage N1; Supplementary Table 4), Wilcoxon signed rank tests were used to compare the two conditions.  $N = 20$ . Serum NE levels measured post-scan were evaluated using a linear mixed model with condition (well-rested vs placebo vs carvedilol) as a fixed effect and subject ID as random effect, with Bonferroni-adjusted p-values.  $N = 20$ . (Supplementary Fig. 5). Linear mixed models were also used to evaluate the effect of treatment on whole-brain log spectral power within the LFO, respiration and cardiac frequency bands as well as on respiration and heart rates. In these models, vigilance state (awake vs NREM sleep), treatment (placebo vs carvedilol), respiration and heart rates (log transformed; only included for resp./card. frequency bands) and the interaction between vigilance state and treatment were included as additive fixed effects, while the random

effect structure was similar to LMM-*i*. P-values and estimates to illustrate the model fits (Fig. 6) were calculated as described in **(ii)** and **(iii)**.  $N = 20$  (number of participants with data in each of the three conditions can be seen in Tables S3 and S4).

### **Power calculation**

The sample size for the study was based on data from Xie et al. [6], which suggest a within-subject cohen's  $d_z$  of 2.2 for brain fluid flow differences between sleep and wakefulness, and 0.9 for the effect of adrenergic inhibition. With an alpha level of 0.01 and 85% power, the estimated sample sizes were  $N = 7$  and  $N = 20$  for the two parts, respectively. Thus, a study cohort of  $N = 20$  was chosen.

### **Supplementary References**

1. Allen PJ, Josephs O, Turner R. A Method for Removing Imaging Artifact from Continuous EEG Recorded during Functional MRI. *NeuroImage*. 2000;12: 230–239. doi:10.1006/nimg.2000.0599
2. Niazy RK, Beckmann CF, Iannetti GD, Brady JM, Smith SM. Removal of FMRI environment artifacts from EEG data using optimal basis sets. *Neuroimage*. 2005;28: 720–737. doi:10.1016/j.neuroimage.2005.06.067
3. Delorme A, Makeig S. EEGLAB: an open source toolbox for analysis of single-trial EEG dynamics including independent component analysis. *J Neurosci Methods*. 2004;134: 9–21. doi:10.1016/j.jneumeth.2003.10.009
4. Klem GH, Lüders HO, Jasper HH, Elger C. The ten-twenty electrode system of the International Federation. *The International Federation of Clinical Neurophysiology. Electroencephalogr Clin Neurophysiol Suppl*. 1999;52: 3–6.
5. Lipsitz SR, Leong T, Ibrahim J, Lipshultz S. A Partial Correlation Coefficient and Coefficient of Determination for Multivariate Normal Repeated Measures Data. *Journal of the Royal Statistical Society: Series D (The Statistician)*. 2001;50: 87–95. doi:10.1111/1467-9884.00263
6. Xie L, Kang H, Xu Q, Chen MJ, Liao Y, Thiyagarajan M, et al. Sleep drives metabolite clearance from the adult brain. *Science*. 2013;342: 373–377. doi:10.1126/science.1241224



# Appendix C

---

# The role of norepinephrine and sleep deprivation on cerebrovascular oscillations in humans

## Authors

Sara Marie Ulv Larsen<sup>1,2</sup>, Anders Stevnhoved Olsen<sup>1,3</sup>, Dorte Bonde Zilstorff<sup>1</sup>, Brice Ozenne<sup>1,4</sup>, Simone Pleinert<sup>1</sup>, Cecilie Lerche Nordberg<sup>1</sup>, Kristoffer Brendstrup-Brix<sup>1</sup>, Pia Weikop<sup>5</sup>, Poul Jørgen Jennum<sup>6,7</sup>, Maiken Nedergaard<sup>2,5,8</sup>, Sebastian Camillo Holst<sup>1,9</sup>, Gitte Moos Knudsen<sup>1,7</sup>

## Affiliations

<sup>1</sup>Neurobiology Research Unit, Copenhagen University Hospital, Rigshospitalet; Copenhagen, Denmark.

<sup>2</sup>Faculty of Health and Medical Sciences (SUND), University of Copenhagen; Copenhagen, Denmark.

<sup>3</sup>Department of Applied Mathematics and Computer Science, Technical University of Denmark; Kgs. Lyngby, Denmark.

<sup>4</sup>Department of Public Health, Section of Biostatistics, University of Copenhagen; Copenhagen, Denmark.

<sup>5</sup>Center for Translational Neuromedicine, University of Copenhagen; Copenhagen, Denmark.

<sup>6</sup>Danish Center for Sleep Medicine, Department of Clinical Neurophysiology, Copenhagen University Hospital, Rigshospitalet; Glostrup, Denmark.

<sup>7</sup>Department of Clinical Medicine, University of Copenhagen; Copenhagen, Denmark.

<sup>8</sup>Center for Translational Neuromedicine, Department of Neurosurgery, University of Rochester Medical Center; Rochester, NY, USA

<sup>9</sup>Roche Pharma Research and Early Development, Neuroscience and Rare Diseases, Roche Innovation Center Basel; Basel, Switzerland

## Correspondence to:

Gitte Moos Knudsen, MD, DMsc

Neurobiology Research Unit, Copenhagen University Hospital

8 Inge Lehmanns Vej, DK-2100 Copenhagen, Denmark

[gmk@nru.dk](mailto:gmk@nru.dk)

## Abstract

**Background:** Cerebrovascular oscillations play a crucial role in driving cerebrospinal fluid flow into and through the brain parenchyma, facilitating the clearance of waste products. While previous studies suggest that these oscillations are influenced by sleep-wake cycles and autonomic arousal, the precise nature of these relationships remains poorly understood.

**Methods:** To examine the role of vigilance and norepinephrine in modulating cerebrovascular oscillations, we examined 20 healthy individuals in a circadian-controlled approach. Participants underwent accelerated neuroimaging with the magnetic resonance sequence multiband echo planar imaging (MB) during three distinct states: rested wakefulness, sleep deprived wakefulness, and NREM sleep (stages N2 and N3).

**Results:** Low frequency oscillations (LFOs) in the 0.011–0.34 Hz band exhibited greater power during sleep deprived wakefulness than in both rested wakefulness (+91%,  $p < 0.001$ ) and sleep (+79%,  $p = 0.011$ ). In rested wakefulness, LFO power was positively correlated with plasma norepinephrine (p-NE) ( $r = 0.59$ ,  $p = 0.022$ ). This relationship persisted during sleep, as changes in p-NE from rested to sleep-deprived conditions were correlated with changes in LFO power from rested wakefulness to sleep ( $r = 0.68$ ,  $p = 0.044$ ). However, during sleep-deprived wakefulness, no significant association was observed between p-NE and LFO power, despite the absence of overt autonomic arousal. Brain pulsations driven by cardiorespiratory forces were, on the other hand, strongly associated with EEG slow waves.

**Conclusion:** Cerebrovascular oscillations are modulated by two distinct factors: sleep pressure and sympathetic activity.

## Introduction

The brain's fluid dynamics are crucial for maintaining neuronal health and overall brain function, not least because of its role in waste clearance<sup>1</sup>. Emerging evidence proposes sleep as a key regulator of brain fluid flow<sup>2,3</sup>, with sleep slow waves promoting influx of cerebrospinal fluid to the brain parenchyma<sup>4,5</sup>, where it exchanges with interstitial fluid and clears away metabolic waste<sup>3,6,7</sup>. Likewise, sleep deprivation has been associated with reduced clearance and a built-up of those same metabolic waste products<sup>8,9</sup>.

This process has been coined 'the glymphatic system'<sup>10</sup>, and its dysfunction has been implicated in the development of neurodegenerative diseases<sup>10</sup> and oedema formation after stroke<sup>11</sup> and traumatic brain injury<sup>12,13</sup>. Advancing our understanding of the brain fluid dynamics and its regulators in humans could therefore be important in preventing and treating these conditions.

Recently developed accelerated Magnetic Resonance (MR) neuroimaging techniques are particularly useful for studying brain-fluid-dynamics across changing vigilance states<sup>14,15</sup> because of their ability to capture different types of physiological brain oscillations. These include low-frequency brain oscillations (< 0.1 Hz), which are believed to propel CSF into the brain along perivascular spaces, as well as brain pulsations driven by cardiorespiratory forces, that likely represent either brain fluid motion or tissue compliance<sup>1</sup>. Two such fast MR sequences are MR Encephalography (MREG)<sup>16</sup> and Multiband echo planar imaging (MB)<sup>17</sup>. MREG acquires 10 full three-dimensional images of the brain per second, theoretically making it ideal for capturing fast, e.g., cardiac activity induced, brain oscillations. MB, on the other hand, offers better spatial resolution and sampling rates between 0.33–4.6 Hz, potentially making it more suitable for detecting LFOs. While both methods have been used for studying LFOs across vigilance states, it remains to be tested to what extent their outcomes are comparable across the different brain oscillation frequency bands.

Previous clinical<sup>15,18–22</sup> and preclinical<sup>23,24</sup> research indicates that LFOs, or cerebrovascular oscillations, are influenced by sleep-wake mechanisms. Some MREG and MB studies suggest that LFO power is enhanced during NREM sleep stages N1 and N2<sup>15,20</sup>, while others report that LFO power already increases during wakefulness with drowsiness<sup>19</sup> and that sleep deprivation specifically amplifies LFOs in N1 sleep<sup>21</sup>. We recently showed that sleep deprivation in humans increases MREG-detected LFOs more than slow-wave-rich sleep (stages N2 and N3) does and that LFO power correlates positively with measures of sleep pressure<sup>25</sup>. Finally, MB studies have shown that in humans, cortical LFO power as well as the oscillatory inflow of CSF into the fourth ventricle is strongest in N1 sleep followed by N2 and N3 sleep<sup>18</sup>. The authors argue that this - rather than being explained by neuronal activity itself - is due to bursts of autonomic arousal associated with K-complexes that occur in light sleep stages<sup>18</sup>, suggesting sympathetic activity as a potential modulator of LFOs.

The aim of this study was to investigate the effects of sleep deprivation and sympathetic activity, as indicated by p-NE levels, on brain cerebrovascular oscillations using a circadian-controlled design. Additionally, we provide the first direct comparison of outcomes between MB and MREG.

## **Materials and methods**

### **Approvals**

The study was conducted at the Copenhagen University Hospital, Rigshospitalet, between January 2018 and May 2019. Approval was granted by the Danish ethics committee of the Capital Region of Denmark (journal ID: H-16045933) and was preregistered at ClinicalTrials.gov (NCT03576664). The study adhered to the principles of Declaration of Helsinki and written informed consent was obtained from all participants before enrolment in the studies.

### **Study design and population**

In a circadian-controlled study, 20 healthy males (aged 18–29 years) with PSG-confirmed normal sleep patterns were alternately scanned with the two accelerated imaging sequences MREG and MB during rested wakefulness, after 35 hours of prolonged wakefulness and during sleep (Fig 1).

Three sessions, comprised of one rested and two sleep deprived scans, with simultaneous MR imaging, electroencephalography (EEG) recordings, and respiration- and heart rate monitoring, were conducted in the evening after 11 hours (rested wakefulness scan) and 35 hours (sleep deprived scans) of wakefulness, respectively. All three scans were conducted at the same circadian time point at known sleep pressure, confirmed by awake EEG, psychomotor vigilance tests and actigraphy. Before the two sleep deprived scans, participants received either a placebo or oral carvedilol in a double-blind, cross-over design. However, only placebo data is used in the current study.

Before inclusion, all participants were confirmed to be normal sleepers and had not crossed multiple time zones in the months prior to the study. Throughout the study, they abstained from alcohol, consumed a maximum of 2 cups of coffee ( $\leq 200$  mg caffeine/day, taken before 2 pm), and did not use any prescription drugs relevant to brain dynamics. To ensure measurements were performed during the same circadian phase and at comparable sleep propensities, participants followed a prescribed 8–16-hour sleep-wake schedule, confirmed with actigraphy and sleep diaries. In the three nights leading up to study days, participants slept in a controlled sleep environments with their sleep monitored with polysomnography (PSG). During prolonged wakefulness periods, participants were supervised by members of the research team, and their vigilance state(s) were monitored using a transportable EEG setup.

Detailed descriptions of the study design, recruitment, and study population, as well as methods for MREG imaging and supporting data (prolonged wakefulness EEG, nocturnal PSG recordings, p-NE, blood pressure, and questionnaires on Morning-eveningness (MEQ), general daytime sleepiness (ESS), sleep quality (PSQI) are available in our previous publication<sup>25</sup>.

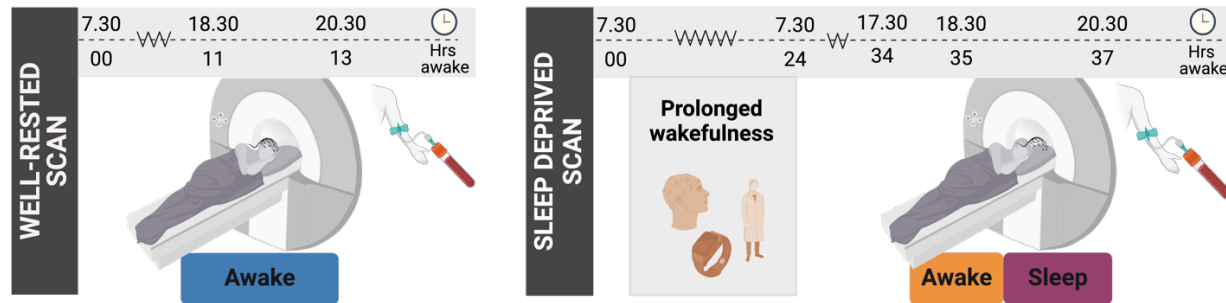


**Fig. 1. Study design.** In a circadian-controlled sleep and sleep deprivation study, MREG and MB data were collected simultaneously with EEG, respiration- and heart rates during wakefulness and sleep in a well-rested and two sleep-deprived scan sessions. A blood sample to assess p-NE was collected ~15 min after scans ended.  $N = 20$ .

*Figure created with BioRender.com.*

## MRI/EEG acquisition

MRI was performed on a Siemens (Erlangen, DE) MAGNETOM 3T Prisma scanner with a 64-channel head coil. For accelerated functional imaging we used both the MREG sequence and a MB sequence developed at the University of Minnesota<sup>26</sup> with a TR = 215 ms, TE = 35ms, Flip angle = 24° and 24 slices with a slice thickness of 4 mm and a voxel size of 3.6x3.6x4mm (3D matrix size: 64x64x24) and a FOV of 229 . We also acquired high-resolution, whole-brain, T1 weighted structural images (MPRAGE) with the following parameters: Inversion time = 900 ms, repetition time = 1900 ms, echo time = 2.52 ms, flip angle = 9°, in-plane matrix = 256 × 256, in-plane resolution = 0.9 × 0.9 mm, slices = 208, slice thickness = 1.0 mm.

To monitor vigilance state and physiological parameters during scans, participants were fitted with an MRI-compatible EEG cap (Electrical Geodesics, Inc., Eugene OR) and electrocardiographic (ECG) electrodes along with a respiratory belt and pulse oximeter wired directly to the scanner during all sessions. Earplugs were provided and memory foam cushions were used to alleviate pressure from the head coil on the EEG electrodes, as well as to restrict head movement.

Each scan session included a wakefulness period of approximately 15 minutes, followed by a sleep opportunity of about 1 hour. During wakefulness scans, the lights remained on, and participants were continuously monitored to ensure they stayed awake with their eyes open. During sleep scans, the lights were turned off, the scanner environment was kept as quiet as possible, and participants were instructed to relax and allowed to sleep. All scans alternated between 5-min MREG and 5-min MB sequences in a 2:1

ratio (MREG-MREG-MB), resulting in approximately twice as much MREG data as MB data (data overview in Fig S1).

### **MB data preprocessing**

MB data were pre-processed similarly to the MREG data in the study. Before analysis, 10 seconds of data (47 images) were excluded from the beginning of all MB-scans to ensure steady-state signal saturation. Next, MB data were pre-processed and analysed using Statistical Parametric Mapping software (SPM12, Wellcome Trust Center for Neuroimaging, UCL) in MATLAB (R2017b, The Mathworks, Inc.). This process included motion correction via realignment and co-registration of the T1 structural image to the MB data. For the co-registration-process, we used FSL's Brain Extraction Tool with a fractional intensity threshold of 0.3 on the first functional volume of each MB scan, to which the structural image was co-registered. Subsequently, the co-registered structural images were segmented into grey matter (GM), white matter (WM) and CSF maps, in which voxels were only included if they had a probability of  $\geq 0.1$  for the relevant tissue type. A whole-brain mask was then defined as the combined GM, WM and CSF masks. Next, an additional CSF region of interest (ROI) was created in the lateral ventricle in order to evaluate CSF oscillations with as little interference of surrounding tissue as possible: A sphere with a radius of 2 cm around a manually selected midpoint of the left ventricle was marked and defined in MNI space (MNI coordinates: 8,-10,24), keeping only the voxels with a segmentation-based CSF probability larger than 0.5. This ventricle CSF ROI was then normalized to each scan session and used for evaluation of CSF oscillations throughout the paper.

### **Scoring and analysis of EEG during MR**

Information on EEG cap placement, EEG acquisition in the MR-environment, the removal of gradient- and ballistocardiographic artefacts from EEG data, and details of EEG delta power quantification can be found in Ulv Larsen & Holst et al., 2024.<sup>25</sup>

EEG recordings obtained during the accelerated MRI scans were visually scored by two independent experts blinded to participant number, treatment, and scan type (lights on vs lights off). Using the DOMINO scoring software (Somnomedics, Germany), the experts scored EEG data in 30-second epochs in accordance with standard AASM criteria (American Academy of Sleep Medicine, 2007). Additionally, they identified epochs with residual MR artefacts and aberrant non-physiological data as “artefacts”.

The final classification of EEG epochs for MB-analysis was based on consensus between the two experts. Epochs were labelled as ‘wakefulness’ if they occurred before the first onset of NREM sleep stages N2 or N3 (scored by either expert) and if both experts agreed on ‘wakefulness’ or if one scored it as ‘wakefulness’

while the other scored it as ‘artifact.’ Epochs were classified as ‘NREM sleep’ if both experts scored them as either NREM sleep stage N2 or N3, and further specified as ‘N2 sleep’ or ‘N3 sleep’ only if both experts agreed on the specific sleep stage.

Delta power ratio was quantified independently of sleep scoring for all epochs that was not classified as ‘artefact’ by both experts, using MATLAB’s bandpower function. The delta power ratio was computed as the average of the ratio between EEG band power ( $\text{mV}^2$ ) the 1 – 4 Hz range and in the 0.5 – 30 Hz range across the C3-M2 and C4-M1 leads.

## **MB spectral analysis**

LFOs: For investigation of MB-detected LFOs, we used the full 5-min MB sequences. We assessed sum of MB spectral power within a frequency ranges based on the clinically described B-waves ( $0.5 - 2$  waves pr. min =  $0.008 - 0.033$  Hz)<sup>27</sup> and in a broader LFO band ( $0.01 - 0.1$  Hz) previously applied by other groups<sup>15,18</sup>. For each 5-min MB scan (= 10 scored EEG epochs), data were high-pass filtered with a 10-order IIR filter (highpass 0.008 Hz). Using the MATLAB periodogram function with a Hanning window and bin width of 0.00227 Hz, spectral analysis was then performed for all individual voxels in a whole-brain mask consisting of voxels within the earlier defined grey matter, white matter and CSF masks. Next, the voxel-wise MB spectra were averaged to create whole-brain or tissue-type-specific MB power spectra. Lastly, all 5-min MB spectra with framewise displacement  $>3$  mm in one or more 30-sec epoch were excluded from analysis. To avoid spill-over effects from the bandpass filtering, the exact frequency intervals for LFO analyses was set to  $0.011 - 0.034$  Hz (B-waves) and  $0.011 - 0.1$  Hz (previously described LFOs). The 5-min MB spectra were selected for LFO-analysis if EEG experts had classified at least 80% (8/10 epochs) of the simultaneously recorded 30-sec EEG epochs as either wakefulness or NREM sleep and only if they occurred in lights-on or lights-off conditions, respectively. Lastly, due to an uneven distribution of 5-min scans with verified vigilance state across participants in the five conditions (rested wakefulness, placebo sleep deprived wakefulness and sleep, and carvedilol treated sleep deprived wakefulness and sleep), we used the mean LFO spectral across scans within each condition for analysis (Table S1)

Respiration- and cardiac-driven brain pulsations: For investigation of brain pulsations related to respiratory and cardiac rhythms, we assessed 30-sec MB-spectra and assessed the sum of spectral power within individually tailored respiration and cardiac frequency bands. Data from all 5-min MB scans were high-pass filtered with a 10-order IIR filter (passband 0.1 Hz), and segmented into 30-sec epochs, which were temporally aligned with corresponding sleep-scored EEG epochs. For each 30-sec epoch, spectral analysis was performed as described for the 5-min LFO dataset, but with a bin width of 0.02 Hz. 30-sec epochs with a framewise displacement above 3 mm or faulty respiration- or cardiac- measures were excluded. We defined epoch-by-epoch heart and respiration rates using temporally aligned data from the

respiratory belt and the pulse oximeter, imported using the TAPAS PhysIO toolbox.<sup>28</sup> The frequency for the dominant peaks in respiration (0.13 – 0.5 Hz; 7.8 – 30 min<sup>-1</sup>) and cardiac frequency ranges (0.67 – 2 Hz; 40.2 – 120 min<sup>-1</sup>) were determined from the periodogram-determined power spectrum of each 30-sec epoch of physiological data. The epoch-by-epoch peak frequencies for respiration and heart rates were then used to define the individually tailored 30-sec epoch-specific respiration and cardiac frequency bands in the MB spectra and the individually tailored respiration and cardiac bands were defined as the epoch-wise respiration rate  $\pm 0.06$  Hz ( $= \pm 3$  bins), and the epoch-wise heart rate  $\pm 0.1$  Hz ( $= \pm 5$  bins), respectively. Epochs with non-physiological values ( $< 40$  or  $> 90$  heart beats per min. and/or  $< 8$  or  $> 25$  breaths per min.) were excluded. 30-sec MB epochs were selected for analyses if experts had classified the corresponding EEG as wakefulness, NREM sleep, N2 sleep or N3 sleep.

### **MREG restricted dataset**

Because the analysed MB datasets (Tables S1–S2) contained less data than the previously investigated MREG datasets<sup>25</sup> (Fig. S1), we conducted sensitivity analyses on two restricted MREG dataset including only the participants and scan conditions per participant available for MB analyses. The restricted 5-min MREG dataset (LFO analyses) data shown in Fig S1A, while the 30-sec restricted MREG dataset (cardiorespiratory pulsations analyses) included what is shown in Fig S1C.

### **Norepinephrine**

Venous blood samples were collected in 6 mL EDTA tubes approximately 15 minutes after scan sessions. Plasma was extracted by centrifugation at 2860 rpm for 7 minutes at 4°C and stored at –80°C until analysis. Plasma norepinephrine (p-NE) levels were measured using microdialysis in batch, according to Weikop et al. (see supplementary methods for details)<sup>29</sup>. The researcher conducting the analysis was blinded to the condition and analysed the samples in a random order.

### **Statistical analyses**

MB spectral power within LFO, respiration, and cardiac frequency bands was log transformed to mitigate skewness in the distribution before analysis. Data from well-rested, sleep deprived awake and sleep scans were analysed using similar approaches and linear mixed models as described in details in Ulv Larsen & Holst et al., 2024<sup>25</sup>. The models included (where appropriate) the following fixed effects: Sleep deprivation (well-rested vs sleep-deprived), vigilance state (awake vs NREM sleep), tissue type (grey matter vs white matter vs CSF), and delta power ratio. Interactions between vigilance state and tissue type as well as between vigilance state and treatment were also included. As random intercepts, we included participant ID, scan

session (well-rested, sleep-deprived session 1, sleep-deprived session 2) and sleep opportunity (lights on, lights off), with sleep opportunity being nested into scan session itself nested into participant ID. To account for the declining spectral power with higher frequencies<sup>30</sup>, epoch-wise respiration or heart rates recorded during the MB scans were also included as fixed effects in analyses of spectral power within respiration or cardiac frequency bands. P-values for fixed effects were obtained using Wald tests. The expected log MB spectral power under various conditions (e.g. awake under sleep deprivation) was computed from the mixed model estimates to illustrate the model fit.

Associations between delta power ratio and log spectral power in respiration and cardiac bands were assessed with Wald tests obtained from linear mixed models (denoted  $p_{\text{adj}}$ ) and corresponding correlations coefficients were deduced from mixed model estimates (denoted  $r_{\text{adj}}$ ).

Pearson's correlation coefficients were used for evaluating associations between NE levels and log spectral power in LFO bands (denoted  $r$ ) and for reference values for  $r_{\text{adj}}$  (regardless of subject ID, scan session, sleep opportunity, respiration- and heart rates and treatment; denoted  $r_{\text{raw}}$ ).

P-values equal to or below 0.05 were considered significant. In analyses evaluating three levels of a fixed effect, P-values were adjusted for multiple comparison using Bonferroni correction. Estimates are reported as mean  $\pm$  standard error of the mean (SEM) unless otherwise stated. Statistical analyses were conducted in R (<http://www.R-project.org/>) using the R packages lme4 (version: 1.1.29), lmerTest (version: 3.1.3), and LMMstar (version: 0.8.9) used for fitting linear mixed models, performing Wald tests, and estimating expected means and correlation parameters, respectively.

## Results

### Investigation of MB-detected physiological brain oscillations in healthy participants

Results from sleep-wake rhythm monitoring, EEG during prolonged wakefulness, PSG-monitored standardised nights and recovery nights as well as psychomotor vigilance performance have been reported elsewhere<sup>25</sup>. Some conditions had missing data. The number of participants in the data sets per condition is presented in Table S1–S2 and FigS1.

In EEG data collected simultaneously with MB scans, 7% of epochs were classified as artefacts, comparable to what was seen during MREG. EEG delta power increased during NREM sleep (delta to total power ratio:  $0.064 \pm 0.016$  AU,  $p < 0.001$ ), with higher power in N3 compared to N2 sleep ( $0.06 \pm 0.024$  AU,  $p = 0.013$ ), confirming the validity of the sleep-scoring.

Physiological data collected during MB-scans showed a borderline significant increase in respiration ( $p = 0.076$ ) and heart rates ( $p = 0.096$ ) with sleep deprivation, while both were decreased during sleep, *see* Table

S2. Previous analyses showed no effect of sleep deprivation on blood pressure and only borderline significant effects on NE levels measured post-scan.

We find a strong correlation between the frequency of measured respiration and heart rates and the corresponding power peaks in the MB spectra in rested wakefulness data (Resp:  $r_{adj} = 0.9$ ,  $p_{adj} < 0.001$ ; Card:  $r_{adj} = 0.99$ ,  $p_{adj} < 0.001$ ; Fig 2), supporting the hypothesis that MB reliably detects respiration- and cardiac-driven brain pulsations.

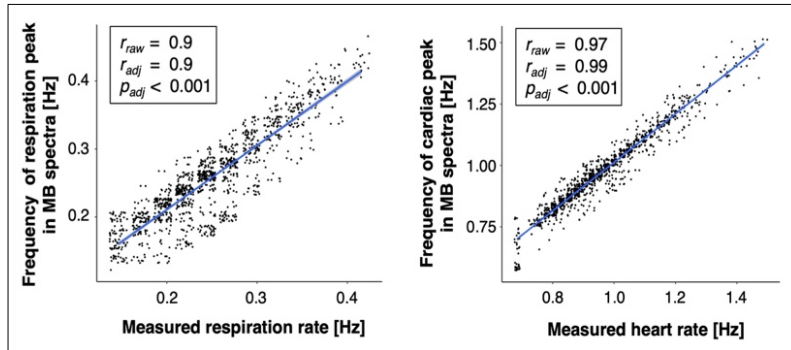


**Fig 2. Frequencies of power peaks in MB spectra correlate with respiration- and heart rates.** Correlation between measured respiration rates and the frequency of respiration-associated peaks in the MB spectra and between measured heart rates and the frequency of the cardiac-associated peaks in the MB spectra from all 30 sec epochs collected during the well-rested scans.  $r_{raw}$  denotes Pearson’s correlation coefficient.  $r_{adj}$  and  $p_{adj}$  denote estimates adjusted for repeated measurements from linear mixed models.  $N = 19$ .

## Spectral power in LFOs, respiration and cardiac frequency bands vary across tissue type

To investigate whether LFOs and respiration- and cardiac-driven brain oscillations differs across GM, WM and CSF, we analysed wakefulness data from the well-rested scan sessions ( $N_{LFO} = 17$ ,  $N_{Resp/Card} = 18$ )

We found that LFO spectral power was higher in GM compared to both WM and CSF, with CSF also showing higher power than WM (tissue main effect:  $p < 0.001$ ; Fig. 3B). These differences were consistent across the B-wave frequency band (0.011–0.034 Hz) and the broader LFO band (0.011–0.1 Hz); in frequencies below 0.05 Hz, the effects in GM were quite distinct (Fig. 3A).

In both the respiration and cardiac frequency bands, spectral power was strongest in CSF, followed by GM and then WM (Tissue main effect:  $p < 0.001$ ; Fig 3A & C).

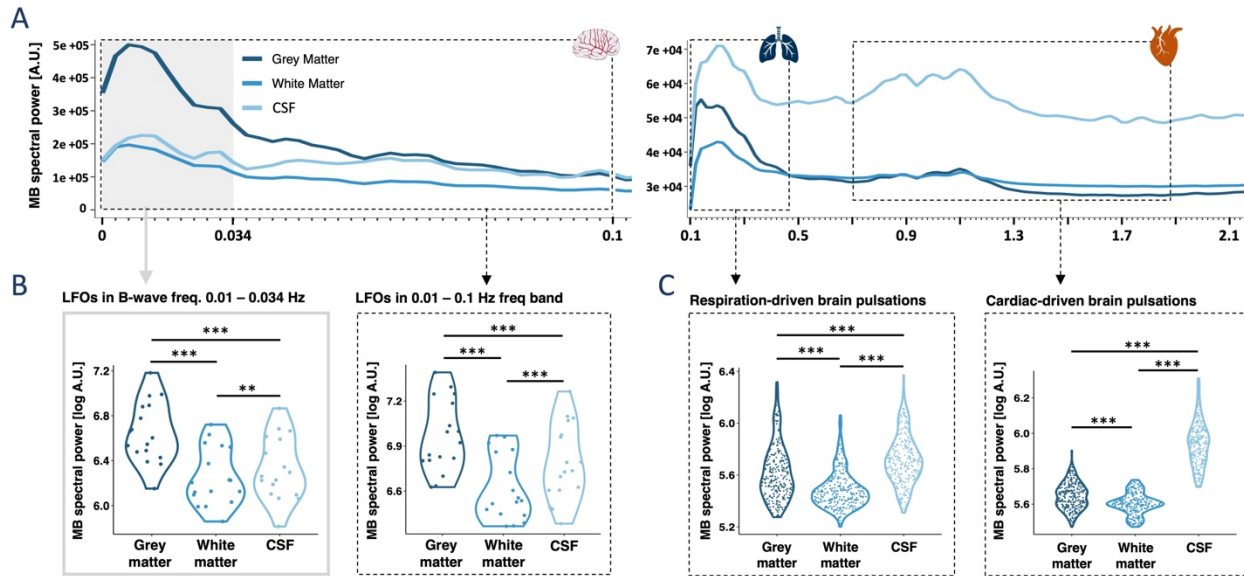


**Fig. 3. Strength of physiological brain oscillations vary across tissue type in rested wakefulness.** (A) Mean MB spectra across participants. Spectral power from 0 – 0.1 Hz (left) was determined from 5 min dataset, while MB spectral power in 0.1 – 2.1 Hz interval was determined from 30-sec dataset. (B,C) Comparison of MB spectral power density across grey matter, white matter and CSF. In (B), each dot represents one participant (average of included 5-min scans for participants with data from >1 scan). In (C), each dot represents a 30-sec epoch.  $p$ -values are from linear mixed models and are corrected for repeated measurements and multiple comparisons between the three tissue types with Bonferroni correction.  $N_{LFO} = 17$ ,  $N_{Resp/Card} = 18$ . \*\* =  $p < 0.01$ , \*\*\* =  $p < 0.001$ .

## LFO spectral power is higher when sleep deprived

Vigilance state effects on LFOs were evaluated in data from rested wakefulness ( $N = 17$ ), sleep deprived wakefulness ( $N = 8$ ) and NREM sleep (stages N2 and N3 combined;  $N = 13$ ). Results are shown for LFO spectral power in the B-wave frequency band, with similar effects observed in the broader frequency band (see Fig 4 B, D)

Sleep deprivation increased LFO spectral power by 91% ( $p < 0.001$ ; Fig 4). While sleep deprived NREM sleep (stages N2 and N3) was not associated with significantly higher LFO spectral power compared to rested wakefulness ( $p > 0.5$ ), it was lower compared to sleep-deprived wakefulness (LFO: -79%,  $p = 0.011$ ; Fig 4). However, it should be noted that even though effects were estimated using a linear mixed model including all data from the three conditions ( $N = 20$ ), only three participants had overlapping data between sleep deprived wakefulness and sleep scans (Fig 4C,E; missing data overview in Fig S1) .

Sleep deprivation and sleep had similar effects on LFO spectral power in GM, WM, and CSF (‘tissue type’  $\times$  ‘sleep deprivation’ interaction:  $p = 0.84$ ; tissue type’  $\times$  ‘sleep’ interaction:  $p = 0.57$ ).

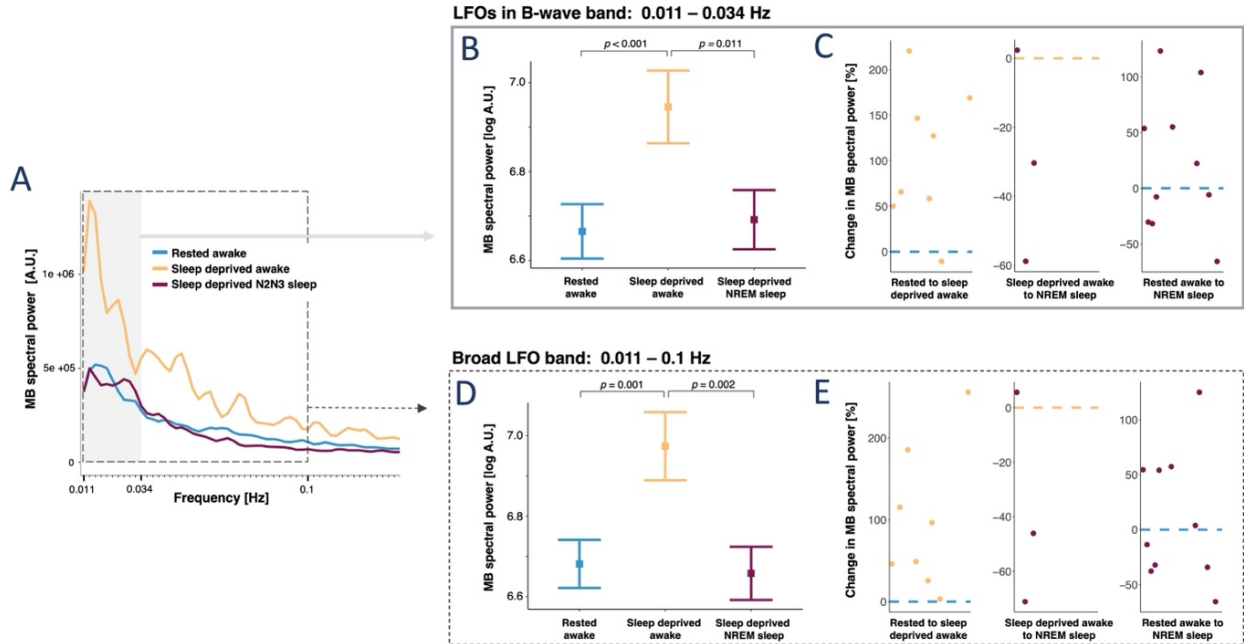


**Fig. 4. LFO spectral power is higher when sleep deprived.** (A) Mean whole-brain MB spectra across participants for rested wakefulness, sleep deprived wakefulness and NREM sleep (combined N2 and N3). Grey and dashed boxes denote frequency ranges for LFOs in a B-wave range (0.012–0.034 Hz) and a broader frequency range (0.011–0.1 Hz), respectively. (B, D) Estimated means  $\pm$  SEM and  $p$ -values are from linear mixed models evaluating effects of sleep deprivation and sleep on MB spectral power within LFO bands. (C, E) Individual percent changes in MB spectral power within the two LFO bands from rested to sleep deprived wakefulness (left), sleep deprived wakefulness to sleep deprived sleep (middle) and from rested wakefulness to sleep deprived sleep (right).

### Association between LFO spectral power and plasma norepinephrine

In rested wakefulness, we found a positive correlation between p-NE and whole-brain spectral power within the B-wave LFO band across participants ( $r = 0.59$ ,  $p = 0.022$ ,  $N = 17$ ).

Next, we investigated whether changes in p-NE correlate with changes in spectral power within the LFO band. We found no significant association between the change in p-NE from rested to sleep deprived wakefulness and the corresponding increase in LFO spectral power ( $r = 0.24$ ,  $p = 0.57$ ,  $N = 8$ ). However, a strong correlation was observed between p-NE changes and the change in LFO spectral power from rested wakefulness to sleep deprived NREM sleep ( $r = 0.68$ ,  $p = 0.044$ ,  $N = 9$ ). Similar effects were observed for the broad LFO band.

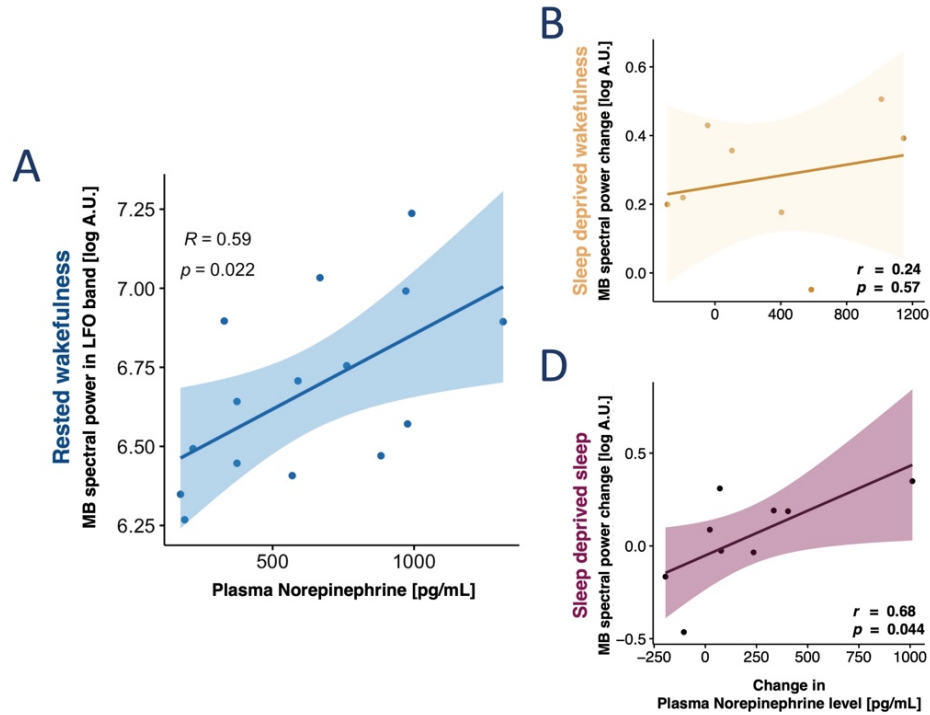


**Fig 5. Strength of LFOs is associated with plasma norepinephrine level (A)** Correlation between p-NE (measures after scan session) and MB spectral power in LFO band (0.011-0.034 Hz) during rested wakefulness,  $N = 17$ . **(B)** Association between absolute change in p-NE level from rested to sleep deprived scans and absolute change in LFO MB spectral power from rested wakefulness to sleep deprived wakefulness and **(D)** NREM sleep.  $N_{SDawake} = 8$ ,  $N_{sleep} = 9$ .  $r$  and  $p$  denote Pearson's correlation coefficient and its related significance level.

## NREM sleep (N2N3) enhances spectral power in the respiratory frequency band

To evaluate, if vigilance state also affects spectral power within the respiratory frequency band, we evaluated data from rested wakefulness ( $N = 18$ ), sleep deprived wakefulness ( $N = 8$ ) and NREM sleep stages N2 and N3 ( $N = 15$ ).

We observed a strong effect of sleep on whole-brain spectral power within the respiration frequency band, exhibiting a 119% increase compared to rested wakefulness ( $p < 0.001$ ) and a 77% increase compared to sleep-deprived wakefulness ( $p = 0.006$ ; Fig 6A-C).

This sleep-effect varied across GM, WM and CSF ('sleep' x 'tissue type' interaction:  $p < 0.001$ ), with separate analysis of the three tissues showing the strongest effect in GM (GM: +75,  $p = 0.012$ ; WM: +54%,  $p = 0.011$ ; CSF: +57%,  $p = 0.05$ ). Sleep deprivation did not increase spectral power in the respiration frequency band. In the cardiac frequency band, MB-spectral power did not differ between NREM sleep and neither rested nor sleep deprived wakefulness ( $p > 0.5$ , Fig 6A,D-E); this was the case for all tissue types ( $p_{all} > 0.5$ ).

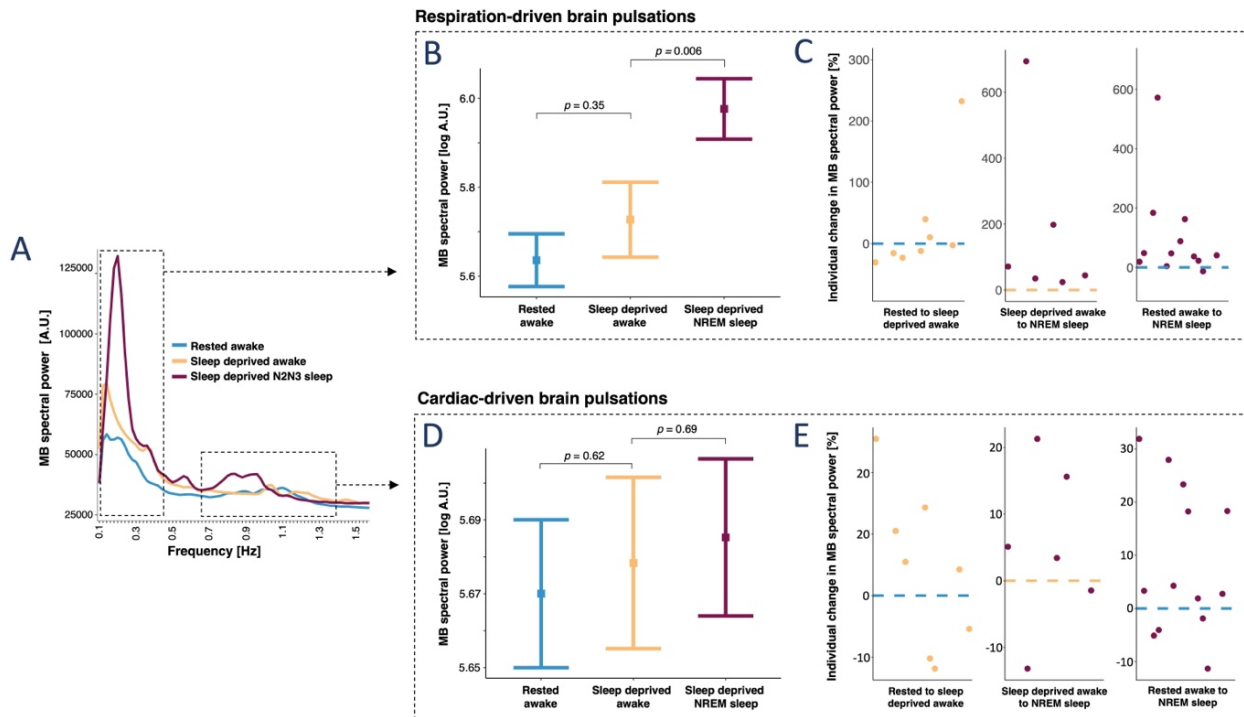


**Fig 6. Slow-wave rich NREM sleep enhances respiration-driven brain pulsations.** (A) Mean whole-brain MB spectra across participants for rested wakefulness, sleep deprived wakefulness (35 hours awake) and NREM sleep (combined N2 and N3). (B, D) Estimated means  $\pm$  SEM and  $p$ -values are from linear mixed models evaluating effects of sleep deprivation and sleep on spectral power in respiration (B) and cardiac (D) frequency bands. (C,E) Individual percent changes in spectral power within respiration (C) and cardiac (E) frequency bands from rested to sleep deprived wakefulness (left), sleep deprived wakefulness to sleep deprived sleep (middle) and from rested wakefulness to sleep deprived sleep (right).  $N_{\text{rest}} = 18$ ,  $N_{\text{SDawake}} = 8$ ,  $N_{\text{sleep}} = 15$ .

## Spectral power in respiratory and cardiac frequency bands correlate with EEG delta power

When we tested EEG delta-power ratio in all 30-sec epochs across well-rested and sleep-deprived scan sessions, regardless of scored vigilance state, against whole-brain spectral power in the respiration frequency band, we observed a significant association ( $r_{\text{raw}} = 0.18$ ,  $r_{\text{adj}} = 0.15$ ,  $p_{\text{adj}} < 0.001$ ; Fig. 7A).

This was also the case in the cardiac frequency band, although the effect size was lower ( $r_{\text{raw}} = 0.096$ ,  $r_{\text{adj}} = 0.11$ ,  $p_{\text{adj}} < 0.001$ ; Fig. 7B).

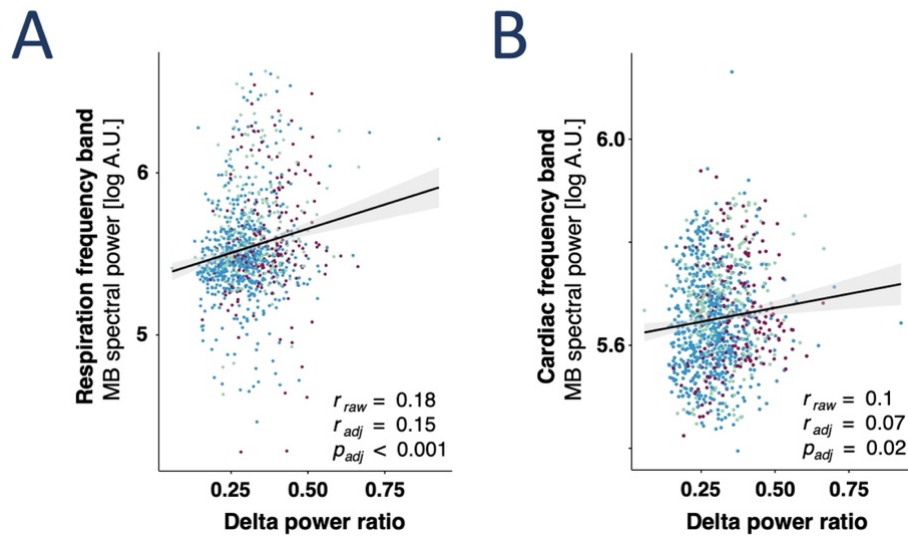


**Fig. 7. Power of respiration- and cardiac-driven brain pulsations correlates with EEG delta power.** Correlation between EEG delta power ratio and MB spectral power within the respiration (A) and cardiac (B) frequency bands across all 30-sec epochs from well rested and sleep deprived scans. Colours represent the scored sleep stages (blue: wakefulness; purple: NREM sleep stage 2 and 3; turquoise: N1 sleep or uncertain scorings) and are included for visualisation, but were not included in analysis.  $r_{raw}$  denotes Pearson's correlation coefficient.  $r_{adj}$  and  $p_{adj}$  denote adjusted estimates from linear mixed models.

## MB versus MREG outcomes

Because the analysed MB datasets (Tables S1–S2) contained less data than the previously investigated MREG datasets (Fig. S1), we conducted sensitivity analyses on a restricted MREG datasets to determine if discrepancies between findings in MB and MREG data were due to power limitations rather than methodological differences.

When the MREG data were reduced to match the MB sample size, the effect of sleep deprivation on MREG spectral power in the LFO band showed similar effect size to MB, while MB had the higher p-value (MREG<sub>Restrict</sub>: +98%,  $p = 0.04$  versus MB: +91%,  $p < 0.001$ ). For the respiration frequency band, we observed a similar effect of sleep in both dataset (MREG<sub>Restrict</sub>: +74%,  $p < 0.001$  versus MB: +77%,  $p = 0.006$ ), whereas sleep deprivation only increased power significantly in the restricted MREG dataset (MREG<sub>Restrict</sub>: +42%,  $p = 0.036$ ; MB +23%,  $p = 0.35$ ). In contrast to MB, the restricted MREG dataset showed that sleep enhanced cardiac spectral power (MREG<sub>Restrict</sub>: +28%,  $p = 0.05$ ; MB: +1.6%,  $p = 0.69$ ).

Restricted analyses were not conducted for EEG delta power correlations, as 30-sec epochs were included in these analyses independently of scan, condition and scored vigilance stage.

## Discussion

In a circadian-controlled design, we used the MB and MREG-sequences to investigate LFOs, generally believed to represent cerebral vasomotor activity<sup>14,15,18</sup>, during rested wakefulness, sleep-deprived wakefulness, and slow-wave-rich sleep. We also assessed p-NE as a marker of sympathetic activity. We demonstrate for the first time that in humans, norepinephrine modulates the cerebral vasomotor oscillations during rested wakefulness and sleep, whereas sleep deprivation enhances these oscillations independently of norepinephrine levels

We show that in rested wakefulness, p-NE is strongly correlated with LFO strength, and that this relationship persists during sleep where an increase in p-NE from rested to sleep-deprived status correlates with the increase in LFO spectral power from rested wakefulness to NREM sleep (stages N2 and N3). Taken together, these findings indicate that sympathetic activity modulates cerebrovascular oscillations in both wakefulness and sleep. Circulating norepinephrine levels decrease as sleep sets in<sup>31</sup>, which aligns with our observation that LFOs decrease in strength with the transition from sleep deprived wakefulness to sleep. Moreover, the progressive decline in norepinephrine levels across deeper sleep stages<sup>32</sup> could explain the finding by Picchioni et al.<sup>18</sup> that MB-detected LFO spectral power is largest in N1, smaller in N2 and even smaller in N3 sleep<sup>18</sup>. Lastly, autonomic arousals associated with K-complexes, which are common during lighter sleep stages but absent in N3 sleep<sup>33</sup>, have been shown to better explain cerebrovascular oscillations than neural slow-wave activity<sup>18</sup>. Combined with potential uncontrolled sleep pressure effects, this may explain why studies focusing on N1-N2 sleep report higher LFO strength during sleep compared to rested wakefulness<sup>15,20,21</sup>, whereas we observe no significant differences between the two.

Notably, sympathetic activity did not explain the stark effect of sleep deprivation on LFOs, as changes in norepinephrine levels from rested to sleep-deprived conditions did not correlate with changes in LFO strength. Likewise, we found no evidence that increased autonomic arousal alone drove the LFO increase, as blood pressure, respiration, and heart rates did not differ significantly between rested and sleep deprived wakefulness. These findings indicate that sleep deprivation promotes cerebrovascular activity independently of sympathetic activity. Aligning with this, our MREG data from the study previously showed<sup>34</sup> that systemic treatment with adrenergic  $\alpha$ 1-,  $\beta$ 1- and  $\beta$ 2-antagonists attenuated LFOs during sleep, but not LFOs during sleep deprived wakefulness. However, likely due to power limitations, this effect was neither replicated in MB data nor in a restricted MREG dataset.

Based on the above findings, we propose two distinct modulators of cerebrovascular oscillations: sleep pressure and sympathetic activity. During sleep, cerebrovascular activity may therefore be influenced by a combination of built-up sleep pressure, bursts of autonomic activity occurring in lighter sleep stages, and fluctuation in norepinephrine levels with changing vigilance and sleep stages. This interpretation agrees

with preclinical findings that, in naturally sleeping mice, transitions between sleep stages, microarousals and wakefulness are associated with distinct constriction-dilation dynamics of cerebral arteries and arterioles. Moreover, the amplitude of low frequency oscillations in these vessels is greater in wakefulness before than after sleep<sup>23</sup>

The MR-based techniques MB and MREG differ in their temporal and spatial resolution. Our direct comparison of the methods presented here helps to inform future studies when choosing which sequence to use and what power is required. We found that MB is comparable, or even superior to, MREG for detection of cerebrovascular oscillations, while for MB, we could not replicate sleep effects on cardiac-associated brain oscillations. This is consistent with the higher temporal (10 Hz) resolution of MREG and underscores its capability to capture all three types of physiological brain oscillations. MB, on the other hand, with its better spatial resolution and a sampling rate of 4.6 Hz was more consistently able to demonstrate changes in vasomotor brain oscillations. Supporting this perspective, we found that in rested wakefulness, MB-measured LFO spectral power was higher in GM than in both WM and CSF. This difference between tissues was not observed with MREG, confirming MB's greater sensitivity to cerebrovascular oscillations, which are expected to be strongest in GM due to its high vascular density<sup>35</sup>. Contrary to expectations based on vascular density, LFOs were also stronger in CSF than in WM. This supports the notion that cerebrovascular oscillations propels CSF into the brain parenchyma, generating a compensatory and oscillating net inflow of CSF to the ventricular system<sup>15</sup>.

Sleep deprivation strongly enhanced LFOs across all tissue types, as also seen with MREG<sup>25</sup>. While the magnitude of this effect was similar between MB and previously reported results for MREG (90% vs. 120%), MB demonstrated stronger statistical evidence, indicating higher measurement precision and/or lower data variability. Supporting this, analysis of a restricted MREG dataset, limited to the data available for MB analysis, showed a comparable effect size to MB (98%), but only a borderline significant effect. Likewise, MB data also revealed a significant negative effect of sleep compared to sleep-deprived wakefulness, whereas this effect was only numerical in MREG data. Altogether, this confirms that MB is more sensitive to cerebrovascular oscillations than MREG, requiring less power to detect differences than MREG.

Lastly, to best capture cerebrovascular activity, we defined a frequency range consistent with clinically described intracranial pressure B-waves (0.011–0.034 Hz), which have been shown to reflect cerebrovascular oscillations<sup>27,36</sup>. To ensure comparability with earlier studies<sup>15,18</sup>, we also evaluated LFO spectral power in a broader frequency band (0.011–0.1 Hz). Both frequency bands produced similar results, though the differences between tissue types and effects of sleep deprivation appeared to be largest within the B-wave range.

To our knowledge, no prior studies have used MB to investigate physiological brain oscillations beyond LFOs, so we first validated MB's ability to do so. We demonstrate a clear temporal relationship between measured respiration and heart rates and their respective power peaks in the MB spectra. Additionally, we show that cardiorespiratory spectral power is highest in CSF, followed by GM and WM. These findings are consistent with what is seen with MREG and support the hypothesis that the strength of these pulsations relates to brain tissue water content<sup>25</sup>.

The power of respiration-driven brain pulsations detected with MB strongly increased during NREM sleep and correlated with EEG delta power. Sleep increased power similarly in MB and in both the original and restricted MREG datasets, suggesting comparable sensitivity between the methods. Our MB findings thus align with our own and previous MREG results<sup>21,34</sup>, reinforcing the proposed relationship between respiration-driven brain pulsations and sleep slow waves. Since these pulsations likely reflect brain fluid motion<sup>1,14</sup>, this provides human translational evidence supporting the preclinical finding that sleep slow waves regulate CSF flow into and through the brain parenchyma<sup>4,5</sup>.

For cardiac-driven brain pulsations detected with MB, we found a correlation with EEG delta power. However, contrary to the original MREG dataset, we observed no significant difference between wakefulness and NREM sleep. Analyses of the restricted MREG dataset showed only a borderline significant effect of sleep, indicating that this null finding was not only due to method differences, but also due to power limits of this smaller MB dataset. From this, we speculate that larger sample sizes are required for detection of sleep effect on cardiac-driven compared to respiration-driven brain pulsations. Aligning with this notion, both ours and earlier studies<sup>20</sup> have reported smaller effects of sleep on cardiac- relative to respiration-driven brain pulsations. Although MB can theoretically capture pulsations up to  $\sim 2.33$  Hz ( $\sim 140$  beats per minute), the proximity of heart rate frequencies to this detection limit might increase the risk of aliasing, which could compromise power estimation under the Nyquist sampling theorem<sup>37</sup>. However, to definitively compare these methods with regards to cardiac-driven brain pulsations, a sufficiently powered study with an intervention of known effect size is needed.

In summary, we demonstrate for the first time in humans that MB-measured cerebrovascular oscillations are modulated by systemic norepinephrine during both rested wakefulness and sleep, and that sleep deprivation enhances these oscillations independently of norepinephrine level. Since cerebrovascular oscillations are believed to drive brain fluid flow and brain clearance, we now show that brain fluid flow is regulated not only by homeostatic sleep mechanisms but also by sympathetic activity and autonomic arousal. Pharmacological modulation of sympathetic activity could therefore play a crucial role in treating and managing neurodegenerative diseases and the progression of brain oedema following stroke and traumatic brain injury.

Moreover, we confirmed our previous MREG findings that the strength of respiration-driven brain

pulsations, which are believed to reflect brain fluid motion, is closely associated with sleep slow waves. Combined with the finding that cerebrovascular oscillations decrease during sleep relative to sleep-deprived wakefulness, this supports the idea that neural slow waves drive brain fluid flow through mechanisms other than a direct link with vasomotion – possibly via synchronized ionic waves in the interstitial fluid, as recently demonstrated in rodents by Jiang-Xie et al.<sup>5</sup> Finally, our results suggests that MB is superior to MREG in detecting cerebrovascular oscillations, while both techniques reliably capture respiration-driven brain pulsations.

## **Data availability**

All data and code supporting the findings of this study are available from the corresponding author, upon reasonable request.

## **Acknowledgments**

We would like to thank Helle Leonthin for sleep staging and Emily Beaman and members of the Center for Translational Neuromedicine lab for their assistance with data collection and supervision of proper sleep deprivation. We also thank Professor Vesa Kiviniemi for his valuable advice on the analysis of accelerated imaging data.

## **Funding**

The research reported in this work was funded by the H2020 Marie Skłodowska-Curie Actions grant: H2020-MSCA-IF-2017-798131 (SCH); the Lundbeck Foundation grant: R264-2017-2778 (SCH); the Lundbeck Foundation grant: R279-2018-1145 (GMK); the Independent Research Fund Denmark grant: 0134-00454B & 7025-00090B (GMK); the Independent Research Fund; Rigshospitalet Forskningspuljer grant: R151-A6534 (GMK); the EU Joint Programme - Neurodegenerative Disease Research 2022-120 (MN, GMK). The funders had no role in research conceptualization, study design, data collection and analyses, decision to publish or manuscript preparation.

## **Competing interests**

S.C.H. is currently an employee of Roche Pharma, which is unrelated to the contents of this manuscript. All other authors declare no competing interests.

## References

1. Rasmussen MK, Mestre H, Nedergaard M. Fluid transport in the brain. *Physiol Rev.* 2022;102(2):1025-1151. doi:10.1152/physrev.00031.2020
2. Ding F, O'Donnell J, Xu Q, Kang N, Goldman N, Nedergaard M. Changes in the composition of brain interstitial ions control the sleep-wake cycle. *Science.* 2016;352(6285):550-555. doi:10.1126/science.aad4821
3. Xie L, Kang H, Xu Q, et al. Sleep drives metabolite clearance from the adult brain. *Science.* 2013;342(6156):373-377. doi:10.1126/science.1241224
4. Hablitz LM, Vinitzky HS, Sun Q, et al. Increased glymphatic influx is correlated with high EEG delta power and low heart rate in mice under anesthesia. *Sci Adv.* 2019;5(2):eaav5447. doi:10.1126/sciadv.aav5447
5. Jiang-Xie LF, Drieu A, Bhasiini K, Quintero D, Smirnov I, Kipnis J. Neuronal dynamics direct cerebrospinal fluid perfusion and brain clearance. *Nature.* 2024;627(8002):157-164. doi:10.1038/s41586-024-07108-6
6. Iliff JJ, Wang M, Liao Y, et al. A paravascular pathway facilitates CSF flow through the brain parenchyma and the clearance of interstitial solutes, including amyloid  $\beta$ . *Sci Transl Med.* 2012;4(147):147ra111. doi:10.1126/scitranslmed.3003748
7. Lucey BP, Hicks TJ, McLeland JS, et al. Effect of sleep on overnight cerebrospinal fluid amyloid  $\beta$  kinetics. *Ann Neurol.* 2018;83(1):197-204. doi:10.1002/ana.25117
8. Eide PK, Vinje V, Pripp AH, Mardal KA, Ringstad G. Sleep deprivation impairs molecular clearance from the human brain. *Brain.* 2021;144(3):863-874. doi:10.1093/brain/awaa443
9. Shokri-Kojori E, Wang GJ, Wiers CE, et al.  $\beta$ -Amyloid accumulation in the human brain after one night of sleep deprivation. *Proc Natl Acad Sci USA.* 2018;115(17):4483-4488. doi:10.1073/pnas.1721694115
10. Xu Z, Xiao N, Chen Y, et al. Deletion of aquaporin-4 in APP/PS1 mice exacerbates brain A $\beta$  accumulation and memory deficits. *Mol Neurodegener.* 2015;10:58. doi:10.1186/s13024-015-0056-1
11. Cerebrospinal fluid influx drives acute ischemic tissue swelling | Science. Accessed December 29, 2024. <https://www.science.org/doi/10.1126/science.aax7171>
12. Braun M, Sevaio M, Keil SA, et al. Macroscopic changes in aquaporin-4 underlie blast traumatic brain injury-related impairment in glymphatic function. *Brain.* 2024;147(6):2214-2229. doi:10.1093/brain/awae065
13. Hussain R, Tithof J, Wang W, et al. Potentiating glymphatic drainage minimizes post-traumatic cerebral oedema. *Nature.* 2023;623(7989):992-1000. doi:10.1038/s41586-023-06737-7
14. Ultra-fast magnetic resonance encephalography of physiological brain activity – Glymphatic pulsation mechanisms? - Vesa Kiviniemi, Xindi Wang, Vesa Korhonen, Tuija Keinänen, Timo Tuovinen, Joonas Autio, Pierre LeVan, Shella Keilholz, Yu-Feng Zang, Jürgen Hennig, Maiken Nedergaard, 2016. Accessed January 16, 2023. <https://journals.sagepub.com/doi/10.1177/0271678X15622047>

15. Fultz NE, Bonmassar G, Setsompop K, et al. Coupled electrophysiological, hemodynamic, and cerebrospinal fluid oscillations in human sleep. *Science*. 2019;366(6465):628-631. doi:10.1126/science.aax5440
16. Hennig J, Kiviniemi V, Riemenschneider B, et al. 15 Years MR-encephalography. *MAGMA*. 2021;34(1):85-108. doi:10.1007/s10334-020-00891-z
17. Barth M, Breuer F, Koopmans PJ, Norris DG, Poser BA. Simultaneous multislice (SMS) imaging techniques. *Magn Reson Med*. 2016;75(1):63-81. doi:10.1002/mrm.25897
18. Picchioni D, Özbay PS, Mandelkow H, et al. Autonomic arousals contribute to brain fluid pulsations during sleep. *NeuroImage*. 2022;249:118888. doi:10.1016/j.neuroimage.2022.118888
19. Gonzalez-Castillo J, Fernandez IS, Handwerker DA, Bandettini PA. Ultra-slow fMRI fluctuations in the fourth ventricle as a marker of drowsiness. *Neuroimage*. 2022;259:119424. doi:10.1016/j.neuroimage.2022.119424
20. Helakari H, Korhonen V, Holst SC, et al. Human NREM Sleep Promotes Brain-Wide Vasomotor and Respiratory Pulsations. *J Neurosci*. 2022;42(12):2503-2515. doi:10.1523/JNEUROSCI.0934-21.2022
21. Helakari H, Järvelä M, Väyrynen T, et al. Effect of sleep deprivation and NREM sleep stage on physiological brain pulsations. *Front Neurosci*. 2023;17:1275184. doi:10.3389/fnins.2023.1275184
22. Krauss JK, Droste DW, Bohus M, et al. The relation of intracranial pressure B-waves to different sleep stages in patients with suspected normal pressure hydrocephalus. *Acta neurochir*. 1995;136(3):195-203. doi:10.1007/BF01410626
23. Bojarskaite L, Vallet A, Bjørnstad DM, et al. Sleep cycle-dependent vascular dynamics in male mice and the predicted effects on perivascular cerebrospinal fluid flow and solute transport. *Nat Commun*. 2023;14(1):953. doi:10.1038/s41467-023-36643-5
24. Turner KL, Gheres KW, Proctor EA, Drew PJ. Neurovascular coupling and bilateral connectivity during NREM and REM sleep. Peyrache A, Colgin LL, Das A, eds. *eLife*. 2020;9:e62071. doi:10.7554/eLife.62071
25. Larsen SMU, Holst SC, Olsen AS, et al. Sleep pressure propels cerebrovascular oscillations while sleep intensity correlates with respiration- and cardiac-driven brain pulsations. Published online October 17, 2024:2024.10.16.24315580. doi:10.1101/2024.10.16.24315580
26. Moeller S, Yacoub E, Olman CA, et al. Multiband multislice GE-EPI at 7 tesla, with 16-fold acceleration using partial parallel imaging with application to high spatial and temporal whole-brain fMRI. *Magn Reson Med*. 2010;63(5):1144-1153. doi:10.1002/mrm.22361
27. Spiegelberg A, Preuß M, Kurtcuoglu V. B-waves revisited. *Interdisciplinary Neurosurgery*. 2016;6:13-17. doi:10.1016/j.inat.2016.03.004
28. Frässle S, Aponte EA, Bollmann S, et al. TAPAS: An Open-Source Software Package for Translational Neuromodeling and Computational Psychiatry. *Frontiers in Psychiatry*. 2021;12. Accessed January 16, 2023. <https://www.frontiersin.org/articles/10.3389/fpsy.2021.680811>
29. Weikop P, Kehr J, Scheel-Krüger J. Reciprocal effects of combined administration of serotonin, noradrenaline and dopamine reuptake inhibitors on serotonin and dopamine levels in the rat prefrontal

- cortex: the role of 5-HT<sub>1A</sub> receptors. *J Psychopharmacol*. 2007;21(8):795-804. doi:10.1177/0269881107077347
30. Gerster M, Waterstraat G, Litvak V, et al. Separating Neural Oscillations from Aperiodic 1/f Activity: Challenges and Recommendations. *Neuroinform*. 2022;20(4):991-1012. doi:10.1007/s12021-022-09581-8
  31. Irwin M, Thompson J, Miller C, Gillin JC, Ziegler M. Effects of Sleep and Sleep Deprivation on Catecholamine And Interleukin-2 Levels in Humans: Clinical Implications1. *The Journal of Clinical Endocrinology & Metabolism*. 1999;84(6):1979-1985. doi:10.1210/jcem.84.6.5788
  32. Rasch B, Dodt C, Mölle M, Born J. Sleep-stage-specific regulation of plasma catecholamine concentration. *Psychoneuroendocrinology*. 2007;32(8-10):884-891. doi:10.1016/j.psyneuen.2007.06.007
  33. de Zambotti M, Trinder J, Silvani A, Colrain IM, Baker FC. Dynamic coupling between the central and autonomic nervous systems during sleep: A review. *Neurosci Biobehav Rev*. 2018;90:84-103. doi:10.1016/j.neubiorev.2018.03.027
  34. Ulv Larsen SM, Landolt HP, Berger W, Nedergaard M, Knudsen GM, Holst SC. Haplotype of the astrocytic water channel AQP4 is associated with slow wave energy regulation in human NREM sleep. *PLoS Biol*. 2020;18(5):e3000623. doi:10.1371/journal.pbio.3000623
  35. Kubíková T, Kochová P, Tomášek P, Witter K, Tonar Z. Numerical and length densities of microvessels in the human brain: Correlation with preferential orientation of microvessels in the cerebral cortex, subcortical grey matter and white matter, pons and cerebellum. *J Chem Neuroanat*. 2018;88:22-32. doi:10.1016/j.jchemneu.2017.11.005
  36. Auer LM, Sayama I. Intracranial pressure oscillations (B-waves) caused by oscillations in cerebrovascular volume. *Acta Neurochir (Wien)*. 1983;68(1-2):93-100. doi:10.1007/BF01406205
  37. Jerri AJ. The Shannon sampling theorem—Its various extensions and applications: A tutorial review. *Proceedings of the IEEE*. 1977;65(11):1565-1596. doi:10.1109/PROC.1977.10771

## Supplementary Figures

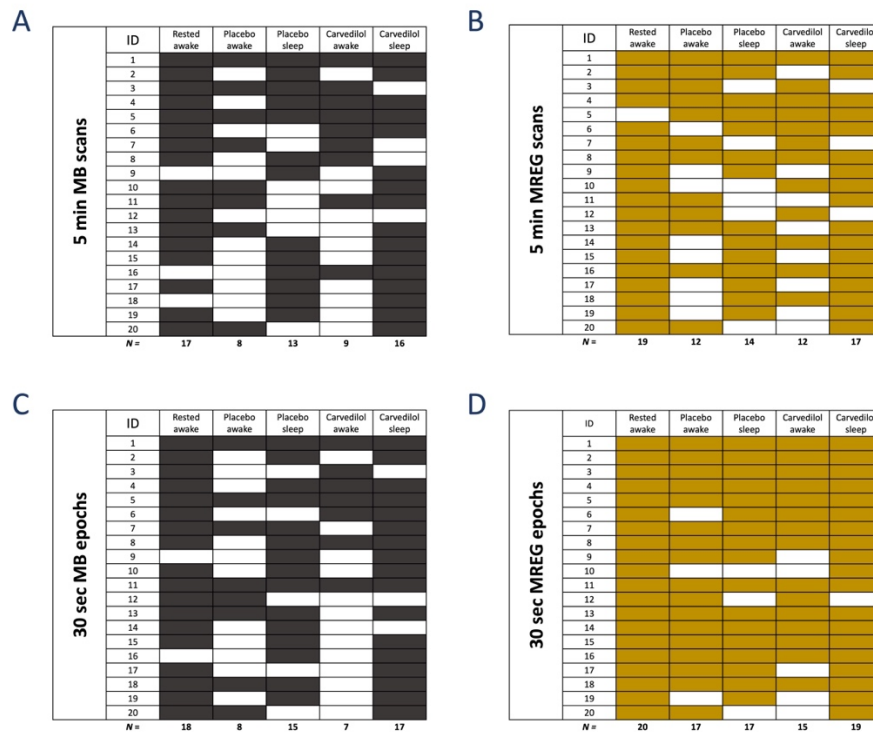


**Fig S1. Data amount across conditions.** (A, B) Included data (and missing data: white slots) in 5-min MREG- and MB-dataset used for analysis of LFOs. (C,D) Included data (and missing data) in 30-sec MREG- and MB-dataset used for investigation of respiration- and cardiac-driven brain pulsations. Data was included in all dataset based on classification of simultaneously recorded EEG-data (see methods)

## Supplementary Tables

**Table S1 Distribution of analysed data in 5-min dataset**

	Well-rested wakefulness	Sleep deprived wakefulness	Sleep deprived sleep (N2&N3)
<b>Participants in analysis (N)</b>	17	8	13
<b>5-min scans pr. participant (n)</b>	1 [1, 1]	1 [1,1]	1.5 [1.1, 1.9]

Data included in the 5-min dataset used for evaluation MB spectral power within the LFO frequency band(s). Participants were included in analysis, if they had at least one 5-min MB scan where a minimum of 80% (8/10 epochs) of the simultaneously collected EEG data was classified as either wakefulness or NREM sleep (stages N2 or N3). The number of scans per participant is presented as a mean with a 95% confidence interval.

**Table S2 Distribution of analysed data in 30-sec dataset**

	<b>Well-rested wakefulness</b>	<b>Sleep deprived wakefulness</b>	<b>Sleep deprived sleep (N2&amp;N3)</b>
<b>Participants in analysis (N)</b>	18	8	15
<b>Included 30-sec epochs (n)</b>	16.7 [12.1, 21.2]	11.0 [7.2, 14.8]	12.5 [8.3, 16.8]
<b>Respiration rate (min<sup>-1</sup>)</b>	15.3 [14.0, 16.7]	17.0 [15.0, 19.2]	13.9 [12.5, 15.3]
<b>Heart rate (min<sup>-1</sup>)</b>	60.5 [56.9, 64.3]	64.4 [59.1, 70.2]	53.9 [49.4, 56.7]

Data included in 30-sec dataset used for MB spectral power within the respiration- and cardiac frequency band. Participants were included in analysis if they had at least one 30-sec MB-epoch where the simultaneously collected EEG data was classified as either wakefulness or NREM sleep (stages N2 or N3). Number of scans per participants as well as respiration- and heart rates across conditions are presented as mean with 95% confidence intervals, determined using linear mixed models to account for interindividual variance.

## Supplementary methods

### NE analysis

p-NE levels were determined with microdialysis according to Weikop et. al. 2007. CMA / 12 4mm probes were prepared and their individual recoveries for norepinephrine were determined. The calibrated CMA / 12 4mm probe was immersed in one ml of EDTA stabilized plasma for 60 min, at a flow of 1  $\mu$ l per min. Subsequently, the flow was set to 0.5 ul/min for another 60 min. The plasma sample was kept at a relatively low temperature  $\leq$  15 degrees Celsius. After calibration to the plasma, a sample of 30  $\mu$ l was collected over 60 minutes and was then analyzed by High-performance Liquid Chromatography (HPLC) with electrochemical detection: The column used was a Prodigy C18 column (100 x 2 mm I.D., 3- $\mu$ m particle size, YMC Europe, Schermbeck, Germany). The mobile phase consisted of 55 mM sodium acetate, 1 mM octanesulfonic acid, 0.1 mM Na<sub>2</sub>EDTA and 7% Acetonitrile, adjusted to pH 3.7 with 0.1 M acetic acid, and was degassed using an on-line degasser. 10  $\mu$ l of the sample was injected and the flow rate was 0.31 mL/min. The electrochemical detection was accomplished using an amperometric detector (Antec Decade from Antec, Leiden, The Netherlands) with a glassy carbon electrode set at 0.7 V, with an Ag/AgCl as reference electrode. The output was recorded on a computer program system CSW (Data Apex, Prague, The Czech Republic), which was used to calculate the peak areas. Concentrations of NE were calculated based on a known standard and adjusted for the recovery of the individual probes. The determined concentration in the 10  $\mu$ l sample was converted to the content in one ml plasma sample.